Development of a chick embryo spinal cord injury model as a platform to test neural tissue engineering strategies

Aina Mogas Barcons

Doctor of Philosophy in Neuroscience

December 2021

This thesis is dedicated to

Manoli Álvarez González, my grandmother.

ABSTRACT

Spinal cord injury is a devastating condition affecting thousands of people every year. The spinal cord does not have the intrinsic capacity for regeneration due to a complex cascade of physical and chemical barriers that prevent axonal growth and lead to neuronal death and, therefore, current treatments are yet to achieve full functional repair. The implantation of encapsulated neural stem cells within 3D matrices offers the advantages of cellular repopulation, release of neurotrophic factors and healthy extracellular matrix mimicking, leading to improved motor function. However, neural tissue engineering strategies face three main challenges: the exclusive use of experimental grade biomaterials for research, the overlooking of the highly aligned structure of the spinal cord and the reliance on complex and expensive *in vivo* rodent animal models, leading to time consuming experiments which make reproducibility challenging. As an alternative, we propose the use of chick embryo spinal cord organotypic slices as a novel spinal cord injury model as it offers a cheaper alternative linked to less ethical implications.

Here, we established for the first time a transecting spinal cord injury model using the chick embryo as a donor of spinal cord slices. We also tested two biomaterials for their capacity to incorporate a relevant cell transplant population: Hemopatch™, a clinically available scaffold, and Cellevate™, an aligned nanofibre biomaterial. We demonstrated the viability of both matrices for incorporating a healthy cell population, we showed improvement of cell distribution through laminin engineering on Hemopatch™ and we described a protocol for measuring cellular alignment with Cellevate™. Finally, we tested the feasibility of biomaterial implantation in the spinal cord injury model described earlier, resulting in the typical cellular responses expected in an adult injury.

The model, which presents comparable responses to those based on murine models, represents a simpler alternative to previously established models. The adoption of this model could lead to impactful research while maintaining a cost-effective and technically

simple methodology. This could have translational potential for other research areas, such as the study of degenerative diseases, and potentially increase the research output on the study of spinal cord injury therapies which, in turn, would lead to a faster translation of functional therapies to higher complexity models and, finally, to the clinic.

TABLE OF CONTENTS

LIST OF FIGURES AND TABLES

LIST OF ABBREVIATIONS

AIS – American spinal cord injury impairment scale

BBB – Blood brain barrier

BDNF – Brain-derived neurotrophic factor

CAC – Sodium cacodylate

CNS – Central nervous system

CSF – Cerebrospinal fluid

CSPG – Chondroitin sulfate proteoglican

CT – Computational tomography

DCML – Dorsal column-medial lemniscal

DiffM – Differentiation medium

E1 – Embryonic day 1

ECM – Extracellular matrix

EGFR – Epidermal growth factor receptor

ESC – Embryonic stem cell

EU – European union

FDA – Food and drug administration

FGF – Fibroblast growth factor

GDNF – Glial cell-derived neurotrophic factor

GFAP – Glial fibrillary acidic protein

GFP – Green fluorescent protein

GMP – Good manufacturing practice

HBDS – Heparin-binding delivery system

HH – Hamburger and Hamilton

IL-6 – Interleukin-6

iPSC – Induced pluripotent stem cell

MEA – Multi electrode array

MLM – Monolayer medium

MPSS – Methylprednisolone sodium succinate

MRI – Magnetic resonance imaging

MSC – Mesenchimal stem cell

NGF – Nerve growth factor

NSC – Neural stem cell

NSM – Neurosphere medium

NT-3 – Neurotrophin-3

OD – Optical density

OEC – olfactory ensheathing cell

OPC – Oligodendrocyte precursor cell

P1 – Postnatal day 1

PBS – Phosphate buffered saline

PEG – Polyethylene glycol

PFA - Paraformaldehyde

PLC – Polycaprolactone

PLLA – Poly-L-lactic acid

PMA – Pre-market approval

PNS – Peripheral nervous system

qPCR – Quantitative polymerase chain reaction

ROS – Reactive oxygen species

SCI – Spinal cord injury

SEM – Scanning electron microscopy

TEM – Transmission electron microscopy

UK – United Kingdom

WHO – World Health Organisation

PUBLICATIONS DURING PhD

Woods, W., Evans, D., Mogas Barcons, A., Tzerakis, N., Adams, C., Chari, M. **Neural Stem Cell Sprays for Neurological Injuries: A Perspective**. Emerging Topics in Life Sciences (2021). doi: 10.1042/ETLS20210113

Mogas Barcons, A., Chari, D. M., & Adams, C. **Enhancing the regenerative potential of stem cell-laden, clinical-grade implants through laminin engineering**. Materials Science and Engineering: C, (2021). doi.org/10.1016/j.msec.2021.111931

Price, J. C., Levett, S. J., Radu, V., Simpson, D. A., Mogas Barcons, A. Adams, C. F., Mather, M. L. **Quantum sensing in a physiological-like cell niche using fluorescent nanodiamonds embedded in electrospun polymer nanofibers.** Small (2019). doi.org/10.1002/smll.201900455

ACKNOWLEDGEMENTS

I am extremely grateful for the privilege it has been to do this PhD which has been the most important project in my life so far. During these four years I have learnt from incredibly talented and brilliant scientists, I have formed new friendships and relationships and I have grown as a scientist and as a person.

I owe this largely to my supervisor, Dr. Chris Adams. Chris, I am incredibly grateful for this opportunity. I am aware that a PhD supervisor has a huge impact on the experience the student has on the project and I feel very lucky to have had your support and guidance during these four years. You have given me valuable guidance and advice when I needed it, but you have also given me freedom to express my ideas and allowed me to be creative and to steer this project in a direction that we are both passionate about. Thank you!

This project would not have been possible without the help and support from all the members of the Neural Tissue Engineering Keele (NTEK) group and collaborators. To everybody who has been and gone in the lab and to everybody who is starting now: thank you for teaching me and sharing many long lab days with me. Especially, I would like to thank Dr. Stuart Jenkins, who was the first person I met when I arrived at Keele, who has constantly taught me and helped me when I needed it the most and who was very kind to agree to proofread this manuscript. I would also like to thank Prof. Dave Furness, Mrs. Karen Walker and Mr. Simon Holborn for their valuable help and assistance at the Electron Microscopy Unit.

Of course, I need to mention the strongest support group I have ever had: the office! In my experience, doing a PhD comes with a lot of up and down moments and it would have been very hard to go through the down moments without them. Farhana, Jess, Yolanda, Emma and Cátia, in you I found a group of inspirational women who taught me how important it is to help each other. In the small space of the office we have shared all kinds

of moments and emotions but I feel very happy to be able to say that our friendship goes beyond these four walls. I wish you all happiness and good luck in all your future projects and I offer you my help and support with anything you need, just as I know you would do for me.

And speaking of support groups, I am incredibly lucky and grateful to have had the constant support and encouragement from Scott Seabridge. Scott, I met you months before I started my PhD and now that I am close to finishing, I can say with absolute certainty that this experience would not have been the same without you. You have witnessed of all the stages I have been through and encouraged me to continue when it felt most difficult and, more importantly, you and your family have made me feel at home in a country that was new to me. Thank you!

Finally, I want to thank my family: my uncles, aunts, cousins (big and small) and, especially, my parents. They were all very surprised when a 16-year-old me told them I wanted to be a scientist, but they have always encouraged and enabled me to pursue my passions even if it meant being an eternal student (as they like to call it) and living away from home. It has been difficult to be away from them, especially through a pandemic, but their love has always felt very close. I also want to thank my grandmother, from whom I like to think I have inherited strength and character (and a passion for books!) and, although she died in January 2020, she is still very present in everything I do.

To all of you, thank you!

Aina Mogas Barcons

1 INTRODUCTION

1.1 OUTLINE

During the course of this introduction, a background on spinal cord injury (SCI) and spinal cord anatomy will be reviewed. Next, the current and experimental therapeutic approaches will be discussed, with special attention to cell therapy and biomaterial implantation as the two approaches that will be taken forward in the experimental chapters. As this thesis focuses on the development of a new model in which to test biomaterial implantation for SCI, the current models in which to test SCI therapies will be reviewed and the chick embryo will be proposed as an alternative model. Finally, the aims and experimental chapters of this thesis will be outlined.

1.2 SPINAL CORD INJURY

1.2.1 Socioeconomic impact of spinal cord injury

SCI is the cause to thousands of people's paralysis around the world, affecting between 250000 and 500000 people every year (WHO, 2018). The average age at the time of injury has increased from 29 years to 43 years since the 70s (National Spinal Cord Injury Statistical Center, 2019) with a male-female ratio of incidence of approximately 2:1 (WHO, 2018).

SCIs can be classified depending on the affected segments of the spinal cord. In this classification, the SCI can result in paraplegia, which refers to the loss of function in the thoracic, lumbar or sacral segments, but not cervical. Therefore, arm functioning is spared, but damage can affect the trunk, legs and/or pelvic organs depending on the level of injury. On the other hand, tetraplegia refers to impairment or loss of motor/sensory function in the cervical segments. Typically, tetraplegia affects the arms as well as trunk, legs and pelvic organs (Kirshblum et al., 2011). Moreover, SCI is associated with higher

risk of developing secondary complications such as thrombosis, urinary tract infections or respiratory complications (WHO, 2018).

However, SCIs are usually classified following the American spinal injury Impairment Scale (AIS), which was created in 1982 with the aim to standardise SCI, guide further treatment, determine which injuries are complete or incomplete and help predict a possible recovery of autonomic functions, such as bowel movements or respiratory functions (Roberts et al., 2017). The AIS consists of a myotomal-based motor examination (following a grading system from 0-6), dermatomal-based sensory examination (following a grading system from 0-2) and anorectal examination. The AIS also classifies the injuries as complete or incomplete. A SCI will be classified as complete if there is no motor or sensory function below the injury. An incomplete SCI will be defined as such when there is some degree of motor or sensory function below the injury (Roberts et al., 2017) (**Table 1.1**).

Table 1.1 SCI classification according to ASIA. *Injury level classification to guide further treatment.*

		American spinal injury association Impairment Scale (AIS)
A	Complete	No motor or sensory function is preserved in the sacral segments S4-S5.
B	Incomplete	Sensory function is preserved but not motor function is preserved below the neurological level and includes the sacral segments S4-S5.
C	Incomplete	Motor function is preserved below the neurological level, and more than half of key muscles below the neurological level have muscle grade less than 3.
D	Incomplete	Motor function is preserved below the neurologivel level, and at least half of key muscles below the neurological level have a muscle grade of 3 or more.
E	Normal	Motor and sensory function are normal.

The leading causes for SCI in the United States are vehicle crashes, followed by falls, violence (primarily gunshot wounds), sports and medical/surgical complications (**Figure 1.1 A**) (National Spinal Cord Injury Statistical Center, 2019). After injury, the average length of hospitalisation in the United States is 11 days of acute care and 31 days of rehabilitation. However, approximately 30% of people are re-hospitalised usually due to diseases related to the genitourinary system (National Spinal Cord Injury Statistical

Center, 2019). By the time of hospital discharge, less than 1% of people experience complete neurological recovery and the level of neurological damage can vary considerably between individuals, with incomplete tetraplegia the most common type of damage (**Figure 1.1 B**) (National Spinal Cord Injury Statistical Center, 2019). People with SCI are 2 to 5 times more likely to die prematurely than people without SCI and the mortality risk is higher during the first year after injury. It increases with injury severity (**Figure 1.1 C**) and it is strongly influenced by timely, quality medical care (WHO, 2018).

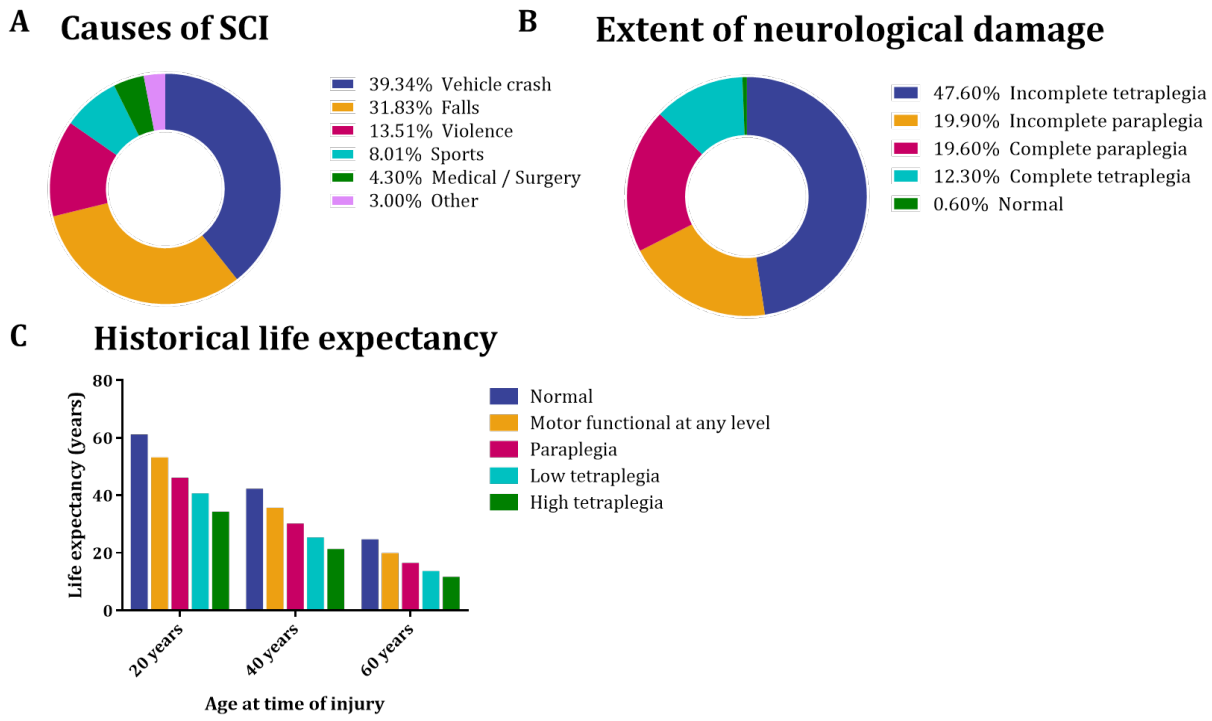

***Figure 1.1 Epidemiology of SCI**. Graphs adapted from data from National Spinal Cord Injury Statistical Center (2019) showing causes of SCI (**A**), extent of neurological damage by the time of hospital discharge (**B**) and life expectancy post-injury after injuries occurring at different ages and with various damage degrees (**C**).*

In regard to the economic impact of such injuries, new SCI cases in the United Kingdom (UK) may incur lifetime costs of over £1.45 billion per year, 71% of which is covered by public funding (Mcdaid & Park, 2019). In fact, according to the World Health Organisation (WHO), the economic impact of SCI is higher compared to other neurological conditions such as dementia or multiple sclerosis, and the costs increase along with the level of severity, meaning finding an effective treatment for SCI is a key clinical goal.

1.2.2 Anatomy of the spinal cord

The spinal cord is a cylindrical structure with a bilateral symmetry. It is extended from the foramen magnum to the first or second lumbar vertebrae in humans. It can be divided into four regions: cervical, thoracic, lumbar, sacral and coccygeal. Each of these regions can be divided into segments: 8 cervical, 12 thoracic, 5 lumbar, 5 sacral and 1 coccygeal (31 in total) (**Figure 1.2 A**). From each segment, two nerve roots emerge on each side, one ventrally and one dorsally. The dorsal nerves are called afferent and carry sensory input to the brain, whereas the ventral nerves serve the function of motor output and are called efferent (Bear, Connors, Paradiso, 2007) (**Figure 1.2 B**).

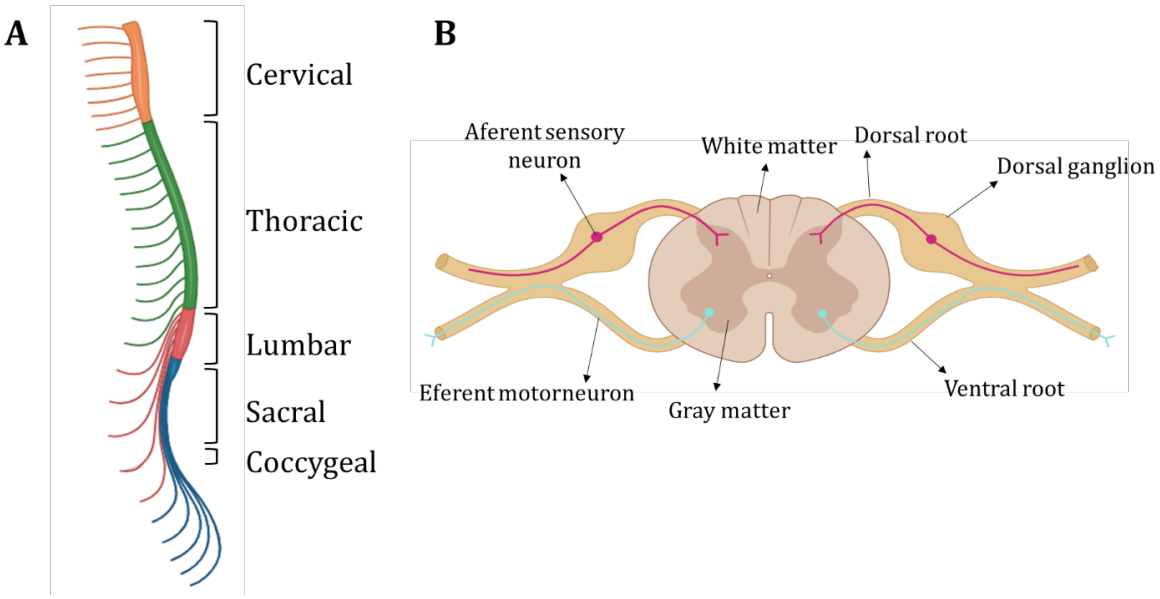

Figure 1.2 Schematic representation of spinal cord anatomy *on a side view (**A**) and cross view (**B**). Image created with Biorender.com. Image based on Bear, Connors, Paradiso, 2007.*

Diverse anatomical structures are found in a cross section of the spinal cord (**Figure 1.2 B**). The grey matter is the region where neuronal bodies are located. It is shaped like a butterfly and it forms a ventral and dorsal horn on each side. The axons are found in the white matter, which surrounds the grey matter. At the centre of the spinal cord is the central canal, where cerebrospinal fluid (CSF) flows, surrounded by a monolayer of ependymal cells. The shape and size of the grey matter varies along the axis due to lower

levels containing fewer afferent axons and more efferent. Moreover, the width of the spinal cord also varies; there is a cervical enlargement, which contains neuronal bodies that innervate the arms, and a lumbar enlargement, which innervates the legs. (Bear, Connors, Paradiso, 2007).

Distributed along the dorsal-ventral axis there are more than 20 types of interneurons, sensory neurons and motoneurons (Alaynick et al., 2011) that can be organized in different groups (**Table 1.2**). Sensory neurons transmit sensory information from the periphery to the brain; motoneurons innervate the smooth and skeletal muscles to which they transmit output from the brain. Interneurons synapse with sensory neurons, motoneurons and other interneurons and form higher complexity circuits (Bear, Connors, Paradiso, 2007).

***Table 1.2 Classification of neurons and their trajectory within the spinal cord**. Table based on Bear, Connors, Paradiso, 2007 describing the origin (soma) and destination (synapse area) of different cell types within the spinal cord, as well as there they can be found in the grey and white matter and what kind of fibre they are according to their function.*

Cell type	Origen	Destination	Grey matter	White matter	Nerve fiber
Motorneurons α,γ	Ventral horn	Skeletal muscle	Ventral horn	Ventral root	Somatic
Preganglionic MN	Lateral horn	Smooth muscle	Lateral horn	Ventral root	Autonomic
Primary Sensory	Soma at spinal ganglion	Dorsal-lateral horn	Dorsal horn	Dorsal root	Sensory
Secondary Sensory	Dorsal-lateral horn	Brain	Dorsal-lateral horn	Dorsal-lateral root	Sensory
Intersegmentary	Segment A	Segment B	All horns	All	Association
Intrasegmentary	Side A of segment	Side B of segment	All horns	None	Association

These neurons are part of complex specialised pathways that innervate different muscles or that transmit input to the brain from various sensory areas (**Figure 1.3**). The ascending or sensory pathways transmit sensory information. The neurons from the dorsal column-medial lemniscal pathway (DCML) carry sensory information regarding fine touch, proprioception and vibration, whereas the neurons from the anterolateral system carry information regarding crude touch, pressure, pain or temperature. The descending or motor pathways can be classified into pyramidal tracts, responsible for conscious

movements, or extrapyramidal tracts that are responsible for unconscious movements. There are two pyramidal pathways: the corticospinal tracts, which supply the musculature of the body; and the corticobulbar tracts, which supply the musculature of the head and neck. The descending extrapyramidal tracts control balance and posture (vestibulospinal tract), muscle tone (reticulospinal tract), fine hand movements (rubrospinal tract) and movements of the head in relation to vision stimuli (tectospinal tracts) (Bear, Connors, Paradiso, 2007).

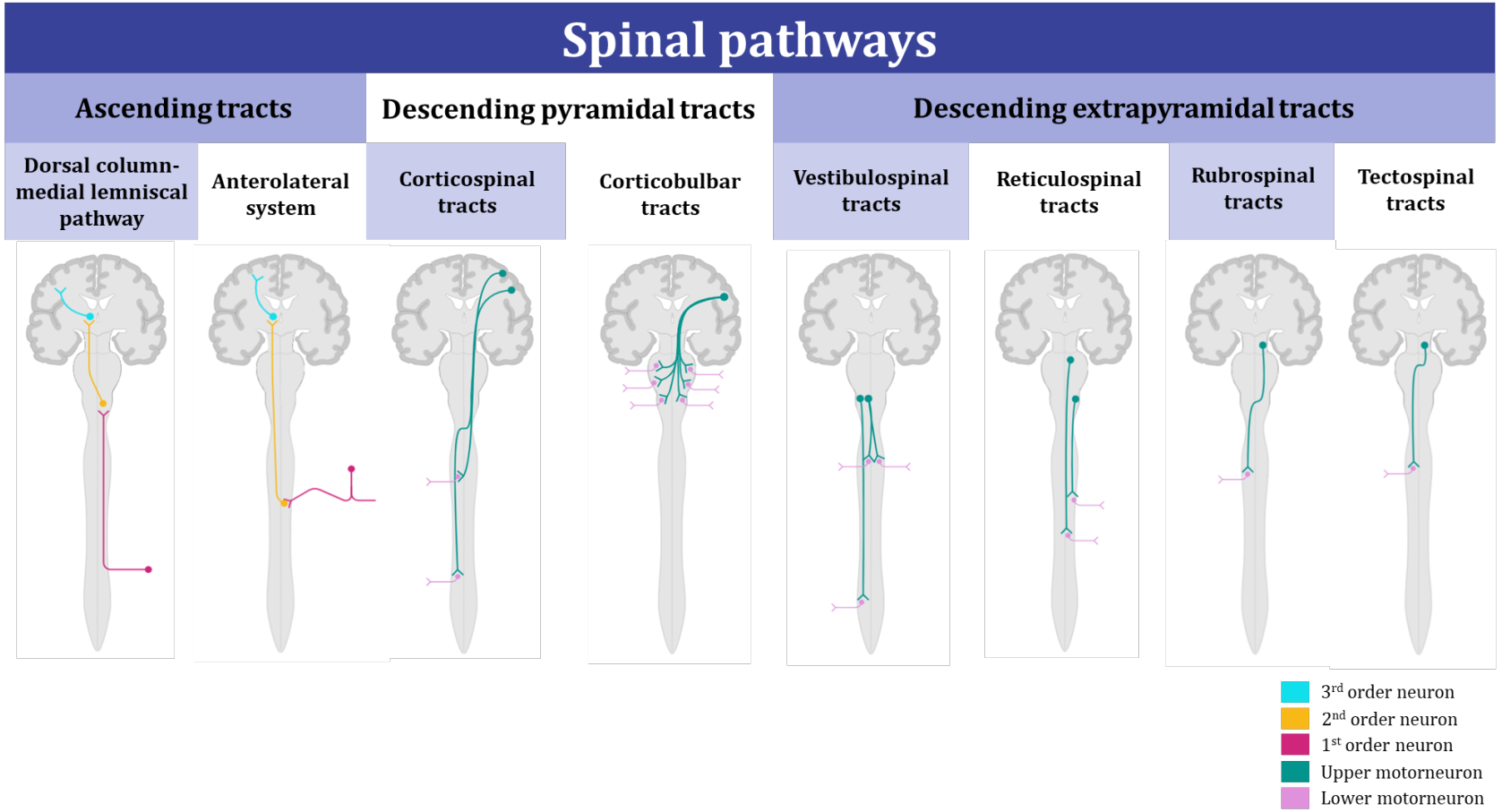

Figure 1.3 Classification of spinal pathways. *Schematic representation of the brain and spinal cord highlighting the trajectory of somatosensory information (in neurons and nerve fibres of the ascending tracts) and motor output (in neurons and nerve fibres of the descending tracts). The dorsal column-medial lemniscal pathway (DCML) carries sensory information regarding fine touch, proprioception and vibration, whereas the anterolateral system carries information regarding crude touch, pressure, pain or temperature. The corticospinal tracts supply the musculature of the body; and the corticobulbar tracts, supply the musculature of the head and neck. The descending extrapyramidal tracts control balance and posture (vestibulospinal tract), muscle tone (reticulospinal tract), fine hand movements (rubrospinal tract) and movements of the head in relation to vision stimuli (tectospinal tracts). Image created with Biorender.com*

In addition to neurons, the spinal cord also consists of glial cells, which provide support to neurons as well as performing multiple other tasks to maintain the homeostasis of the central nervous system (CNS). Astrocytes are the most abundant glial cell type, they provide structural support to the tissue, as well as form tight junctions around the blood vessels to form the blood brain barrier (BBB) and provide nutrients to the neurons. Furthermore, they clear the excess neurotransmitters around synapses to prevent excitotoxicity and re-establish optimal concentrations for signalling. Oligodendrocytes are found within the white matter surrounding the axons with a myelin sheath that increases the action potential transmission speed and has been shown to provide trophic support to neurons (Krämer-Albers et al., 2007). Microglia act as the macrophages of the CNS and have the ability to phagocyte cellular debris and clear any potential threat to the CNS (F. Bear, Connors, Paradiso, 2007).

Finally, the spinal cord is surrounded by three meninges, which are special connective tissue structures that protect the spinal cord. At the most outer part is the dura mater, which is made of dense connective tissue and is highly vascularized. In the middle, there is the arachnoid membrane, composed of 5 to 8 layers of fibroblasts under which the CSF flows. In between the dura matter and arachnoid membrane there is the subdural space, a virtual space which indicates that these two meninges are not adhered. In the inner part, there is the pia matter, adhered to the neural parenchyma (F. Bear, Mark; W. Connors, Barry; A. Paradiso, 2007).

Damage to the spinal cord can affect some or all of these structures and cell types, which leads to a highly complex succession of events that form the SCI. These events and their inhibitory effect on regeneration will be explored in the next section, but it should also be noted that any successful repair will have to attempt to restore the complex cytoarchitecture described in this section – one of the major challenges of developing new therapies.

1.2.3 Barriers to regeneration after SCI

Far from being stable, the SCI develops through different stages. The timeline of injury development can be divided into acute (<48h), subacute (48h to 14 days), intermediate (14 days to 6 months) and chronic (>6 months) (Ahuja et al., 2017b). The acute phase is characterised by the initial trauma that causes mechanical damage to cells and vasculature, leading to cell death, haemorrhage and initial inflammatory response. These responses lead to the subacute phase, characterised with the rise of excitotoxicity and release of pro-inflammatory molecules due to the immune response. Vasculature damage also leads to prolonged ischaemia, which contributes to further cell death. During the intermediate phase, and maintained through the chronic phase, the glial scar and cystic cavities are formed (Ahuja et al., 2017b). These phases are discussed in more detail below.

Damage is usually caused by a mechanical compression of the spinal cord, completely disrupting the nerve fibres at the centre of the pressure point, damaging the surrounding axons and causing haemorrhages (Kakulas, 1999). As seen in an *in vitro* model of murine dorsal root ganglia, severed axons have an intrinsic capacity to seal themselves and maintain internal homeostasis after axotomy, while they can still transmit nerve impulses (George et al., 1995). However, a few days after the axons have been disrupted, there is an entry of intracellular stored and extracellular calcium which activates calpain, an essential protease for cytoskeletal degeneration (George et al., 1995). This degenerative process is called Wallerian degeneration, (Waller, 1850) and it leads to cellular death and loss of information transmission capability. Moreover, the release of neurotransmitters, such as glutamate, around the synaptic cleft can rise to toxic levels due to the impaired function of glutamate transporters after the injury. This leads to excitotoxicity of the neurons, which occurs when receptors are overactivated, and results in cellular death, as seen in *in vivo* and *in vitro* rat models (Azbill et al., 2000).

Following a compression injury in live rats, the tight junctions that form the BBB are compromised, allowing blood cells to penetrate the injury site, stimulating an inflammatory response (Gray et al., 2007), which creates a toxic environment for cell growth. The first cells to migrate to the damaged tissue are macrophages from the blood stream and activated microglia from the surrounding tissue (Fawcett & Asher, 1999). Upon injury, macrophages and microglia are induced to switch from an anti-inflammatory subset (M2) towards a proinflammatory subset (M1) (Kigerl et al., 2009), which act to clear myelin debris and damaged cells. However, these also create a neurotoxic environment through the release of oxygen reactive species and, therefore, balancing the M1/M2 ratio towards an anti-inflammatory phenotype could be key in order to promote regeneration (Kigerl et al., 2009).

After traumatic brain injury in mice, stimulated microglia can activate naïve astrocytes to a neuroprotective phenotype (Shinozaki et al., 2017) that migrate to the injury site and synthesize growth inhibitory factors such as chondroitin sulphate proteoglycans (CSPGs) (McKeon et al., 1999). CSPGs create an inhibitory environment for axonal growth (Davies et al., 1997). In fact, delivery of chondroitinase (which breaks down CSPGs) to the injury site has been shown to promote regeneration of ascending and descending tracts (Bradbury et al., 2002), demonstrating the inhibitory nature of these molecules. In *in vivo* murine models of SCI, local astrocytes then upregulate glial fibrillary acidic protein (GFAP) and hypertrophy to surround the endbulbs of dystrophic axons (Frisén et al., 1995). This creates a barrier that isolates the injured from the healthy tissue and stops an uncontrolled inflammatory response and degradation (Faulkner et al., 2004), but that also prevents axonal growth. This astrocytic phenotype and upregulation of growth inhibitory extracellular matrix is commonly referred to as the glial scar and is widely regarded as a major barrier to regeneration. On the other hand, there is some evidence in live mouse SCI models suggesting that astrocytes also produce growth supportive molecules, such as

laminin, which could help axonal regeneration (Anderson et al., 2016). In fact, this study showed that ablating scar-forming astrocytes did not result in increased axonal infiltration. Instead, growth factor delivery promoted axonal regeneration past the astrocytic scar (M. A. Anderson et al., 2016), suggesting that there are other mechanisms present in the lesion that contribute to the lack of regenerative capacity of the spinal cord.

Oligodendrocyte precursor cells (OPCs) are also present in the lesion, differentiating into mature oligodendrocytes for remyelinating the tissue (Zawadzka et al., 2010). However, some of these OPCs stay undifferentiated and there is some evidence suggesting they act as reactive astrocytes, upregulating their expression of CSPGs in rats with incomplete SCI (Levine, 1994). Degraded myelin also has growth inhibitory effects due to the exposition of myelin-associated proteins such as neurite outgrowth inhibitor A (Nogo A), myelin-

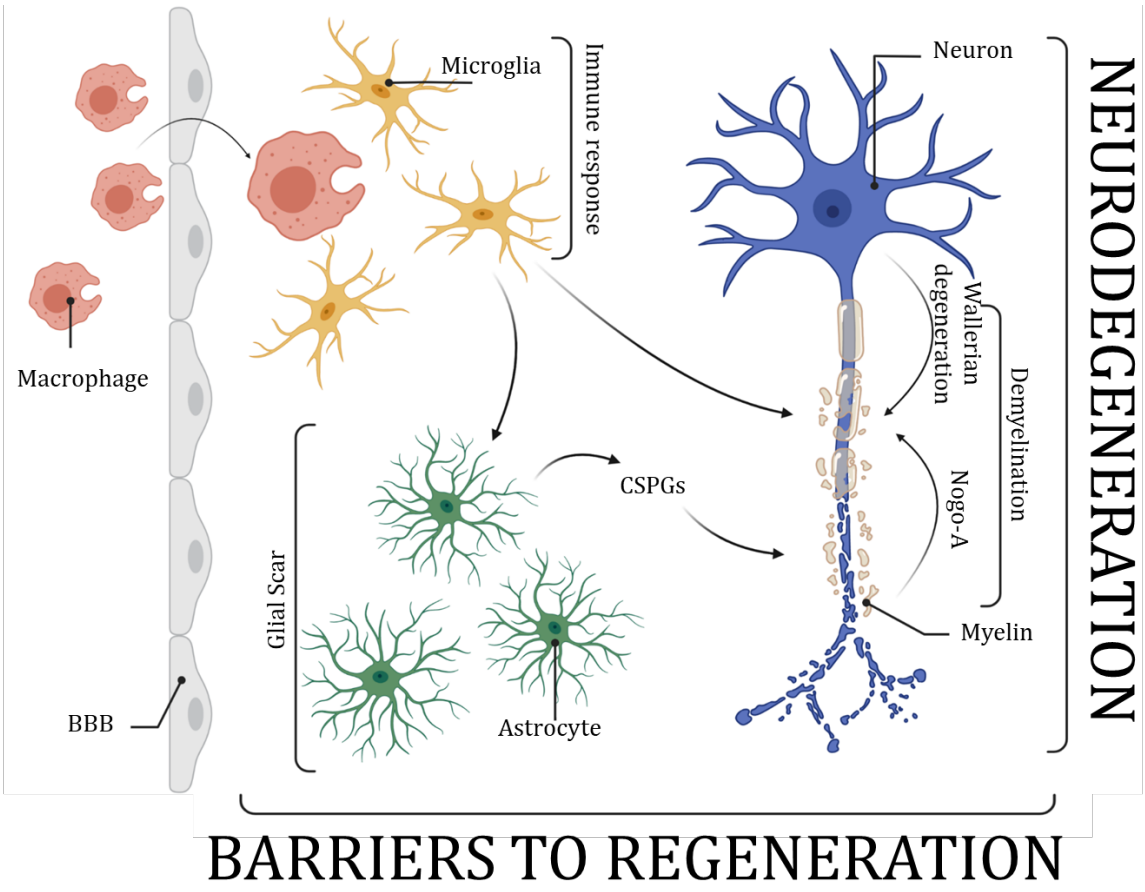

Figure 1.4 Barriers to regeneration*. Schematic representation of cellular processes leading to neurodegeneration and barriers to repair after SCI. Represented here are macrophage infiltration and microglial activation, activation of astrocytes, formation of the glial scar and release of CSPGs, demyelination and Wallerian degeneration. Image created with Biorender.com*

associated glycoprotein and oligodendrocyte-myelin protein (Ahuja et al., 2017a). The binding of these proteins to cell receptors activates a downstream cascade leading to neurite retraction and apoptosis (Ahuja et al., 2017a) (**Figure 1.4**).

Therefore, in order to achieve effective repair, multiple clinical goals need to be targeted in the context of the complex injury mechanisms. These include replacing lost or damaged cells, increasing viability and regeneration of injured neurons and creating an environment that is more conducive to repair. This is a major clinical challenge and, to date, no effective combinatorial therapy has been described.

1.2.4 Current treatments and limitations

At the site of the incident where the injury has occurred, the spinal cord has to be immobilized both in suspected and confirmed injuries, especially in the case of cervical damage. Once at the hospital, the level of neurological damage and baseline function must be established using computational tomography (CT) or magnetic resonance imaging (MRI) (Ahuja et al., 2017b). Blood pressure has to be kept stable and surgical decompression of the spinal cord is needed in order to allow blood flow and avoid

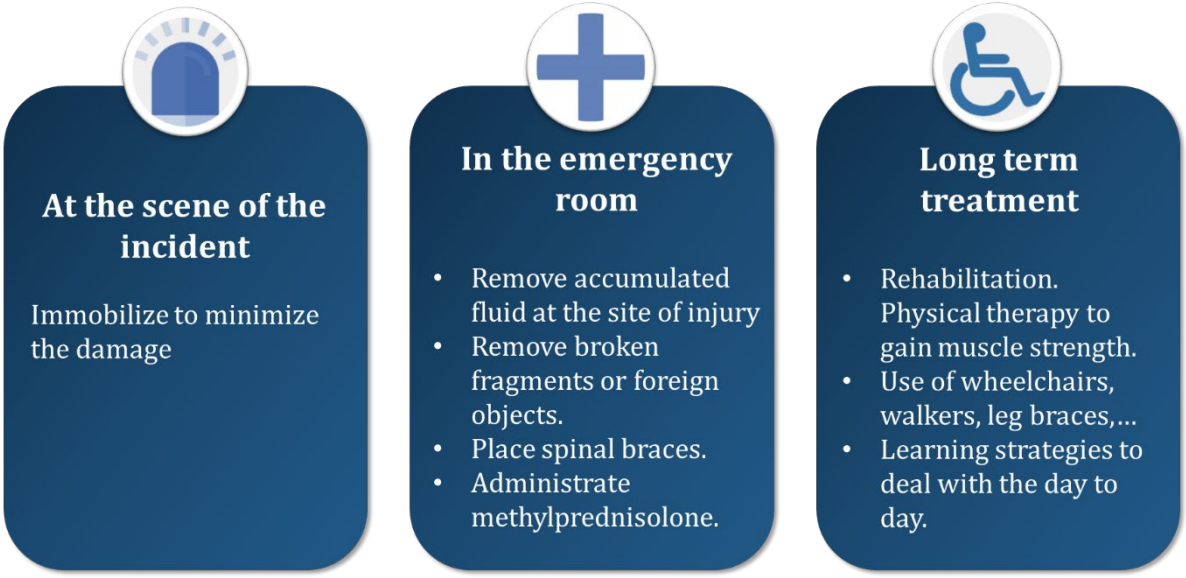

Figure 1.5 Timeline of response to SCI with current treatments. *Pharmacological treatment and rehabilitation are the main treatment approaches.*

ischaemia (Ahuja et al., 2017a). Once the level of neurological damage is established, it will be possible to act in accordance (**Figure 1.5**).

At the moment, drug administration to patients with SCI, together with rehabilitation, are the main treatment approaches. Methylprednisolone is a glucocorticoid that upregulates anti-inflammatory cytokine release and enhances cell survival in preclinical models of SCI (Ahuja et al., 2017a). In a 2006 poll, 86% of the 305 interviewed surgeons indicated that they would choose to administrate methylprednisolone sodium succinate (MPSS) to patients with acute SCI (Eck et al., 2006). Even though it has been widely prescribed, animal studies show mixed results towards functional recovery. According to a 2009 systematic review, only 34% of animal studies show beneficial effects after MPSS administration, 58% of studies show no advantages and 5% show mixed results (Akhtar et al., 2009). Moreover, a recent review of clinical studies show that the treatment has no impact on long term neurological recovery unless it starts within 8 hours post injury, in which case it has a small beneficial effect and should be considered for treatment (Fehlings et al., 2017).

Although pharmacological treatment has shown to enhance functional recovery to some extent, drug delivery only addresses one of the many factors involved in the SCI cascade. Therefore, a better approach has to be taken to maximize this effect and to treat multiple symptoms.

1.2.5 Experimental treatments

Three main regenerative approaches have been proposed for treatment of SCI and are being tested in ongoing pre-clinical and clinical trials:

1) Administration of pharmaceutical compounds that can stimulate growth (neurotrophic), inhibit degeneration (neuroprotective) or mitigate the toxic environment (neutralizing).

2) Transplantation of cells, such as stem cells, to the injured area to promote endogenous repair.
3) The implantation of biocompatible scaffolds to create an environment for repair and axonal growth.

Administration of minocycline inhibits microglial activation and, therefore, reduces the release of pro-inflammatory molecules (Seabrook et al., 2006). An intraperitoneal injection of minocycline every day for 28 days after injury in mice, resulted in improved hind limb function and reduced lesion size (Wells et al., 2003). These studies have been taken further into a clinical trial. Intravenous injection of minocycline twice a day during 7 days after acute SCI resulted in 6 points greater motor recovery of patients treated with the drug (27 patients) compared to the 25 placebo-treated patients, especially in the case of cervical injury. However, no recovery was observed in patients with thoracic SCI. In addition, although these results show a tendency to recovery enhanced by drug administration, they are not statistically significant (Casha et al., 2012).

GM-1 is a component of cell membranes that has the ability to promote neuronal plasticity and regeneration (Ahuja et al., 2017a), and presents low levels after injury (Imanaka et al., 1996). Administration of GM-1 has been shown to reduce neuronal retrograde death in hippocampus-injured rats (Sofroniew et al., 1986). Daily intraperitoneal injections of GM-1 to spinal cord injured rats over 13 days resulted in its incorporation in axons and myelin sheaths surrounding the lesion site, and a faster functional recovery than in controls (Imanaka et al., 1996). The intravenous injection of this drug to 37 patients, 18 to 39 days post injury, resulted in a better functional recovery in a first study (Geisler et al., 1991), but no statistical significance was found in a later study with a population number of 180 patients (Geisler et al., 1991).

One of the biggest obstacles for pharmacological therapies is the system of delivery. Peripheral drug delivery to the CNS is impeded by the tight junctions that surround the capillaries and that form the BBB. Therefore, there is often a need for a direct delivery system such as the commonly used bolus injection or a catheter/minipump system (Pakulska et al., 2012). However, both systems present challenges that must be overcome. On the one hand, bolus injection consists of injection of the drug in the intrathecal space, but it is hindered by the flow of the CSF, that washes it off, disperses the drug and minimizes its localized release. Therefore, it has to be injected periodically. On the other hand, the catheter/minipump system requires invasive surgery for implantation, which makes it prone to dislodgement and increases the risk of infection. (Pakulska et al., 2012).

Although helpful, pharmacological treatment does not offer a multifaceted approach to the treatment of the complex injury. On the contrary, cell therapy offers an approach of neuroprotection and cell replacement and biomaterial implantation offers a neuroprotective effect instead of the toxic environment of the lesion (Ahuja et al., 2017a). However, it is the combination of these two therapies that has given more promising results. Therefore, cell therapy and biomaterial implantation for SCI will be discussed below.

1.3 CELL THERAPY AS AN EXPERIMENTAL APPROACH TO SPINAL CORD INJURY REPAIR

1.3.1 Pro-regenerative mechanisms of cell therapy

The study of cell therapy for CNS repair first originated when a section of peripheral nerve was used to bridge the two sides of an injured spinal cord in rats, resulting in elongation of the severed spinal cord axons (David & Aguayo, 1981). This outcome was associated with the modification of the glial environment, in particular, to the presence of Schwann cells, which seem to guide axonal regeneration in the peripheral nervous system (PNS)

(David & Aguayo, 1981). Consequently, a series of experiments were carried out in order to isolate Schwann cells for implantation (Bunge, 2016).

Since then, multiple cell types have been tested for CNS regeneration. The most used cell types are Schwann cells, neural stem cells (NSCs), olfactory ensheathing cells (OECs) and mesenchymal stem cells (MSCs) (Ahuja et al., 2020; Assinck et al., 2017). These have been shown to promote functional recovery through mechanisms of neuroprotection and cell replacement, which will be covered in more detail in the subsequent paragraphs.

Neuroprotection is defined as the mitigation of secondary damage caused by cellular responses to injury, which is usually mediated by the secretion of neurotrophic factors (Assinck et al., 2017). Depending on their structure, neurotrophic factors can be divided into three categories: neurotrophins, glial cell-derived neurotrohpic factor (GDNF) family and neuropoietic cytokines (Boyd & Gordon, 2003). Neurotrophins, such as nerve growth factor (NGF), brain-derived neurotrophic factor (BDNF) or neurotrophin-3 (NT-3), play a role in cell survival and differentiation (Boyd & Gordon, 2003). The GDNF family, has also been associated with cell survival. Finally, neuropoietic cytokines, like interleukin-6 (IL-6) and IL-11, have been associated with the regulation of the immune response, cell proliferation, differentiation and neurite outgrowth (Boyd & Gordon, 2003).

An imbalance in the levels of neurotrophic factors following SCI has been reported with conflicting results, sometimes suggesting upregulation in *ex vivo* rat spinal cord tissue (Hawryluk et al., 2012) and sometimes downregulation in adult live rhesus monkeys (Zhang et al., 2008). This could be due to the experimental differences between the studies which suggest an initial downregulation of neurotrophic factors during the first 3-7 days after injury (Hawryluk et al., 2012) followed by a slight increase after 7 days (Hawryluk et al., 2012; Zhang et al., 2008). Increased levels of immature neurotrophins have also been reported after lesion (Fan et al., 2018), which have been associated with a

detrimental role after spinal cord laminectomy in rats (Wong et al., 2010). Transplant cell populations have the capacity to release neurotrophic factors, which has been correlated with increased axonal regeneration and functional recovery (Ahuja et al., 2020; Assinck et al., 2017). Cell transplantation has also been correlated with an immunomodulatory effect, probably mediated by the release of anti-inflammatory cytokines (Assinck et al., 2017), which could be the cause and/or the consequence of increased levels of spared tissue (neuroprotection).

Cellular repopulation into the cystic cavity has been associated with the secretion of extracellular matrix (ECM) molecules, such as laminin, which can potentially facilitate the attachment of host axons and, therefore, enhance axonal regeneration (Assinck et al., 2017). Moreover, differentiation of transplanted cells into mature neurons can also lead to the formation of new synapses with the host tissue, which has been correlated with increased functional outcome (Assinck et al., 2017). These mechanisms, can lead to potential cell replacement.

To date, numerous studies involving cell implantation into SCI have been carried out. However, the response to the therapy varies greatly across reports due to different experimental settings. Probably, the most consequential variation is the cell type used.

1.3.2 Advantages and limitations of therapeutic cell types for spinal cord injury

The most commonly used cell types for implantation are MSCs, Schwann cells, OECs and NSCs. MSCs, Shwann cells and OECs can be derived directly from the patient to avoid immunosuppressive responses. However, harvest and propagation of these cell types is costly due to the complexity of the procedure. On the other hand, NSCs can be derived from embryonic tissue in an easier process. However, harvesting cells from embryonic tissue is associated with more ethical implications (Ahuja et al., 2020). Key advances in the neuroregenerative effects of each cell type, including clinical trials, have been

extensively reviewed elsewhere (Ahuja et al., 2020). Below, the most common experimental outcomes for each cell type, and its advantages and limitations, will be discussed.

MSCs are multipotent cells found in connective tissue throughout the body (Ahuja et al., 2020). They can be harvested from the bone marrow, adipose tissue and skeletal muscle, which makes them a good candidate for autologous transplantation (Ahuja et al., 2020; Assinck et al., 2017; Quertainmont et al., 2012). Injection of MSCs in *in vivo* models of spinal cord contusion in rats has resulted in improved locomotor recovery (Nakajima et al., 2012; Quertainmont et al., 2012) and increased axonal infiltration into the lesion (Ankeny et al., 2004). MSC injection has also been correlated with an increase of neurotrophic factors in the lesion site (Himes et al., 2006; Nakajima et al., 2012; Quertainmont et al., 2012), which could be the cause of the presence of increased spared tissue after injection (Ankeny et al., 2004; Himes et al., 2006; Nakajima et al., 2012) and of an immunomodulatory effect (Nakajima et al., 2012). Despite these promising results, there is conflicting evidence on the regenerative potential of this cell type as suggested by studies that present no locomotor recovery after injection of MSC in similar rat *in vivo* models of spinal cord contusion (Ankeny et al., 2004; Himes et al., 2006). In addition, despite the multipotent nature of these cells, there is also conflicting evidence on the capacity of MSCs to differentiate into a neural lineage, with some studies reporting neuronal differentiation (J. He et al., 2021) and others suggesting that these cannot differentiate into fully functional neurons, as suggested by the lack of voltage-gated ion channels necessary for the transmission of action potentials (Hofstetter et al., 2002).

Schwann cells are the myelinating cell type in the PNS and they seem to guide regenerating axons after injury in the PNS (Assinck et al. 2017). Injection of Schwann cells into the lesioned CNS has been correlated with enhanced axonal remyelination after a contusion lesion in live rats (Biernaskie et al., 2007; Honmou et al., 1996) as well as

functional recovery (Biernaskie et al., 2007). However, they show poor migration capacity into the astrocyte-containing CNS, which leads to the formation of a boundary between the cells and the damaged tissue (Wiliams & Bunge, 2012). Moreover, Schwann cells do not have the intrinsic capacity to differentiate into CNS cells.

OECs are found in the nasal mucosa, and protect olfactory neurons by ensheathing them, phagocytosing debris and releasing neurotrophic factors (Ahuja et al., 2017b). Similarly to Schwann cells, OECs support the growth of damaged neurons into the olfactory bulb (Ahuja et al., 2020). Moreover, due to their presence in the nasal mucosa they are easily accessible and targeted for autologous transplantation (Féron et al., 2005). Injection of OECs has resulted in increased locomotor recovery and axonal regeneration after spinal cord transection in rats (Li et al., 1997; Nakhjavan-Shahraki et al., 2018; Ramón-Cueto et al., 2000). They have also been reported to enhance remyelination, neuroprotection and immunomodulation (Ahuja et al., 2020). Therefore, OECs seem to have potential therapeutic effects in neuroprotection and remyelination, leading to increased motor recovery and axonal regeneration. However, these cells are not multipotent and, therefore, cannot contribute to the repopulation of lost neurons.

NSCs can be harvested from embryonic tissue or from the subventricular zone or central canal in adults and bear the capacity to differentiate into neurons, astrocytes and oligodendrocytes, therefore, they can provide tissue replacement for the injury and trophic support (Liu et al. 2018). Implantation of NSCs into the lesioned spinal cord has resulted in increased functional recovery, remyelination, axonal regeneration and formation of new synapses between grafted cells and host tissue (Ahuja et al., 2020).

From a therapeutic point of view, both NSCs and MSCs have the capacity to respond to SCI with both mechanisms mentioned previously: neuroprotection and cell replacement (**Table 1.3**). While Schwann cells and OECs can provide neuroprotection through

remyelination and, in the case of OECs, neurotrophic factor release, these cells do not have the capacity to differentiate into neurons. Therefore, these are not able to form new synapses with the host tissue. On the other hand, MSCs and NSCs have the capacity to release trophic factors for neuroprotection. In addition, they are multipotent and therefore, have the potential to differentiate into myelinating cell types and neurons. Although MSCs have the advantage of autologous transplantation, literature shows conflicting results in regard to functional recovery and their differentiation capacity. Instead, NSC implantation has robustly shown pro-regenerative outcomes. As a limitation, NSC harvesting is ethically challenging due to their presence in embryonic tissue. Nevertheless, in recent years NSCs have also been obtained through differentiation of induced pluripotent stem cells (iPSCs) and injected in the injured spinal cords of mice with promising results (Nori et al., 2011), providing an ethical alternative for NSC implantation. For these reasons, the experimental chapters of this thesis are based on the use of primary NSC cultures.

Table 1.3 List of advantages and disadvantages to the use of different cell types for SCI treatment. *This table describes the main pros and cons of the use of mesenchymal stem cells (MSCs), Schwann cells, olfactory ensheathing cells (OECs) and neural stem cells (NSC) as cell therapy for spinal cord injury (SCI)*

CELL TYPE	PROS	CONS
MSCs	• Autologous transplantation • Multipotency • Remyelination • Neurotrophic factor release	• Conflicting results • Non-functional derived neurons
Schwann cells	• Autologous transplantation • Remyelination	• Poor migration capacity • No differentiation • No neurotrophic factor release
OECs	• Autologous transplantation • Remyelination • Neurotrophic factor release	• No differentiation
NSCs	• Multipotency • Remyelination • Neurotrophic factor release	• Difficult to source ethically

1.3.3 Experimental advances and limitations on the use of neural stem cells for spinal cord injury therapy

Due to the above stated advantages, NSC implantation after SCI has been extensively studied *in vivo* (**Table 1.4**), resulting in survival of NSCs at the lesion site and migration into the host tissue (BJ Cummings, N Uchida, 2005; Iwanami et al., 2005; Karimi-Abdolrezaee et al., 2006; Nori et al., 2011; Parr et al., 2007). Grafted cells have also been reported to differentiate into astrocytes, neurons and oligodendrocytes. However, the differentiation ratios differ across reports. While some studies report approximately 20% (Iwanami et al., 2005), 30% (BJ Cummings, N Uchida, 2005) or 50% rate of neuronal differentiation (Nori et al., 2011), others report 0-1% of neuronal differentiation with

Table 1.4 Examples of existing literature featuring NSC implantation for the treatment of SCI. *The top part of the table describes the methodology used in different research articles looking at cell therapy for spinal cord injury (SCI). The second part of the table summarises the relevant results.*

Reference	Model	Lesion type	Implantation time	Injection	Experimental duration
Nori *et al.* 2011	Mouse	Contusion	9 dpi	Lesion epicenter	56 dpi, 112 dpi
Cummings *et al.* 2005	Mouse	Contusion	9 dpi	Bilaterally	112 dpi
Parr *et al.* 2007	Rat	Contusion	9 dpi, 28 dpi	Lesion epicentre and bilaterally	112 dpi
Karimi-Abdolrezaee *et al.* 2006	Mouse	Compression	14 dpi, 56 dpi	Intraspinal	10 weeks post implantation
Iwanami *et al.* 2005	Marmoset	Contusion	9 dpi	Lesion epicenter	56 dpi

Reference	Graft survival	NSC differentiation	Synapse formation	Trophic factor release	Re-myelination	Locomotor recovery
Nori *et al.* 2011	✓	✓	✓	✓	✓	✓
Cummings *et al.* 2005	✓	✓	✓	N/A	✓	✓
Parr *et al.* 2007	✓	✓	N/A	N/A	N/A	×
Karimi-Abdolrezaee *et al.* 2006	✓	✓	N/A	N/A	✓	✓
Iwanami *et al.* 2005	✓	✓	N/A	N/A	N/A	✓

most cells differentiating into oligodendrocytes and astrocytes (Karimi-Abdolrezaee et al., 2006; Parr et al., 2007).

Due to differences in the phenotypical fate of the grafted NSCs, there is also outcome differences with some studies reporting new synapse formation between grafted cells and host cells (BJ Cummings, N Uchida, 2005; Nori et al., 2011) and some reporting remyelination of axons (BJ Cummings, N Uchida, 2005; Karimi-Abdolrezaee et al., 2006; Nori et al., 2011). Despite these differences, most studies report increased locomotor recovery after treatment (BJ Cummings, N Uchida, 2005; Iwanami et al., 2005; Karimi-Abdolrezaee et al., 2006; Nori et al., 2011).

Since the publication of these studies, efforts have been made in order to understand and control the variability of outcomes upon implantation. For example, it has been suggested that the presence of the myelin protein Nogo-66 promotes the differentiation of NSCs into an astrocytic lineage (Wang et al., 2008) and that Wnt4-modified NSCs differentiate into neurons at higher rates than controls upon implantation, promoting functional recovery (Xiang Li et al., 2020). These studies highlight the versatility of NSC manipulation and open the possibility to finely tune this transplant cell population to a desired outcome.

In clinical trials, the safety of NSC grafting was first studied for the treatment of liposomal storage disorder (Selden et al., 2013). NSC implantation has also been studied clinically for the treatment of traumatic, non-penetrating, cervical SCI resulting in improved locomotor recovery in all 5 patients (Anderson et al., 2017).

Despite these advantages, cell therapy faces challenges in maintaining optimal cell survival and distribution in the lesion. For example, multiple studies report a decrease in NSC survival after implantation in a chronic compression lesion compared to acute in rats (Karimi-Abdolrezaee et al., 2006; Parr et al., 2007). In addition, other studies report a time-dependent decrease in the number of grafted cells found in the lesion area in a

similar model (Himes et al., 2006; Nakajima et al., 2012) and an uneven distribution of grafted cells, which partially fill the lesion cavity, also in a compression lesion in rats (Ankeny et al., 2004). There is evidence suggesting that intravenously injected cells in rats will not reach the injury area, they will only be detected in the injury when they are directly injected in the intrathecal or intralesional space after a contusion injury in rats (Takahashi et al., 2011). However, in this study 95% of the intrathecal-injected cells died within 1 week after injection and only attached to the healthy pia mater instead of invading the injury, and 70% of the intralesion-injected cells died within 6 weeks (Takahashi et al., 2011).

The cause of transplant cell population death has been attributed to two mechanisms: the mechanical forces exerted on the cells when protruded through a very fine needle and anchorage-depended death (Mitrousis et al., 2018). Within the syringe, cells are exposed to shear and extensional forces that increase in the needle/syringe interface due to the smaller diameter of the needle. These forces lead to necrotic cellular death but they also trigger apoptotic death once the cells are implanted (Mitrousis et al., 2018). On the other hand, cell anchorage to the ECM sends pro-survival signals, which are lost when cells are implanted into a degenerating environment, leading to cell death. These pro-survival signals are mediated by membrane integrins when these bind to ECM components such as collagen on laminin (Mitrousis et al., 2018).

Taken together, these results suggest that, despite the therapeutic potential of NSC implantation to treat SCI, a more effective delivery approach has to be taken. NSC therapy alone offers several strategies to repair SCI such as cell replacement, myelination of spared axons, trophic factor release or restoration of neuronal circuitry (Mothe & Tator, 2012). However, the combination of an NSC delivery approach with the implantation of a biomaterial matrix has been seen to improve host cell regeneration (Bonner et al., 2011)

and hindlimb function (Ogawa et al., 2002) with more positive results than a non-combinatorial approach.

1.4 ENCAPSULATION OF NEURAL STEM CELLS IN 3D BIOMATERIALS

1.4.1 Pro-regenerative mechanisms of biomaterial implantation for spinal cord injury repair

From the perspective of regenerative medicine, biomaterials are three-dimensional scaffolds that partially mimic the natural environment created by the ECM. They are of interest due to their capacity to provide a substrate to which host cells can adhere and their potential to encapsulate drugs or cell transplant populations. Therefore, they can serve as a platform for a combinatorial therapy (Drury & Mooney, 2003; Macaya, D; Spector, 2012; Morteza Bahram, 2012; Pakulska et al., 2012). Cell-biomaterial interactions are typically mediated by the same components that mediate cell-ECM interactions, the integrins, a cell membrane receptor that anchors to the ECM, binding it with the cytoskeleton (Takada et al., 2007). However, in the case of artificially implanted biomaterial, the biocompatibility of the implant is extremely important in order to avoid fibrous encapsulation of the implant, which would isolate it from the cells and impair it's primary function (Sanz-Herrera & Reina-Romo, 2011). Biomaterials can be formed of natural (such as collagen) or synthetic polymers (such as polycaprolactone (PCL)). Natural polymers promote cell adhesion and are easily degraded by natural occurring enzymatic reactions. However, they have a higher risk of disease transmission and immunogenic reaction. On the other hand, the degradation rate and stiffness of synthetic biomaterials can be easily customised but the reactants or the degradation residues can cause biocompatibility issues (Macaya, D; Spector, 2012). According to their structure, biomaterials can be classified into gels, sponges or tubes.

If these biomaterials are meant to be implanted into a SCI as a repair strategy, their structure should permit axonal growth through the biomaterial, preferably directed to the

other end of the lesion. The material should be biocompatible and biodegradable once its purpose has been served. It is also important that the reactants and degradation products are non-immunogenic and non-toxic, and that the degradation rate is on the same time scale as axonal growth in order to allow full recovery. Its stiffness should match that of the spinal cord to mimic the host tissue and pore size has to allow nutrient delivery and cell ingrowth and motility. Moreover, an injectable hydrogel that could support all of the above would be advantageous for clinical application instead of an implantable one. Evidence for the application of hydrogels in each of these areas will be discussed in the next few paragraphs.

Suspension of fibroblasts in a viscous carrier, like an alginate hydrogel instead of saline, resulted in protection against the forces in the needle (Amer et al., 2015). Encapsulation of NSCs within a 3D matrix prior to implantation has also resulted in increased cell survival. In this case, when NSCs were seeded onto a laminin-based scaffold and implanted into a brain injury in mice, there was enhanced cell survival and better performance of mice in a space learning task than when cells were implanted in media alone 8 weeks post implantation (Tate et al., 2009).

Moreover, biomaterial encapsulation of NSCs has also been reported to improve cell retention at the lesion site. Some hydrogels, for example, a combination of hyaluronan and methylcellulose hydrogel, have fast gelling properties and can be injected as a viscous liquid before gelling in the lesion site (Ballios et al., 2015). 7 days after NSC injection with this type of hydrogel, 86% of mice (6 of 7) still retained cells at the injury site compared to 57% (4 of 7) when injected with CSF (Ballios et al., 2015). In a 2016 study, 46% of biomaterial-transplanted cells were still found in the injury site 7 days post grafting, compared to 29% of cells transplanted in medium (Führmann et al., 2015).

Biomaterials can also be functionalised to manipulate cell behaviour. For example, scaffolds can be embedded with a heparin-binding delivery system (HBDS) which can gradually release growth factors, such as NT-3 and platelet derived growth factor, to enhance neuronal differentiation compared to cells delivered in media or hydrogel alone (Johnson et al., 2011). Therefore, encapsulating cells within biomaterials can lead to increased cell survival and distribution (**Figure 1.6**).

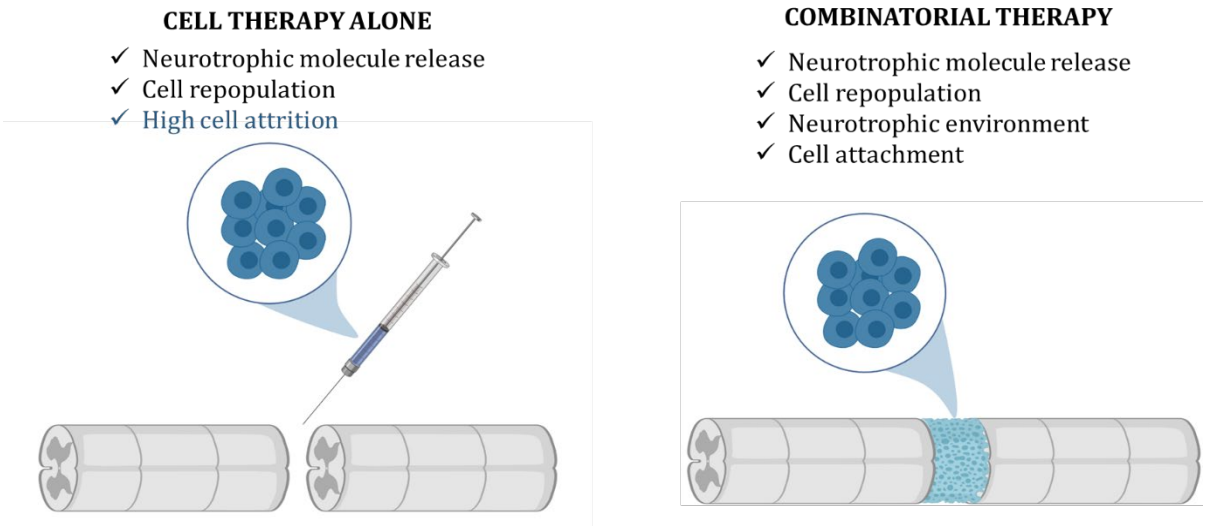

Figure 1.6 Outcomes of the use of cell therapy alone* vs. *combinatorial therapy. *This schematic represents the main outputs of cell therapy alone compared to a combinatorial therapy (cell+biomaterial implantation) for spinal cord injury (SC). Image created using Biorender.com*

Biomaterial implantation has been extensively studied *in vivo* (**Table 1.5**). The increasing numbers of available biomaterials (*i.e.*: gelatine, alginate, chitosan, hyaluronic acid, graphene or collagen), which can be functionalised or not and could encapsulate transplant cell populations or not, has led to an increasing number of possible permutations to test in diverse animal models and diverse lesion types.

For example, an *in vivo* study carried out in dogs suggested that the implantation of a cell-biomaterial construct into a transecting lesion improved mobility recovery with better rates than biomaterial implantation alone (Wu et al., 2018). In this study, a mixed culture

of Schwann cells and neurons derived from NSCs was implanted in a thoracic transecting lesion in beagles. The initial 4mm injury gap was reduced 6.5 months after surgery, presenting a narrower gap in cell-biomaterial implanted dogs than with biomaterial alone implantation. Moreover, gradual functional recovery was rated higher after cell-biomaterial implantation. Post-mortem histological analyses also showed implanted cell integration with host ascending and descending neuronal tracts.

Table 1.5 Examples of existing research using biomaterial implantation to treat SCI and summary of outcomes. *This table summarises the methodology of research articles which studied biomaterial implantation* in vivo *(top section of the table) and the relevant results (bottom part of the table).*

Animal model	Lesion type	Level	Biomaterial	Functionalisation	Cell type	Duration of treatment	Reference
Dogs	Transecting	T10	Gelatine	N/A	Swann cells + MSCs	6.5 m	*Wu et al. 2018*
Rat	Transecting	T9-T10	Calcium alginate	N/A	N/A	154 d	*Galli et al. 2018*
Rat	Transecting	T7-T8	Chitosan tube	NT-3	N/A	1 y	*Yang et al. 2015*
Rat	Transecting	T9-T10	Hyaluronic acid	TEMPO	N/A	28 d	*Zhang et al. 2020*
Rat	Hemisection	C6	Graphene microfibres	N/A	N/A	120 d	*Dominguez-Bajo et al. 2020*
Mouse	Compression	-	Porous collagen	N/A	NSCs	12 w	*Kourgiantaki et al. 2020*

Reference	Increased motor recovery	Increased sensory recovery	Increased axonal infiltration	Reduced glial scarring	Reduced microglial infiltration	Reduced demyelination
Wu et al. 2018	✓	N/A	✓	N/A	N/A	N/A
Galli et al. 2018	✓	N/A	✓	×	N/A	✓
Yang et al. 2015	✓	✓	✓	N/A	N/A	✓
Zhang et al. 2020	✓	N/A	✓	N/A	N/A	N/A
Dominguez-Bajo et al. 2020	×	N/A	×	×	×	N/A
Kourgiantaki et al. 2020	✓	N/A	✓	✓	×	N/A

A study in rats with implanted alginate hydrogels after SCI suggested that the number of axons infiltrating the lesion was similar between treated and control rats and that the lesion gap 154 days after implantation was bigger in treated animals than in controls. However, the same study also showed lower tract demyelination in treated animals,

correlated with increased motor recovery from 7 days post-implantation (Galli et al., 2018).

Implantation of a chitosan tube functionalised with NT-3 in a rat SCI resulted in myelinated axonal regeneration from both ends of the tubes towards the centre, forming new functional synapses. Moreover, the presence of Nestin-positive cells inside the tube suggested migration of NSCs towards the injury, which could then have differentiated into neurons (as suggested by Nestin and Tuj-1 double positive cells). These histological results were also correlated with a higher motor and sensory recovery 1 year post injury when compared to untreated controls or rats treated with unfunctionalized chitosan tubes (Z. Yang et al., 2015).

Effective recovery of motor function and increased axonal infiltration were also reported after hydrogel implantation in a transecting SCI in rats. In this case, a hyaluronic acid hydrogel functionalised with 2,2,6,6-tetramethylpiperidinyloxy (TEMPO) to reduce ROS responses was implanted and significant differences between treated and control groups were seen 28 days after implantation (Y. Zhang et al., 2020).

In a mouse model of a compressive injury, porous collagen scaffolds laden with NSCs were implanted. Their results show an increased locomotor recovery 12 weeks post injury compared to non-treated controls, with no statistical differences compared to uninjured controls. They also show signs of increased axonal infiltration and reduced glial scarring. The implanted BrdU labelled NSCs were still seen at the lesion area 12 weeks post lesion, although some had migrated at 200μm from the scaffold. Finally, colocalization of BrdU with Tuj-1 or GFAP suggested that these had differentiated towards neurons and astrocytes after implantation (Kourgiantaki et al., 2020).

Taken together, these findings suggest that, in most cases, biomaterial implantation correlates with better motor recovery and axonal infiltration (**Table 1.5**), highlighting the therapeutic potential of this procedure.

A key requirement in developing such therapeutic biomaterials is the ability to test them in relevant neuromimetic models. However, the complexity of the *in vivo* models hinders the capacity to reliably and reproducibly analyse histological changes in the tissue, such as the formation of a glial scar, microglial infiltration or demyelination (**Table 1.5**), which, in combination with increasing possible permutations of biomaterial testing, highlight the importance of a simpler model in which to carry out these tests before escalating to higher complexity models.

1.5 EXPERIMENTAL MODELS OF SPINAL CORD INJURY

1.5.1 Current animal models for the study of spinal cord injury

In vitro animal models of SCI rely on the use of cell cultures (neurons, astrocytes and oligodendrocytes) to study different aspects of the lesion whether it is the study of pro-regenerative techniques or the underlying mechanisms of neurodegeneration. Such studies can be carried out in 2D and offer the possibility of studying axonal outgrowth, astrocyte reactivity or myelin degradation (Abu-Rub et al., 2010). 3D *in vitro* models, achieved through cell culture on bioscaffolds, also offer the possibility of studying cell migration, focal adhesions and the dynamics of neuronal growth (Abu-Rub et al., 2010).

For example, *in vitro* astrocyte alignment induced through an electric field has been used to determine the extent to which aligned astrocytes affect directed axonal growth (Alexander et al., 2006). As mentioned previously, *in vitro* cell alignment can also be tested through culture on aligned substrates, such as aligned electrospun fibres (A. Weightman et al., 2014). In order to replicate primary responses to injury, the cell stretch model consists of cell culture on a flexible substrate, which induces cellular damage upon

stretching (Ellis et al., 1995), and has been seen to induce an astrocytic response similar to that of the glial scar (Cullen et al., 2007). Although such models are useful for the study of specific neurodegenerative mechanisms, the lack of external physiological input forces the use of higher complexity models when aiming to study the applicability of SCI therapies.

Therefore, *in vivo* models constitute the majority of models for the study of SCI. These can be classified, according to the injury type, into contusion or transection injury models (Robins & Fehlings, 2008). Contusion or compression injuries can be inflicted by dropping a weight on the spinal cord (mimicking a traumatic injury) or by slowly compressing the spinal cord by slowly adding weights or inflating a balloon (mimicking trauma created by extradural tumours) (Robins & Fehlings, 2008). As the most physiologically relevant injury model, this is also the most used in experimental studies (Sharif-Alhoseini et al., 2017). This type of injury results in loss of normal locomotor ability, which is not recovered 8 weeks post injury. Moreover, it also results in damage to the corticospinal tract and upregulation of pro-inflammatory genes and genes associated with glial scarring (Forgione et al., 2017).

Transecting injuries are the second most common type of injury in experimental models (Sharif-Alhoseini et al., 2017). A partial transecting injury refers to those injuries where some axonal tracts remain intact. For example, in a unilateral lesion. On the other hand, a complete transecting lesion refers to that in which all tracts are damaged (Robins & Fehlings, 2008). Transecting injuries are not as physiologically relevant as contusion injuries, as it is less likely they occur naturally (Robins & Fehlings, 2008). Therefore, these are not indicated when the aim of the study is to determine certain pathophysiological responses to injury. Nevertheless, they provide a reliable platform to study the outcome of neuroregenerative strategies because they allow to discriminate between neuroprotection and *de novo* axonal regeneration (Robins & Fehlings, 2008). Similarly to

contusion injuries, transecting injuries result in loss of locomotor function, axonal degeneration, inflammatory response, glial scarring and demyelination (Galli et al., 2018).

Although *in vivo* models are essential for the study of SCI therapies, current research relies heavily on adult mammalian models, resulting in expensive, time-consuming and technically challenging experiments. Moreover, animal suffering is inevitable. Because of these reasons, a high rate of variability is introduced among biological repeats and experimental reproducibility becomes challenging. This, in combination with increasing numbers of new biomaterials for SCI, highlight the necessity of a relevant model in which to test the pro-regenerative capacity of such materials while reducing animal suffering and increasing reproducibility before moving to expensive and complex *in vivo* models.

1.5.2 Organotypic slices as spinal cord injury models

Organotypic slice cultures are an *ex vivo* technique that aim to represent the *in vivo* structure and function of a specific organ or tissue in isolation from the body. They differ from *in vitro* cellular cultures in that they preserve the tissue structure and cellular connections, providing the system with more *in vivo*-like properties. Despite its most obvious disadvantage against animal *in vivo* models, which is the disconnection with the rest of the animal's organs, this culture closely mimics the pathological features of the SCI in resonance with the 3R's principles for animal experimentation. Moreover, the *in vitro* aspect of such cultures provides the system with easier manipulation and analysis procedures than those used in *in vivo* research. This model allows for the introduction of a SCI following similar protocols to *in vivo* models, but the easiness of *in vitro* models.

The first organotypic culture was used to study the differentiation of the chick embryo eye and the technique was first tested for CNS tissue on rat hypophysis (Pandamooz et al., 2018). In rodents, donor age plays a crucial role on the survival of the CNS organotypic culture. Tissue from embryonic donors older than E14 seems to increase in size with time

and survive better than tissue from postnatal mice due to its high cellular plasticity (Humpel, 2015). Viable organotypic spinal cord slices from chick embryos have been obtained from embryonic day 5 (E5) (K. Sharma et al., 1994) to E16 (Nuria Brunet et al., 2007) donors. Tissue from postnatal donors younger than post-natal day 12 (P12) offer a more mature alternative, however, it also displays low viability rates (Humpel, 2015). Despite these advantages, it has been reported that sagittal spinal cord slices from mice older than P6 were not viable for culture (Bonnici & Kapfhammer, 2008). Therefore, although tissue from adult donors could be more clinically relevant, these tend to be used for acute, short term experiments due to low survival rates in the long term (Humpel, 2015).

Similarly to *in vitro* techniques, the dissected slices need access to culture media to survive. However, these cannot be submerged in the culture medium due to poor oxygenation of the slice. Long term survival of the tissue can be achieved through three different methods: the *in oculo* method, the roller tube method or the semipermeable membrane method (Humpel, 2015).

The *in oculo* method consists of the implantation of a slice of brain tissue in the rodent's eye chamber, which is highly vascularised, so it survives in total isolation. Although this technique does not impair the animal's vision, its major disadvantages are the difficult manipulation of the slice and the highly animal dependant nature of the technique (**Figure 1.7 A**).

On the contrary, the roller tube method consists of the attachment of the slice on a glass coverslip using a fibrin clot, which is placed in a rotating tube coming in and out of the media. Although this method offers an easily accessible alternative to the *in oculo* method, it faces complications due to detachment of the samples during rotation. Moreover, it

would complicate the lesion process due to the fibrin clot covering the slice (**Figure 1.7 B**).

Finally, the semipermeable membrane method, consists of placing the samples on a semipermeable membrane sitting on the media. This allows the samples access to media while being oxygenated. These samples are typically kept in normal incubators and only moved and handled during medium change (**Figure 1.7 C**). Therefore, this method does not depend on live animals and it allows for easy access to the cultured tissue. These characteristics make it a desirable model of SCI (Abu-Rub et al., 2010), and it is the model used in this thesis for biomaterial implantation.

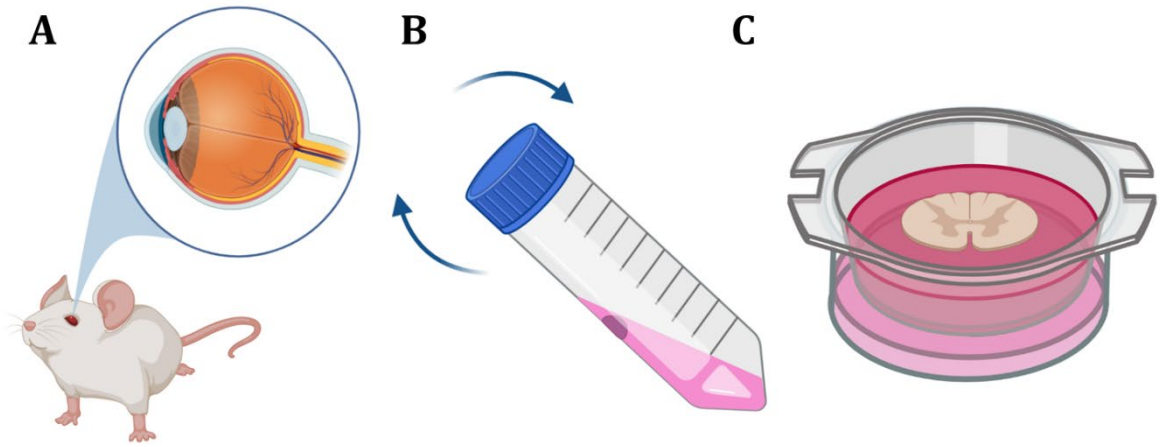

***Figure 1.7 Schematic representation of the three different methods for establishing organotypic cultures**:* in oculo *(**A**), roller tube (**B**) and semipermeable membrane (**C**).*

1.5.3 Spinal cord injury research within the framework of the 3Rs principle

The 3Rs principle refers to the replacement, reduction and refinement of animal use for experimentation (NC3Rs, 2021). In addition to promoting ethical use of animals in experimentation, this principle has also led to better experimental practice, more reproducible and more cost-effective research (MacArthur Clark, 2018).

As discussed above, *in vitro* experimentation does not replicate all physiological aspects of the lesion and, therefore, most research uses an *in vivo* approach to study treatment. As a result, SCI research relies heavily on the use of live protected species. In fact,

approximately 88% of all animals used for SCI research are rodents, with rats being the most used animal (Sharif-Alhoseini et al., 2017). The number of animals used per study ranges significantly between studies, with some reporting the use of 15 rats (Domínguez-Bajo et al., 2020), 42 (Galli et al., 2018) or even 342 rats per study (Z. Yang et al., 2015). In reference to the 3Rs principle, the use of organotypic slices can help reduce the number of animals used per study, as multiple sections of tissue can be retrieved from each animal. In order to replace the use of protected animal models for experimentation, we propose the chick embryo as an alternative to adult mammalian models.

Replacement refers to those approaches that directly replace the use of conscious, living animals. Replacement can be full (completely avoiding the use of any animal) or partial, which includes the use of animals that are not considered capable of experiencing suffering such as invertebrates and immature forms of vertebrates. According to the Animals (Scientific procedures) Act of 1986, mammals, birds and reptiles are considered protected species after starting the last third of their gestation or incubation period. In this case, the chick embryo is considered protected after E14. Moreover, due to its development inside an egg, the embryo can be accessed without harming the mother.

Reduction refers to methods that allow minimising the number of animals used in experimentation. Therefore, it requires adequate experimental design and data analysis in order to maximise the data acquired from each animal. It also encourages the sharing of data and resources between research groups. Finally, refinement refers to methods that minimise pain and suffering. This includes improving animal welfare in housing, using appropriate anaesthesia to minimise pain and training to cooperate with procedures in order to minimise distress. In this case, the use of organotypic slices, offers the possibility of acquiring multiple spinal cord slices from a single individual, reducing the number of animals per experiment. Moreover, all lesioning procedures are carried out *in vitro*, minimising the pain and suffering on the animals.

The chick embryo has been widely used as a developmental model because of its easy accessibility, simple manipulation techniques and cost-effectiveness. Because of these features it allows for the study of regenerative medicine while replacing the use of adult and complex animal models and minimizing the number of animals used per experiment and, therefore, minimising animal suffering. Therefore, this thesis will focus on the development of a SCI model using chick embryo organotypic slices.

1.6 THE CHICK EMBRYO

1.6.1 Relevance of the chick embryo as a neural tissue engineering platform

From ancient Egyptians to Aristotle, the chick embryo has captured the attention of scientists and philosophers through time, when eggs were opened at different stages to study development (Stern, 2005). It was also the model that William Harvey used in 1628 to discover the function of capillary vessels to connect arteries and veins and the model that lead to the discoveries by Marcello Malpighi (1675) of the existence of the neural tube, the somites and that the heart starts beating before blood is formed. With the improvement of microscopy, staining and sectioning techniques in the 1800s, embryology became more accessible, changes between the embryonic stages were described and the terminology of the anatomical components of the embryo was established by a new generation of comparative histologists (Stern, 2005). In 1951, Hamburger and Hamilton published "A series of normal stages in the development of the chick embryo", which set up a reference for further investigations such as the embryonic development of the CNS (Schoenwolf & Smith, 1990).

The chick embryo has been widely used as a model for developmental biology, pharmacology, immunology and cell biology amongst others (Bjornstad et al., 2015; Rashidi & Sottile, 2009). Although it has often been overlooked as a regenerative medicine model, the chick embryo spinal cord is very similar to the mammalian spinal cord. It possesses all major cell types and neural system tracts (Ferretti & Whalley, 2008).

Furthermore, the chick spinal cord cannot regenerate after injuries made after E13 (Hasan et al., 1993; Shimizu et al., 1990), which opens the possibility to test regenerative responses following biomaterial implantation. Moreover, the underlying mechanisms of its development have been extensively studied, making data interpretation more complete. Furthermore, the embryo develops inside an egg, which makes it very easily accessible and technically straightforward. This feature also allows for embryonic studies while preserving the mother's life.

1.6.2 Spinal cord development in the chick

When working with embryonic tissue, it is crucial to understand the developmental stages of the species in order to be able to identify different structures and cell types. Therefore, this section focuses on the spinal cord development of the chick embryo.

The formation of the CNS is initiated by the process of neurulation or neural tube formation, which consists of two phases: primary and secondary neurulation (Schoenwolf & Smith, 1990). During primary neurulation, the neural plate (portion of the ectoderm that will become neural tissue) extends longitudinally, narrows transversally and thickens apicobasally (H. W. Van Straaten et al., 1996). Simultaneously, a medial hinge point appears in a transverse section forming a neural groove that deepens and widens to finally form the neural walls and the neural tube lumen ((H. W. M. Van Straaten et al., 1997). Only the most dorsal part of the neural walls, the neural folds, bend inwards during convergence, after which they appose, adhere and finally fuse (H. W. Van Straaten et al., 1996). This process starts *de novo* in three different closure points: 1) Mesencephalic closure (during Hamilton's embryonic stages 4 to 6 (18 to 25h)). 2) Rombocervical closure (stages 6 to 8 (23 to 46h)) and 3) Posterior neuropore closure (stages 7 to 18 (23 to 69h)) (H. W. Van Straaten et al., 1996). This folding process requires higher concentration of microfilaments in the apical region and longer cell cycles at hinge points,

thereby narrowing the apices of these regions (Sadler, 2005). The neural tube will later differentiate into the spinal cord and the brain during secondary neurulation.

Signalling along the rostral-caudal axis of the neural tube establishes the main subdivisions of the CNS: forebrain, midbrain, hindbrain and spinal cord, whereas dorsal-ventral and medial-lateral signalling establishes the differentiation of progenitor cells (Jessell, 2000; Lu et al., 2015). There is also a temporal factor that influences cell fate, different cells differentiate at various times (Lu et al., 2015). The position of a cell in these axes will determine its fate. Caudalization of the neural tube is mediated by the combined actions of four factors that promote the specification of midbrain, hindbrain and spinal cord: fibroblast growth factor (FGF), paraxial-mesoderm caudalizing (PMC) activity, retinoic acid and a rostralizing factor (Muhr et al., 1999).

In the dorsal-ventral axis, adjacent cells to the floor of the neural tube will give rise to motoneurons, and cells dorsally to motoneurons will become several classes of interneurons. Cells of the most dorsal part of the neural tube will form the neural crest, and the cells lateral to it will differentiate into dorsal sensory interneurons (K. J. Lee & Jessell, 1999).

Non-neural epidermal cells from the ectoderm send inducing signals to the dorsal cells next to the neural crest, triggering their differentiation into sensory neurons (K. J. Lee & Jessell, 1999). This signal is transmitted by the secretion of proteins of the TGFβ family (Hemmati-Brivanlou & Melton, 1994). The cells from the neural tube floor, together with the notochord, trigger the differentiation of the ventral cells through a gradient of the glycoprotein Sonic hedgehog (Shh) (Patten & Placzek, 2000). Neurons at the more ventral region of the neural tube (closer to the notochord) require a higher concentration of Shh for differentiation than cells at the more dorsal part of the ventral region (J. Ericson et al., 1997). These progenitor cells have two classes of homeodomain proteins: class I proteins

are repressed by Shh and class II are activated (Briscoe et al., 2000). The interactions between these two classes of proteins will eventually convert the Shh gradient into activation of discrete progenitor domains for differentiation (Briscoe et al., 2000). In the end, within an ideal spinal cord segment, 13 pools of progenitor neurons can be found along the dorsal-ventral axis. There are 8 dorsal pools of interneuron progenitors: p1-6, pdILA, pdILB; 4 dorsal progenitor subdivisions: p0-3 and one motoneuron progenitor domain pMN (Alaynick et al., 2011).

In all vertebrates, the region at the roof of the neural tube is called the neural crest (Le Douarin, 2004). The neural crest cells are special for their migration capacity and their pluripotent state (Le Douarin, 2004). Those that migrate along a dorsolateral pathway will give rise to pigment cells, and those migrating along a ventrolateral pathway will give rise to autonomic ganglia, Schwann cells and dorsal root ganglia (or sensory ganglia) (Charles W., George P., 2009).

Colonization of microglia in the spinal cord coincides with vascularization (Charles W., George P., 2009). In the developing chick spinal cord, microglia act as phagocytes to remove dying cells (Jordi Calderó et al., 2009). OPCs arise from the ventricular surface as a response to Shh signals from the notochord (Nigel P. Pringle et al., 1996). These precursor cells migrate and enter the white matter, where they will stop and undergo final differentiation (Robinson et al., 1998). Astrocytes also arise from the same region and play a role in axonal guiding (Masahira et al., 2006).

1.6.3 Timeline of development

Chick embryos need to be incubated during 21 before hatching (**Figure 1.8**). Gastrulation occurs within the first day of incubation or E1. By the end of E1, neural folds begin to appear, indicating that neurulation has begun. Neural folds first meet at the region of the head, and somites begin to form on each side of the notochord. By the end of the second

day, the head begins to turn onto the left side and the embryo flexes forming a C shape. At the 4th day most somites are formed and the embryo has completely turned to its left side. The caudal-rostral specification is initiated between Hamburger & Hamilton (HH) stages 3 and 4 (Muhr et al., 1999).

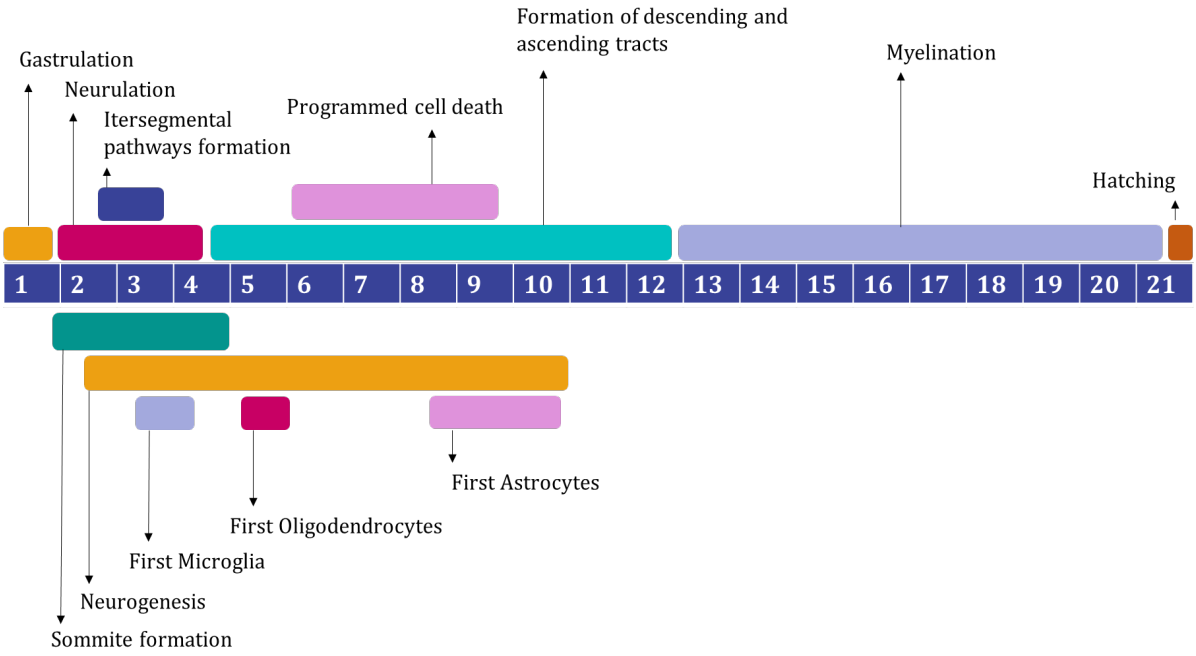

Figure 1.8 Schematic representation of key events which occur during the timeline of CNS development in the chick embryo*. The central numbers indicate days post-fertilisation. And each coloured line indicates the period of time in which a relevant developmental stage occurs.*

Different cell types appear at different time points. Neurons begin to differentiate at E2, motoneuron progenitors are born between HH stages 15-17 (corresponding to E3) (Johan Ericson et al., 1992). However, some neurons from the dorsal horns don't appear until E8 or E9 (Ferretti & Whalley, 2008). Many motoneurons are born, but only those that make synapses will survive, the others will die following a programmed cell death that peaks at E6 and ends at E9 (Yamamoto & Henderson, 1999). At E11, there still seems to be neurogenesis, but at a very slow rate (Katherine Whalley et al., 2009). Microglia appear at E3 (Jordi Calderó et al., 2009). Oligodendrocytes appear at E5 (Ono et al., 1995) and myelination starts at E13 and ends at hatching (Dobbing et al., 1957). Finally, astrocyte

precursors begin to be detected at the end of neurogenesis at E8, but GFAP (glial fibrillary acidic protein) can only be detected after E10 (N. P. Pringle, 2003).

Intersegmental projections are formed between E2.5 and E3.5 (Yaginuma et al., 1990). The formation of ascending and descending neural tracts occurs prior to the onset of spontaneous limb movements, which begin at E6 (Okado & Oppenheim, 1985). Based on Okado and Oppenheim's findings in 1985 after retrogradelly tracing neurons with horsereadish peroxidase (HRP), descending tracts from the brainstem to the cervical region of the spinal cord are formed between E5 and E8. These tracts reach the lumbar region between E5.5 and E12.

As previously mentioned, chick embryos are a protected species during the last third of the incubation period. Therefore, it is considered that they are not capable of pain and suffering before E14. At this stage, all CNS cell types are already present and most structures, including ascending and descending tracts are already formed. It has also been established that the chick embryonic spinal cord will not regenerate after an E13 lesion. For these reasons the E14 chick embryo has been chosen to establish a new SCI model in this thesis.

1.7 KNOWLEDGE GAPS AND THESIS AIMS

In summary, after a lesion, the spinal cord does not have the intrinsic capacity for regeneration and current treatments are yet to achieve full functional repair. The injection of NSCs after SCI in clinical trials has led to an increased motor and sensory recovery. However, this therapy faces high cell attrition due to the forces inflicted on the cells when protruded through a fine needle. Alternatively, the implantation of encapsulated cells within 3D matrices offers the advantages of cell protection and healthy ECM mimicking, leading to improved results compared to cell injection alone. Although promising, the translation of this therapy to the clinic can be delayed for years due to the exclusive use

of experimental grade biomaterials. Moreover, most research conducted to date overlooks the highly aligned nature of the spinal cord, neglecting the need for patterned implantable scaffolds. In addition, the raising numbers of available biomaterials rely on complex and expensive *in vivo* rodent animal models, leading to time consuming experiments which make reproducibility challenging. As an alternative, the use of organotypic spinal cord slices offers a simpler, more controlled environment to study SCI therapies while maintaining the spinal cord structure. Although few, these experiments have already shown promising results. However, they still rely on murine models. The chick embryo offers a cheaper alternative as a spinal cord slice donor, linked to less ethical implications. Here, we propose the use of chick embryo organotypic slices for testing biomaterial implantation for SCI.

Therefore, this thesis aims to develop a SCI model using chick embryo organotypic slices in order to provide a platform in which to test biomaterial implantation within the framework of the 3Rs principle.

In order to do so, lesioning time points and cellular responses to injury will be researched in **Chapter 3** in a chick embryo organotypic slice SCI model. Following, two biomaterials will be explored for their ability to encapsulate NSCs: Hemopatch™ (**Chapter 4**), a clinically available biomaterial, and Cellevate™ (**Chapter 5**), a patterned nanofibre scaffold. Finally, Hemopatch™ will be implanted in the organotypic model previously established and cellular responses to implantation will be studied (**Chapter 6**).

2 METHODOLOGY

2.1.1 OUTLINE

Within this section, I will detail the relevant methodology for all experimental chapters. For ease of reference, the list of culture media and antibodies are detailed below and split into tables (**Section 2.2**) and all experimental groups are detailed in **Section 2.3**. **Sections 2.4** to **2.10** cover the methodology for live cell and tissue cultures set up. Cell and tissue processing are covered in **Sections 2.11** to **2.16**. Finally, sample and data analyses are covered in **Sections 2.17** to **2.20**.

2.2 LIST OF MEDIA AND ANTIBODIES

Table 2.1 details the list of media used for spinal cord and NSC culture.

Table 2.1 List of media used for organotypic spinal cord slice culture and NSC culture*. This table lists all the reagents used to make the different media for cell and tissue feeding.*

List of media for organotypic spinal cord slice culture and NSC culture	
Slicing medium	HEPES (2.5%) (BioSera L0180-100), EBSS (97.5%) (Invitrogen 24010-043).
Culturing medium	Pen-strep (1%) (Fisher 11528876), 13% glucose (5%), EBSS (19%), horse serum (25%) (BioSera S0910-500), MEM (50ml) (Invitrogen 42360-024).
Neurosphere medium (NSM)	DMEM (72.2%) (Fisher 41966029), F-12 (24.6%) (Fisher 21765-029), B-27 (2%) (Fisher VX17504044), bFGF (0.05%) (Peprotech 100-18B) and EGF (0.05%) (RnD Systems 236-EG-200), Heparin (0.1%) (Sigma H3149), Pen-strep (1%) (Fisher 11528876).
Monolayer medium (MLM)	DMEM (49%) F-12 (49%) N2 (1%) (Fisher VX17502048), bFGF (0.05%), EGF (0.05%), Heparin (0.1%), Pen-strep (1%).
Differentiation medium (DiffM)	DMEM (72.2%), F-12 (24.6%), B-27 (2%), Heparin (0.1%), Pen-strep (1%) (Fisher 11528876), FBS (1%)

Table 2.2 details a list of primary and secondary antibodies used for immunolabelling.

***Table 2.2 List of primary and secondary antibodies used for immunostaining**, detailing cellular target, concentration, host and purchase code. The last item was discontinued after experiments.*

Primary and secondary antibodies				
Name	**Target**	**Conc.**	**Host**	**Code**
Nestin	NSCs	1:200	Mouse	BDbiosciences 611658
Sox-2	NSCs	1:1000	Rabbit	Sigma Aldrich AB5603
GFAP	Astrocytes	1:500	Rabbit	BioLegend 644702
Tuj -1	Neurons	1:500	Rabbit	BioLegend 802001
MBP	Oligodendrocytes	1:200	Rat	BioRad 160223
Lectin biotinylated	Microglia	1:200		VectorLabs B1175-1
Anti mouse Ab FitC	Mouse	1:200	Donkey	Stratech 715-095-151
Anti rabbit Ab FitC	Rabbit	1:200	Donkey	Stratech 711-095-152
Anti rabbit Ab Cy3	Rabbit	1:200	Donkey	Stratech 711-165-152
Anti rat Ab FitC	Rat	1:200	Donkey	Stratech 712-095-153
Anti Biotin Ab FitC	Biotin	1:200		

2.3 EXPERIMENTAL GROUPS FOR EACH DATA CHAPTER

For ease of reference, this section specifies the experimental groups and timelines of each chapter. Details of assay procedures and experimental set up are explained in the subsequent sections.

In **Chapter 3**, we wanted to establish an *in vivo* and an *in vitro (*or *ex ovo)* model in which to test biomaterial implantation after SCI in the chick embryo. Therefore, two experimental groups were established for the *in vivo* experiments of **Chapter 3**: the "shell" group refers to those embryos incubated in their eggshell, while "shell-less" refers to those incubated in a cup outside their shell. The aim was to determine which of the two would allow easier manipulation for lesioning and biomaterial implantation.

In the *in vitro* experiments of **Chapter 3**, four different groups were established (**Figure 2.1**). Spinal cords were dissected from E14 chick embryos and were injured at two different time points: 4 days post dissection (I4) and 12 days post dissection (I12). Each of these groups were split and fixed at two different time points: 4 days post injury (I4F4 and I12F4) or 12 days post injury (I4F12 and I12F12). The viability of each of these time points was controlled with an uninjured spinal cord slice that was fixed at the same time. These timepoints were required to investigate the effects of an early *vs.* late injury and whether the response to injury changed over time. We expected to choose the most representative time point for the implantation experiments in **Chapter 6**.

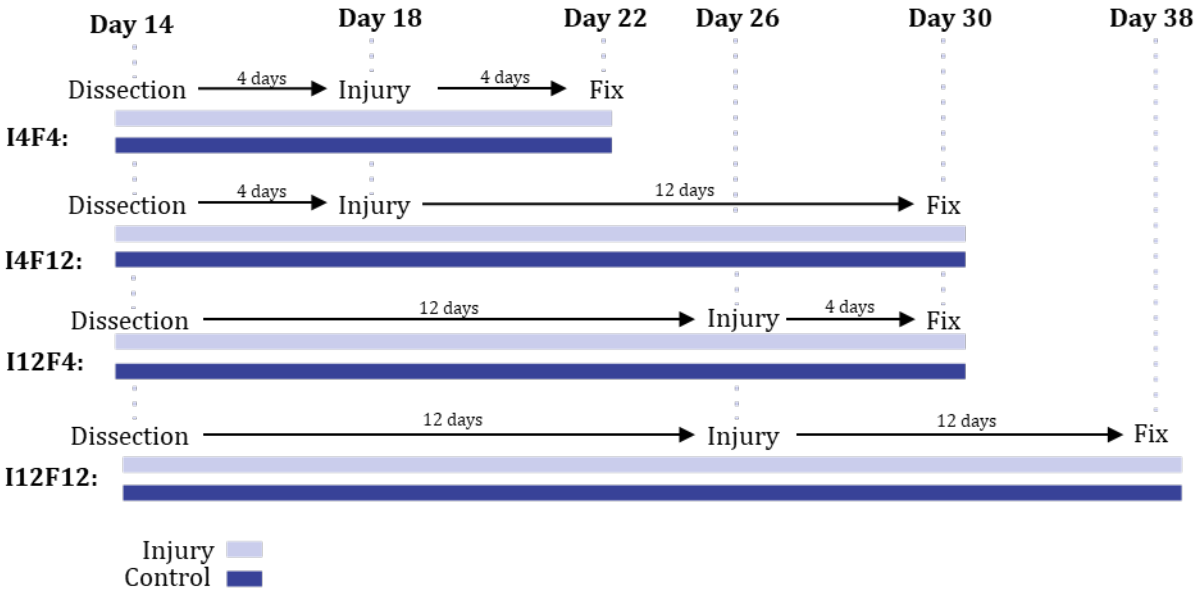

Figure 2.1 Schematic representation of the dissection, injury and fixation timepoints used for the organotypic spinal cord slice culture model in Chapter 3*. This timeline aims to represent the timepoints at which the spinal cords were lesioned and fixed.*

In **Chapters 4 and 5** we aimed to study the capacity of different biomaterials to support an NSC population. The experimental conditions for **Chapter 4** included: (i) laminin and poly-ornithine coated coverslips, (ii) uncoated Hemopatch™ and (iii) laminin and poly-ornithine coated Hemopatch™. **Chapter 5** included the following experimental groups: (i) glass coverslips, (ii) random Cellevate™ fibres and (iii) aligned Cellevate™ fibres.

Finally, in **Chapter 6**, we used the previously established *in vitro* SCI model in **Chapter 3** to test biomaterial implantation, in this case, the same biomaterial tested in **Chapter 4**. The time points were adapted from the previous findings in **Chapter 3** resulting in three groups: Injury, Injury + Hemopatch™ and Sham (**Figure 2.2**). All slices except those in the "Sham" group were lesioned 4 days post dissection. The "Injury" group was lesioned but was not treated with Hemopatch™, the "injury + Hemopatch™" group was injured and the material was implanted in the lesion directly after injury. All slices were fixed 24 days post dissection.

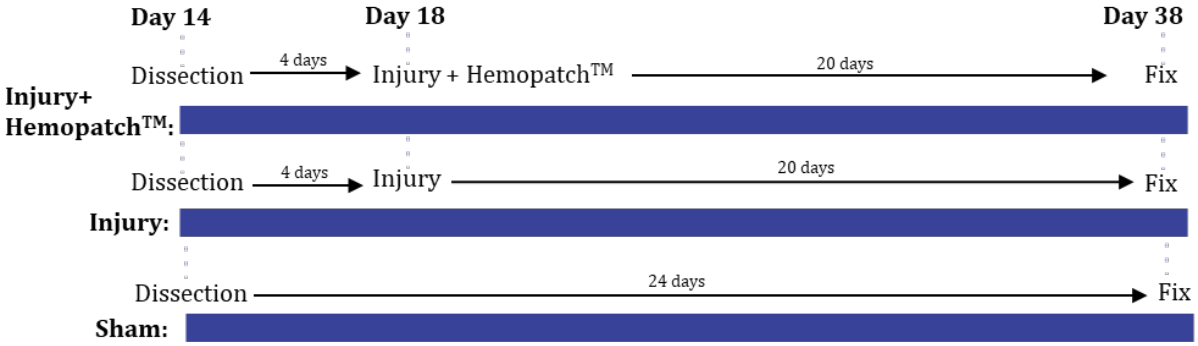

Figure 2.2 Schematic representation of the dissection, injury, biomaterial implantation and fixation timepoints used for the organotypic spinal cord slice culture model in Chapter 6. *This timeline aims to represent the timepoints at which the spinal cords were lesioned and fixed and the biomaterial was implanted.*

2.4 CULTURE OF CHICK EMBRYOS IN SHELL AND SHELL-LESS

Chick embryos were incubated inside their shells or shell-less in order to establish which method allowed for easier manipulation of the model.

Fertilized Bovans Brown eggs (Henry Stewart & Co.) were incubated at 37°C and 47% humidity for 56 hours. Then, as appropriate depending on the experiment, some eggs were left in the incubator (shell) and the rest were cultured without the shell (shell-less) as follows. For the shell-less culture (adapted from Tahara & Obara, 2014), a culture vessel had to be designed and constructed. For this, a plastic cup was filled with 40 mL of dH2O and covered with cling film. The film was then pressed downwards using a light bulb to form a 5 cm deep concave shape mimicking the shape of the shell. Finally, 2mL of

dH2O and 300mg of calcium lactate were added on the cling film. To transfer the embryos to the culture vessel, the eggs were removed from the incubator after 56h, and 6mL of albumin were extracted from the shell and added to the plastic cup. Next, the eggs were placed vertically and the top of the egg was surrounded with scotch tape to avoid cracks and cut with fine scissors. Finally, the contents of the egg were gently poured inside the cup, with the embryo facing upwards. Using a needle, 10 holes were made at the top of the cling film to allow transpiration of the embryo (mimicking the pores in the shell), the cup was covered with the lid of a petri dish and all the embryos were kept in an incubator at 37°C (**Figure 2.3**).

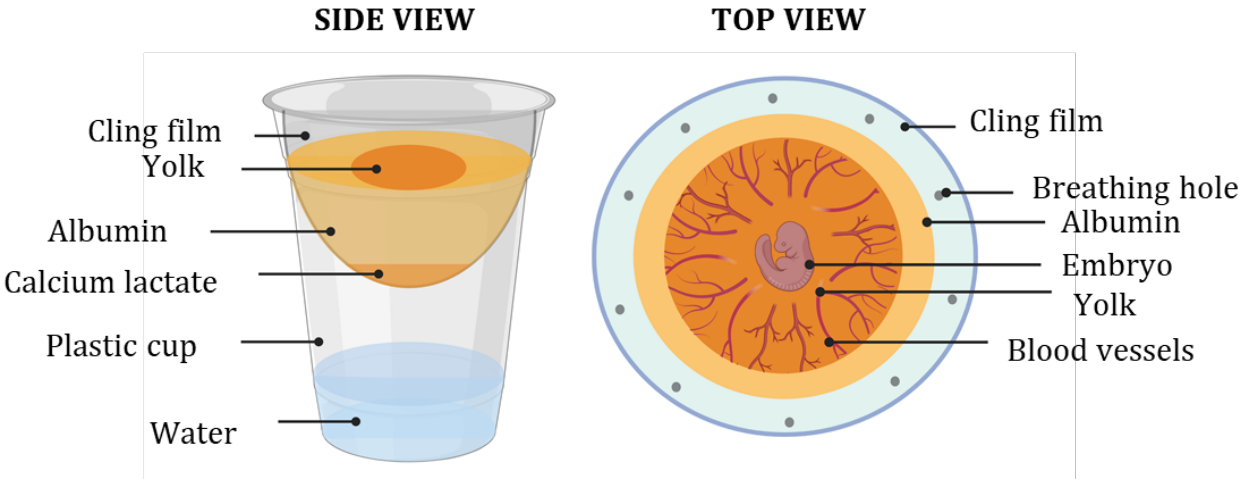

Figure 2.3 Representation of the shell-less culture vessel *with a side view (left) and top view (right). Image created with Biorender.com*

2.5 INTRODUCTION OF A SPINAL CORD TRANSECTING LESION *IN VIVO* IN THE CHICK EMBRYO

The feasibility of chick embryo lesioning was tested as follows. 4mL of albumin were extracted from the shell embryos at E3 to prevent the membrane from attaching to the shell. At E5, a small window was opened on the shell to expose the embryo. Under a dissection microscope, a small gap was cut on the amniotic membrane and the embryo was lifted upwards using a curved glass rod. Then, with fine scissors or a needle, a lesion

was cut from the centre of the spinal cord towards the outside in the cervical or lumbar region. The window in the shell was sealed with scotch tape and the egg was returned to the incubator. After 0h, 24h or 48h, the window was widened, the embryo was removed from the shell and the spinal column was dissected and fixed with 4% paraformaldehyde (PFA) overnight and cryosectioned (See **section 2.10**) or the whole embryo was fixed in 4% PFA for a week and stained (See **section 2.11**). The same lesioning protocol was used for Shell-less embryos (excluding removal of albumin and windowing). In some cases, a 0.1 mm piece of acellular Hemopatch™ (stained with green food colouring dye for easier visibility) was implanted inside the injury gap with the mechanical help of a needle (**Video 1**). Some embryos were kept in the incubator until E14 to study survival.

2.6 ESTABLISHMENT OF THE EMBRYONIC SPINAL CORD SLICE ORGANOTYPIC CULTURE

A more simplistic SCI model was established through the use of chich embryo spinal cord organotypic slices as follows. Fertilized Bovans Brown eggs (Henry Stewart & Co.) were incubated at 37°C and 47% humidity in a specialised egg incubator (Brinsea) (Incubation parameters were chosen as indicated by Brinsea). After 14 days, the shells were cracked and the contents were poured in a large glass petri dish. Then, the embryos were decapitated with fine scissors and the limbs were cut off (**Figure 2.4 A, B**). A ventral incision was made to remove all internal organs and the skin around the spinal column was removed (**Figure 2.4 C, D**). Using a scalpel, the cervical segment of the spinal column was isolated (**Figure 2.4 E**). Finally, the cervical segment of the spinal cord was extracted from the spinal column by ejecting a powerful stream of slicing medium (**Table 2.1**) through the spinal canal (**Figure 2.4 F**). When it was not possible to extract the cervical segment of the spinal cord, the thoracic segment was used. All spinal cords were kept in slicing medium on ice until use (**Figure 2.4 G**).

The spinal cord slice organotypic culture and lesioning protocols were adapted from Weightman et al. (2014). Here, each spinal cord was sliced longitudinally at 350µm thickness with a McIlwain Tissue Chopper (**Figure 2.4 H**), collected in a small petri dish containing ice-cold slicing medium and kept on ice for 30 minutes (**Figure 2.4 I**).

Meanwhile, the culture chambers were prepared. A permeable insert was placed in a small petri dish and three 0.45µm pore, 0.5cm^2 size membranes (Omnipore JHWP04700) were placed on top of the insert. The space between the petri dish and the insert was filled with 1.1mL of culturing medium (**Table 2.1**).

After 30 minutes, the spinal cords were collected with a wide-bore transfer pipette and placed on the membranes (one spinal cord slice/membrane) (**Figure 2.4 J**). Finally, the small petri dishes were placed on a large square petri dish for easier transportation and for better sterile protection and kept inside an incubator at 5%CO_2 and 37°C. The slices were fed every other day by 50% medium change.

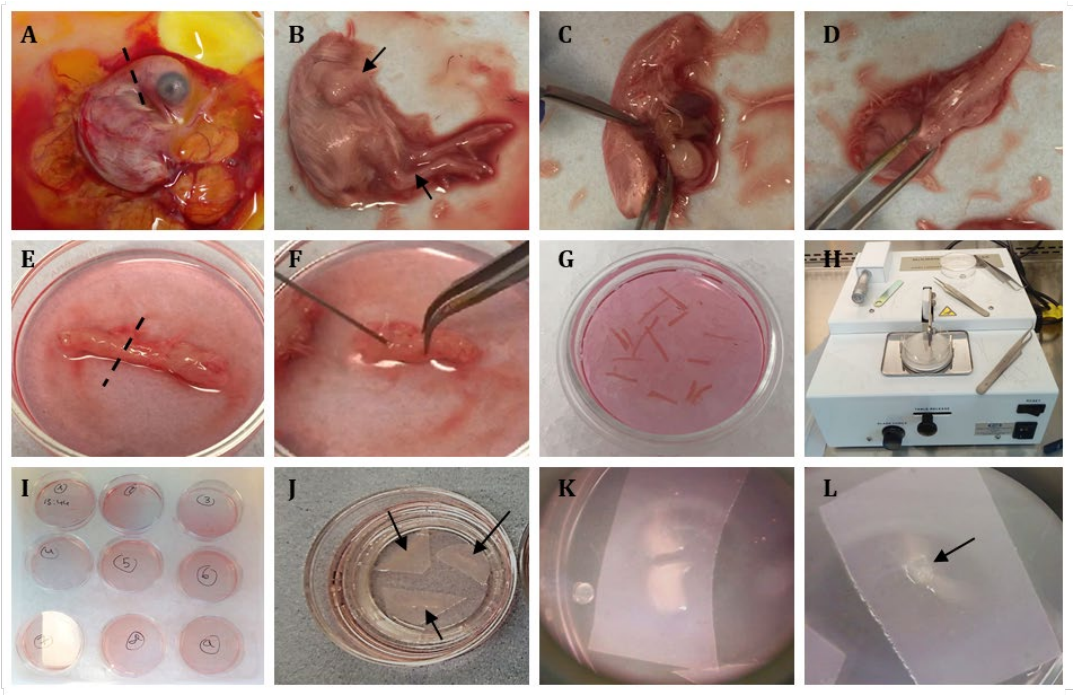

Figure 2.4 Representative pictures of the dissection, culture set up, lesioning and biomaterial implantation of chick embryo organotypic spinal cord slices. *Discontinuous lines represent cutting areas. Arrows in B point to limbs, arrows in J point to spinal cord slices and arrow in L points to implanted biomaterial.*

2.7 INTRODUCTION OF A TRANSECTING LESION IN THE ORGANOTYPIC SPINAL CORD SLICES AND IMPLANTATION OF HEMOPATCH™

Transecting lesions were implemented in sterile conditions under a dissection microscope. A double-blade scalpel was used to mark the lesion edges to ensure equal injury size in all slices. Then, the spinal cords were completely sectioned with a standard scalpel aided with a needle following the marks of the double-bladed scalpel (**Figure 2.4 K**). The slice debris between the two injury margins was removed with tweezers.

For the experiments in **Chapter 6**, a 250μm thick slice of uncoated and acellular Hemopatch™ (See **Section 2.9** for slicing methodology) was placed adjacent to the slice and further cut to the size of the lesion with a scalpel. Then, it was implanted to bridge the gap between two sides of the lesion (**Figure 2.4 L**).

Finally, the slices were kept in the incubator and fed with culturing medium (**Table 2.1**) (50% change) until they were transferred into 24-well plates, fixed with 4% PFA for 1h and kept at 4°C for further staining. See **section 2.2** for lesioning and fixing time points.

2.8 ESTABLISHMENT OF A NEURAL STEM CELL PRIMARY CULTURE

NSC cultures for seeding onto biomaterials were set up following the previously established protocols in our laboratory (Fernandes et al., 2015). Mouse brains were dissected from postnatal day 1 (P1) to P3 mice and kept in PBS on ice until use. Under a dissection microscope, the subventricular zone was isolated from all brains using a scalpel and kept in 1mL of neurosphere medium (NSM) (**Table 2.1**). The tissue was incubated at RT with DNAse I (Sigma Aldrich 10104159001) for 1 minute and then mixed by pipetting up and down until all large clumps had dissipated. The sample was centrifuged for 5 minutes at 1000rpm and resuspended in 0.5mL of NSM. The solution was passed through a cell strainer (70μm pore size) and diluted with NSM to a final volume of 3mL. Then, the density of viable cells was calculated by mixing 10μL of cell solution with Trypan blue

(Sigma Aldrich T8154) in a 1:5 solution, with cell counting performed using a hemocytometer.

In a separate tube, the cells were diluted with NSM at a density of $1x10^5$ cells/mL and transferred into T25 flasks (5mL of cell solution in each flask). These were incubated at 5% CO_2 and 37°C. NSCs were allowed to proliferate as neurospheres (**Figure 2.5**).

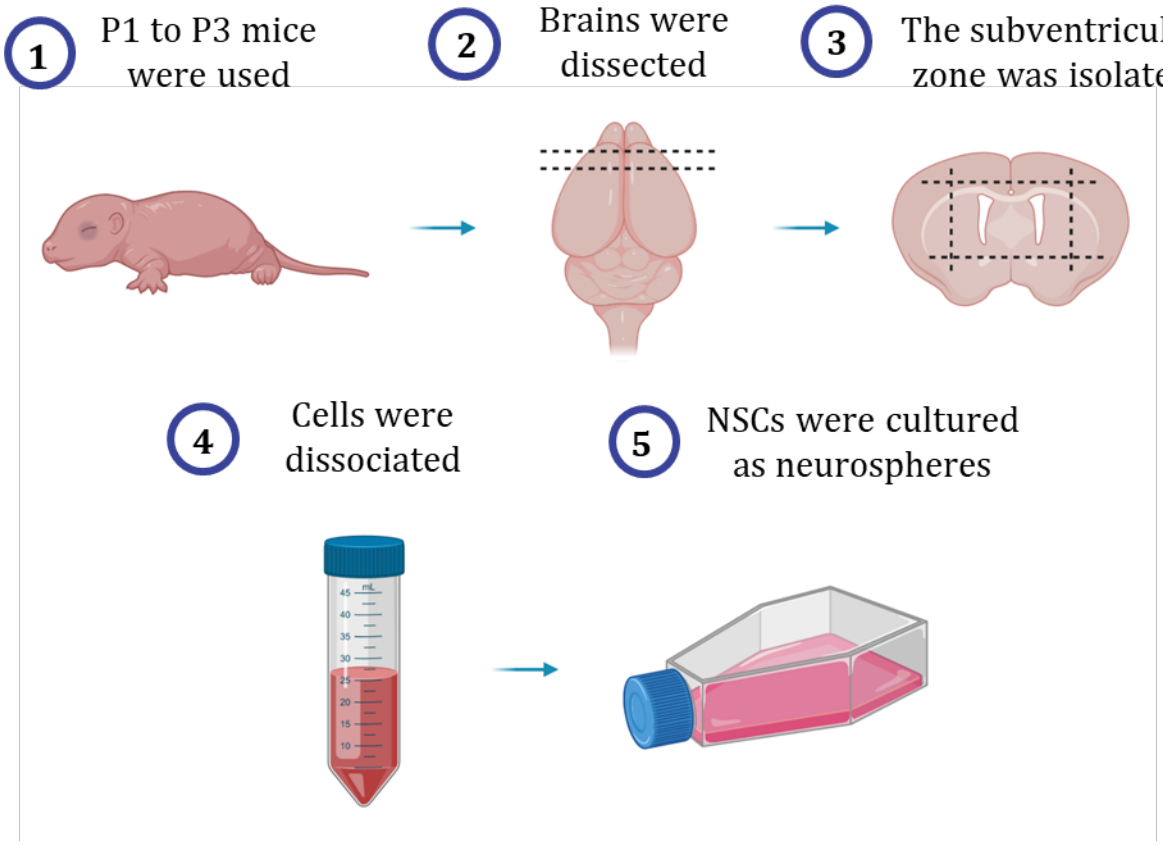

Figure 2.5 Primary NSC culture set up*. Step by step schematic representation of the protocol for the establishment of a primary NSC culture and neurosphere formation. Image created with Biorender.com*

Once the neurospheres had reached an optimal density (5 to 7 days) (**Figure 2.6**) they were pooled into a falcon tube and centrifuged at 1000rpm for 5 minutes. The pellet was resuspended in PBS and centrifuged again with the same parameters. Then, the neurospheres were dissociated into single cells by incubation with a DNAse I /Accutase mix (1:10) for 5-10 minutes. 1mL of NSM was added to inactivate the mix and the solution was centrifuged once more. The density of viable cells was calculated following the same protocol as before and the cells were diluted with MLM (**Table 2.1**) at the required

density for each experiment (See **sections 2.9** and **2.10**) or NSM (**Table 2.1**) for further propagation in T25 flasks.

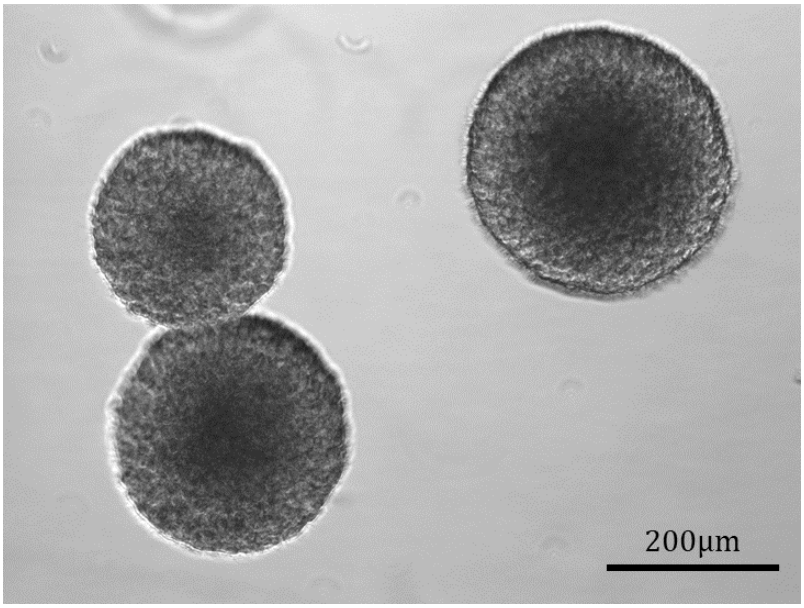

Figure 2.6 Neurospheres*. Light microscope representative image of three neurospheres at optimal density for passaging.*

2.9 HEMOPATCH™ FUNCTIONALISATION AND EXPERIMENTAL SET UP

Hemopatch™ was kindly donated by Baxter Healthcare Technologies. Under sterile conditions, a 0.5 cm^2 piece of Hemopatch™ was cut with a scalpel and then chopped with a McIlwain Tissue Chopper set to 250 µm.

It should be noted that Hemopatch™ is also coated with a 250µm thick layer of NHS-PEG (polyethyleneglycol) bound to one side of the material, designed to enhance its tissue adherance properties (**Figure 2.7A**). However, we consider the impact of this PEG layer on cellular function to be negligible in these experiments due to the following reasons: the material was cut vertically (to fit the culture well), perpendicular to the PEGylated layer to generate a piece of Hemopatch™ approximately 5000 (length) x 1000 (width) x 250 (depth) µm. The 250µm thick PEGylated layer was therefore solely situated along one of the widths of the final piece. Moreover, during culture, the material was orientated

sideways (with the thin PEGylated side as one of the lateral walls) (**Figure 2.7 B**) so as to minimise PEG interaction with cells. Further, it is likely the PEG layer was dissolved in water during the preparation steps prior to seeding the cells on the material (personal communication, Baxter), so would not have affected the outcomes.

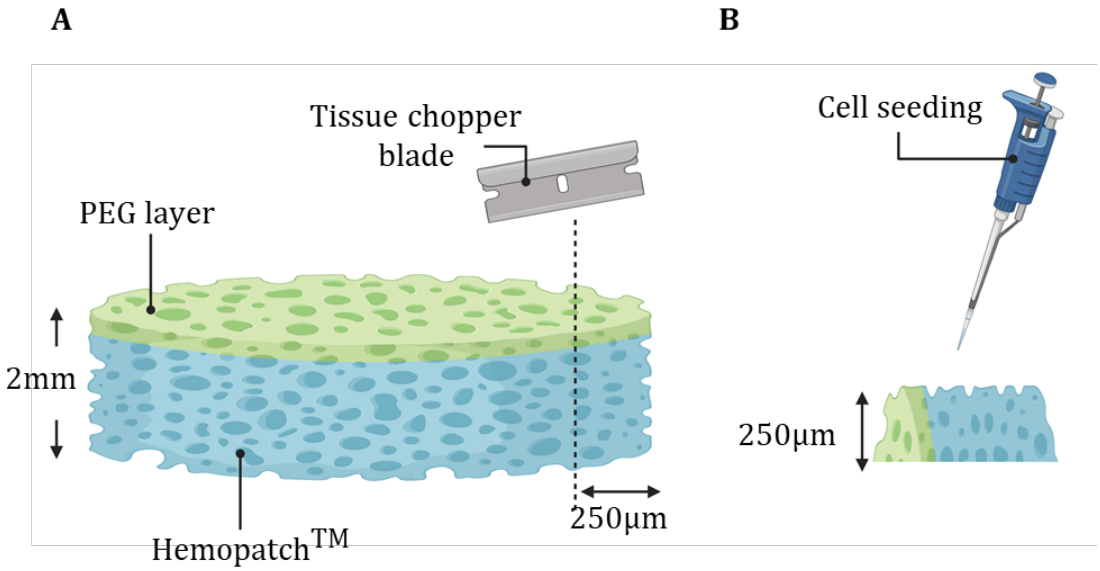

Figure 2.7 Slicing of Hemopatch™. *Schematic representation of the Hemopatch™ slicing process and orientation (**A**) and orientation of the piece for cell seeding (**B**). Image created with Biorender.com*

Some pieces of Hemopatch™ and glass coverslips were rinsed with ethanol and then incubated at 37°C with poly-ornithine (1:5) (Sigma P4957) for 1 hour. Then, they were washed with water and incubated again with laminin (1:200) (Sigma L2020) for 1 hour. Finally, they were washed three times with water and stored in the incubator until use. Alternatively, some slices of Hemopatch™ were left uncoated and kept in water until use.

The glass coverslips were placed at the bottom of 24 well plates and the cells were seeded on top suspended in 600 µL of MLM at a density of $1.5x10^5$ cells/mL. Each piece of Hemopatch™ (coated and uncoated) was placed in a different well from the same plate and the cells were seeded on top of the biomaterial in a 10 µL drop at a density of $1x10^7$cells/mL. The cells were allowed to settle for 30 minutes in the incubator and then 600 µL of medium was added in each well.

Cells were grown in MLM (designed to retain NSCs) for 5 days, with 50% medium change every other day. Once the cells on the coverslips were confluent (**Figure 2.8**), cells in all experimental conditions were either fixed with 4% PFA for 1 hour (for assessment of NSC growth and health) or were allowed to differentiate for 7 days by swapping the MLM to differentiation medium (DiffM) (**Table 2.1**) (to assess any effects of materials on differentiation). All plates were fed every other day with a 50% medium change. Prior to fixing, some cells were stained for survival (Live/Dead) and proliferation (Edu) assays (See **sections 2.19.1** and **2.19.2**).

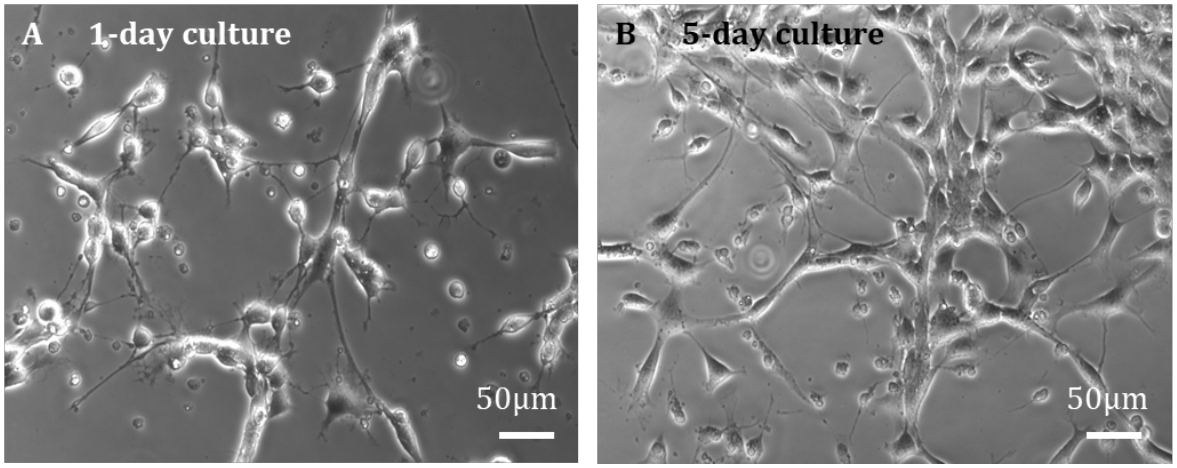

Figure 2.8 NSCs on glass coverslips*. Representative light microscopy images of NSCs cultured on glass coverslips one day after seeding (**A**) and 5 days after seeding (**B**).*

2.10 CELLEVATE™ FUNCTIONALISATION AND EXPERIMENTAL SET UP

incubated again with laminin (1:200) (Sigma L2020) for 1 hour. Finally, they were washed three times with water and stored in the incubator until use.

After neurosphere dissociation (**Section 2.7**), NSCs were seeded on the fibres and glass coverslips in 600 µL of MLM at a density of 1.5 x 10^5 cells/mL. The cells were fed every other day with a 50% medium change. NSCs were allowed to proliferate for 5 days before being fixed with 4% paraformaldehyde (PFA) for 30 minutes or allowed to differentiate to astrocytes, neurons and oligodendrocytes by swapping the medium to DiffM. The latter were kept in the incubator for a further 7 days, with medium changes every 2-3 days, before being fixed with 4% PFA.

2.11 CRYOSECTIONING OF CHICK EMBRYOS

The head and limbs of some PFA fixed embryos from the shell and shell-less cultures were cut off with a scalpel in order to isolate the spinal column alone. The samples were submerged in a solution of 30% sucrose overnight and then frozen in OCT at -80°C for 2 hours. Then, the samples were cryosectioned at 12 to 20µm, mounted on glass slides and incubated in a 37°C oven for dehydration and optimal attachment to the slide. Following this, the slices were washed with PBS (3 times, 5 minutes) and stained following the standard immunostaining protocol (**Section 2.12**).

2.12 CHICK EMBRYO WHOLE MOUNT STAINING

Some embryos from the shell and shell-less experiments were kept intact after fixing and stained as a whole. First of all, the embryos were permeabilized overnight at 4°C with a PBS-TxD solution consisting of 2% Triton x-100 and 20% DMSO in PBS. The following day, the samples were incubated with Tuj-1 (1:200) in PBS-TxDB (PBS-TxD + 1% BSA + 0.1% fish gelatine) and kept for 4 days at 4°C. Then, they were washed 5 times for 30 minutes with PBS-Tx (without DMSO or gelatine) and incubated with secondary antibody in PBS-TxDB for 4 days at 4°C. Following this, samples were rinsed with PBS-Tx for 30 minutes

and then with TNT (100mM Tris-HCl + 140mM NaCl + 0.05% Tween) for 30 minutes and finally with TN (TNT without Tween) 3 times for 5 minutes. Samples were then dehydrated through a methanol/TN series of 15 minutes each (20%, 50%, 75% and 100%). Finally, the embryos were moved to glass containers and the tissue was cleared with a BABB solution containing 1 part of benzyl alcohol and 2 parts of benzyl benzoate, the samples were stored at 4°C in BABB until imaging. This protocol was adapted from Zukor et al. (2011).

2.13 IMMUNOHISTOCHEMISTRY

After fixing, cells, spinal cord organotypic slices and chick embryo cryosectioned slices were washed 3 times for 5 minutes in PBS and then incubated with blocking solution (PBS + 0.3% Triton X-100 (Sigma T9284) + 10% Normal Donkey Serum (Jackson ImmunoResearch 017-000-121)) for 30 min at RT. Then, the samples were incubated at 4°C overnight with the appropriate primary antibody (**Table 2.2**) suspended in blocking solution. The next day, the samples were washed and incubated with the appropriate secondary antibodies (**Table 2.2**) in combination with DAPI (4′,6-diamidino-2-phenylindole) (5.0 µg/mL) in blocking solution for 2h at RT in the dark and then washed 3 times, 5min/wash. Finally, the samples were mounted on glass slides with Vectashield mounting medium (Vector H-1000) and covered with a glass coverslip.

2.14 DAB STAINING

DAB (3,3'-diaminobenzidine) staining was carried out with Vector Laboratories Vectastain Elite ABC kit and DAB Peroxidase Substrate (SK-4100). The samples were washed with PBS and incubated at RT for 30 min with blocking solution (0.3% Triton X-100 in PBS + 10% normal donkey serum). Then, the slices were incubated overnight with primary antibody (**Table 2.2**). Following a 5 min wash, the samples were incubated for 30 minutes with the diluted biotinylated secondary antibody solution and washed again with PBS. Then, the samples were incubated for 30 minutes with the Vectastain ABC

reagent and washed with PBS. Finally, the samples were incubated with peroxidase substrate solution until the desired stain intensity developed. The samples were rinsed with water, mounted and imaged.

2.15 LIVE/DEAD ASSAY

30 minutes prior to fixing, some samples were incubated with 3µl/mL Ethidium homodimer (Sigma E1903), 1µl/mL of Calcein AM (VWR 89139-470) and 2µl/mL of DAPI in DMEM, incubated for 20 minutes in 5% CO2 at 37°C, washed with PBS, mounted on glass slides and imaged live.

2.16 PROLIFERATION ASSAY

Selected samples from each condition in **Chapters 4 and 5** were also incubated with the reagent EdU A (1 µM) for 6 hours prior to fixing. EdU is a thymidine analog which is incorporated during DNA duplication and therefore labels proliferating nuclei. After cell fixation, the samples were incubated at RT for 40 minutes with 0.3% Triton X-100 in PBS and then washed 4 times (5 minutes/wash) with 3% BSA in PBS. Then, the samples were incubated for 1h (RT, dark) with the Invitrogen Click-iT® EdU reaction cocktail and washed again with BSA. Finally, the samples were washed with PBS and subsequently immunostained (**Section 2.12**).

2.17 SCANNING ELECTRON MICROSCOPY

For a high resolution and detailed imaging of Hemopatch™ and Cellevate™, some samples were fixed with 2.5% Glutaraldehyde diluted in 0.1M sodium cacodylate (CAC) in preparation for SEM. Then, these samples were processed with the OTOTO protocol established by Fernandes *et al.*, (2015) as follows.

First of all, the samples were washed 3 times for 5 minutes with CAC and then incubated at RT with osmium tetroxide for 1 hour. Following this, they were incubated for 20 minutes with a saturated solution of thiocarbohydrazide, a high affinity osmium binding

agent, in distilled water. Then, the samples were washed 6 times for 5 minutes and the process was repeated two more times. After the third incubation with osmium tetroxide, the samples were washed again with water and then dehydrated through a series of 30-minute incubations of increasing concentrations of ethanol (70%, 80%, 90%, 100% and 100% dry ethanol). Finally, the samples were dried to the critical point with CO_2 as the transition fluid and mounted on SEM stubs.

To enhance conductivity, the edges of the coverslips were coated with silver paint before imaging. SEM imaging was carried out at the standard setting of 5Kv and images were taken at x3k magnification.

2.18 FLUORESCENCE IMAGING

Images of cells, spinal cord organotypic slices and chick embryo cryosectioned slices were taken under a fluorescence microscope (Leica DMC 2500 LED) equipped with a CCD camera (DFC350 FX) unless stated otherwise. The software used for imaging was Leica Application Suite X v.1 (2017). All spinal cord slice images were taken at consistent light exposure parameters throughout the experiments. Images from chick embryo whole mount staining were obtained with a Zeiss Axiozoom v16. and z-stack images were obtained with an AxioObserver.Z1 equipped with an AxioCam MRm. Both microscopes were powered by Zen 2 (blue edition) software (Carl Zeiss MicroImaging GmbH, Goettingen, Germany).

Cryosectioned chick embryos were imaged at 50x magnification (with as many fields as necessary to acquire an image of the full section). Organotypic spinal cord slices (**Chapters 3 and 6**) were imaged at 5x magnification (1 field), 100x magnification (1 field), 200x magnifications (with as many fields as necessary to acquire an image of the full width of the lesion) and 40x magnification in 3 areas: slice centre, lesion edge and

lesion gap (3 fields/area). Cells on glass coverslips or on biomaterials (**Chapter 4 and 5**) were imaged at 5x magnification (1 field) and 400x magnification (3 fields/sample).

Image processing and data acquisition from images was done with the software ImageJ Fiji and all statistical analysis of data was carried out with GraphPad Prism unless stated otherwise.

2.19 QUANTIFICATION AND STATISTICAL ANALYSIS OF NEURAL STEM CELL CULTURE ON BIOMATERIALS

For these experiments, each mouse litter was counted as one biological repeat or 'n'. A non-Gaussian distribution was assumed for all data sets and all statistical analyses were carried out using GraphPad Prism unless stated otherwise. Unless stated otherwise, data significance was analysed with a non-parametric Kruskal-Wallis test and all values are expressed as the mean ± standard error of the mean. For each experimental group, at least 170 cells were counted in each biological repeat.

2.19.1 Survival

DAPI staining was used to count the total number of cells for each field and compared to the number of Ethidium homodimer positive nuclei (which colocalised with DAPI). For each sample, the results from each field were added and the percentage of dead cells was calculated. The resulting value was subtracted from 100% to obtain a survival percentage. Finally, the survival percentage for each biological repeat was averaged and plotted.

2.19.2 Proliferation

Similarly to survival analysis, DAPI staining was used to count the total cell number per field. Then, those nuclei which were also positive for Edu were counted. The results for each field were added and a percentage of Edu-positive cells was calculated. Then, the percentages for each biological repeat were averaged and plotted.

2.19.3 Cellular markers

DAPI staining was used to count the total cell number per field. Then, those cells which were also positive for the relevant cellular marker (Nestin, Sox-2, GFAP, Tuj-1 or myelin basic protein (MBP)) were counted. The results for each field were added and a percentage of marker-positive cells were calculated. Then, the percentages for each biological repeat were averaged and plotted.

2.19.4 Neurosphere formation

Cell distribution on **Chapter 4** was analysed as the number of neurospheres/μm^2. A group of cells was counted as a neurosphere only if it was visible in 5x magnification images in a spherical formation, detached from other cell groups and with a maximum diameter of 100μm.

2.19.5 Cell and fibre alignment

The alignment of cells and fibres was analysed for **Chapter 5**. The cell and fibre orientation for each sample was automatically calculated with the "Directionality" plug-in for ImageJ Fiji. For each sample, a low magnification fluorescence image (showing the stained cells) and the corresponding bright field image (showing the fibres) were analysed. A Fourier components method was selected as the analytical pathway to calculate the orientation of fibres and cells in the image within a 90º to -90º angle range, as seen in **Figure 2.9 A, B**. The resulting list indicating the number of structures in a given direction (**Figure 2.9 C**) was used later for analysis.

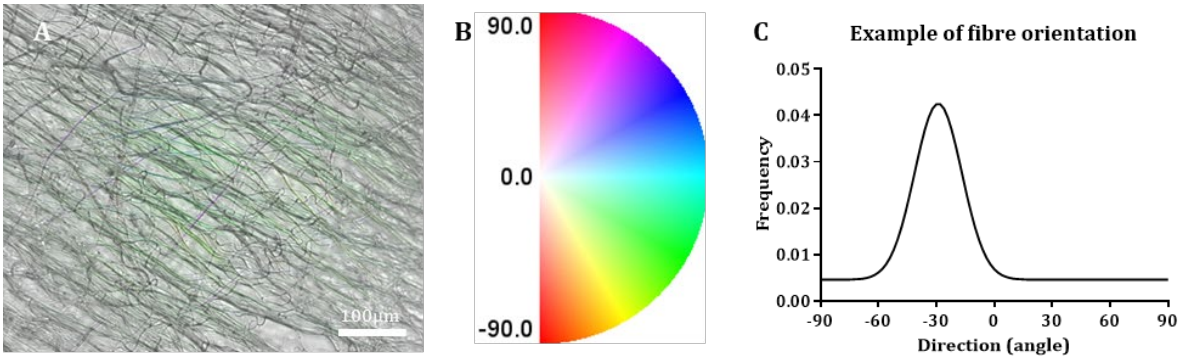

Figure 2.9 Orientation analysis protocol*. Example of fibre orientation analysis. (**A**) Representative light microscopy image of aligned Cellevate™ fibres. The coloured areas represent those that will be analysed by the software. (**B**) Legend indicating the colour that represents each angle from -90° to 90°. (**C**) Example of the resulting graph indicating the frequency (Y-axis) at which fibres are present for each direction (X-axis).*

To confirm that the images of the aligned Cellevate™ constructs showed aligned fibres and that the images of random constructs were completely random, the exact orientation peak (angle in which more fibres are oriented) of the data acquired from the bright field images was found with Excel Office using the following formula. For example, the orientation peak in **Figure 2.9 C** would be approx. -30°C.

$$f(x) = IF(AND(X2 > X1, X2 > X3),\text{"PEAK"},\text{"0"})$$

Then, values were systematically corrected, such that the most highly represented direction was referred to as zero angle (0°), with all orientations now being represented as deviations from this "zero" angle (**Figure 2.10**), a process equivalent to rotating the original image to obtain horizontal fibres. The rotation process aimed to normalise the data for future comparison between biological repeats. Therefore, this process was repeated for each biological repeat and the rotated frequencies were averaged and plotted for both random and aligned fibres (these plots were created with ggplot2 in R studio).

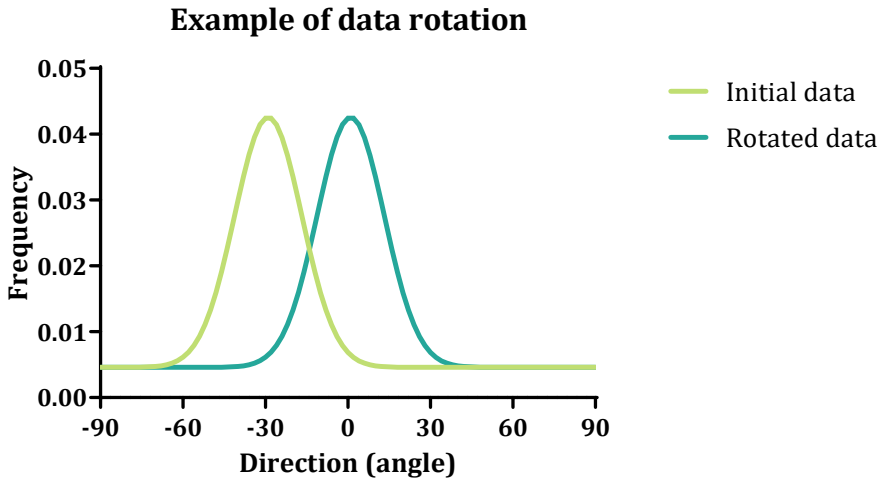

Figure 2.10 Data rotation protocol*. Example of data rotation showing data plotted before rotation (with peak at -30°) and after rotation (peak at 0°).*

The area under the curve of the orientation peaks (between the angles -30° and 30°) was calculated for both random and aligned fibres in each biological repeat and normalised in respect to the total area under the curve. This was done in order to compare the relative number of aligned fibres in aligned constructs *vs.* random constructs. Then, the results were plotted and analysed with a Wilcoxon test for paired samples.

A similar process was followed to determine cell orientation. In this case, the orientation peak was determined only on the bright field image for aligned fibres and rotated to 0º. The orientation data from the other images (fluorescence on aligned fibres, bright field on random fibres and fluorescence on random fibres) was rotated symmetrically according to the peak on the bright field aligned fibres. The process was repeated for each biological repeat and the resulting data was averaged and plotted. These XY orientation graphs, were designed using ggplot2 in R studio.

Next, in order to statistically determine whether the cells were following a similar orientation pattern as the fibres they were seeded on, a correlation coefficient was calculated. To analyse the correlation coefficient of the cell orientation versus the fibre

orientation, the previously averaged data sets were plotted in a linear graph, with the fibre frequencies for each orientation in the X-axis and the cell frequencies for each orientation as the Y-axis. A two-tailed Spearman correlation test with a 95% confidence interval was carried out to test for significance.

2.20 QUANTIFICATION AND STATISTICAL ANALYSIS OF ORGANOTYPIC SPINAL CORD SLICES

2.20.1 Survival

Images of stained spinal cords taken at 5x magnification were used for this analysis. First, the images for each channel (red and green for Ethidium homodimer staining and Calcein AM staining respectively) were converted to 8-bit, inverted and calibrated. Then, the optical density (OD) background value was obtained for each channel as the mean OD of 5 different areas of the image outside the spinal cord. Then, the mean OD value of the full image for each channel was obtained and corrected by subtracting the background. The corrected values were added to obtain a total fluorescence value and, finally, a viability index was obtained as the percentage of corrected viable OD relative to the total OD value.

The survival data for **Chapter 3** was analysed with a two-way ANOVA and Tukey correction test due to the presence of two independent variables and more than two groups. The data for **Chapter 6**, was analysed in a similar fashion. However, a Kruskal-Wallis test with Dunn's correction was chosen due to there being only one independent variable and more than two groups. The viability analysis for infiltrated cells on Hemopatch™ was carried out the same way as the spinal cord slice but only for the section occupied by the Hemopatch™ piece instead of the whole image. Statistical significance was tested with a Mann-Whitney test due to there being only one independent variable and two groups.

2.20.2 GFAP expression

5x images of GFAP stained spinal cords were converted to 8-bit, inverted and calibrated. A 400µm line was drawn from the lesion margin towards the centre of the slice and the OD profile of the line was generated (**Figure 2.11**). The process was repeated three times along the width of the slice and the OD values of each distance point were averaged. Then, the OD value of the baseline was calculated by averaging the mean OD value of three different regions outside the slice in each image. Finally, the baseline value was subtracted from the previously averaged slice OD values to obtain a corrected OD value for each spinal cord.

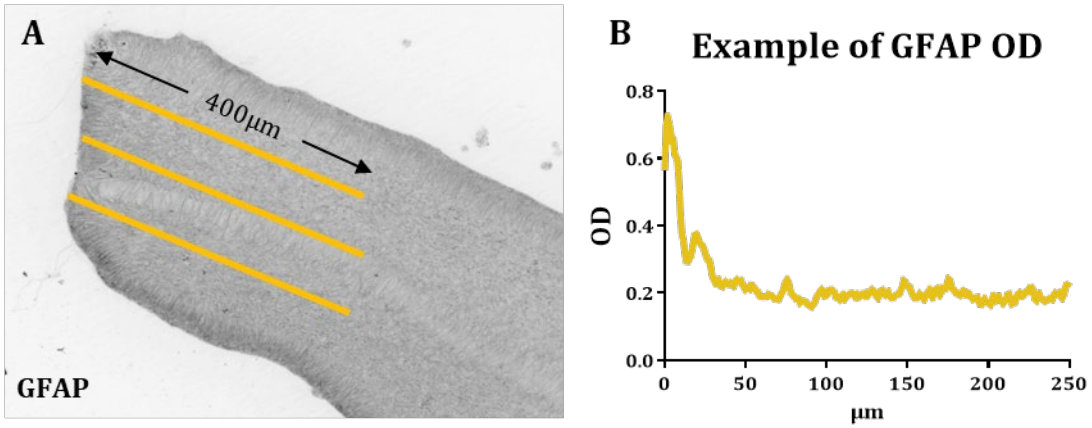

Figure 2.11 GFAP analysis protocol*. Example of GFAP OD analysis. (**A**) Representative image of an inverted GFAP fluorescent image. The yellow lines represent the lines from which the OD values were calculated. (**B**) Graphical representation of the OD values obtained in one of the lines from **A**.*

According to their position relative to the lesion edge, the values from each spinal cord were grouped in three groups: 0-10µm, 50-60µm and 100-110µm. The values from each group were averaged so as to obtain a mean OD value from each distance.

A repeated measures two-way ANOVA with Sidak's multiple comparison test was used to statistically analyse the data.

2.20.3 Optimisation of the analysis of axonal infiltration in the lesion gap

20x magnification consecutive images of the whole width of the lesion were fused together in a panoramic image using Microsoft PowerPoint 2016 and opened with ImageJ

Fiji, converted to 8-bit, inverted and calibrated. Then, a single line was traced above the lesion margin following the length of the spinal cord. In those cases in which the lesion margin was not flat, multiple lines were traced in order to avoid the line overlapping with the slice (**Figure 2.12 A**). The OD profile of the line was plotted (**Figure 2.12 B**) and the values were transferred into a Microsoft Excel 2016 sheet. Each OD peak in the plot corresponded with a fibre sprouting from the slice. The following formula was used to determine those values that were higher than the previous and following ones, which corresponded to the peaks in the plot (A. P. Weightman et al., 2014):

$$f(x) = IF(AND(X1 < X2, X3 < X2), "1", "0")$$

Each peak value was given a value of 1 in the next column, whereas the rest of the numbers were given a value of 0. These were then added to obtain the total number of peaks or fibres sprouting from that spinal cord. Finally, the exact width of the spinal cord slice was measured from a 5x magnification image and the number of peaks/mm was calculated.

This protocol, however, seemed to account for debris and background staining as if they were sprouting fibres. Therefore, a Pearson correlation test between these results and manually counted axons was carried out using GraphPad Prism (95% confidence interval) (**Figure 2.13 C**).

The negative, non-significant correlation result (r=-0.41) suggested that the number of peaks that were automatically counted using OD did not correlate with the manually counted fibres. In fact, the results differed by more than 10-fold. For this reason, this quantification method was discontinued.

In order to eliminate the background, a threshold was applied to the image (**Figure 2.12 D**). The threshold value was calculated as the mean OD value of the whole panoramic image. Following this, the same method of quantification and formula were used and compared to the manual count. The positive correlation result (r=0.54) (**Figure 2.12 E**)

seemed to indicate that this quantification method was more reliable, however, it was not significant. For this reason, we decided to base the analysis of sprouting fibres on the manual quantification procedure rather than an automated analysis.

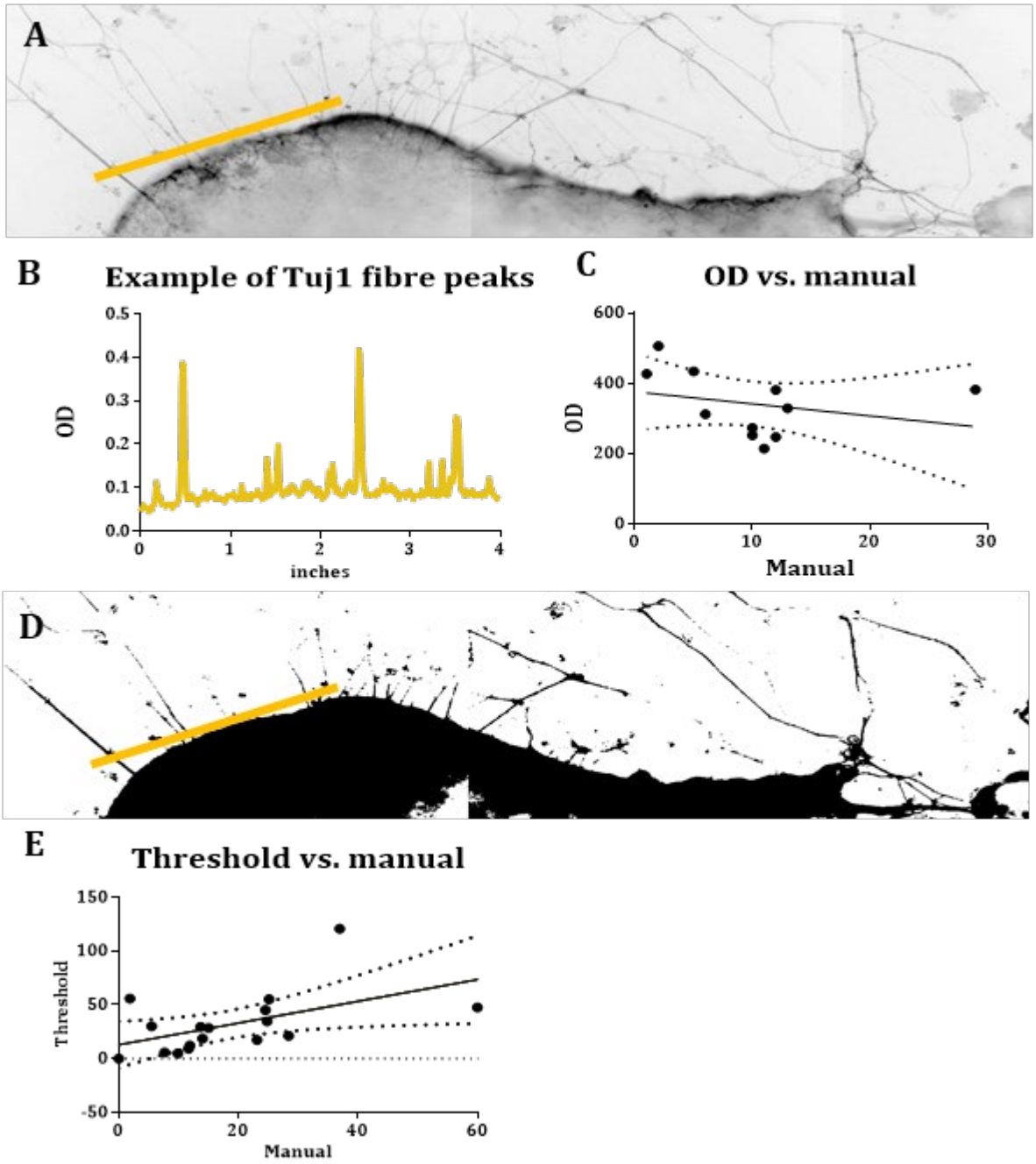

Figure 2.12 Tuj-1 analysis manual optimisation*. (**A**) Inverted panoramic fluorescence image of Tuj-1. Yellow line represents the area at which OD values were obtained. (**B**) Graph representing the OD profile of putative sprouting Tuj-1 fibres. (**C**) Correlation of manual count vs. OD count. (**D**) Inverted panoramic fluorescence image of Tuj-1 after threshold application. (**E**) Correlation of manual count vs. OD count after threshold application.*

2.20.4 Axonal infiltration in the lesion gap

In **Chapter 3**, the total number of axons infiltrating the lesion gap was analysed. 20x magnification consecutive images of the whole width of the lesion were fused together in a panoramic image using Microsoft PowerPoint 2016 and opened in ImageJ Fiji, converted to 8-bit and inverted. All axons that were sprouting from the lesion margin into the lesion gap were counted and divided by the full width of the slice (mm).

However, this protocol was not usable after biomaterial implantation (**Chapter 6**). Due to the intricate web of axonal infiltration within the material, it was impossible to count single axons. Therefore, the total length of all infiltrated axons was calculated instead (**Section 2.20.6**).

2.20.5 Optimisation of measuring total length of infiltrated axons analysis

In **Chapter 6**, 40x images taken at random areas of the injury gap or in implanted Hemopatch™ were either opened with the ImageJ plugin "Axon Tracer" (for an automated quantification) or converted to 8-bit and uploaded in the plug in "NeuronJ" (for a manual quantification) (**Figure 2.13 A-D**). The axons present in the image were either manually

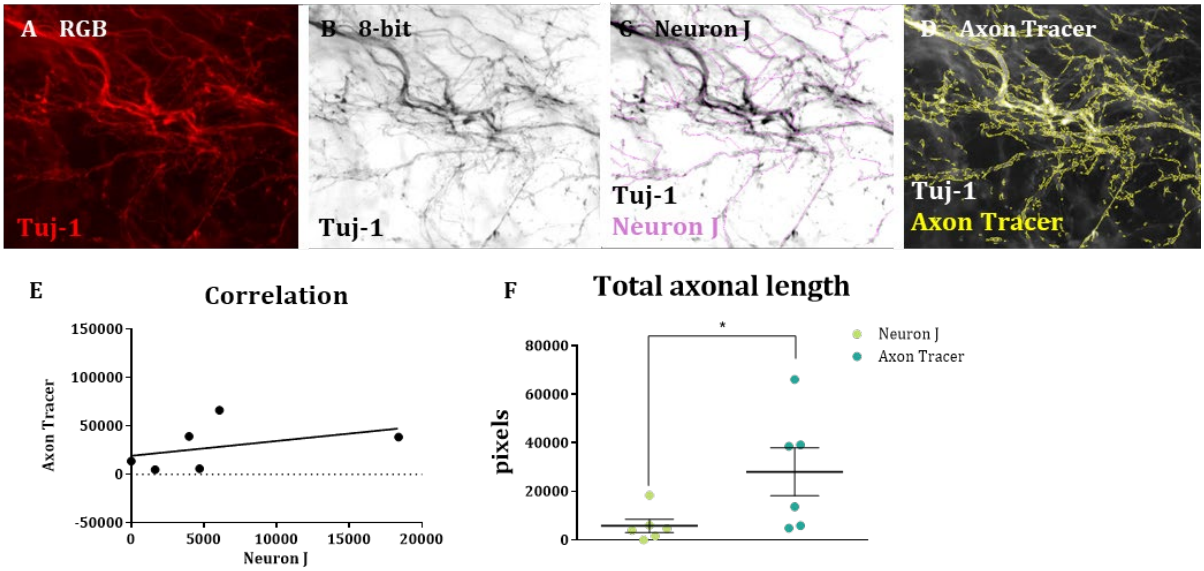

***Figure 2.13 Tuj-1 analysis automated optimisation**. (**A**) Original Tuj-1 fluorescence image. (**B**) Image converted to 8-bit and inverted. (**C**) Neuronal fibres manually traced with NeuronJ. (**D**) Neuronal fibres automatically traced with Axon Tracer. (**E**) Correlation of axonal length counted with Neuron J (X-axis) vs. Axon Tracer (Y-axis). (**F**) Graph representing the significant difference between the total axonal length counted with each method.*

traced on NeuronJ or automatically picked up by Axon Tracer to obtain the total axonal length in each image.

The results of these analytical methods were positively correlated (r=0.486) (**Figure 2.13 E**), but the automated method seemed to account for debris or unspecific staining for axons and, therefore, counting approximately two-fold more axons than the manual approach (Mann-Whitney test, p=0.041) (**Figure 2.14 F**). Therefore, the total axonal length was quantified using NeuronJ.

2.20.6 Total axonal length in the injury gap

In **Chapter 6**, from each spinal cord, three 40x images were taken at random areas of the lesion gap or the implanted Hemopatch™ and uploaded on NeuronJ. The axons were traced and the total length of traced axons in μm was obtained. The results from each field were added and then averaged with the other spinal cords from the same experimental group. A Kruskal-Wallis test with Dunn's correction was performed for statistical analysis.

2.20.7 MBP expression

40x images were taken at the centre of the spinal cord, the edge of the lesion and the lesion gap or Hemopatch™. The total length of MBP positive tracts in each image was quantified using NeuronJ. The results of each area were added to obtain a total length of myelinated tracts in each spinal cord. Then, a percentage of myelinated tracts was calculated for each region relative to the total myelinated tracts in that spinal cord. Finally, the results for each area were averaged with the other spinal cords and plotted. A repeated measures two-way ANOVA with Sidak's multiple comparison test was performed for statistical analysis.

2.20.8 Lectin expression

Lectin quantification was achieved by counting the number of lectin-positive cells that were detached from the spinal cord slice per unit area (1 mm^2) at the lesion site using a

standard size grid overlaid onto each image. The total number of lectin positive cells per area was averaged for each slice. The results were plotted and statistically analysed with a Kruskall-Wallis test with Dunn's correction.

3 ESTABLISHMENT OF THE CHICK EMBRYO AS A SPINAL CORD INJURY MODEL

3.1 BACKGROUND

3.1.1 Requirements for alternative spinal cord injury models as tissue engineering platforms

As covered in **Chapter 1**, numerous clinical and preclinical treatments for SCI are currently being investigated, such as the delivery of a replacement cell population to the injury site, the implantation of pro-regenerative biomaterials to bridge the lesion gap or a combination of both. Testing these new therapies is usually carried out in rodents (Sharif-Alhoseini et al., 2017) due to the high costs and ethical implications of using large mammals or primates. However, rodent models also require ethical approval, which might take years to acquire, are associated with high maintenance costs and require housing facilities, professional caring personnel and food supply which, in turn, inflate the cost of experimentation. In contrast, the exponentially increasing numbers of new biomaterials and various treatment ramifications to be tested need a trial platform that is easy, cost-effective and free of ethical implications.

The chick embryo spinal cord possesses all major cell types and neural system tracts when compared to that of an adult human (Ferretti & Whalley, 2008). Furthermore, the embryo develops inside an egg, which makes it easily accessible and technically straightforward. Moreover, chick embryo maintenance requires the space of a standard cell incubator compared to a full animal facility and does not require food supply, as everything the embryo needs is inside the egg. The oviparous nature of the chicken also allows for embryonic studies while preserving the mother's life. The nervous tracts that allow the embryo to feel pain are not fully formed until E13 (Okado & Oppenheim, 1985), because of this, experimentation before E14 does not require licensing under ASPA

(1986). Furthermore, it is simple and cost-effective meaning it could be adopted widely by various laboratories.

3.1.2 Relevance of the chick embryo as a spinal cord injury model

The chick embryo has already been used as a model for spinal cord injury. In 1990, a research group studied the differences between spinal cord regeneration after transections made at E2, E5, E10 and E15 (Shimizu et al., 1990). Their results suggest that spinal cord regeneration is possible before E10, but for transections made at E15, regeneration is not possible anymore. They showed that after an E2 transection, full continuity of the neural tube was restored at 12h post-surgery. After an E5 transection, restoration was completed in 48h and between 2 to 8 days after E10 surgery. In these three cases, some chicks were aided to hatch or were able to do it on their own, but their post-hatching behaviour was no different from that of sham chicks. On the contrary, neural tube continuity was not restored after E15 transections and those chicks showed degenerating axons by E19. Moreover, none of them was able to hatch on their own or to support their weight afterwards.

In 1993, Hasan et al. narrowed down this time period when they showed that regenerating axons were only observed before E13. In their experiments they injected two retrograde labelling dyes: the first one was injected two days before transection and the second one 7 to 8 days post-transection. Double labelled axons suggest that repair is due to a true regeneration process. Their results showed that the percentage of double-labelled brainstem-spinal cord neurons was 5.1% for transections made at E10, and 21.7% for transections made at E12 compared to 0% for transections made after E13.

Whalley et al., (2006) suggested that the main difference between the regeneration permissive stage and the non-permissive stage was the tissue vascularization. They showed that vascularisation increased significantly around E13 and that increase was

associated with an increase of apoptotic cells and tissue cavitation after injury. Moreover, the use of desmopressin in E15 embryos to reduce haemorrhage, resulted in less apoptotic cells and less cavitation, similar to E11. On the other hand, injection of diazepam to increase haemorrhage in E11 embryos resulted in a similar injury to that of E15 embryos.

Given the regenerative potential of NSCs, the response of endogenous NSCs to injury has also been studied in the chick embryo. In this case, it was demonstrated that, at E16, healthy NSC proliferation decreases significantly compared to E11. Interestingly, after an injury made at E11, neurogenesis does not increase. However, after an injury made at E16, NSC proliferation increases, probably resulting in new born glial cells instead of neurons (Whalley et al., 2009). This increase in NSC proliferation after SCI has also been observed in rodent models, leading to the formation of new reactive astrocytes within the centre of the glial scar and oligodendrocytes in the surrounding white matter (Grégoire et al., 2015).

The chick embryo has also been used to test stem cell behaviour post-transplantation into the spinal cord. Delivery of human hematopoietic stem cells (HSC) within the spinal cord of E3 chick embryos, results in the differentiation of these HSC into neurons, but only in a regenerative environment after injury (Sigurjonsson et al., 2005). Moreover, injected NSC from adult mouse into the amniotic cavity of E1 chick embryos integrate into the host system and differentiate to give rise to adult neurons (Clarke et al., 2000). These results highlight the potential of exogenous cell implantation within the chick embryo SCI. Moreover, they indicate the possibility of interfacing NSCs from a different species (*i.e.:* human or mouse) into the chick embryo tissue for experimental purposes.

Despite these promising findings, no-one has yet investigated whether we could use the chick embryo as a model in which to test cell-biomaterial combinatorial therapies designed to repair the spinal cord.

3.1.3 Physiological relevance of the spinal cord organotypic culture for spinal cord injury

Whilst *in vivo* models of SCI based on the chick embryo may be a viable option, as highlighted in the **Chapter 1**, organotypic slice cultures are an alternative *ex vivo* technique that aims to represent the *in vivo* structure and function of a specific organ or tissue in isolation from the body. They differ from *in vitro* cellular cultures in that they preserve the tissue structure and cellular connections, providing the system with more *in vivo*-like properties. This is due to the preservation of cell-cell and cell-ECM intercellular junctions, which are not represented in 2D models (Shamir & Ewald, 2014). Moreover, the *in vitro* aspect of such cultures provides the system with easier manipulation and analysis procedures than those used in *in vivo* research.

The suitability of organotypic slice cultures as SCI models has been investigated extensively in rodent models. A recent study aimed to assess cellular viability of the slices after different types of lesion infliction in live rats: stab, contusion and transection. Over 10 days of culture, all slices showed more live cells than dead after injury, although uninjured controls showed a higher viability rate. Only in the case of transected slices, a reduction in cell viability was observed over time (Patar et al., 2019b).

After 2 weeks of culture, sagittal slices of mouse spinal cords were reported to maintain neuronal survival and differentiation, and the characteristic ventro-dorsal polarity of the spinal cord was preserved (Bonnici & Kapfhammer, 2008). The presence of synaptic contacts and oligodendrocytic myelination were also reported in the same cultures (Bonnici & Kapfhammer, 2008). One week after transection, the injury gap was easily

recognised due to the inability of the majority of fibres to regenerate. In fact, the number of spontaneous regenerating axons decreased with the maturation of the slice *in vitro* but not with the age of the donor from P0 to P6 (Bonnici & Kapfhammer, 2008).

Organotypic slices have also been reported to present *in vivo*-like glial responses to physical insult such as an increase in reactive astrocytes and NG-2 proteoglycans 10 days after a stab or a transection injury in rats (Patar et al., 2019a). Six days after a complete transecting injury, mouse spinal cord organotypic slices presented signs of reactive astrocytes and limited nerve fibre outgrowth (Weightman et al., 2014).

3.1.4 The chick embryo as a donor for organotypic spinal cord slices

There are several examples of successful chick embryo spinal cord organotypic slices. One of the first models was established as a proof of concept to add validity to the study of the CNS *in vitro*. Spinal cord slices were obtained from E10 chick embryos and cultured for up to 16 days during which the uptake kinetics of neurotransmitters were studied (Tunnicliff et al., 1973). A similar culture was used to study the development of cutaneous sensory projections in the spinal cord. Spinal cords with attached dorsal root ganglia and peripheral nerves were dissected in thick transversal slices from E5-E7 embryos and were maintained *in vitro* for 2-3 days (Sharma et al., 1994; Sharma et al., 1998). Neurite outgrowth in 3D has also been examined after embedding E7 chick embryo transversal slices of spinal cord in a fibrin matrix. Neurites from the young embryonic tissue grew radially and reached lengths up to 3mm after 5 days without treatment (Rösner & Vacun, 1997).

The first case of testing neuroregeneration in chick embryo spinal cord slices was aimed at screening drugs for motor neuron disease. The transversal slices, which were obtained from E16 embryos, provided a model with mature, target independent motoneurons, that could be maintained for at least 4 weeks *in vitro* (Brunet et al., 2007). This model was later

used as a platform for screening glutamate receptor agonist and antagonist drugs, which appear to play an important role in motoneuron degeneration in amyotrophic lateral sclerosis (Núria Brunet et al., 2009; J. Calderó et al., 2010).

Despite clear advantages shared by both organotypic slice cultures and the chick embryo as a model, such a system has never been established.

3.1.5 Knowledge gaps and aims

In summary, protocols for administering a SCI to the chick embryo have been established, with similar responses to that of adult injury. As also described, organotypic slices have been repeatedly demonstrated to provide a physiologically relevant model of spinal cord injury, mostly using rodent tissue. These types of slices have also been successfully derived from the chick embryo at different developmental stages. However, longitudinal spinal cord slices have never been derived from the chick embryo spinal cord. Further, it has never been tested whether a transecting injury can be induced in the slices and the subsequent response to this injury has not been investigated.

Consequently, the aims of this chapter are to investigate:

1. The feasibility of establishing a SCI in the chick embryo with implantation of a bioscaffold.
2. The feasibility of establishing organotypic spinal cord slices from chick embryo tissue.
3. The neuropathological responses to a transecting injury in organotypic spinal cord slices from chick embryo tissue.

3.2 RESULTS

3.2.1 Shell-less culture of chick embryos was feasible and allowed greater access for manipulation

Fertilised chicken eggs were purchased and the embryos were incubated either inside their shells in a specialised incubator or removed from the shell and placed into culture vessels inside the incubator (**Chapter 2**) in order to test which culture type offered easier access for a transecting lesion.

A total of 74 chick embryos were incubated in their shell (**Figure 3.1 A**) and a total of 28 embryos were incubated outside their shell (shell-less) (**Figure 3.1 B**). A small window was opened on the shell of the first group to introduce a transecting lesion in the spinal cord of E5 embryos, while the second group were already exposed and the lesion was inflicted without the need of windowing.

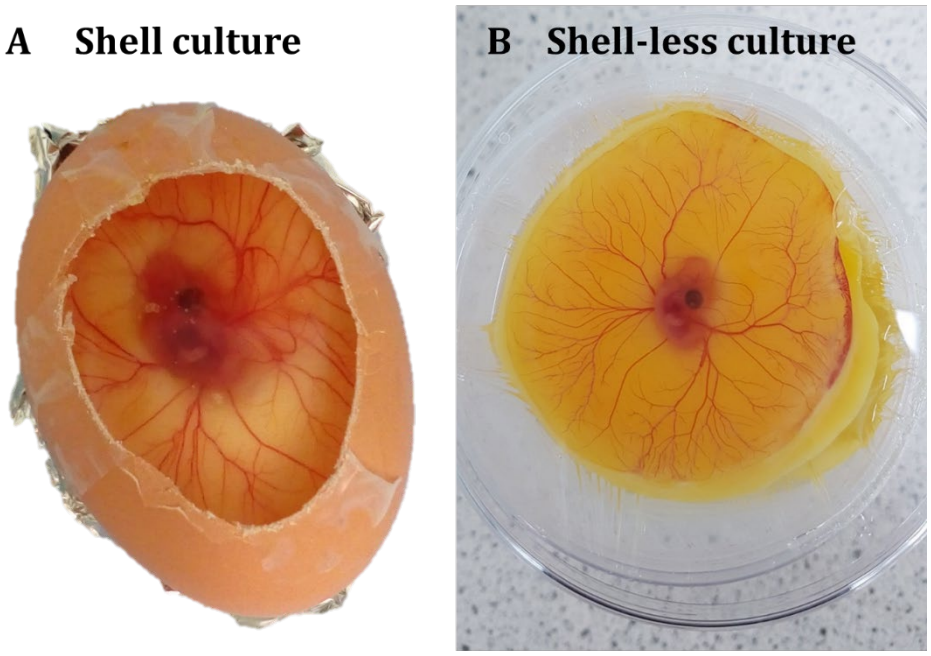

***Figure 3.1 Chick embryo culture**. Representative images of E5 chick embryos in shell (**A**) and shell-less cultures (**B**).*

As shown in **Figure 3.2 A**, embryo survival was higher for Shell cultured embryos than those cultured using our first Shell-less procedures. As the survival curve in **Figure 3.2 B** shows, there was a point shortly after introducing the embryo into the culture vessel (E3)

where approximately 30% of embryos died (n=28). This potentially suggests the embryos underwent trauma upon transfer to the vessel. Therefore, we refined the culture technique to try a gentler transfer of embryos into the vessel. Instead of cracking the egg straight into the vessel, 6mL of albumin were extracted from the egg and added to the vessel. Then, the top of the shell was cut off with a pair of fine scissors. Finally, the contents of the egg were gently poured into the vessel. This protocol change led to a marked improvement in survival. In more detail, it led to a 40% survival of embryos (n=29) compared to approximately 15% (n=28) when using the initial method. (**Figure 3.2 A, B**).

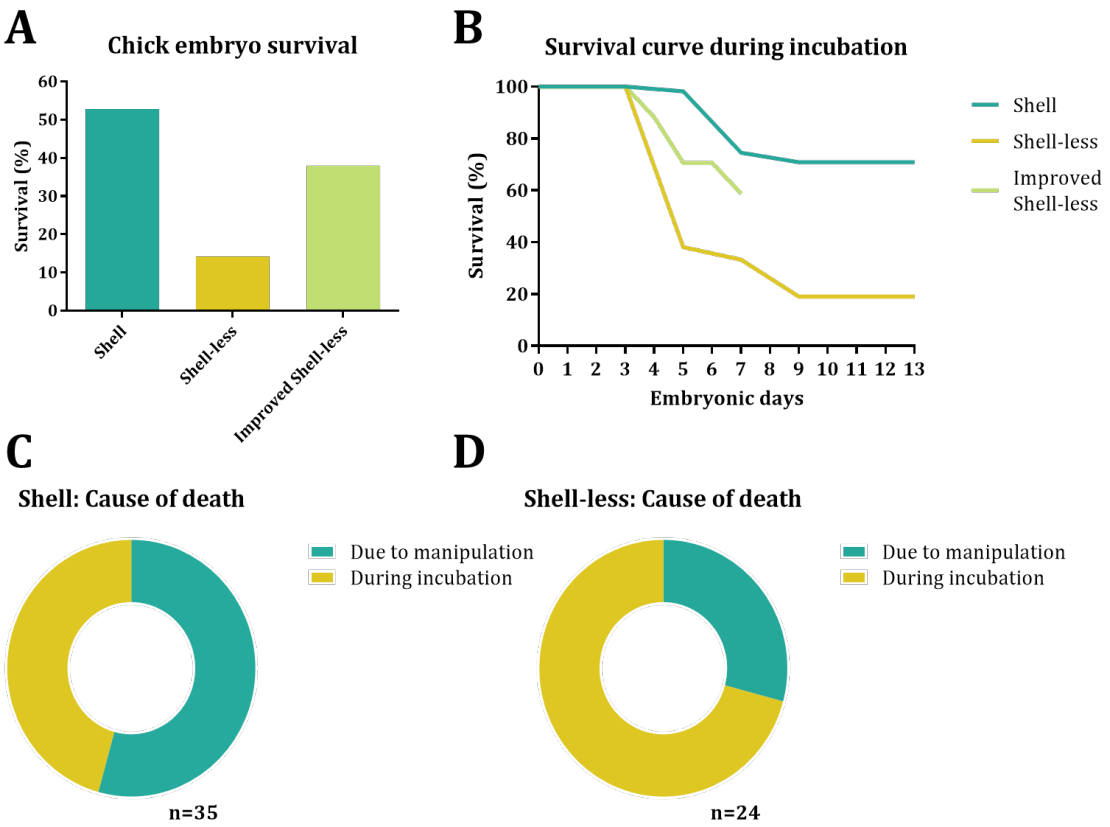

Figure 3.2 Chick embryo survival. *Graphical representations of chick embryo survival (**A**) and survival curve during incubation (**B**) in which only natural deaths that were not caused by manipulation were counted. Graphical representation of the cause of death in the "Shell" group (**C**) and in the "Shell-less" group (**D**). 35 embryos were used in the "Shell" group, 24 in the "Shell-less" group and 17 in the "improved shell-less" group. The percentages represent the percentage of embryos that survived relative to the total number of embryos in each group. The results are expressed as percentages. These graphs indicate that chick embryo survival decreases in the shell-less culture, but that manipulation is easier and leads to less deaths due to surgery.*

Embryo lesioning through a small window in the shell was challenging, especially at later developmental stages, mainly due to poor visibility and movement of the embryo combined with a small space to move the lesioning tools. In this regard, the Shell-less embryo provided a wider manoeuvre space, resulting in less deaths due to embryo surgery: 54.3% of deaths in the Shell culture (n=35) compared to 29.1% in the Shell-less culture (n=24) (**Figure 3.2 C, D**). A death due to surgery was described as such when a blood vessel was distinctively punctured, causing haemorrhage. Although survival of Shell-less embryos improved after the protocol optimisation, a decrease in survival was noted during incubation for unknown causes, mostly in the Shell-less group (**Figure 3.2 C, D**). These deaths, occurred mostly between E4 and E6 in the Shell culture and between E3-E4 in the Shell-less group, followed by another drop in survival between E5 and E9 (**Figure 3.2 B**).

3.2.2 *In vivo* chick embryo lesioning was successful

Under a dissection microscope, a thoracic transecting lesion was introduced with a 21-gauge needle (**Figure 3.3 A**). The lesioned embryos were then either removed from the egg for immediate fixation (E5) or the window was re-sealed with scotch tape and the embryos cultured for a further 24h (E6) and 48h (E7).

Whole mount staining of the embryo allowed for lesion localisation at high (**Figure 3.3 B**) and low magnification (**Figure 3.3 C, D**). In addition, key features of the developing spinal cord could be identified such the dorsal root ganglia and spinal nerves (**Figure 3.3 B**). Although it was possible to see axonal tracts, some areas were obscured, probably due to the thickness of the sample, making quantification of any possible regeneration unreliable.

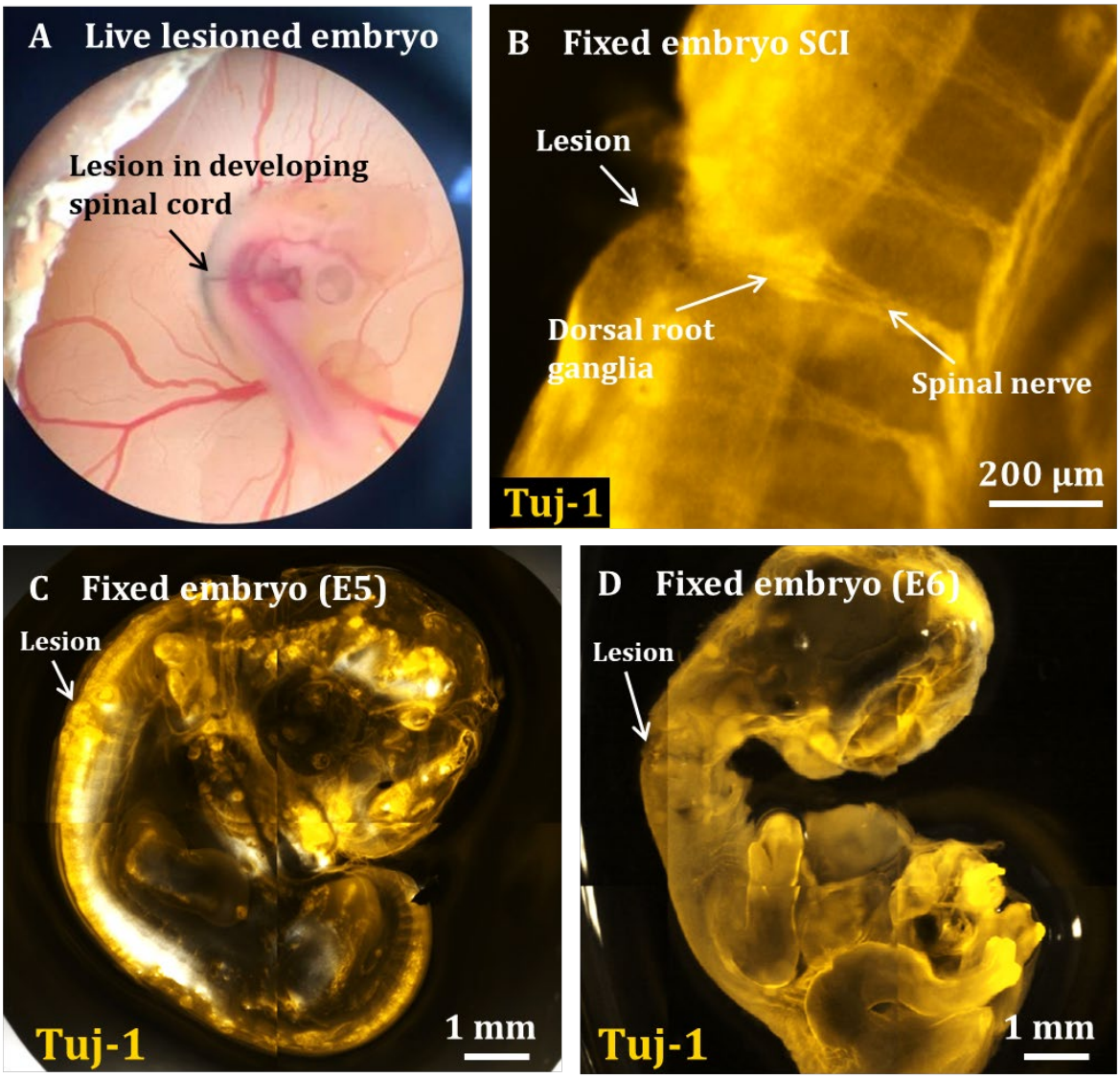

Figure 3.3. Whole-mount staining of chick embryos*. Representative image of a live E4 chick embryo in its shell and after lesioning. Lesion visible after injection of blue food colouring. Image donated by Dr. Chris Adams (**A**). Representative image of the lesion site (**B**) and the stained whole mount embryos at E5 (**C**) and E6 (**D**). B, C and D were stained using the neuronal marker Tuj-1. Whole-mount staining allowed for gross visualisation of spinal cord architecture.*

As an alternative method of visualising the lesioned spinal cord of chick embryos in higher detail, we employed cryosectioning and staining for nerve fibre marker Tuj-1 (**Chapter 2**). In a frontal section (**Figure 3.4 A-C**) it was possible to see the ascending and descending neuronal tracts surrounded by dorsal root ganglia. In the case of E5, the ascending and descending tracts are either developing or in a different plane, therefore, an apparent gap in the tracts appears at the centre of the spinal cord (**Figure 3.4 A**). At 24 and 48h post-injury the tracts were detected in the slices but we were not able to conclusively locate the injury, possibly due to regeneration of the tissue (**Figure 3.4 B, C**).

Tract swelling, which has previously been associated with a site of spinal injury in the chick embryo (Shimizu et al., 1990), was noted in E7 embryos, potentially indicating an area of regeneration after injury (**Figure 3.4 C**). The lack of injury detection in any of the sections, led us to slice sagittal sections of the spinal cord, in which a potential lesion gap was found (**Figure 3.4 D**).

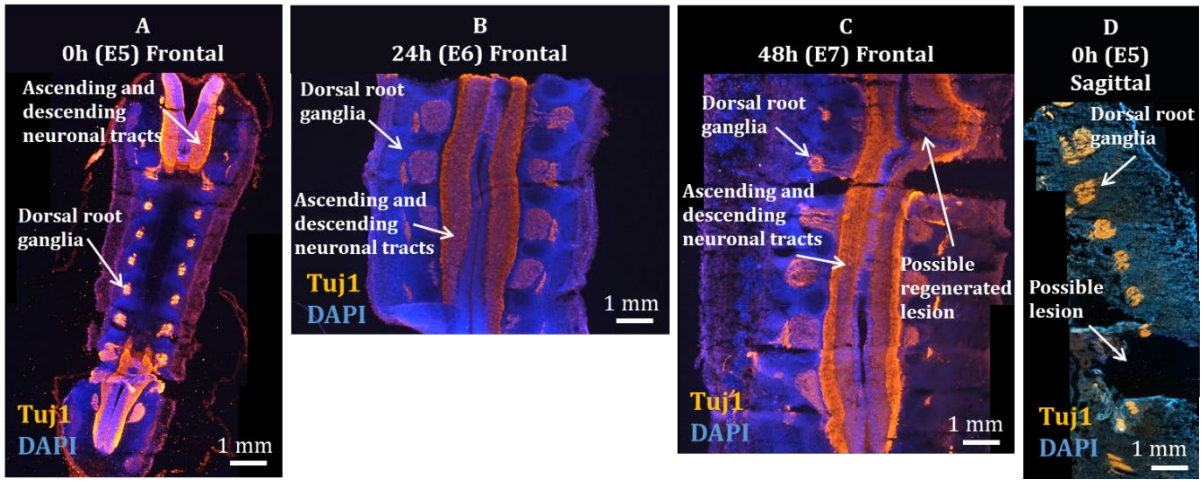

***Figure 3.4 Chick embryo spinal cord cryosectioning**. Representative fluorescence images of chick embryo spinal cords after cryosectioning frontally on E5 (0h post injury)) (**A**), E6 (24h) (**B**) and E7 (48h) (**C**) and sagitally on E5 (0h) (**D**). The slices were stained with Tuj-1 (orange) and DAPI (blue). Sagittal slices at 0h allowed for potential lesion gap visualisation.*

3.2.3 *In vivo* biomaterial implantation after injury was successful

After the establishment of the Shell-less culture and lesioning protocols we attempted a preliminary trial for implantation of Hemopatch™ in E5 lesioned embryos (**Figure 3.5**). Under microscopic observation it appeared that Hemopatch™ was successfully

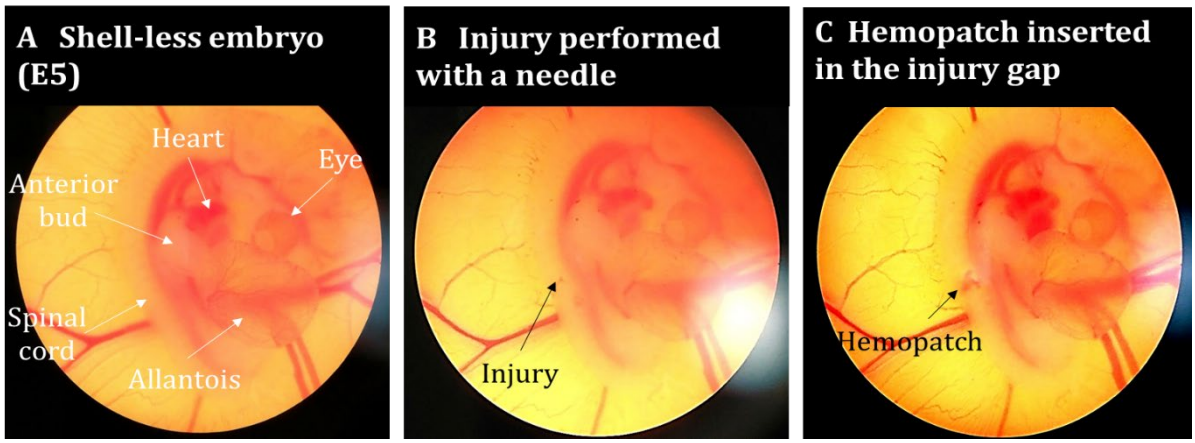

***Figure 3.5 Live chick embryo**. Representative frames from Video 1 showing a live embryo (**A**), the embryo after SCI (**B**) and after biomaterial implantation (**C**). HemopatchTM implantation was possible after lesioning.*

implanted into the lesion site (**Figure 3.5** and **Video 1**), without causing further damage to the tissue.

Posterior observation after DAB staining with a neuronal marker revealed the implant still in the injury site (**Figure 3.6**). Although the implant is near the ascending and descending axonal tracts, it seems that it is not fully inserted in the spinal cord (**Figure 3.6 C**). However there seemed to be axonal tracts infiltrating the implant (**Figure 3.6 D**).

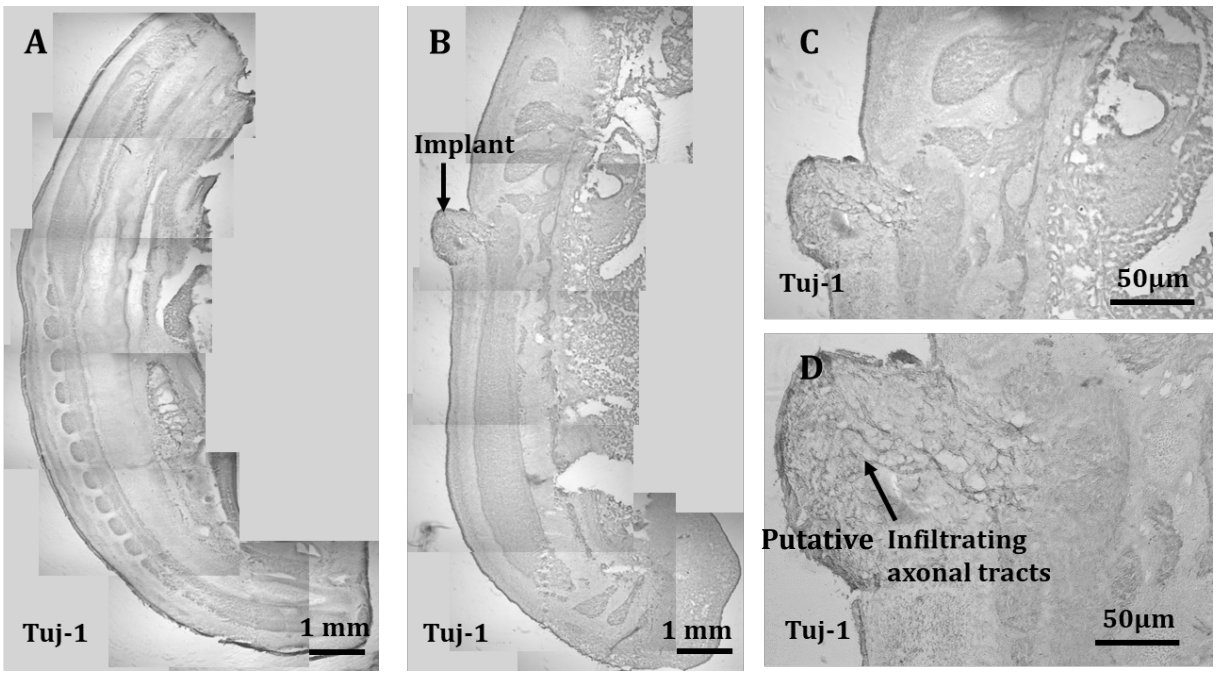

Figure 3.6 Chick embryo spinal cord after biomaterial implantation*. Representative images of cryosectioned spinal cord slices of a sham embryo (**A**) and after injury and biomaterial implantation (**B**). Images **C** and **D** show the implanted biomaterial at a higher magnification and putative axonal infiltration. Slices were stained with the neuronal marker Tuj-1 which was subsequently detected using DAB staining. Biomaterial implantation might have allowed axonal infiltration.*

Although survival rates increased after improving the culture technique and despite successfully inflicting a transecting lesion and implanting Hemopatch™, we were unable to reliably analyse possible cell regeneration with our current tools. Therefore, all further experiments were carried out with organotypic spinal cord slices.

3.2.4 Spinal cord organotypic slices were viable regardless of lesion or time point

In order to assess the cellular responses over time and to different lesioning times, we established 4 timepoints for lesioning and fixing the samples (**Chapter 2**).

All spinal cords were highly stained with Calcein AM, an indicator of cellular health, regardless of whether they had been lesioned or not (**Figure 3.7 A, B**). At high magnification it was possible to see single dead cells spread across the spinal cord (**Figure 3.7 C**), which were mostly accumulated outside the edges of the slice. Approximately, between 60 and 80% of the spinal cord was stained with Calcein AM. There were no statistically significant differences in survival between injured and uninjured slices or between time points (**Figure 3.7 D**).

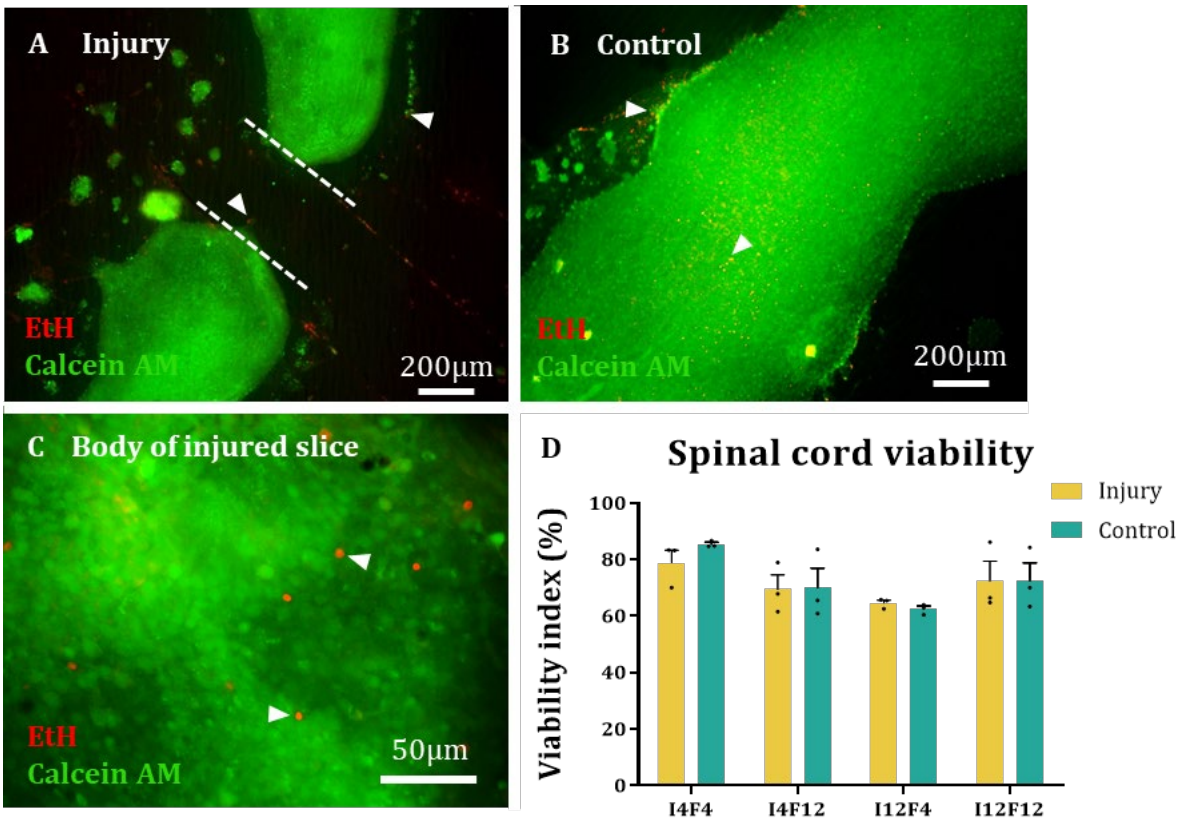

Figure 3.7 Survival of spinal cord organotypic slices*. Merged fluorescence images of the survival assay on an injured spinal cord organotypic slice (**A**) and on an uninjured slice (**B**) and a high magnification image showing the centre of an injured spinal cord slice away from the lesion (**C**). Green staining corresponds to live cells stained with Calcein AM and red staining corresponds to dead cells stained with Ethidium homodimer (EtH) in the centre of the spinal cord after injury. Arrows point at dead cells. All images correspond to the I4F12 time point. **D** depicts the graphical representation of the viability index for each timepoint (expressed as the percentage of Calcein AM staining compared to total OD of the image) and compares the viability of injured spinal cords vs. controls (Two-way ANOVA, n=3, p≥0.05). The percentages represent the Calcein AM OD relative to the total Calcein AM + Ethidium homodimer OD. Each dot in the graph represents one biological repeat (one organotypic slice). Spinal cord viability was similar in both injured and uninjured slices in all experimental groups.*

3.2.5 A reproducible transecting injury could be administered to the slice

All spinal cords were lesioned with a double-bladed scalpel to ensure a reproducible lesion width. After fixation and staining, the edges of the spinal cord were established as the areas where DAPI staining ended and the width of the lesion was calculated for 10 spinal cords from each group. Although in some cases one side of the spinal cord moved slightly from its original position during antibody washing, there were no statistical differences in lesion width between groups, with an average width ranging from *ca.* 400 to 500µm (**Figure 3.8**).

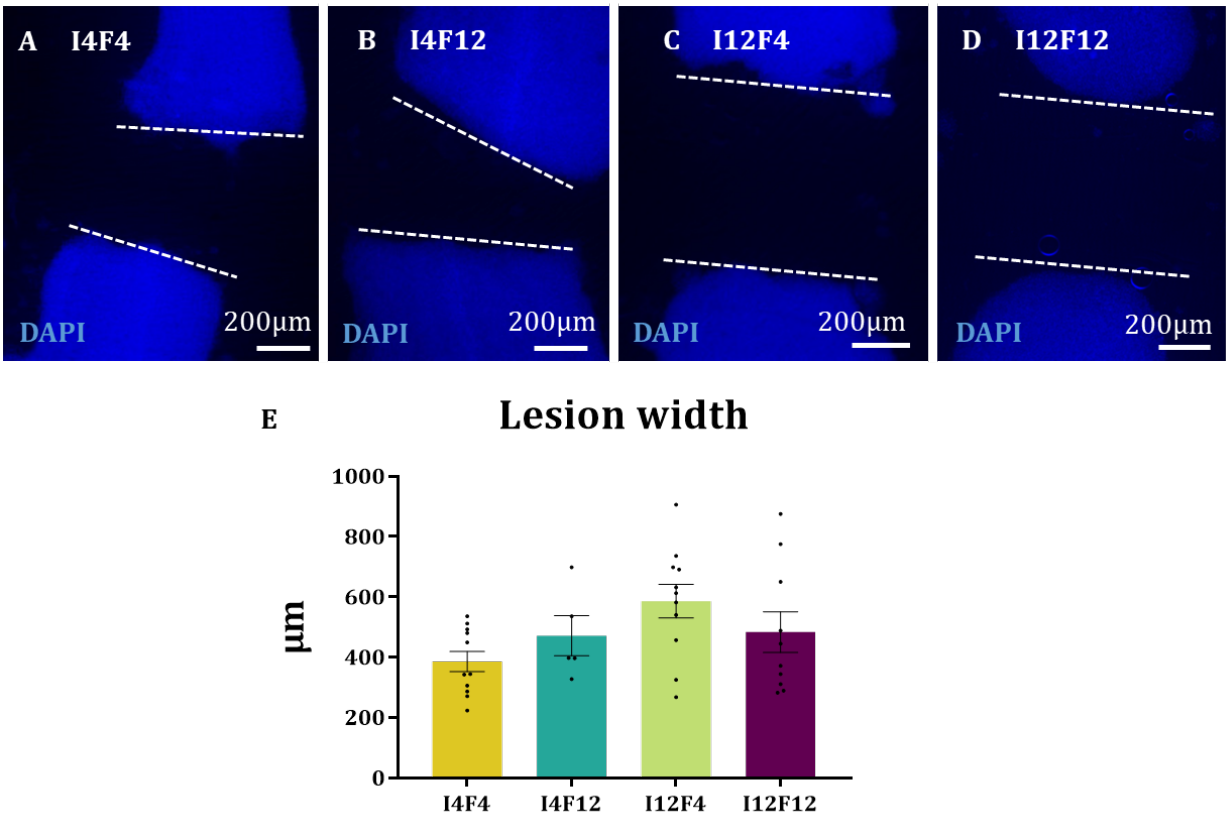

Figure 3.13 Width of SCI*. Representative DAPI images showing the lesion and the two slides of the spinal cord at each time point (**A-D**) and graphical representation of the lesion width across time points (One-way ANOVA, n=10, p≥0.05). Y axis represents the µm between the two edges of the lesion. Dots in graph represent one biological repeat (one organotypic slice) (**E**). Dotted lines represent the edges of the lesions. There were no statistical differences in lesion width across experimental groups.*

Following this, the cellular responses to injury were studied in order to characterise standard responses to injury. In particular: the formation of glial scar, impaired axonal regeneration, loss of myelination and microglial infiltration.

3.2.6 GFAP expression was higher at the edge of the lesion than at the centre of the spinal cord 12 days post injury.

To measure the possible formation of a glial scar in our injury slice models, we analysed GFAP expression. During microscopic observation it was noted that the lesion margins of some spinal cords were brighter than the centre of the spinal cord when stained with an anti-GFAP antibody (**Figure 3.9 A-D**). Upon observation at higher magnification, the GFAP-positive cells observed at the lesion margins of the slices with higher GFAP expression, presented distinct morphologies when compared to the centre of the slices. At the edge of the lesion, morphologies were characterised by elongated somas and processes, distributed in parallel to each other and perpendicularly to the lesion and at a high density (**Figure 3.9 E, F**). OD analyses revealed a significantly higher GFAP expression between 0-10μm from the lesion margin than at 50-60μm and 100-110μm from the lesion margin for the spinal cords that were fixed 12 days post injury (I4F12 ($p=0.006$) and I12F12 ($p=0.02$)). This higher GFAP expression was not seen for those that were fixed earlier, at 4 days post injury (I4F4 and I12F4) (**Figure 3.9 G**). In more detail, I4F4 presented OD levels of 0.097±0.04 at 0-10μm, 0.083±0.026 at 50-60μm and 0.076±0.023 at 100-110μm. I4F12 presented OD values of 0.092±0.033 at 0-10μm, 0.053±0.017 at 50-60μm and 0.046±0.012 at 100-110μm. I12F4 presented OD values of 0.068±0.05 at 0-10μm, 0.048±0.019 at 50-60μm and 0.046±0.017 at 100-110μm. Finally, I12F12 presented OD values of 0.063±0.007 at 0-10μm, 0.039±0.010 at 50-60μm and 0.035±0.007 at 100-110μm.

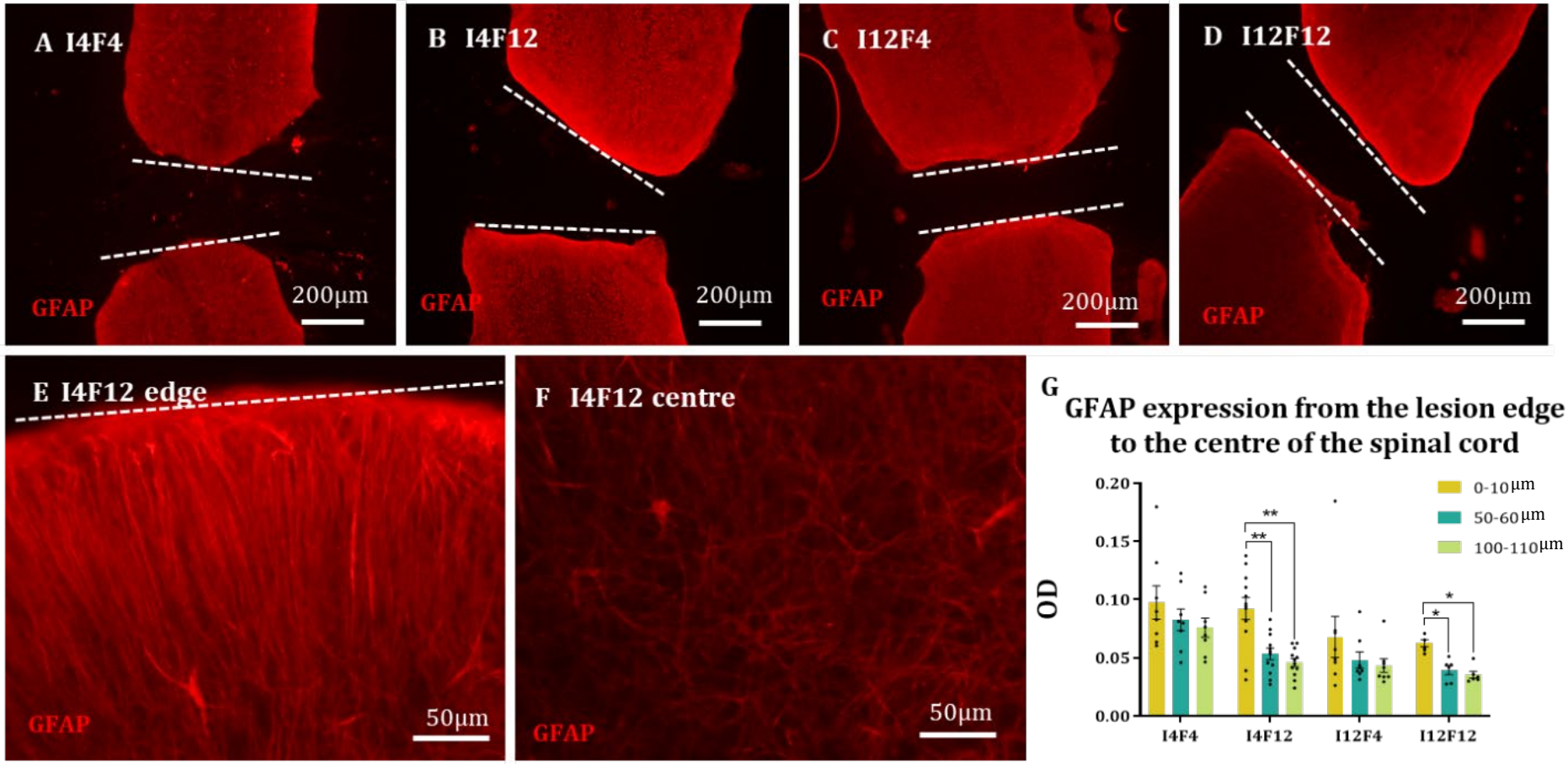

Figure 3.9 GFAP expression after injury*. Fluorescence images showing a spinal cord slice after lesioning and GFAP staining at low magnification at different time points (**A-D**) and high magnification at the lesion edge (**E**) and centre of the spinal cord (**F**). Dotted lines representing the edges of the lesions. The graph (**G**) represents the OD values of GFAP staining from the lesion edge (0-10µm) to the centre of the spinal cord (100-110µm) across all time points (Two-way ANOVA, I4F4: n=8, p≥0.05; I4F12: n=12, p=0.006; I12F4: n=8, p≥0.05; I12F12: n=6, p=0.02). * p<0.05; **p<0.01. Y axis refers to GFAP OD. GFAP OD values were higher at the edge of the lesion when slices were fixed 12 days after injury.*

3.2.7 Regenerating axons were observed in the lesion gap but never reconnecting both sides

Tuj-1 staining allowed for the detection of regenerating axonal fibres into the lesion gap. It was noticed that axonal growth was not always directed to the opposite end of the lesion. Instead, some fibres grew perpendicularly to the injury or in a haphazard fashion.

Weak axonal sprouting was observed in the lesion gap but these never appeared to reconnect both sides of the lesioned spinal cord (**Figure 3.10 A, B**). Approximately 20 axonal fibres were counted per mm from one side of the lesion with a relatively high variation amongst slices (between 20 and 60 fibres/mm) within the same time point

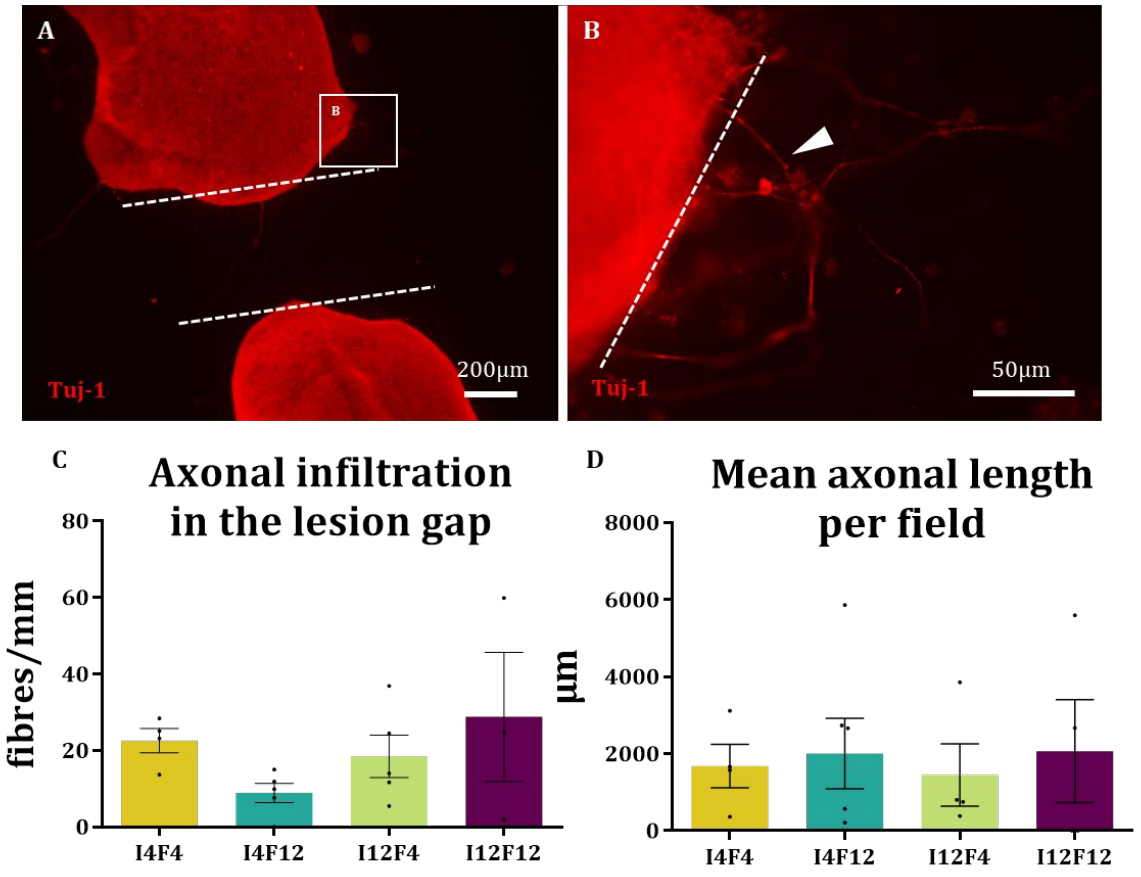

Figure 3.10 Axonal sprouting in SCI organotypic slices*. Representative fluorescence images of a I4F12 spinal cord slice after injury and Tuj-1 staining at low magnification (**A**) and hight magnification at the lesion edge (**B**) showing spontaneous axonal sprouting. Dotted lines representing the edges of the lesion. Arrow pointing and sprouting axon. The bar graphs represent the number of single fibres per mm infiltrating the lesion gap in each time point (Kruskal-Wallis test, I4F4: n=4; I4F12: n=4; I12F4: n=5; I12F12: n=3, p≥0.05) (**C**) and the mean total axonal length of the infiltrating fibres of each field (Kruskal-Wallis test, I4F4: n=4; I4F12: n=5; I12F4: n=4; I12F12: n=3, p≥0.05) (**D**). No differences were found in axonal infiltration among experimental groups.*

(**Figure 3.10 C**). The total length of sprouting axons per field was also highly variable (from 0 to 6000µm), with no statistical differences between time points ($p>0.05$) (**Figure 3.10 D**).

3.2.8 The density of MBP-positive tracts was higher at the centre of the spinal cord than at the lesion edge

Most spinal cords presented MBP-positive tracts. However, sometimes those were only present on one side of the lesion. In some cases no MBP was observed or the amount of MBP-positive structures varied across spinal cords. Therefore, only those slices that presented MBP-positive tracts were selected for analysis.

When MBP-positive cells were observed, those seemed to form tracts following the direction of Tuj-1-positive fibres, possibly ensheathing them as myelination tracts (**Figure 3.11**).

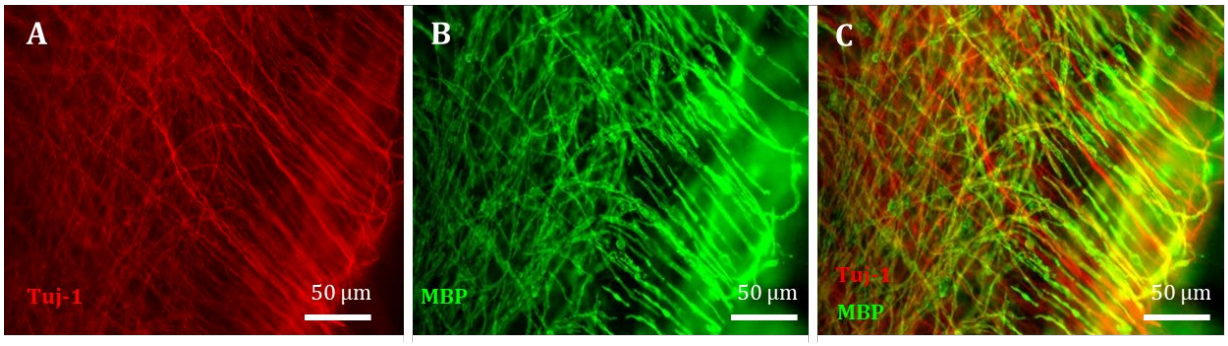

Figure 3.11 Presence of myelin tracts in chick embryo spinal cord organotypic slices. *Example images of spinal cord slices with Tuj-1 positive fibres (**A**) and MBP-positive fibres (**B**) following similar position patterns, as seen by colocalization of staining in a merged image (**C**).*

However, the density of MBP-positive tracts seemed to be less at the edge of the lesion than at the centre of the spinal cord (**Figure 3.12 A-C**). The quantification analysis suggested that approximately four times the level of MBP staining was detected in the centre of the cord compared to the lesion margin ($p<0.05$). This was true for all time points except I12F12 (**Figure 3.12 D**).

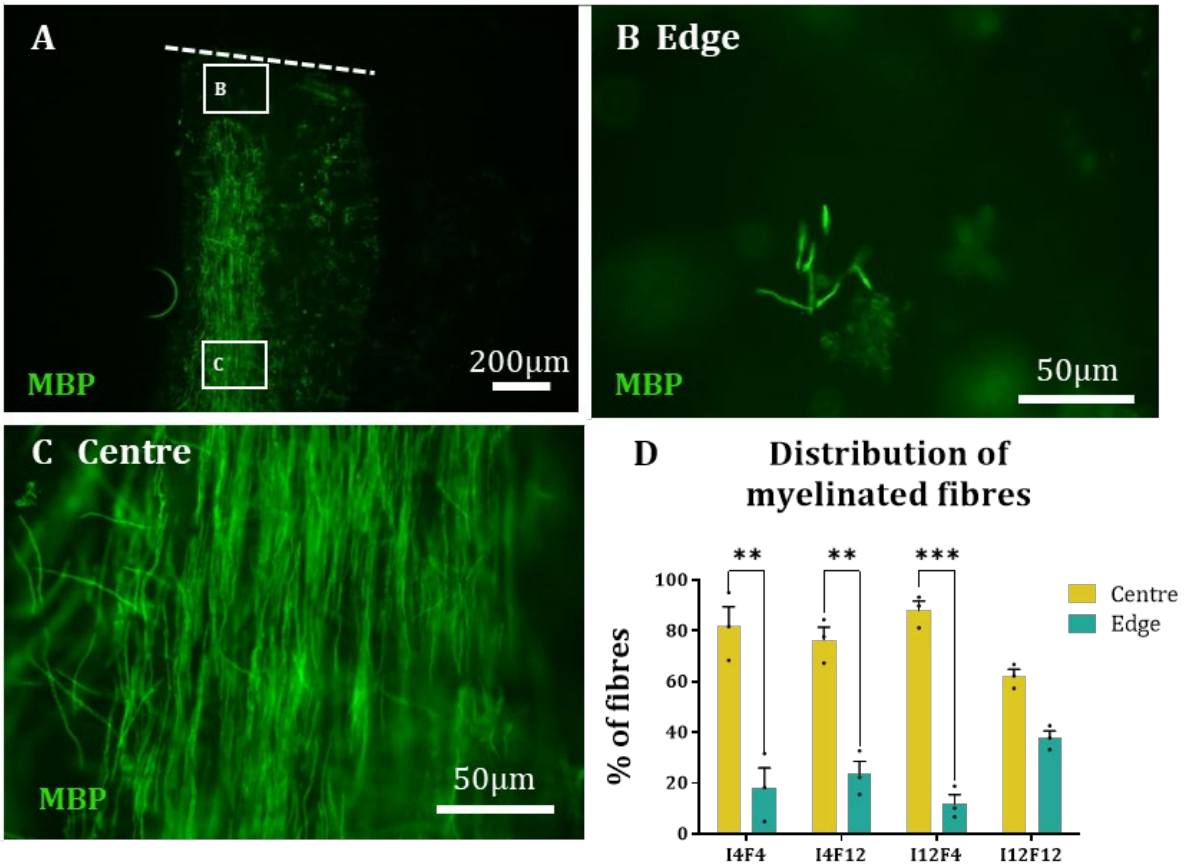

Figure 3.12 Myelination of slices after injury*. Representative fluorescence images of a spinal cord slice after injury and MBP staining at low magnification (**A**) and high magnification at the lesion edge (**B**) and centre of the spinal cord (**C**). All images corresponding to a I4F12 slice. The bar graph represents the percentage of MBP-positive tracts in the centre of the spinal cord compared to the edge for each time point (Two-way ANOVA, n=3, p≤0.05) (**D**). Y axis represents the percentage of fibres in either the edge of the slice or the centre relative to the total number of fibres in the slice. Most MBP-positive tracts were found at the centre of the spinal cord compared to the edge in the first three timepoints.*

3.2.9 Lectin-positive cells infiltrated the lesion gap

Finally, microglia, detected as lectin-positive cells, were seen infiltrating the lesion gap. The cells infiltrating the lesion presented an amoeboid morphology (**Figure 2.13 A**) while cells visualised within the centre of the slice appeared more ramified (**Figure 3.13 B**). As suggested by the statistical analysis, the number of infiltrated cells per unit area was similar in all time points (**Figure 3.13 C**).

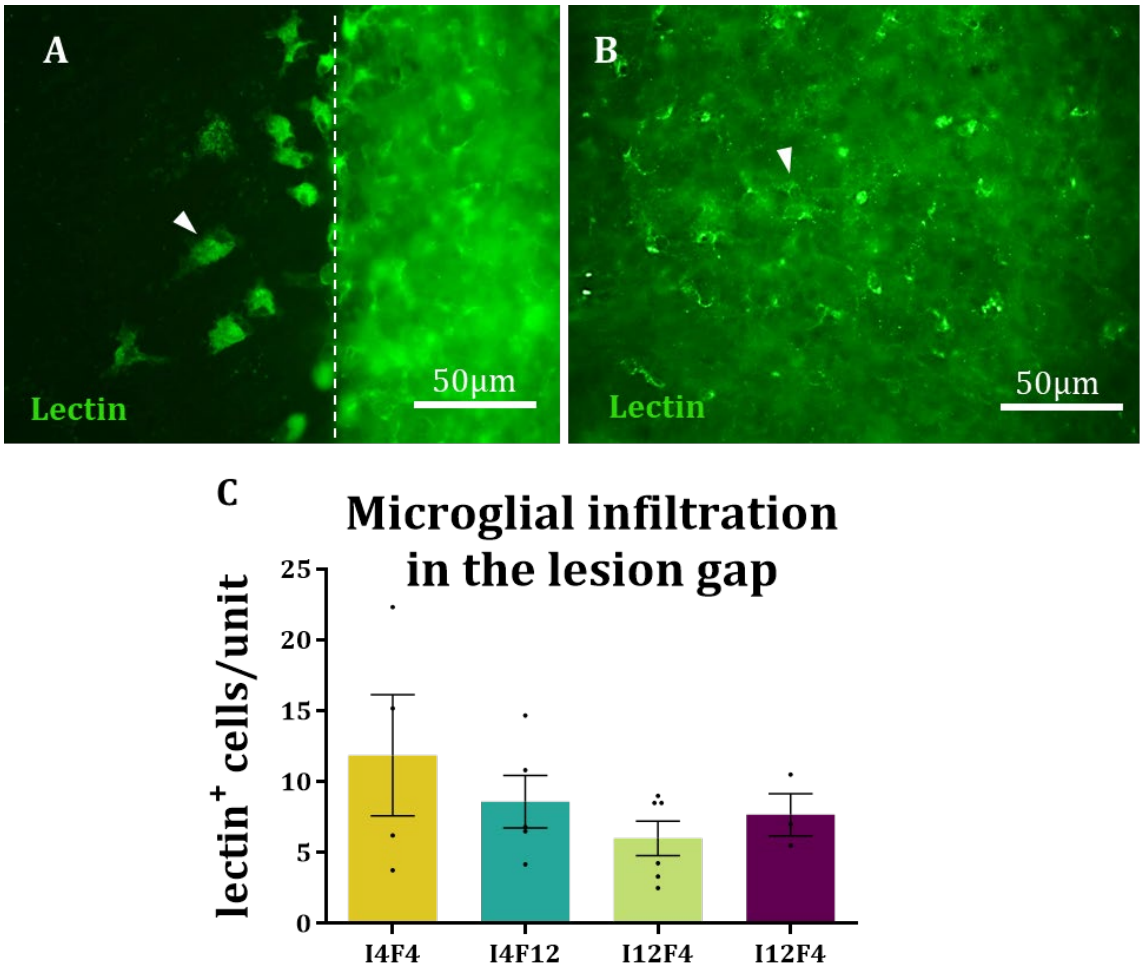

Figure 3.13 Infiltration of microglia in the injury gap*. Fluorescence image of a I4F12 slice representing lectin-positive cells infiltrating the lesion gap (**A**), lectin-positive cells in the centre of the spinal cord (**B**) and graphical representation of the number of lectin-positive cells per unit area in the lesion gap for each time point (Kruskal-Wallis test, I4F4: n=4; I4F12: n=4; I12F4: n=6; I12F12: n=3, p≥0.05) (**C**). Dotted line representing the edge of the lesion and arrows pointing at examples of cells. There were no differences in the number of lectin-positive cells among experimental groups.*

3.3 DISCUSSION

3.3.1 Summary of aims and results

Here, we have shown that it is possible to create a SCI and implant a therapeutic biomaterial to the lesion in the live chick embryo. However, the technique faces low survival rates and presents analytical difficulties. Instead, the establishment of an organotypic SCI model using chick embryo spinal cord was shown. These data indicate that the chick embryo slice model could be used as a novel platform for testing possible therapies. This is due to the high slice survival *in vitro* and its replication of the most common cellular behaviours following traumatic SCI: astrocytic hypertrophy, inhibited axonal regeneration, microglial infiltration and potential loss of myelinating oligodendrocytes. Moreover, as stated in **Chapter 1**, the use of the chick embryo offers significant advantages over rodent models. In short, it is cheaper to maintain, easier to manipulate and it is restricted to less ethical implications offering wider availability throughout the scientific community. These outcomes will be discussed in the following sections.

3.3.2 The chick embryo as an *in vivo* model of spinal cord injury

In this chapter we showed that chick embryos can develop in culture vessels outside their shell, as initially showed by Tahara & Obara (2014), and that it is possible to inflict a transecting injury to their spinal cord. Furthermore, a small piece of the biomaterial Hemopatch™ was successfully implanted into the spinal cord after lesioning. This culture protocol allowed for a wider manipulation area compared to the small window in "shell" cultured chicks. In the "shell" group, creating a small window allowed to insert tools to inflict a transecting lesion while maintaining all the egg contents in place. However, this window was too small to move the lesioning tools freely, often resulting in blood vessel puncture and death. Therefore, the "shell-less" group provided an advantage regarding the lesioning procedure. However, the process of transferring the embryo to the culture

vessel and perhaps the suboptimal conditions in the culture vessel led to a marked decrease of embryo survival during incubation. The survival rate was increased by modifying the transfer procedure of the embryo to the culture vessel. The optimised procedure resulted in a gentler transfer, reducing the impact force and, possibly, the trauma inflicted on the embryo upon transfer. Despite the fact that the shell-less group showed increased survival after manipulation, and that we were able to increase survival rates, these still showed a tendency to die during the incubation period even without manipulation of the embryos at higher rates than the "shell" group.

The embryos were stained with two different methods: whole-mount staining or immunostaining after cyosectioning. Although the lesion was located and some neural fibres were observed after whole mount staining, the thickness of the tissue did not allow for a clear visualisation of neural structures and therefore, any possible quantification would have been unreliable and not reproducible. On the other hand, sagittal sections of the spinal cord allowed for lesion localisation 0h after lesioning and implant localisation after 24h. The lesion was not localised with frontal sections, perhaps due to the lesion being in a different plane or due to regeneration. Here, we used E5 – E7 chick embryos. This time point was chosen due to the fact that neurons, OPCs and microglia should already be present (**Chapter 1**), and the embryo was small enough to manipulate through the shell window. As a limitation, the E5 chick embryo spinal cord can regenerate after a lesion and, therefore, this model would only allow for the evaluation of cell infiltration upon biomaterial implantation instead of regeneration permissiveness.

In conclusion, chick embryos developing in culture vessels were more appropriate for lesioning procedures despite a survival decrease during incubation. In regard to sample manipulation, cryosectioning the samples before staining resulted in clear visualisation of structures for potential reliable quantification. Despite this, and after optimising culturing methods, chick embryo survival was only approximately of 40% and would need

further optimisation to increase survival. In addition, and in the context of this thesis, the organotypic slice culture model offers a more simplistic, higher throughput model in which to test biomaterial implantation. Importantly, the organotypic model offers the possibility of working with older tissue, which does not spontaneously regenerate. Therefore, we proceeded to study and analyse cellular responses on the *in vitro* model in order to establish a reproducible and robust testing platform for neural tissue engineering.

3.3.3 Chick embryo spinal cord slices as an *in vitro* model of spinal cord injury

The organotypic spinal cord slice culture was set up following the protocol established by Weightman et al., (2014). The culture was set up at day E14 of development to ensure there would be no spontaneous spinal cord regeneration after injury (Hasan et al., 1993) as an attempt to mimic the response of adult tissue. The slices were lesioned at two time points (4 or 12 days after dissection) to assess whether the age of the slice and potential maturation had any impact on the cellular responses to injury. Moreover, the slices were fixed at two time points: 4 or 12 days after injury. The goal was to study any possible differences in cellular response over time.

The slices were kept in the incubator for 8, 16 or 24 days depending on the lesioning/fixing time point, with no statistical differences in survival between groups. Similar transverse slice models have been shown to survive *in vitro* for up to 3 weeks in rat (Cho et al., 2009) and up to 4 weeks in chick (Brunet et al., 2007). Transverse spinal cord slices derived from human tissue after autopsy have been cultured for up to 14 days *in vitro* (Jeong et al., 2011). There is also previous evidence of longitudinal slices derived from mice surviving for up to 2 weeks in culture, showing 96%±2% survival (Weightman et al., 2014).

The slice viability analysis in our study was reproduced from previously published protocols (longitudinal rat spinal cord organotypic slices with transection lesions) (Guijarro-Belmar et al., 2019; Weightman et al., 2014), and resulted in approximately 70-80% slice viability. In line with other reports, microscopical observation of the slices after staining with Calcein AM and Ethidium homodimer seem to suggest a higher viability rate that we estimated to be ≥95%. This disparity could be due to the fact that we compared OD measurements from two different markers in two different channels (red and green), and that each marker is associated to a different level of fluorescence. For example, although ethidium homodimer (red) covered a smaller area of the field, the OD per red pixel was higher than the OD per green pixel (Calcein AM), resulting in a slightly biased result. All images across experimental repeats were taken at the same exposure. Therefore, the survival rates resulting from the analysis are treated as a survival index, that allows for the comparison between groups leading to the conclusion that there is no difference in survival over time or regardless of lesioning. Meanwhile, microscopy observation permitted a qualitative approximation of the slice survival. Other studies using spinal cord organotypic slices used TUNEL staining to measure cell death (Cho et al., 2009; Krassioukov et al., 2002). This technique results in a bright blue staining of dead cells' nuclei. However, this technique would not have been feasible due to the large number of cells per field in our longitudinal spinal cord slices compared to other transverse slices.

In summary, our results show that chick embryo spinal cord organotypic slices can survive *in vitro* for at least 24 days, similarly to previously published literature focusing on rodent models, and that survival does not decrease after a transecting lesion. These data suggest the slices are a robust model in which to test lesioning procedures and analysis of responses over time.

In regard to astrocyte behaviour, tightly-packed, proliferative, hyperfilamentous astrocytes producing long processes are referred to as reactive or hypertrophic (Fawcett & Asher, 1999). *In vivo*, naïve astrocytes become reactive at 14 days after lesioning in a mouse SCI model, undergoing hypertrophy, extending processes and showing increased GFAP expression (Faulkner et al., 2004; Hara et al., 2017). Similarly, the glial scar starts to form at 14 days post injury in humans (Ahuja et al., 2017b). Increased reactivity of astrocytes at 7 and 12 days post injury described by high GFAP expression and hypertrophic morphologies in organotypic spinal cord slices after injury has been reported before in rats (Guijarro-Belmar et al., 2019; Weightman et al., 2014).

In our study, GFAP staining revealed increased OD values at 0-10μm from the lesion edge when compared to 50-60μm and 100-110μm from the edge at 12 days after injury, but not at 4 days after injury. Similarly, Weightman et al., (2014) reported higher GFAP expression at 0-100μm from the lesion compared to 100-200μm 6 days post lesion in mice organotypic spinal cord slices and reported hypertrophic astrocytes at the lesion edge. In a brain stab wound in mice, hypertrophic astrocytes were also described as polarized, forming elongated processes directed towards the lesion site 7 days post injury (Bardehle et al., 2013). Both Weightman et al., (2014) and Guijarro-Belmar et al., (2019) report small numbers of infiltrating reactive astrocytes into the lesion gap, which we did not find in any of our slices. It is important to mention that we also noted increased GFAP OD at the sides of the spinal cord slices, where the spinal cords were sliced with the tissue chopper to set up the model and, therefore, do not represent a controlled injury environment for experimentation. Therefore, the side edges of the slices were not counted for analysis. However, it might be beneficial to study how the OD profile of the spinal cord edge compares to uninjured slices in future studies in order to determine whether a previous lesion (in this case created when setting up the culture) can affect the cellular responses

to the experimental lesion or whether the experimental lesion has effects in other areas of the spinal cord besides the lesion margin.

In conclusion, astrocytes in the chick embryo model for SCI present a reactive phenotype 12 days post injury, similar to that found in rodent SCI models, which has been described as a typical glial scar phenotype after SCI (Fawcett & Asher, 1999). Moreover, similarly to a naturally occurring injury in adult humans, the astrocytic response develops over time. These findings suggest that our model could serve as a platform in which to study astrocytic responses to possible SCI therapies.

Such hypertrophic astrocytes have also been suggested to act as a barrier to neurite outgrowth in a transecting lesion in a rat spinal cord organotypic slice culture 7 days post lesion, as seen by the presence of collapsed axonal growth cones confronted with highly reactive astrocytes (Guijarro-Belmar et al., 2019). In fact, it is widely established that the adult CNS does not possess the capacity for axonal regeneration after injury. For example, after complete spinal cord transection in rats, no serotoninergic fibres were detected caudally to the transection 14 days post lesioning *in vivo* (Coumans et al., 2001).

According to our data, weak, spontaneous axonal sprouting was observed in all timepoints. In addition, the number of sprouting axons and the total axonal length infiltrating the lesion was similar between experimental groups. Importantly, the growth orientation of these axons seemed random and not directed towards the other end of the lesion, and they were never seen reconnecting both sides. In contrast, transverse sections of E7 chick embryo spinal cord slices embedded in a fibrin gel showed robust radial axonal growth at 5 days *in vitro*, reaching lengths of approximately 3mm (Rösner & Vacun, 1997). However, as already established in the literature, axons do not seem to regenerate after an E15 lesion in the chick embryo *in vivo* (Shimizu et al., 1990) and our cultures were established at E14, with lesions inflicted 4 or 12 days after. In rodents, extensive nerve

fibre outgrowth from the lesion was reported 7 days after lesioning in slices from P0 mice in contrast to limited nerve fibre outgrowth in slices from P5 mice. However, in neither of the timepoints, directed axonal growth was reported (Weightman et al., 2014). The low levels of axonal regeneration and undirected nature of growth in the chick embryo model indicate that this model is comparable to the rodent model of a transecting spinal cord injury *in vivo* and *in vitro*, suggesting that it is a viable platform for testing potential therapies aimed at increasing and directing axonal outgrowth.

Demyelination, likely due to the loss of oligodendrocytes, is a typical response following traumatic SCI (Duncan et al., 2019; Fawcett & Asher, 1999). Longitudinal spinal cord slices from P6 mice, have been reported to feature myelination tracts after day 7 *in vitro* (Bonnici & Kapfhammer, 2008). Our results suggest that MBP-positive tracts are present in some of the slices, but we did not find this phenomenon in all slices. MBP, or myelin basic protein, is a biomarker expressed by myelin sheaths. Taking into consideration that the process of myelination starts approximately at E13 in the chick embryo (Dobbing et al., 1957) (**Chapter 1**), and that the spinal cords were dissected at E14 and kept in the incubator, it seems plausible to assume that not all slices will have developed myelin tracts. However, the presence of MBP-positive fibres suggests that this process had undergone in other slices, which were chosen for quantification.

Our results seem to indicate that MBP-positive tracts, when present, were denser at the centre of the spinal cord than at the edge of the lesion, suggesting a possible loss of oligodendrocytes due to the lesion. This was not the case for the last time point (I12F12), in which the overall MBP expression seemed lower than in the other time points. Although this could be due to a lower level of MBP-positive tracts present in the slice from the beginning, due to the fact that this was repeated in all the slices in that time point, we believe the phenomenon is due to the age of the slices, which may have caused oligodendrocyte loss from the lesion edge but also from the edges of the slice (where it

was sliced to set up the culture). This potential loss of myelinating oligodendrocytes at the lesion edge would have to be corroborated with appropriate tests, such as transmission electron microscopy (TEM) of transverse sections with comparison at the centre and edge of the spinal cords.

Finally, microglial infiltration to the lesion area has been reported in rodent organotypic spinal cord slices before (Guijarro-Belmar et al., 2019; Weightman et al., 2014). We observed microglial invasion (detected by lectin staining) at the lesion site with no statistical differences within groups. In comparison, microglial infiltration in other studies was reported to increase from day 0 to 5 and then decrease again at day 10 (Weightman et al., 2014). On the other hand, other studies suggest that the elevated numbers of activated microglia persist in the lesion site for weeks after injury (Fawcett & Asher, 1999). Despite this contradiction in results, most studies describe infiltration of activated or reactive microglia, characterised by bigger somas and amoeboid morphology, while microglial cells remaining in the unlesioned tissue present smaller somas and a ramified morphology, more characteristic to a resting state (Guijarro-Belmar et al., 2019; Weightman et al., 2014). In concordance with published results, we have also observed microglia presenting a reactive-like morphology infiltrating the lesion, compared to resting-like microglia within the centre of the spinal cord.

This microglial response has been correlated with the acute response to SCI *in vivo*, and act to phagocyte debris and release inflammatory cytokines (Fawcett & Asher, 1999) (**Chapter 1**). Our results suggest that this activation profile is represented in chick embryo spinal cord organotypic slices, highlighting another representative feature of this model in comparison to a naturally occurring SCI in adult humans. Moreover, an important factor to consider when implanting biomaterials for the treatment of SCI, is the immune response these might activate, our results highlight the possibility of using this model to study microglial activation in response to biomaterial implantation.

3.3.4 Future directions

There are several potential routes for future research based on this work, which could be divided into three categories: continued optimisation and characterisation, further development and neural tissue engineering applications.

In the first place, the survival of the *in vivo* model could be improved by perhaps inflicting a contusion or compression injury, which might provoke a smaller degree of injury while avoiding the use of sharp objects that might damage surrounding tissue, including blood vessels. Moreover, these techniques would also represent more accurately the majority of natural occurring injuries (Patar et al., 2019b). In addition, a relevant analytical method would need to be established to study cellular responses to the insult. These could potentially be similar to those described for the *in vitro* culture if cryosectioned slices were to be used. Moreover, our results suggest that full restoration of circuitry is potentially achieved at least 48h after injury. This would be in accordance with previous studies using *in vivo* chick embryos (Hasan et al., 1993; Shimizu et al., 1990). Therefore, in order to study the regeneration permissiveness of potential therapies, a non-regenerative environment would have to be established. We hypothesised that by creating a wide lesion (*e.g.:* through removal of a 400-500µm-thick piece of tissue) the axonal tracts would not spontaneously regenerate.

On the other hand, the presence of potential myelination tracts in the *in vitro* model would have to be corroborated, perhaps by analysing the colocalization of Tuj-1-positive and MBP-positive fibres or by analysing the presence of myelin associated proteins, such as Nogo-A. In the same line, it might be interesting to characterise the molecular responses to injury, such the presence of inflammatory cytokines (IL-1, IL-6) or CSPGs. In addition, the model could be further characterised by studying cellular proliferation and differentiation at or near the site of injury.

Further development of the model could be achieved by adding another dimension to the histological/cytological study described here. For example, it might be desirable to study the electrical profile of the culture, particularly the synchronicity of neuronal bursts before and after lesioning. Such studies might be able to improve the understanding of the possible functionality of therapeutic outcomes. This could be potentially studied by using calcium sensitive dyes combined with time-lapse imaging as done previously in chick spinal cord organotypic slices (O'Donovan et al., 2005). Alternatively, voltage-sensitive dyes could be used with a similar approach (Steyn & Andras, 2017). For a more direct and detailed study, it might be desirable to investigate the electrical profile of the samples through the use of recording electrodes, for example, from a multi electrode array (MEA). Such devices have been previously used in combination with neural tissue organotypic slices (Plenz et al., 2011) and open the door to the study of tissue responses to electrical stimulation. It is important to note that the main disadvantage of organotypic models is the inevitable disconnection from the rest of the body. Therefore, although the slices appear to maintain their ascending and descending axonal architecture, some tracts are disconnected from the site of origin and synapse functionality can only be studied considering that the possible synchronicity of neuronal bursts would not directly correlate to the re-establishment of previous ascending and descending tracts, only of neurons whose somas are present in the slice.

Finally, the *in vitro* model established here could be used for the study of neural tissue engineering applications towards finding a treatment for SCI. For example, it would be interesting to study the response of the tissue to the implantation of stem cells (Jeong et al., 2011) or biomaterial implantation (Guijarro-Belmar et al., 2019; Weightman et al., 2014). The latter will be addressed in **Chapter 6**.

4 ENHANCING THE REGENERATIVE POTENTIAL OF STEM CELL-LADEN, CLINICAL-GRADE IMPLANTS THROUGH LAMININ ENGINEERING

4.1 BACKGROUND

4.1.1 Cell-laden biomaterials for spinal cord injury treatment

As explained **Chapter 1**, repairing the multifaceted pathology of SCI is a major challenge requiring breakdown of the glial scar, removal of inhibitory myelin fragments and restoration of complex circuitry. Numerous pre-clinical and clinical studies have demonstrated NSC transplantation offers promise in this regard, providing cell replacement and trophic factor release and enhancing functional outcomes (Ogawa *et al.*, 2002; Bonner *et al.*, 2011; Nemati *et al.*, 2013; Ahuja *et al.*, 2017; Anderson *et al.*, 2017).

In addition, encapsulation of transplant cell populations within implantable, biocompatible matrices may offer several translational advantages. These materials offer (i) a porous structure mimicking the ECM to facilitate cell attachment and tissue ingrowth; (ii) 'soft' mechanical properties to match the stiffness of the native CNS (important for implant acceptance) (Pakulska et al., 2012) and allow surgical moulding into diverse injury sites and; (iii) improved cell survival and distribution in injury sites after implantation. For example, *ca.* 85% mice retained NSCs 7 days after injection within a hyaluronan-based hydrogel compared to *ca.* 55% of mice when NSCs were injected in CSF (Ballios et al., 2015).

4.1.2 Clinical translation of biomaterials

Despite the clinical potential of using biomaterials for encapsulated cell delivery, most studies use experimental grade biomaterials to provide proof-of-concept data. This means the biomaterials tested for therapeutic cell encapsulation and delivery to SCI still

require clinical approval and to be manufactured under good manufacturing practice (GMP).

In the European Union (EU), the CE marking association ensures that all products within the EU market comply with the relevant EU legislation, including medical devices (CE-Marking, 2020). Similarly, the American Food and Drug Administration (FDA) is responsible for ensuring the safety of drugs, biological products and medical devices prior to their regulated use in the clinic (FDA, 2020). The CE marking process focuses primarily on the safety of the product, while the FDA process also focuses on its efficacy and value (Mishra, 2017).

A cell-laden biomaterial falls in the category of "combination products" (FDA, 2020) and, therefore, obtaining approval requires consideration of the material as both an inert device and a biological implant. Moreover, Class III devices, those which "support or sustain human life", require pre-market approval (PMA), which is the most rigorous process required by the FDA (Van Norman, 2016). The PMA process also requires the payment of the highest user fee asked by the FDA, amounting to $365,657 (FDA, 2020). It has been estimated it takes an average of 3 to 7 years for a new device to be approved by the FDA, and approximately 12 years for a new drug to be approved (Van Norman, 2016). In addition, any major changes in the manufacturing process as experimental biomaterials are translated to clinical grade materials (e.g. through scale-up) necessitate further biological tests to ensure that the safety and functionality of the material have not changed, increasing the time to clinic and costs of development.

It is clear therefore that strategies to reduce the cost and time associated with these procedures, would be highly advantageous to healthcare providers and patients. In this regard, relevant pre-existing evidence of the device's safety upon clinical use can be used to back up the FDA approval request, significantly decreasing the time and costs of the

procedure. Legally marketed devices which have previously undergone the PMA approval process already count with most of the necessary evidence for safety upon clinical use as well as an established manufacturing process. Consequently, medically approved devices may offer a potential alternative to experimental grade biomaterials for SCI implantation while decreasing the time to clinic.

4.1.3 Clinical materials for cell transplantation

Both natural and synthetic polymeric implants are already routinely used within the clinic and approved for uses such as tissue sealants, sutures and wound dressings (Maitz, 2015) (**Table 4.1**). The most commonly used natural surgical adhesives are fibrin or collagen based such as Tisseel VH or Duragen™ respectively (Duarte et al., 2012). However, there are also gelatine or polysaccharide-based adhesives, such as Floseal™ or Chitoflex, respectively (Duarte et al., 2012). Synthetic polymeric adhesives, such as Glubran2 or DuraSeal are also available as FDA approved biomaterials (Duarte et al., 2012).

Most of these materials present advantageous properties for cell encapsulation and implantation, such as biocompatibility, porosity, biodegradability, and flexibility to conform to irregular wound surfaces. However, in the majority of cases, these have not been tested for potential cell transplant applications.

Table 4.1 List of clinically available synthetic and natural surgical adhesives (Baxter Healthcare Corporation, 2019; Celox-Medical, 2020; Dhillon et al., 2011; Dunn et al., 2001; Finch et al., 2020; Integra-Life, 2020; Kassam et al., 2003, 2004; Kawasaki et al., 2017; Leonardi et al., 2002; Prior et al., 1999; Shuliang Chen, Peter Novick, 2017; Tricol-Biomedical, 2020).

Main component	Name	CNS uses	Properties	Company
Fibrin	Tisseel VH	Prevention of CSF leaks in humans, safety upon application on primate brains.	3D, porous, biodegradable (10-14 days), precise placement, fibrin clot	Baxter (US)
	Crosseal	Dural sealing	3D, human-based, biodegradable, fibrin clot	OMRIX (Belgium)
	TachoComb	None reported	3D, porous, dry (sponge), biodegradable (3 -6 weeks), collagen coated with fibrin	Takeda (Japan)
Collagen	CoStasis	None reported	Sprayable, consisting of collagen, thrombin and autologous plasma, gel	Cohesion Technologies (US)
	Duragen	Dural sealing on brain and spinal cord, NSC culture	3D, porous, flexible, biodegradable (3-8 weeks), ultra pure collagen, dry sponge	Integra LifeSciences Corp. (US)
	Hemopatch	Dural sealing	3D, porous, flexible, biodegradable (6-8 weeks), collagen with PEG coating, dry sponge	Baxter (US)

Gelatine	Floseal	Hemostasis in spinal surgery	3D, conform to irregular wound surfaces, gelatin granules and human thrombin, gel	Baxter (US)
Chitosan	HemCon	Indicated for neurovascular intervention	3D, flexible, antibacterial, for emergency use, positively charged	Tricol biomedical inc. (US)
	Celox- A	None reported	Granules, emergency use, small penetrating injuries.	Medtrade Products (UK)
Cyanoacrylate	Glubran2	Endovascular use in neurradiology	Surgical glue, indicated for internal use.	GEM (Italy)
Polymeric hydrogels	SprayGel	None reported	Sprayable film, PEG-based, biodegradable (days)	Confluent Surgical Inc (US)
	DuraSeal	Dural sealant, prevention of CSF leakage in brain and spinal cord	PEG-based, gel, Biodegradable (4 -8 weeks), blue colorant for visualisation, flexible applicator	Integra LifeSciences Corp. (US)

One study has demonstrated Duragen™, a surgical sealant manufactured from clinical grade, bovine collagen can support NSC growth, including genetically engineered populations (Finch et al., 2020). Here, highly viable populations of NSCs could be grown throughout the material with no effect on key regenerative properties of the stem cells including proliferation, stemness and differentiation (Finch et al., 2020).

These promising findings demonstrate that clinical grade sealants can potentially be used for cell transplantation in routine biomaterial therapy after SCI. Moreover, as shown in **Table 4.1**, the varying physicochemical properties of these biomaterials may be applicable to different injury types. For example, for injuries of difficult access, such as traumatic brain injury, it might be desirable to use an injectable material with a long and flexible applicator, such as DuraSeal™. Therefore, it is important to establish a bank of potential clinically approved biomaterials for SCI implantation.

4.1.4 Hemopatch™, a collagen sealant for potential cell encapsulation

Another clinically approved material with a number of potential translational advantages for use in cell transplantation is Hemopatch™. Hemopatch™ is a sealing hemostatic dressing approved for medical use during surgical procedures to reduce bleeding and induce hemostasis (Baxter Healthcare Corporation, 2019). Within the CNS, it has been safely used to close dural defects and avoid post-operative CSF leakage in humans (Nowak et al., 2019).

Hemopatch™ is flexible, allowing for easy handling by surgeons with potential for moulding into sites of injury, and is naturally degraded within 6 to 8 weeks (Baxter Healthcare Corporation, 2019). This material is approved as a CE-marked medical device and is already manufactured for a global market (**Figure 4.1**). It is a porous structure made from ultrapure bovine collagen, with a 200 μm coating of PEG on one surface, to improve tissue adhesiveness.

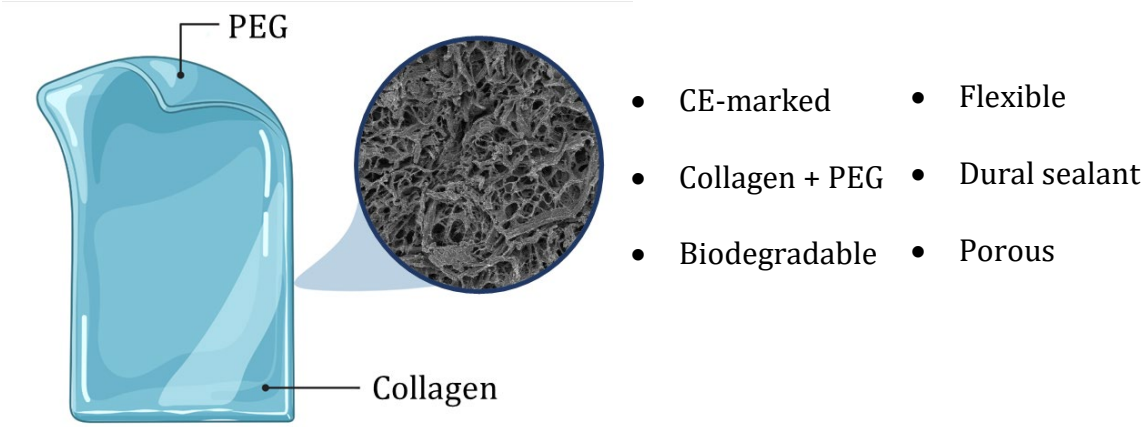

Figure 4.1 Schematic representation of Hemopatch™. *Representation and main advantages of Hemopatch™ for SCI implantation, Image created with Biorender.com*

In humans, collagen is the most prevalent component of the ECM and can be found both in the basal lamina and nervous tissue parenchyma of the CNS (Gregorio et al., 2018). Typically, it is formed of three polypeptide strands coiled around each other to form a triple helix (Shoulders & Raines, 2009), and has been seen to interact with other ECM components and cell membrane receptors (Gregorio et al., 2018). Moreover, due to its abundance, it plays an important role in tuning the stiffness and mechanical properties of the ECM (Gregorio et al., 2018), a key parameter for SCI repair. These characteristics, together with biodegradability, weak antigenicity and biocompatibility make collagen a desirable material for biomedical applications (Lee et al., 2001).

In vitro, collagen has been reported as a substrate in which neurons can survive (Drury & Mooney, 2003) and neural stem cells can differentiate (Ma et al., 2005). Implantation of collagen hydrogels in a transected spinal cord has shown to promote axonal growth 5 days post-injury and functional recovery 12 days post-injury in rats (Yoshii et al., 2004), as well as cell infiltration and vascularization within the implanted hydrogel (de la Torre, 1982).

In vivo studies of combinatorial therapies have been tested with different cell types. Implantation of Schwann cells in a collagen hydrogel into a rat spinal cord resulted in higher cell survival and cell number increase than in media-injected cells (Patel et al.,

2010). In a different study, neonatal astrocytes were delivered to the rat spinal cord within a collagen hydrogel. These astrocytes remained confined into the hydrogel, showing poor migration capacity. However, an increase of ingrowing fibres into the hydrogel was highly correlated to the astrocyte-containing hydrogel group instead of the hydrogel alone-implanted group (Joosten et al., 2004). In a recent study, implantation of encapsulated NSCs within a porous collagen scaffold resulted in locomotion recovery 12 weeks post injury in live mice, at which point there were no statistical differences to uninjured controls (Kourgiantaki et al., 2020).

Collagen bioscaffolds can also be functionalised to incorporate other molecules. NSC have been delivered to a rat spinal cord within an epidermal growth factor receptor (EGFR) neutralizing antibody-treated collagen hydrogel (Xiaoran Li et al., 2013). EGFR has been shown to enhance astroglial differentiation and inhibit the formation of a neuronal lineage (Ayuso-Sacido et al., 2010). The neutralization of EGFR in this study resulted in an increase in the number of neurons from 13% to 25% in the treated hydrogels at 4 weeks post injury, correlating with an increase in functional recovery (Xiaoran Li et al., 2013).

Given the previous evidence, Hemopatch™, a collagen-based tissue adhesive, could be suited for SCI implantation. However, it has never been tested for its potential for cell encapsulation.

4.1.5 Extracellular matrix modifications for material optimisation

Tissue adhesives, such as Hemopatch™, were created with the aim of blood or CSF leakage prevention. Although their properties have great potential for cell encapsulation, these materials are optimal for tissue sealing. Therefore, it might be desirable to enhance their regenerative properties when aiming to repurpose them for SCI treatment. It is well established that 3D scaffolds based on ECM molecules, such as collagen, or

biofunctionalisation of scaffolds with pro-regenerative ECM molecules, *e.g.* laminin, can add significant regenerative potential to the material.

Engineering ECM molecules or epitopes into scaffold design has been shown to improve NSC survival and distribution throughout injury sites after implantation in a collagen matrix in a contusion SCI in mice (Tate et al., 2009) and enhance neuronal differentiation of encapsulated stem cells and nerve fibre and neural cell infiltration into an alginate scaffold (Barros et al., 2019). Laminins, an ECM molecule, are glycoproteins heterotrimers of high molecular weight (400- 900 kDa), and are a major component of the basal lamina (Miner & Yurchenco, 2004). Typically, a laminin protein consists of three chains or arms (α, β and γ) in a cross-like formation, forming a coiled structure in one of the ends (Miner & Yurchenco, 2004). The α unit extends beyond the coil to form the G-domain. Its activity can be broadly classified into matrix assembly and cell membrane interaction, with the short α, β and γ subunits mostly confined to non-cellular ECM binding and the G-domain mediating cell interaction (Miner & Yurchenco, 2004). Due to these properties, laminin is widely used *in vitro* to promote even cell distribution and cell attachment to glass coverslips (Miner & Yurchenco, 2004). In fact, laminin from the basement membrane has the capacity to interact with cells, mainly, through the membrane receptors integrins (Carmignac & Durbeej, 2012), which act as binding proteins between the ECM and the cytoskeleton, and can trigger signal transduction processes to modulate adhesion, survival, proliferation, etc (Takada et al., 2007). Human NPCs have been reported to present several isoforms of integrins (α3, α6, α7, β1, and β4) and the blockage of the α6 in human NPCs resulted in decreased migration of cells on laminin-treated substrates, indicating the importance of the role of integrins in laminin-induced migration (Flanagan et al., 2006). Laminin-binding forms of integrins are also present in neurons, astrocytes, oligodendrocytes and microglia (Nirwane & Yao, 2019).

There is also increasing evidence of laminin promoting even cell distribution in 3D constructs. For example, coating a porous scaffold with laminin supported the attachment and growth of iPSC 3 weeks after seeding but had no impact on cell differentiation (Ruzicka et al., 2019). In a different study, NSCs growing on a naturally occurring biomimetic substrate also showed higher attachment to the substrate instead of neurosphere formation when the substrate was functionalised with laminin, showing a slight increase in proliferation compared to negative controls and no signs of cytotoxicity (Luo et al., 2018). Moreover, laminin functionalisation has also been reported to increase the length of neurite outgrowth on electrospun nanofibres when compared to non-functionalised controls (Koh et al., 2008).

It is clear that laminin functionalisation can enhance the regenerative capacity of a bioscaffold and also of the encapsulated cell population. Despite the evidence, ECM functionalisation has never been tested on any clinically available biomaterial for SCI implantation.

4.1.6 Knowledge gaps and aims

In summary, routine clinical application of bioscaffold implantation for SCI repair is delayed due to the lack of medically approved biomaterials. Surgical tissue adhesives are a potential alternative to experimental grade biomaterials for cell encapsulation and implantation due to their already established clinical use.

To date, only one medical device has been tested for cell encapsulation with promising results of NSC survival, proliferation and differentiation (Finch et al., 2020). This opens the possibility for a new family of biomaterials to be tested for their neuroregenerative capacity in order to create a bank of clinically available bioscaffolds that may suit different injury types.

In addition, it might be desirable to optimise the regenerative properties of such materials, which are currently used as tissue sealants, by functionalisation with laminin, to further mimic the tissue ECM and enhance repair.

Given all the previously described data, we hypothesise that Hemopatch™, a clinically available, porous, collagen surgical sealant could encapsulate NSCs for implantation into sites of SCI. The addition of laminin to the surface of the Hemopatch™, may also improve implant regenerative capacity through promoting cell attachment, cell growth or even cell distribution through the matrix.

Therefore, in order to test these hypotheses, the two objectives of this chapter are to:

1. Test whether Hemopatch™ can support NSC growth and differentiation.
2. Examine the feasibility and effect of biofunctionalisation of Hemopatch™ with the ECM molecule laminin on encapsulated NSC populations.

4.2 RESULTS

4.2.1 NSCs were successfully cultured in 3D within Hemopatch™

Five days after cell seeding, NSCs had dispersed through the biomaterial from the initial seeding area and distributed three-dimensionally, as seen by the presence of cells out of the plane of focus. Z-stack images (**Figure 4.2**) show nestin-positive cells (an NSC marker) in a 3D distribution. Importantly, cells can be observed in the Z-axis of the image at a depth from 0 to at least 50 µm into the Hemopatch™ piece. Unfortunately, imaging of cells further into the material was not possible due to the distortion of light caused by the thick layer of collagen scaffold. This distribution is true for both uncoated and coated pieces of Hemopatch™, although the Z-stack images suggested the distribution of cells in the XY-axis was different, with grouped cells in sphere formation in the uncoated group compared to single cells dispersed through the laminin coated group.

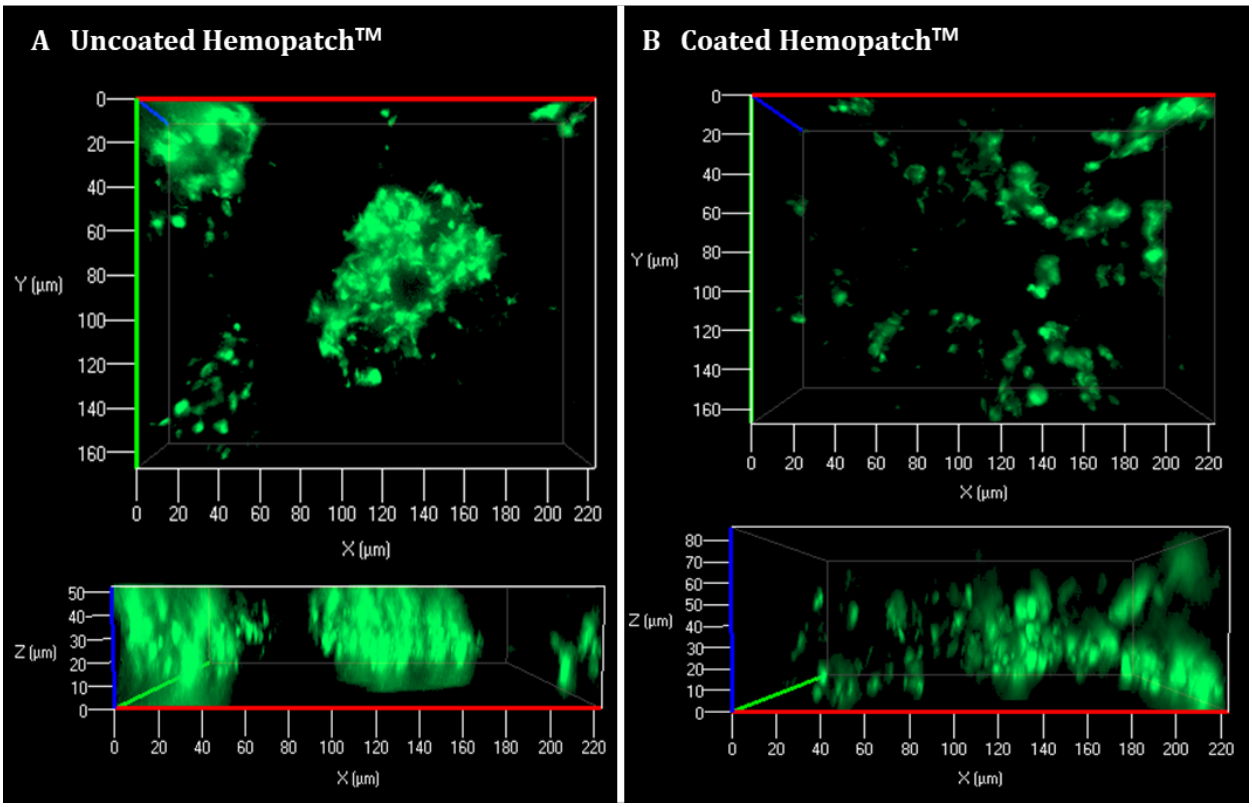

***Figure 4.2 3D distribution of NSCs**. Representative Z-stack images showing nestin-positive cells (a marker for NSCs; green) in the XYZ plane in uncoated Hemopatch™ (**A**) and coated Hemopatch™ (**B**). Top images showing a top-down view and bottom images showing a side view. These images aim to represent the 3D distribution of the cells on the material.*

4.2.2 Laminin coating improved cell distribution through the material

In the XY-axis, NSCs were evenly distributed and present as individual cells over the surface of the coverslips and the coated Hemopatch™, while cells within uncoated Hemopatch™ consistently appeared to form spheres dispersed in the gel (**Figure 4.3 A-C**). After quantification, it was found that between 1 and 3 neurospheres/field and between 0 and 1 neurospheres/field were counted for the glass and coated Hemopatch™ conditions respectively compared to 15-19 neurospheres/field in uncoated Hemopatch™, with a significant statistical difference (p=0.003) between coated and uncoated Hemopatch™ (**Figure 4.3 D**).

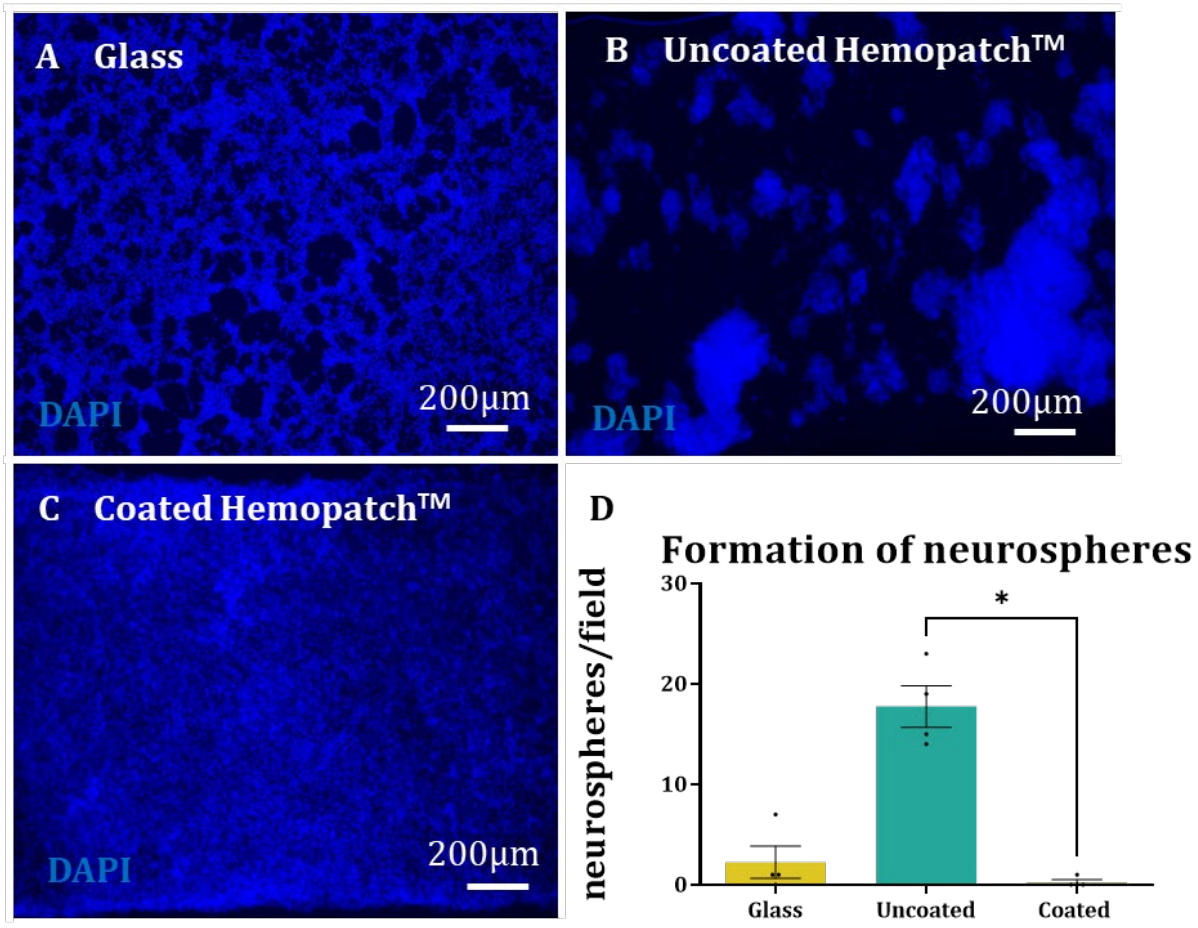

Figure 4.3 Cell distribution in the biomaterial. *Representative images of DAPI-labelled NSCs (blue) showing distribution on glass coverslips (**A**), uncoated Hemopatch™ (**B**) and coated Hemopatch™ (**C**) and scatter plot representation of cell distribution as the number of neurospheres per field (Kurskal-Wallis test, n=4, p=0.003) (**D**). Star representing p<0.05. A higher number of neurospheres were found in uncoated than in coated Hemopatch™.*

Under microscopic observation, a similar distribution pattern was recognised in all cardinal points of the glass coverslips and the Hemopatch™ pieces (*e.g*. centre, corners). However, a higher cell density was usually found in a single point of the scaffold, probably correlating to the cell seeding spot.

4.2.3 Neural stem cell survival remained high regardless of treatment

Cell survival was high across experimental groups as suggested by high calcein AM staining, which is a marker for live cells, compared to sparse red dots, indicative of dead cells stained with ethidium homodimer (**Figure 4.4 A-C**). NSCs in all conditions displayed over 80% viability, with no significant statistical differences between experimental groups (**Figure 4.4 D**).

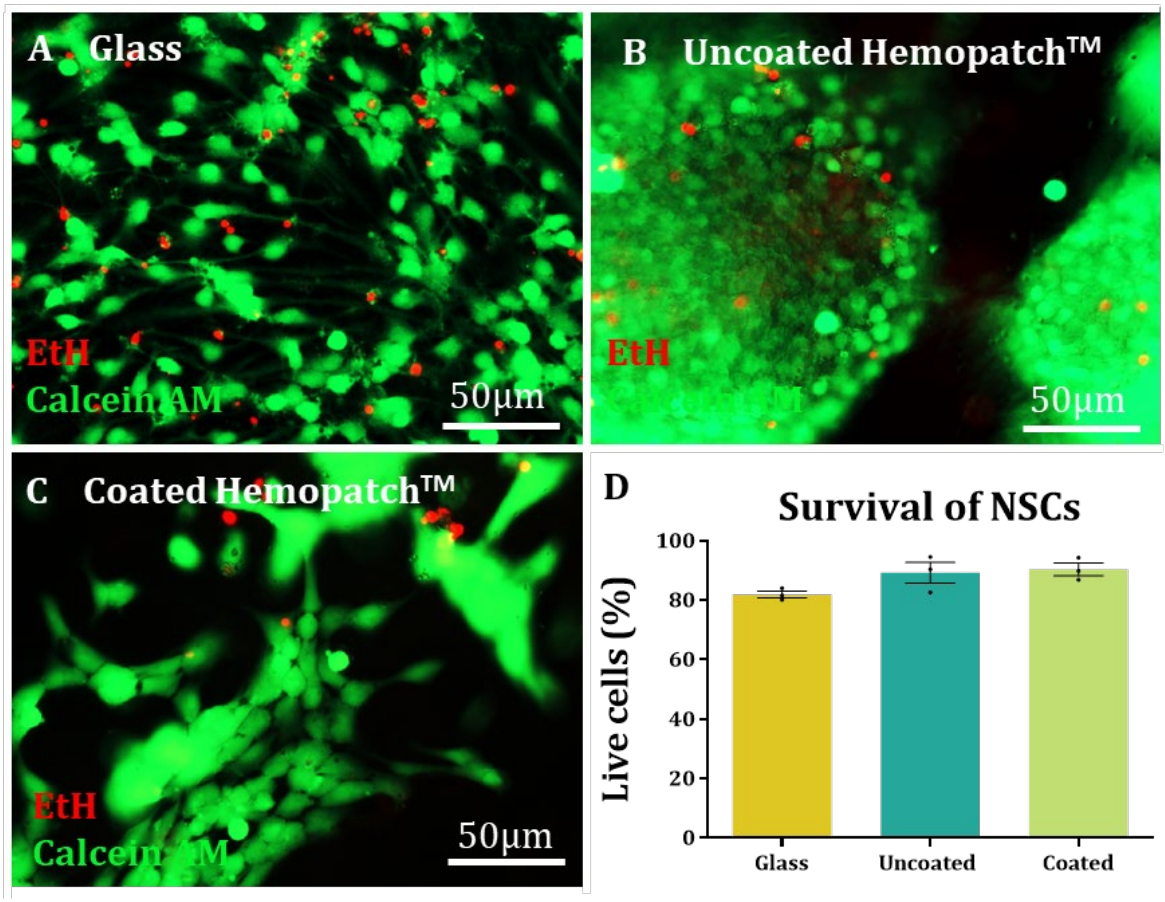

Figure 4.4 NSC survival in Hemopatch™. *Representative fluorescent merged images of NSC survival on glass coverslips (**A**), uncoated Hemopatch™ (**B**) and coated Hemopatch™ (**C**) with scatter plot representation of live cell percentages (Kurskal-Wallis test, n=3, p≥0.005) (**D**). Green channel representing Calcein AM staining and red channel representing ethidium homodimer (EtH) staining. No statistical differences were found between groups.*

4.2.4 Proliferation rates were similar in all conditions

EDU staining was detected across all samples and, as expected, was confined to the nucleus when observed in the NSCs. The number of EDU$^+$ nuclei, an indicator of proliferation, also remained similar in all groups (**Figure 4.5 A-C**). Approximately 20% of NSCS in all experimental groups had proliferated after 6 hours of incubation with EDU A (**Figure 4.5 D**).

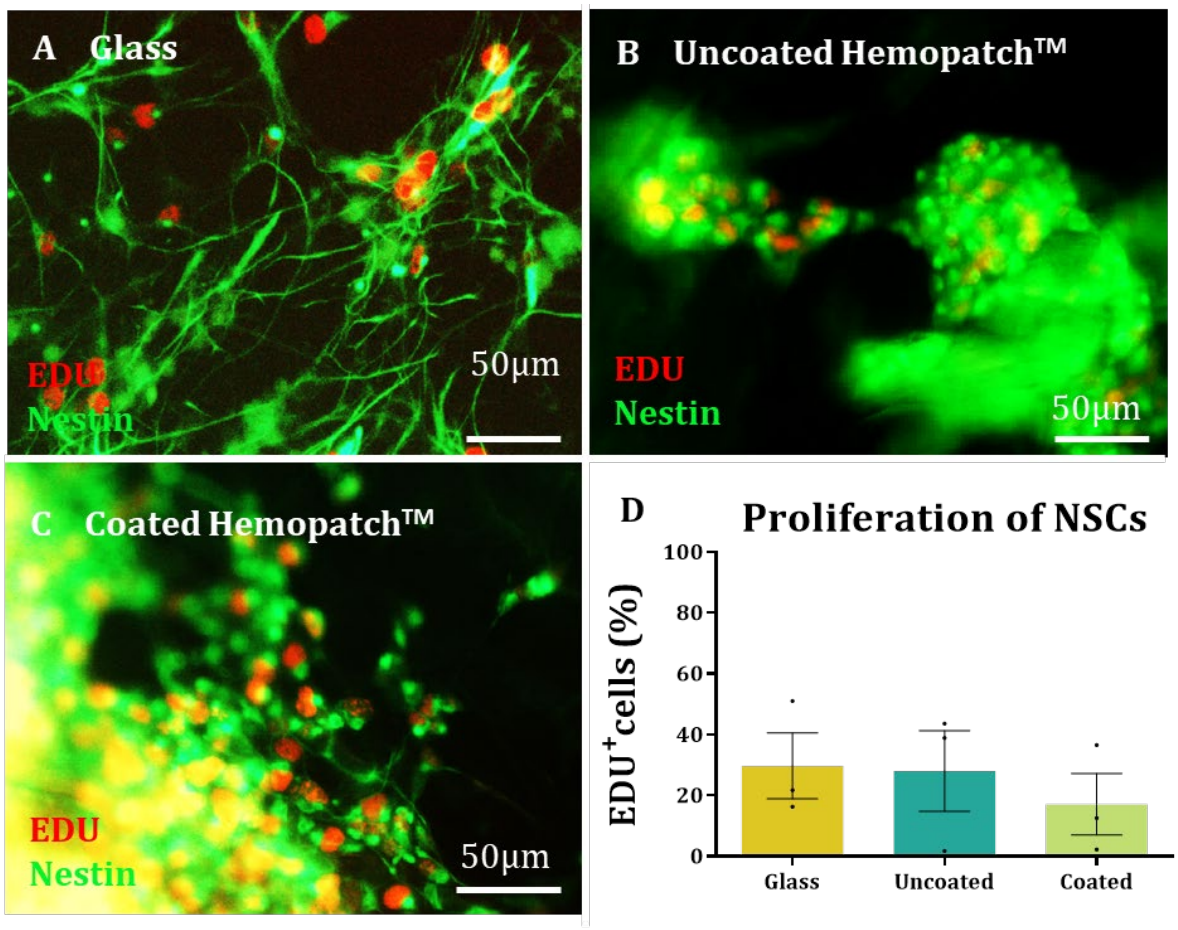

Figure 4.5 NSC proliferation in Hemopatch™. *Merged fluorescent images of EDU (red) and nestin (green) representing NSC proliferation on glass coverslips (**A**), uncoated Hemopatch™ (**B**) and coated Hemopatch™ (**C**) with scatter plot representation of percentage of proliferative cells (Kurskal-Wallis test, n=3, p≥0.005) (**D**). No differences were found between groups.*

4.2.5 Cell stemness was maintained for 5 days in all conditions

Nestin staining, an NSC marker, was carried out to determine the percentage of cells in the culture that were NSCs. All groups displayed high proportions of cells positive for Nestin with >98% of cells recorded as positive across all experimental groups (**Figure 4.6 A-C, G**), suggesting we obtained highly pure cultures of NSCs that were maintained after plating for, at least, 5 days. Cells generally displayed classical bipolar morphologies

associated with the NSC phenotype on glass with some evidence for this seen within the coated Hemopatch™ samples. NSC morphology was harder to discern in the uncoated Hemopatch™ where cells tended to form into neurospheres (**Figure 4.6 A-C**). The cultures were also stained with an anti-Sox-2 antibody, another marker for cell stemness, in order to provide more accuracy to our results. Sox-2 staining correlated with Nestin staining (as seen by co-expression of markers in one cell), indicating a robust identification of stem cells. (**Figure 4.6 D-F**). Similarly to Nestin, quantification of Sox-2 revealed >98% of positive cells for the marker (**Figure 4.6 H**).

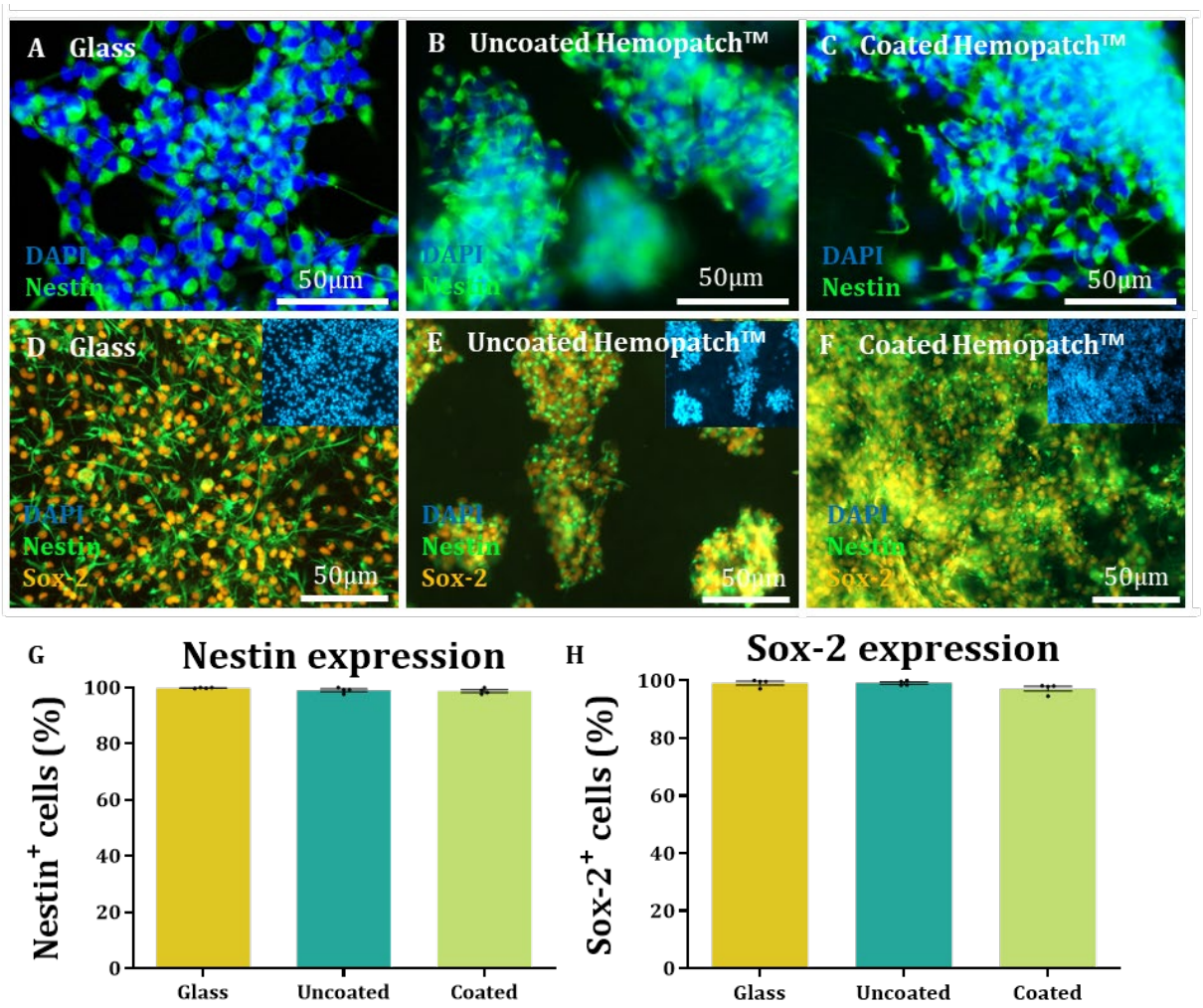

Figure 4.6 NSC markers in Hemopatch™. *Representative images of nestin-positive cells (green) merged with DAPI channel (blue) in glass (**A**), uncoated Hemopatch™ (**B**) and coated Hemopatch™ (**C**). And representative merged images of nestin (green) and sox-2-positive (orange) cells in glass (**D**), uncoated Hemopatch™ (**E**) and coated Hemopatch™ (**F**). The insets are DAPI stained counterparts. Scatter plots showing the proportions of cells expressing Nestin (**G**) (Kurskal-Wallis test, n=4, p≥0.005) or Sox-2 (**H**) Kurskal-Wallis test, n=4, p≥0.005) under each experimental condition. No differences were found between groups.*

4.2.6 Cell viability was maintained after differentiation in all groups

After seven days in differentiation conditions (NSC medium without EGF or FGF and with addition of 1% FBS), cell viability remained high. Calcein AM (green) stained the intact membranes of all cell types present in the culture: astrocytes, neurons, oligodendrocytes and, probably, a small amount of undifferentiated NSCs. Similarly, ethidium homodimer (red), stained the nuclei of all dead cells present in the culture (**Figure 4.7 A-C**). The proportion of viable cells was higher than 80% in all groups as judged by live/dead staining (**Figure 4.7 D**), indicating a highly viable culture 12 days after plating and 7 days after differentiation.

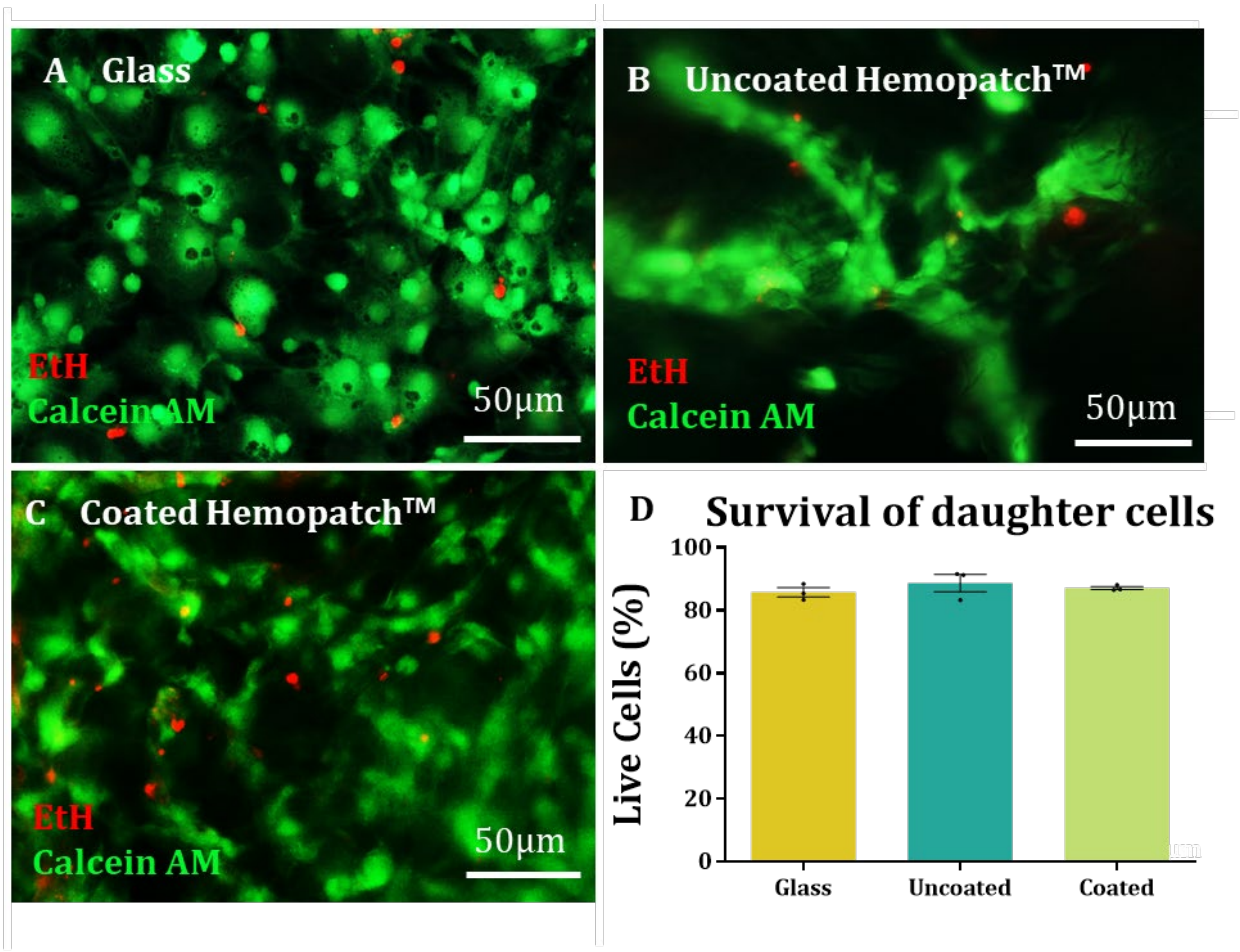

Figure 4.11 Daughter cell survival in Hemopatch™. *Fluorescence merged images of Calcein AM (green) and ethidium homodimer (EtH) (red) representing daughter cell survival in glass coverslips (**A**), uncoated Hemopatch™ (**B**) and coated Hemopatch™ (**C**) with scatter plot representation of Calcein AM⁺ cells relative to total number of cells (Kurskal-Wallis test, n=3, p≥0.005) (**D**). No differences were found between groups.*

4.2.7 Proliferation rates decreased after differentiation at a similar rate in all groups

Proliferation rates decreased after differentiation as expected due to the lower proliferative capacity of daughter cells compared to NSCs. The presence of EDU$^+$ cells in Hemopatch™, both coated and uncoated, was similar to coverslips after differentiation (**Figure 4.8 A-C**), with *ca.* 5% staining positive for EDU incorporation in each condition (**Figure 4.8 D**). No statistical differences were found between experimental groups.

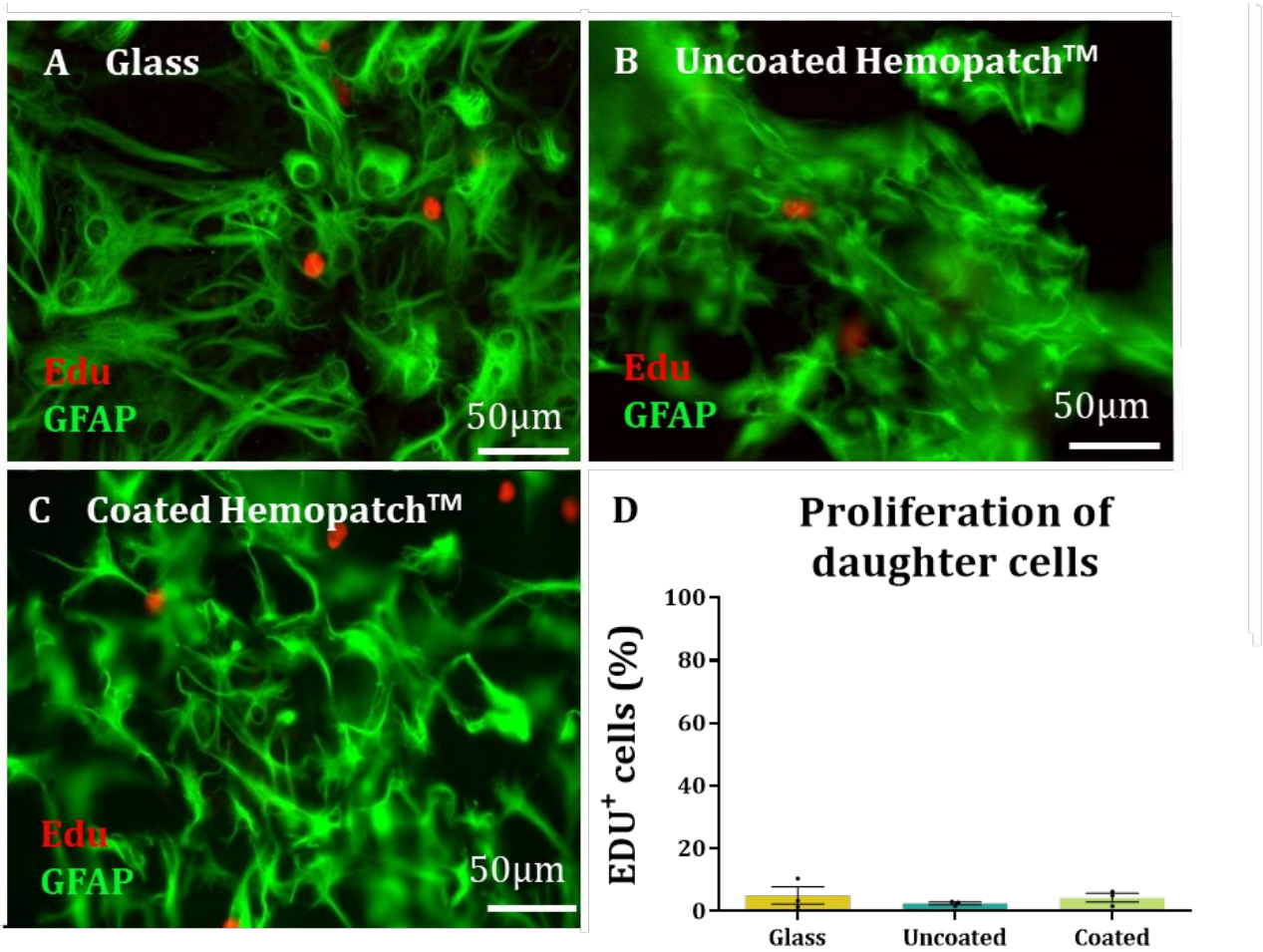

Figure 4.8 Proliferation of daughter cells in Hemopatch™. *Merged fluorescence images of Edu (red) and GFAP (green) representing daughter cell proliferation in glass coverslips (**A**), uncoated Hemopatch™ (**B**) and coated Hemopatch™ (**C**) with scatter plot representation of proliferating cell percentages (Kurskal-Wallis test, n=3, p≥0.005) (**D**). No differences were found between groups.*

4.2.8 No differences were found in the percentages of phenotypes after differentiation

Immunocytochemistry revealed that the NSCs had differentiated in all conditions into the expected phenotypes, namely astrocytes (**Figure 4.9 A-C**), neurons (**Figure 4.9 D-F**) and oligodendrocytes (**Figure 4.9 G-I**). Overall, more than 60% of the cells differentiated into

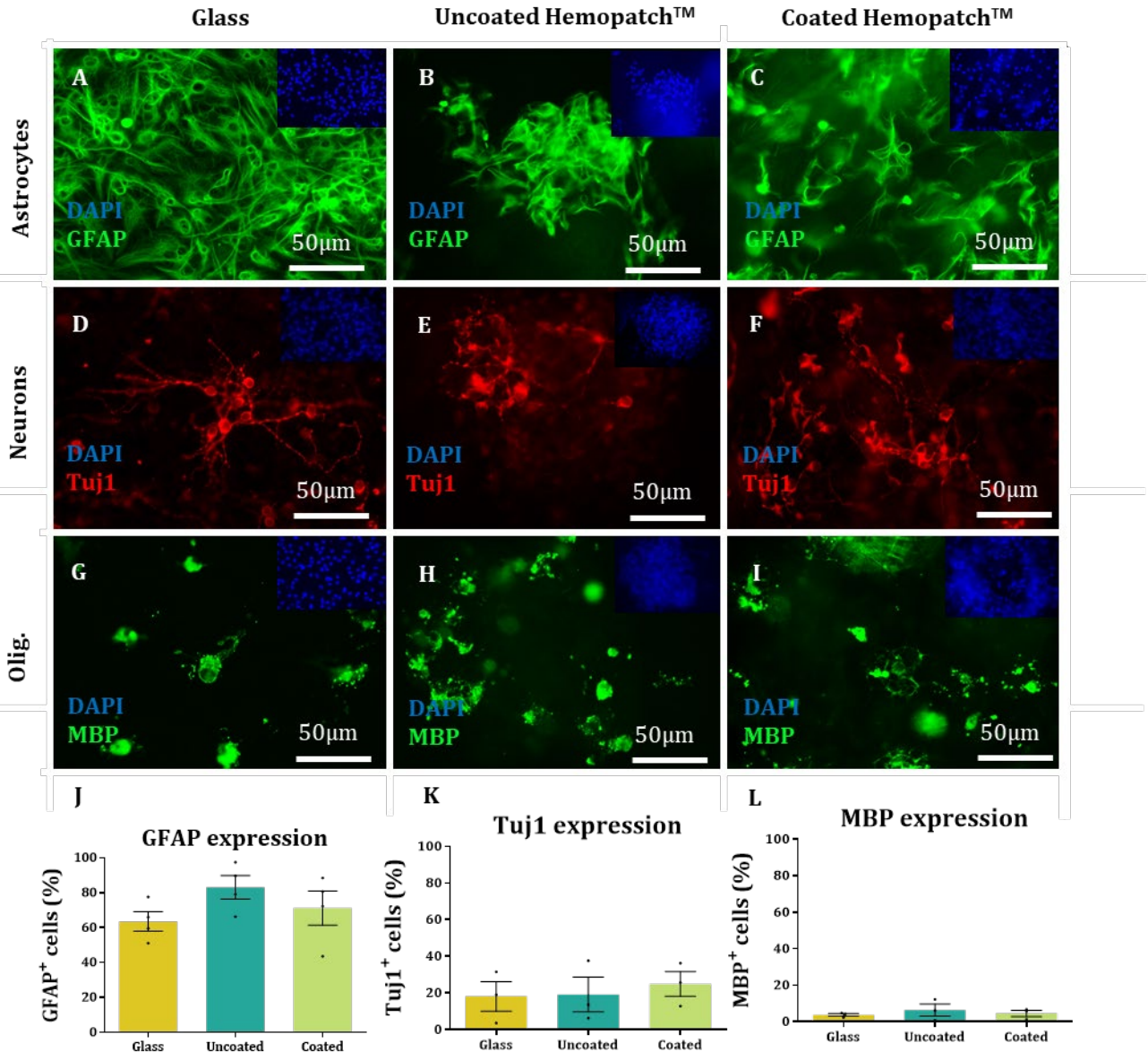

Figure 4.9 Astrocyte, neuron and oligodendrocyte markers in Hemopath™. *(**A-C**): Representative fluorescence images of GFAP stained astrocytes in glass (**A**), uncoated Hemopatch™ (**B**) and coated Hemopatch™ (**C**). (**D-F**): Tuj-1 stained neurons in glass (**D**), uncoated Hemopatch™ (**E**) and coated Hemopatch™ (**F**). (**G-I**): MBP stained oligodendrocytes in glass (**G**), uncoated Hemopatch™ (**H**) and coated Hemopatch™ (**I**). (**J-L**): Scatter plots show the proportions of each cell type: astrocytes (Kurskal-Wallis test, n=4, p≥0.005) (**J**), neurons (Kurskal-Wallis test, n=3, p≥0.005) (**K**) and oligodendrocytes (Kurskal-Wallis test, n=3, p≥0.005) (**L**). Image insets show DAPI stained counterparts. No differences were found between groups.*

astrocytes (**Figure 4.9 J**), >18% into neurons (**Figure 4.9 K**) and >3% into oligodendrocytes (**Figure 4.9 L**) in a consistent manner across the experimental groups with no statistically significant differences observed. The rest of the cells remained unidentified and were possibly undifferentiated stem cells. The daughter cells appeared to retain the pattern of distribution seen for the NSCs, with cells in the uncoated samples remaining in groups and an even distribution noted in the coated samples. In general, daughter cells displayed normal morphologies as expected in *in vitro* culture conditions.

However, astrocytes grown in Hemopatch™ did appear more processed compared to the broad, flattened appearance of astrocytes grown on glass coverslips. In general, cell projections were observed extending throughout the construct and travelled in and out of the plane of focus, highlighting the 3D nature of the culture as compared to glass coverslips. In general, astrocytes were found dispersed within the material, and forming the main body of the spheres in the case of uncoated Hemopatch™. Neuronal somas were usually found in groups, possibly associated with astrocytes judging by the high number of non-stained nuclei around them, with projections in all directions. Oligodendrocytes, fewer in number, were also found associated with other cell types. In some cases, projections could be observed. However, no clear myelination tracts were observed in any of the conditions, perhaps due to the short duration of the culture.

Finally, we showed the feasibility of processing these constructs for imaging via SEM. Here, we were able to visualise the porosity of the material (**Figure 4.10 A**) and the presence of neurospheres on uncoated Hemopatch™ but not on the coated Hemopatch™ (**Figure 4.10 B-C**). Moreover, we were able to identify differentiated NSCs on the collagen fibres (**Figure 4.10 D-I**). Putative cell subtypes are highlighted in **Figure 4.10 (D-F)**, although these need to be confirmed through combinatorial techniques such as

immunogold labelling. The original SEM images are below for comparison (**Figure 4.10 G-I**).

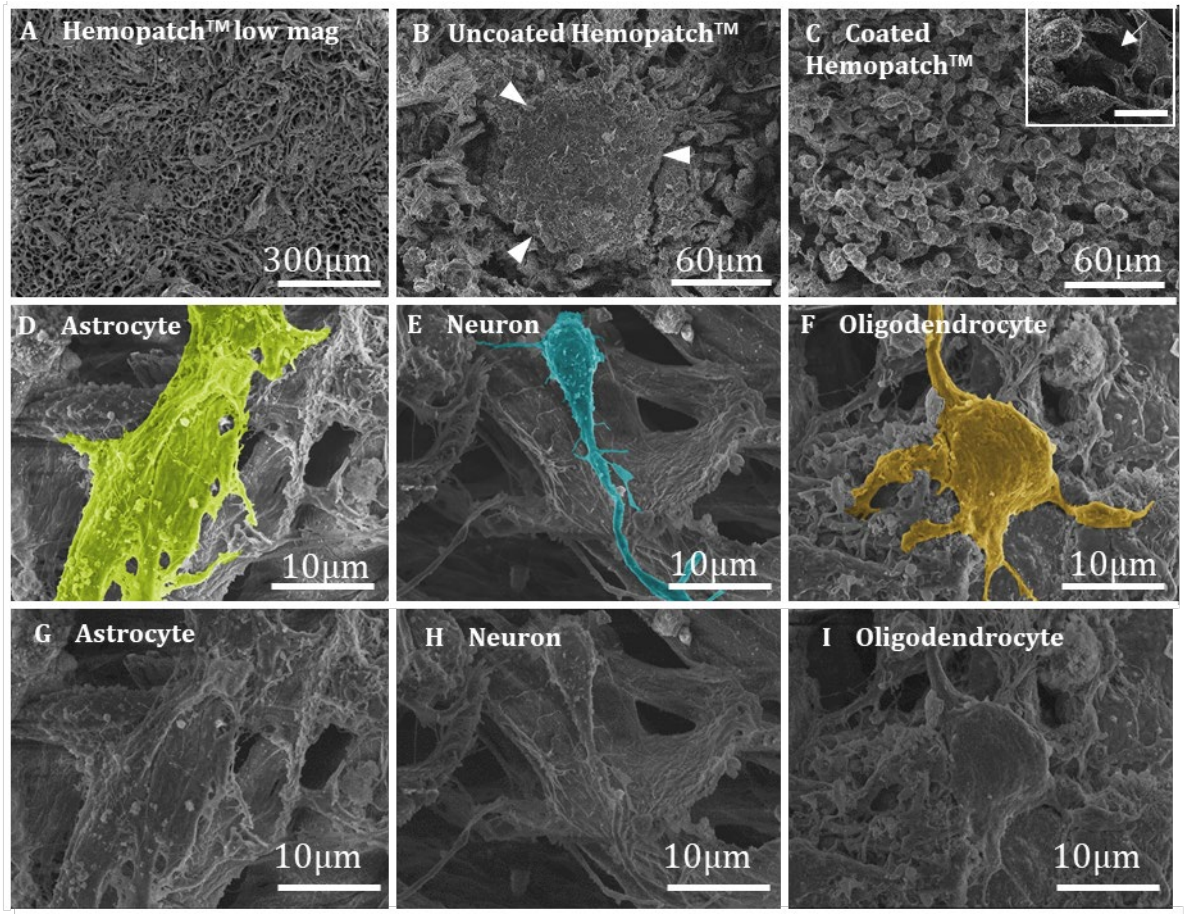

***Figure 4.10 SEM images from OTOTO prepared samples**. (**A-C**): Low magnification image of coated Hemopatch™ depicting the porosity of the construct (**A**), cells in a neurosphere formation on uncoated Hemopatch™ (**B**) and single cells on coated Hemopatch™ Arrows indicate edges of the neurosphere (**C**) Inset showing a single cell on the material. Scale bar: 10µm. (**D-F**): Differentiated NSCs on coated Hemopatch™: astrocyte (**D**), neuron (**E**) and oligodendrocyte (**F**). Colour indicates our interpretation of the cell bodies. (**G-I**): Original SEM images for D, E and F. SEM images allowed for the direct visualisation of cells on the biomaterial.*

4.3 DISCUSSION

4.3.1 Summary of aims and results

Here we show that a clinically relevant primary NSC population can be safely cultured within Hemopatch™ and that this does not affect the survival, proliferation or differentiation of the cultured cells. In addition, we also show that a simple biofunctionalization step with laminin can induce improved cell distribution through the material. Our results corroborate the fact that clinically available materials have translational potential for implantation in SCI with potential implications in reducing the time it takes for such therapies to reach the clinic. Additionally, we were able to modify the scaffold through laminin engineering, opening the possibilities of finely tuning the characteristics of these surgical biomaterials in order to optimise them for cell encapsulation. These findings will be discussed in the following sections.

4.3.2 Hemopatch™ as a scaffold for neural stem cell transplantation to spinal cord injury

According to our results, Hemopatch™ allows for the culture of NSCs and their progeny with high survival rates and without affecting proliferation or differentiation rates. Therefore, our findings suggest the surgical sealant Hemopatch™ could be used as a bioscaffold for SCI implantation. This might have potential implications in shortening the translation time of bioscaffold implantation for SCI to the clinic due to an already established clinical use of this material.

In terms of physicochemical properties, Hemopatch™ is a porous, sponge-like structure mainly fabricated using collagen type I, a material with several benefits for implantation into sites of SCI (Lee et al., 2001). Porous collagen scaffolds have been previously reported to support NSC encapsulation for SCI implantation with associated motor recovery in mice (Kourgiantaki et al., 2020). Our data indicates that the surgical sealant Hemopatch™

could also support the encapsulation of the clinical transplant population of NSCs without affecting normal cell behaviour, *e.g.* survival, proliferation and differentiation when compared to standard glass cultures, supporting our hypothesis.

The pores in Hemopatch™, which are approximately 10μm in diameter, allowed for cell infiltration and attachment throughout the material, as suggested by the presence of cells in different focal planes of the Z-axis. Once implanted, the porosity of the material may also facilitate nerve fibre in-growth and cellular infiltration. The infiltration of macrophages and lymphocytes within Hemopatch™ has been previously reported in the rat liver (Nissen et al., 2017). The implantation of a material which allows host cell penetration is crucial to allow full repair of spared axons that might persist in the injured tissue. Unfortunately, our microscope only allowed imaging up to, approximately, 50μm of depth in the Z-axis. This was possibly due to high distortion of the light due to a thick layer of collagen scaffold. For a detailed characterisation of the 3D distribution of cells within the material, confocal imaging might be an alternative to obtaining high quality images. This might also allow quantification of cell morphology or axonal length.

Besides its physicochemical properties, Hemopatch™ is currently manufactured as a 2 mm thick sheet of flexible collagen, in approximately 15 x 4 cm dimensions. This can be simply cut to a desired shape and is conformable allowing ease of handling. An average intramedullary lesion length size for cervical injuries was reported to be *ca.* 7 cm (Aarabi et al., 2017), suggesting the patches in their current form could cover most injuries (although the largest lesions were up to 19 cm in length). It can be envisaged that these could be cut to size, seeded with NSCs, cultured for up to 5 days then implanted into the site of injury.

Furthermore, Hemopatch™ has a CE-marking certificate for clinical use and, therefore, has been reported safe for implantation in humans. This, combined with an already

established manufacturing process and routine clinical use, means that this tissue sealant might not require to go through a strict PMA process to be clinically used as a bioscaffold implant. This is crucial for the translation to the clinic of this therapy, which is now facing long delays due to the extended use of experimental grade, laboratory fabricated scaffolds.

Although the safety of Hemopatch™ upon implantation has already been tested, its efficacy as a bioscaffold remains unknown. Here, we report its ability for cell encapsulation and, later on, its permissiveness for host cell infiltration. In the future, it will have to be tested, with and without encapsulated NSCs, in *in vivo* animal models and in clinical trials before becoming routinely used.

4.3.3 Enhancing the regenerative properties of Hemopatch™ through laminin functionalisation

We also found that a simple coating step of Hemopatch™ with laminin promoted an even pattern of cell distribution through the material instead of the sphere formation observed in uncoated samples, without affecting survival, proliferation or differentiation of cells. This finding has implications in reducing cell aggregation after transplantation which can lead to uneven repair and, therefore, to incomplete recovery. Our findings are in accordance with other studies in which laminin improved cell distribution in 3D scaffolds (Luo et al., 2018).

The cellular mechanism underpinning these differences is not yet clear, but it could be that the presence of ECM molecules facilitates migration of the cells through the material whereas in their absence the cells remain in place and divide to become neurospheres (Flanagan et al., 2006). Both systems may have advantages. On one hand, improving cell distribution by coating the material with ECM molecules could avoid the issue of cell aggregation and ultimately enhance even repair throughout injury sites. On the other

hand, higher survival rates have been observed after transplantation of NSCs as neurospheres compared to dissociated cells in sites of SCI in rats (Mothe et al., 2008), potentially providing additional protective benefit to the encapsulated cells. Both formats would need to be tested in sites of *in vivo* SCI to examine which could lead to the greatest functional recovery.

As far as we are aware, laminin is not yet used clinically and ECM coating would require additional safety testing steps for CE-marking approval. However, a number of companies already produce chemically defined and animal component-free, human laminin isoforms using commercially scalable processes adaptable to producing clinical grade laminin.

4.3.4 Future directions

Alongside the expansion in biofunctionalisation of scaffolds designed to support cell transplant populations and further enhance regenerative responses, tuning cellular and tissue responses to the scaffold through other techniques might be desirable to obtain a fully optimised product.

Our data shows that NSC culture within Hemopatch™ with or without laminin functionalisation does not affect the NSC differentiation outcomes. However, it has been reported that, once implanted in the injury environment, NSC differentiation towards a neuronal phenotype can be impaired by myelin associated proteins, which promote astroglial differentiation (Wang et al., 2008). Therefore, in order to restore lost neuronal populations, various studies report the incorporation of different factors that might promote neuronal differentiation. For example, functionalisation of collagen scaffolds with EGFR antibody (Xiaoran Li et al., 2013) or a microtubule-stabilising agent (Xiaoran Li et al., 2018) directed NSC differentiation towards a neuronal phenotype. It seems feasible that Hemopatch™ could be further functionalised for directed neuronal differentiation in a similar fashion if desired.

Further, the pores in Hemopatch™ are randomly ordered but the spinal cord displays highly ordered, aligned structures such as the corticospinal tracts. It may therefore be desirable to enhance cell alignment within the construct to aid repair of these structures. Application of an 80 mV/mm alternating current to neurons cultured in a 3D silk protein matrix resulted in axons growing in parallel to the electrical field. (Tang-schomer, 2018). Given the porous, open nature of Hemopatch™, it seems feasible that this strategy could be employed here to influence encapsulated cell behaviour.

One of the most evident complications when it comes to SCI treatment is the different types of injury, *e.g.* transecting, compression, complete, incomplete, etc. Therefore, it makes sense to provide each type of injury with an adapted treatment. However, this can prove to be extremely complex and expensive (*e.g.* training of personnel in multiple techniques, acquisition of specialised reagents and equipment, wide variety of possible side effects, years of delay in experimental grade research, etc.). Since the main variation between different SCI types is of a physical nature, providing specialised physical treatment combined with routine biological treatment can be the key to a specially designed but simple and cost-effective treatment. This could be achieved through implantation of NSCs in combination with an appropriate bioscaffold to each lesion type. In addition, as demonstrated in this study and others (Finch et al., 2020), clinical tissue adhesives have great potential for cell encapsulation and can be adapted to different lesions.

For example, porous matrixes might provide the most optimal scaffold for host cell infiltration and transplant cell encapsulation. Although most of these, like Hemopatch™ or Duragen™, are flexible and can be cut to a desired size and shape, they might induce further injury when implanted within an incomplete injury. Therefore, an injectable gel might be more suited to this type of injury. For example, Tisseel™ is a porous, fibrin-based sealant that gels *in situ*, adapting to the environment's shape. In other scenarios, when

there is an open wound and emergency treatment is needed, a sprayable matrix, like CoStasis™ or SprayGel™, could provide an alternative to other scaffolds.

Given the previous evidence, our data can provide manufacturers a framework (identifying suitable material physiochemical properties and biofunctionalisation strategies) to develop their own materials and protocols for repurposing existing medically approved scaffolds for neural cell transplantation. The ultimate goal is to create a bank of clinically available bioscaffolds to suit different types of SCI. Moreover, these could be further functionalised to enhance their regenerative properties through *e.g.* promotion of even cell distribution, directed neuronal differentiation or promotion of cell alignment.

5 TARGETING ORIENTED AXONAL GROWTH THROUGH NEURAL STEM CELL CULTURE ON ALIGNED NANOFIBRE CONSTRUCTS

5.1 BACKGROUND

5.1.1 The aligned nature of the spinal cord

The spinal cord consists mainly of ascending and descending axonal tracts, providing the tissue with a highly oriented structure. As discussed in **Chapter 1**, these tracts are unable to regenerate upon injury due to the toxic environment of the lesion gap. The combinatorial effects of cell therapy and bioscaffold implantation might be key to achieving effective repair due to their ability to target multiple aspects of the lesion through, for example, cellular repopulation and providing neurotrophic support (Kourgiantaki et al., 2020).

Due to the highly aligned nature of the spinal cord, an important factor to consider when aiming to regenerate severed axons is the direction in which these grow. Directed axonal growth is crucial in order to re-establish highly organised connections and prevent unnecessary and non-functional connections. In fact, implantation of a construct of aligned nanofibres in rats after SCI resulted in extensive cellular penetration, similarly to implantation of random constructs (Liu et al., 2012), suggesting that the aligned constructs do not impair the regenerative capacity of the biomaterials. In addition, the spinal cords treated with aligned biomaterials appeared more structurally intact when compared to random controls (Liu et al., 2012). Moreover, longer axonal length of cultured neurons on aligned fibres has been suggested when compared to random fibres (F. Yang et al., 2005).

Despite the evidence, the vital importance of porosity in the bioscaffold implant to allow cell infiltration has led to the fabrication of, mostly, porous, randomly oriented materials. Consequently, the effects of cellular alignment to SCI repair remain understudied and

translation to clinic will take longer. Therefore, there is a need to optimise directed axonal growth and study the underpinning mechanisms involved.

5.1.2 Guidance cues for directed axonal growth

The elongated tips of growing axons, known as "growth cones", express guidance receptors, which interact with attractive and repulsive guidance cues from their environment to, ultimately, lead the axon towards its final synapsis site (Stoeckli, 2018). Evidence suggests that such cues could be provided by cell surface adhesion molecules and chemotactic molecules from glial cells (N. Zhang et al., 2005).

For example, astrocytic Ca^{2+} waves have been reported to guide growing axons towards remote areas of neuronal activity (Hung & Colicos, 2008). In a 2D setting, electric field-induced astrocyte alignment, directed future neurite outgrowth and alignment (Alexander et al., 2006). Similar research has been translated to a 3D *in vitro* environment, in order to provide the model with the dimensional characteristics of the tissue, with similar results. The *in vitro* formation of 3D aligned astrocyte conduits, permitted neuronal attachment and enhanced aligned neural extension (Katiyar et al., 2018). In another study, the seeding of neurons on 3D collagen constructs containing aligned astrocytes, resulted in greater neurite growth and alignment than on non-aligned astrocytic areas (East et al., 2010).

In addition, neuronal alignment has been attempted through other methods. For example, the exposure of cortical neurons to an alternating current for 4 days resulted in an increase of axonal length and parallel alignment of axons to the electric field (Tang-schomer, 2018).

However, due to the simplicity of the process, probably the most popular alignment methodology is the culture of cells on readily aligned materials. Electrospinning is a relatively new alternative to creating fibre constructs that can overcome some of the

limitations associated with traditional nerve guidance conduits. For example, they exhibit high porosity and high surface area, increasing cell-scaffold interactions, and the fibre diameter can vary from nanometers to micrometers (F. Yang et al., 2005). In addition, they can be functionalized via encapsulation of bioactive molecules and can be collectively orientated, a desirable property for axonal guidance (Xie et al., 2010). This versatile technique allows the formation of aligned constructs with different materials such as poly (l-lactic) acid (PLLA) (F. Yang et al., 2005), PCL (Xiaoran Li et al., 2016), polyethersulfone (PES) (Christopherson et al., 2009), etc.

PCL is a synthetic polymer of the polyester family (Dwivedi et al., 2020). It has a melting temperature between 59 and 64°C, meaning that it attains a rubbery state at physiological temperatures resulting in a strong and elastic material (Dwivedi et al., 2020). Importantly, it is biocompatible and biodegradable (Dwivedi et al., 2020). Moreover, it is a malleable biomaterial, and can be conformed into multiple structures (Siddiqui et al., 2018). In fact, PCL biomaterials can be conformed as porous or fibrous scaffolds (Dwivedi et al., 2020). Fibrous scaffolds can be electrospun with a random or an aligned orientation (Dwivedi et al., 2020), providing the material with potential characteristics for axonal guidance (Liu et al., 2012). These types of fibres have been used in combination with neural-derived cell culture (Xiaoran Li et al., 2016; Sharifi et al., 2016; Silantyeva et al., 2018; Soliman et al., 2018).

5.1.3 Tests with electrospun biomaterials

Previous studies have successfully cultured cells on aligned electrospun fibre constructs (**Table 5.1**).

Table 5.1 List of previous evidence regarding the study of stem cells on aligned electrospun nanofibers*. This table summarises the methodology of previous research on the use of electrospun biomaterials for cell culture.*

Type	Material	Cell type	Culture duration	Reference
In vitro	PCL	ESC	14 days	*Silantyeva et al. 2018*
In vitro	PLLA	NSC	5 days	*He et al. 2010*
In vitro	PCL	NSC	7 days	*Sharifi et al. 2016*
In vitro	PLLA	NSC	2 days	*Yang et al. 2005*
In vitro	Gelatine + PCL	Neuroblastoma x gliome hybrid cell line	5 days	*Soliman et al. 2018*
In vitro	PLGA	ESC	14 days	*Sperling et al. 2017*
In vivo	PLLA	-	4 weeks	*Hurtado et al. 2011*

For example, NSCs differentiated into neurons and seemed to align at ≤10° of the fibre direction (Sharifi et al., 2016; F. Yang et al., 2005). In addition, neurite length was reported higher on aligned fibre constructs than on random fibre constructs (F. Yang et al., 2005). NSCs seeded on radially aligned fibres seemed to respond with a higher migration rate with the presence of chemotactic cues provided by a gradient of stromal-cell-derived factor-1α (SDF1α) (Xiaoran Li et al., 2016).

In another study, the functionalization of aligned fibres with a peptide sequence found in laminin seemed to allow cell survival and alignment of neurons with the fibres. Furthermore, mouse embryonic stem cells (mESC) seemed to express mature neuronal markers at earlier time points than when cultured on laminin coated coverslips (Silantyeva et al., 2018). Similarly, mESC grown on aligned fibres differentiated towards a neuronal phenotype at a higher rate than when the mESC where seeded on random fibres or a gelatin control (Sperling et al., 2017).

In vivo, the implantation of a conduit of aligned electrospun fibres on a complete transection of the spinal cord in rats resulted in robust and long distance axonal regeneration when compared to random fibre controls (Hurtado et al., 2011). Such fibres have also been reported to allow incorporation and slow release of molecules of varying sizes (e.g.: NT-3 and miR-222) for SCI treatment, enhancing axonal regeneration in rats (Nguyen et al., 2017).

5.1.4 Knowledge gaps and aims

These recent advances in the field highlight the need to test and develop a clinically relevant, aligned cell implant. However, current research has relied on use of cell lines or ESC derived NSCs. Such cell lines have inherent risks associated with teratoma formation, especially if residual ESCs are present, and they lack robust and reproducible differentiation protocols (Mothe & Tator, 2012; Tapia & Scholer, 2016) (**Chapter 1**). Further, part of the therapeutic potential of NSCs is to differentiate into their daughter cells and it can be predicted that alignment of both NSCs and daughter cells will facilitate repair. However, there is limited systematic assessment of alignment of NSCs and daughter cells on aligned electrospun nanofibres and, to date, there is no established methodology to statistically compare alignment between biological repeats, making data interpretation qualitative and not reproducible.

Given the above, this study aims to:

1. Develop a new and reproducible quantification strategy to characterise alignment in fibres and associated alignment in neural cells.
2. Systematically assess alignment of a primary culture of NSCs and differentiated progeny
3. Examine the safety of the aligning NSCs on manufactured, electrospun nanofibres.

5.2 RESULTS

5.2.1 The nanofibres provided either random or aligned substrates for cell culture

Phase microscopy revealed matrices of random or aligned nanofibres (**Figure 5.1 A, B**), forming a compact but porous structure that would potentially allow for a thin 3D culture of cells. The fibres provided by the company were delivered in individual inserts placed in 24-well plates, with each insert consisting of a plastic ring holding all the edges of the fibres under tension. The computational analysis showed that the fibres from aligned constructs were indeed aligned, as represented by a high frequency of fibres oriented towards the same direction, as seen by a directionality peak that was approximately 4-fold higher than on random fibres (**Figure 5.1 C**). In order to analyse whether this

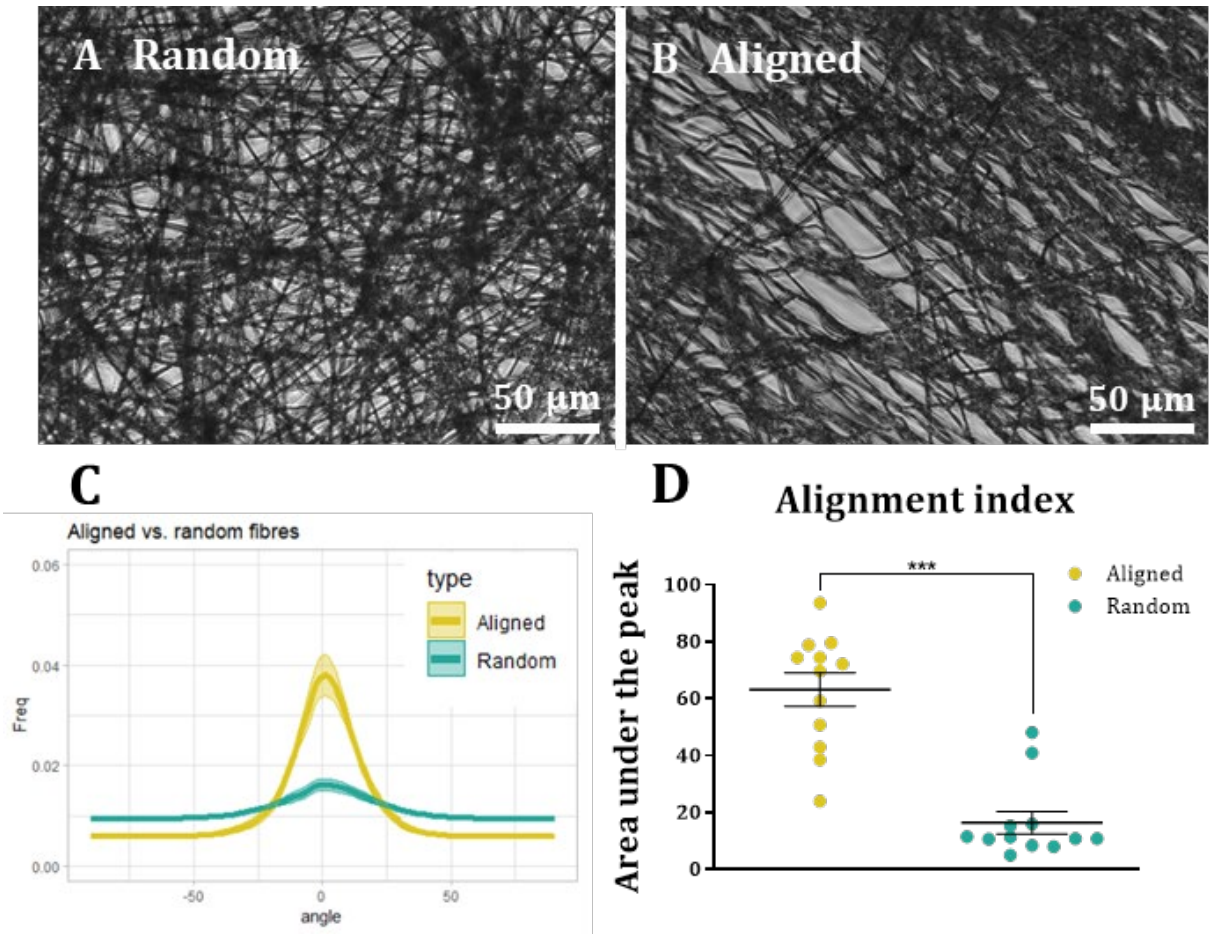

Figure 5.1 Orientation of random and aligned fibres*. Representative bright field images of random (**A**) and aligned (**B**) fibres with orientation graph showing the frequency at which the fibres (Y) were orientated towards each angle (X) (**C**) and comparison of alignment indexes (area under the peak) between random and aligned fibres (**D**) (Wilcoxon test for paired samples, n=12, p=0.0005). The stars represent p<0.05 and each dot represents one construct analysed. These data indicate that alignment is higher in aligned constructs than in random.*

difference was statistically significant, the area under the peak for each fibre type was calculated. Then, a t-test of the average results showed a significant difference between the orientation peak of the two types of fibres (**Figure 5.1 D**), confirming that the aligned materials had greater consistency of fibre orientation.

5.2.2 A healthy population of NSCs was aligned along the nanofibers

NSCs were seeded onto glass coverslips and scaffolds of random fibres and aligned fibres. A survival assay revealed over 90% NSC survival across all conditions after 5 days *in vitro* (**Figure 5.2 A-C**), with no statistical differences between groups (**Figure 5.2 D**). In addition, a proliferation assay also revealed no statistical differences in proliferation rate across conditions after 6h of incubation with Edu reagents (**Figure 5.2 E-H**).

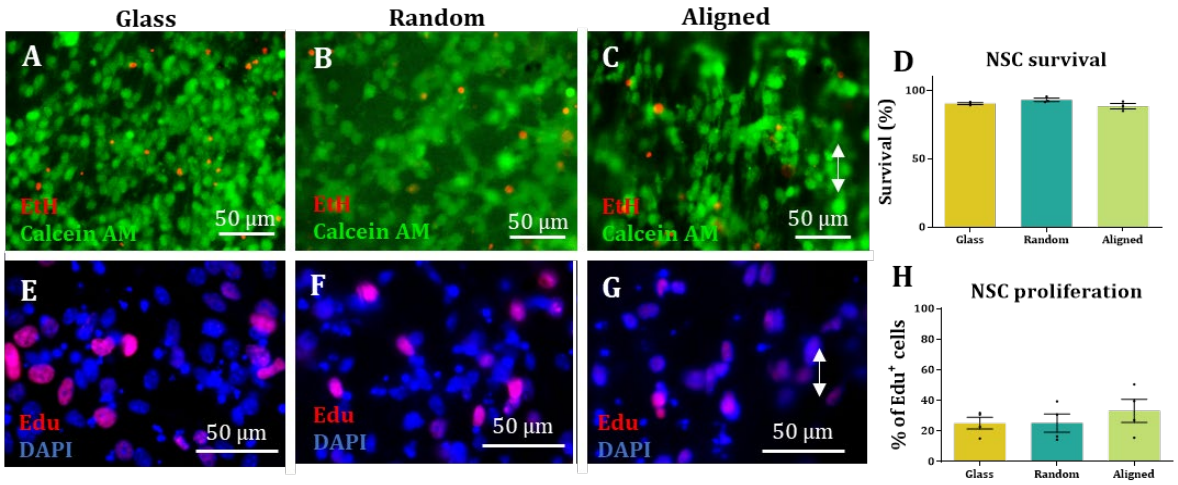

Figure 5.2 Survival and proliferation of NSCs on fibres*. NSC survival assay (**A-D**): Representative images of NSCs stained with Calcein AM, indicating live cells (green) and Ethidium homodimer (EtH), indicating dead cell nuclei (red) on glass (**A**) random fibres (**B**) and aligned fibres (**C**) and graphical representation of survival rates (Kurskal-Wallis test, n=3, p≥0.005) (**D**). NSC proliferation assay (**E-H**): Representative images of NSCs stained with DAPI, a cell nuclear marker (blue) and Edu, a proliferative cell nuclei marker (red) on glass (**E**), random fibres (**F**) and aligned fibres (**G**) with graphical representation of proliferation rates (Kurskal-Wallis test, n=4, p≥0.005) (**H**). No differences were found between groups.*

After 5 days of culture they were fixed and stained with Nestin (a cytoskeleton marker) and Sox-2 (a nuclear marker) (**Figure 5.3 A**). In all three conditions, approximately 100% of cells were positive for both markers, with no statistical differences between groups (**Figure 5.3 B, C**).

Cells seeded on random fibres (**Figure 5.3 D**) were randomly oriented, suggested by the absence of a pronounced peak of cell orientation (**Figure 5.3 E**). Moreover, a correlation analysis indicated there was no correlation between fibre and cell orientation (r=0.184; p=0.080) (**Figure 5.3 F**). However, when NSCs were seeded on aligned fibres a peak of

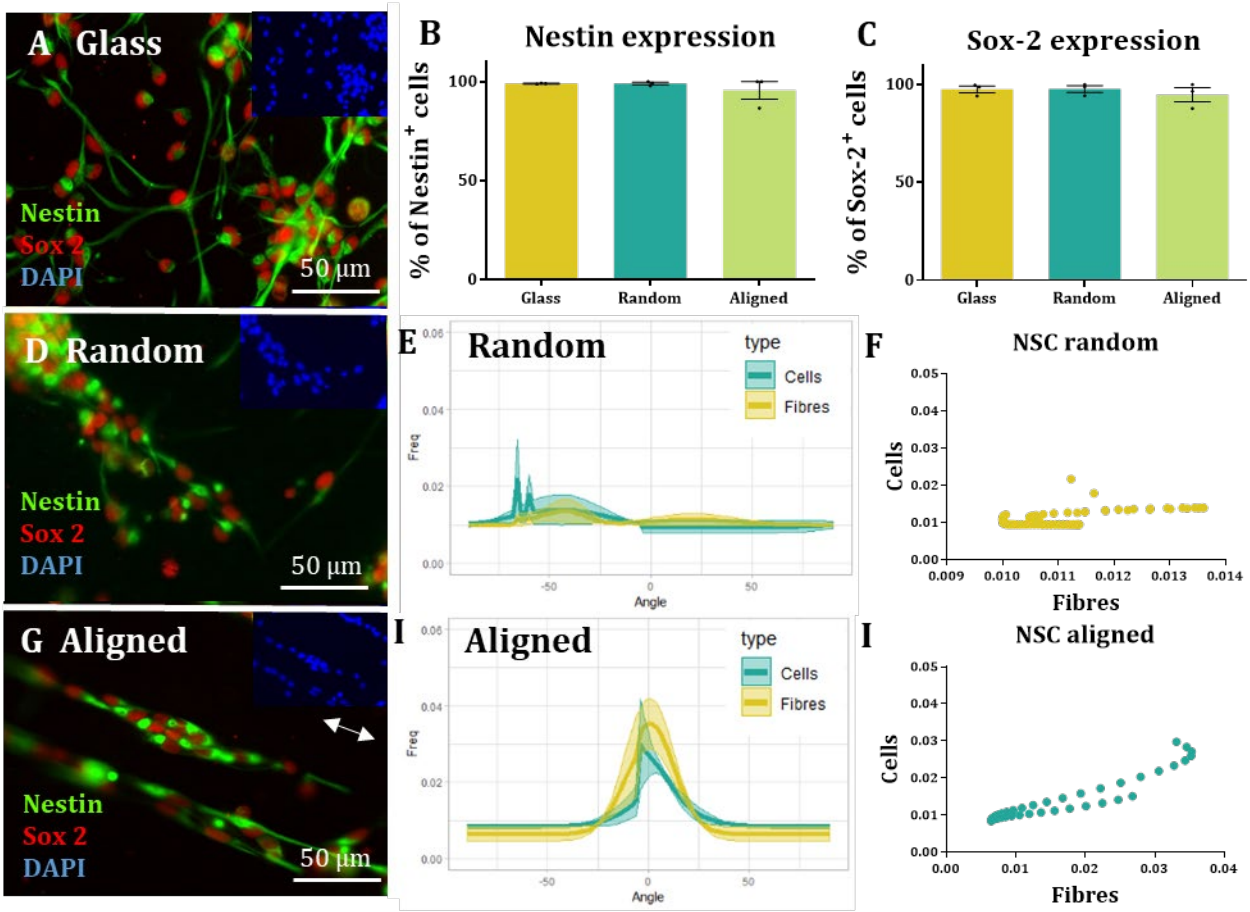

Figure 5.3 Phenotype and orientation of NSCs on electrospun fibres*. Representative image of NSCs on glass stained with NSC cytoskeleton marker Nestin (green) and NSC nuclear marker Sox-2 (red) with insets showing nuclear marker DAPI (blue) (**A**). Bar graphs represent the percentages of Nestin positive cells on glass, random and aligned substrates (Kurskal-Wallis test, n=4, p≥0.005) (**B**) and Sox-2 positive cells (Kurskal-Wallis test, n=4, p≥0.005) (**C**). Error bars indicate SEM and scatter dots indicate the mean values of each biological repeat. (**D**) is a representative image of Nestin and Sox-2 positive cells on random substrates, with inset representing DAPI stained counterpart. XY graph indicates the frequency at which cells and random fibres are oriented at each angle, with halo representing the SEM (**E**). Scatter plot representing the correlation of directionality between cells and fibres on random substrates (r=0.1842, p>0.0804) (**F**). Image (**G**) is representative of Nestin and Sox-2 positive cells on aligned fibres, with blue inset representing the DAPI stained counterpart and the white arrow indicating the direction of the fibres. XY graph represents the frequency at which cells and fibres are oriented at each angle on aligned constructs, and halos represent SEM (**H**). Finally, the scatter plot represents the correlation of orientation between cells and fibres in aligned constructs (r=0.9680, p>0.0001) (**I**). Blue dots on scatter plots indicate strong correlation (r>0.5) and yellow dots indicate weak correlation (r<0.5) (n=3, two-tailed Spearman correlation test with a 95% confidence interval). The cells were oriented towards the same angle as the aligned constructs.*

cell directionality was visible, corresponding to a peak of fibre directionality with a positive correlation (r=0.9680, p>0.0001) (**Figure 5.3 G-I**).

5.2.3 Differentiated neurons and astrocytes, but not oligodendrocytes, also align with the aligned nanofibers

7 days after removing the growth factors from the medium, approximately over 90% of the cell population was alive at the time of the survival assay, with no statistical differences between groups (**Figure 5.4 A-D**). A proliferation assay revealed approximately 5% of proliferating cells during a 6h incubation with Edu reagents, with no statistical differences between groups either (**Figure 5.4 E-H**).

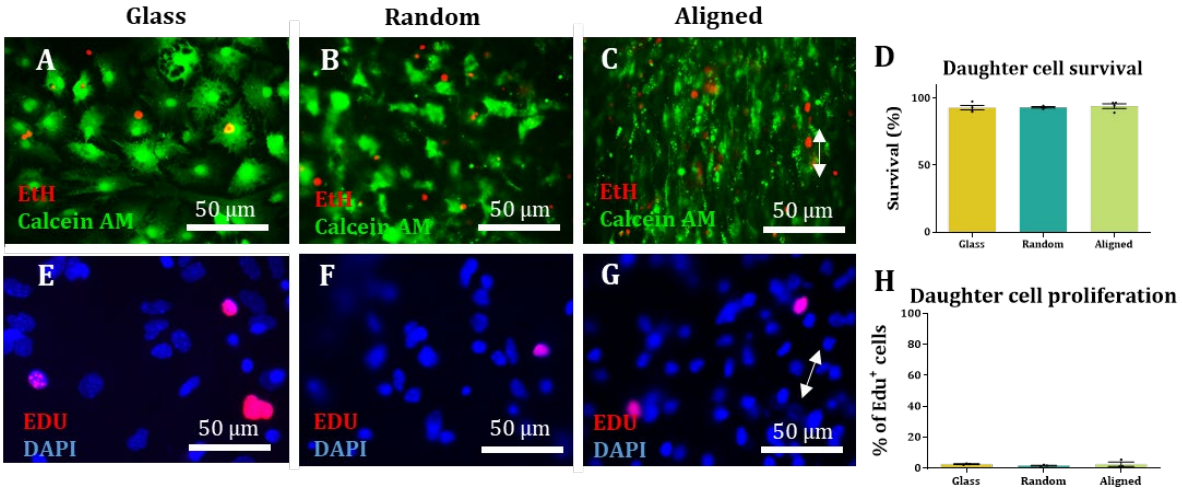

Figure 5.4 Survival and proliferation of daughter cells on fibres*. Daughter cell survival assay (**A-D**): Representative images of daughter cells stained with Calcein AM, indicating live cells (green) and Ethidium homodimer (EtH), indicating dead cell nuclei (red) on glass (**A**) random fibres (**B**) and aligned fibres (arrow indicating fibre direction) (**C**) and graphical representation of survival rates (Kurskal-Wallis test, n=3, p≥0.005) (**D**). Daughter cell proliferation assay (**E-H**): Representative images of daughter cells stained with DAPI, a cell nuclear marker (blue) and Edu, a proliferative cell nuclei marker (red) on glass (**E**), random fibres (**F**) and aligned fibres (arrow indicating fibre direction) (**G**) with graphical representation of proliferation rates (Kurskal-Wallis test, n=4, p≥0.005) (**H**). No differences were found between groups.*

7 days after growth factor removal, cells were fixed and stained. GFAP staining (**Figure 5.5 A, B**) revealed that approximately 60% of the NSCs had differentiated towards an astrocytic phenotype, with no statistical differences between groups. Astrocyte morphology appeared more elongated on random fibres than on coverslips (**Figure 5.5 C**), cell orientation seemed random (no directionality peak) and there was no correlation

between cell and fibre orientation (r=0.249; p=0.017) (**Figure 5.5 D-E**). Astrocytes on aligned fibres also appeared more elongated compared to control (**Figure 5.5 F**). In this case, the computational analysis revealed the presence of an orientation peak, positively correlated with a peak in fibre orientation (r=0.979; p<0.0001) (**Figure 5.5 G, H**).

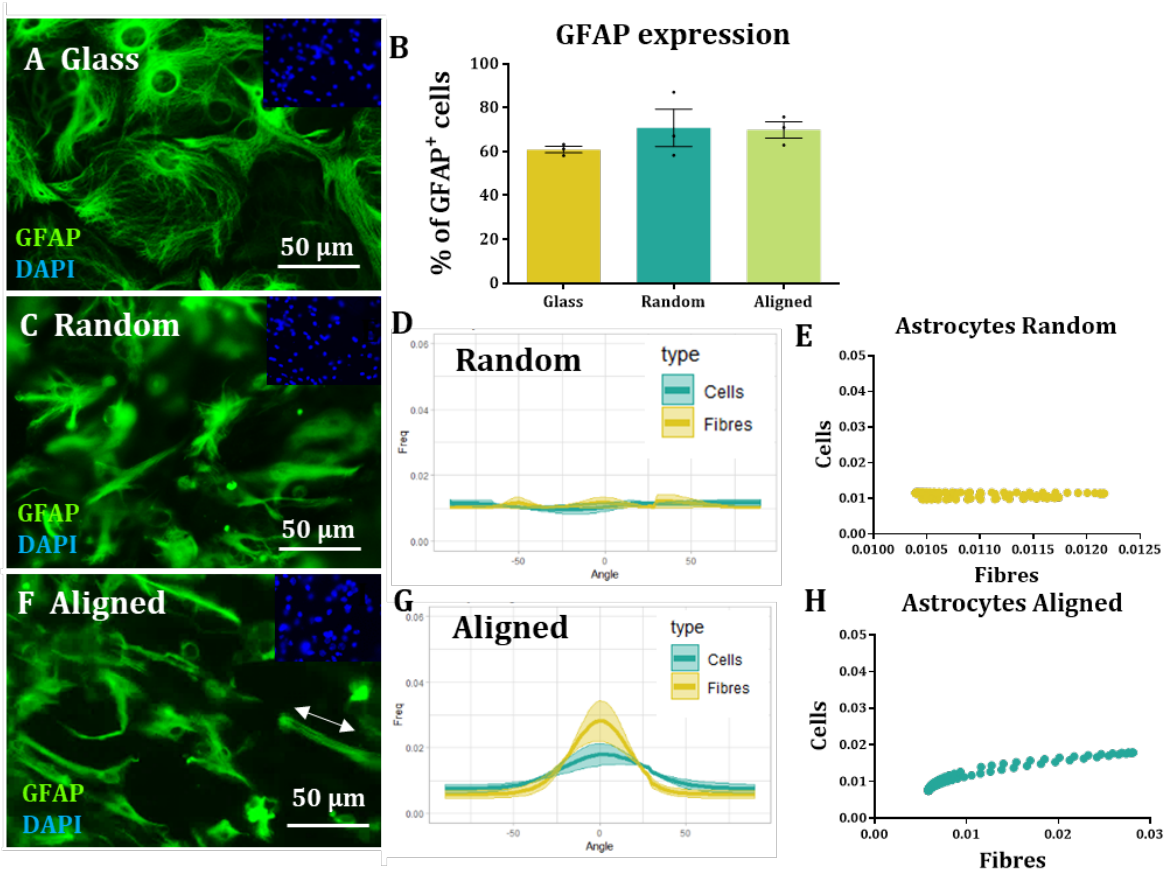

Figure 5.5 Phenotype and orientation of astrocytes on electrospun fibres. *Representative image of astrocytes on glass stained with astrocyte cytoskeleton marker GFAP (green) with insets showing nuclear marker DAPI (blue) (**A**). Bar graph represents the percentages of GFAP positive cells on glass, random and aligned substrates (Kurskal-Wallis test, n=4, p≥0.005) (**B**). Error bars indicate SEM and scatter dots indicate the mean values of each biological repeat. (**C**) is a representative image of GFAP positive cells on random substrates, with inset representing DAPI stained counterpart. XY graph indicates the frequency at which cells and random fibres are oriented at each angle, with halo representing the SEM (**D**). Scatter plot representing the correlation of directionality between cells and fibres on random substrates (r=0.2490, p=0.0173) (**E**). Image (**F**) is representative of GFAP positive cells on aligned fibres, with blue inset representing the DAPI stained counterpart and the white arrow indicating the direction of the fibres. XY graph represents the frequency at which cells and fibres are oriented at each angle on aligned constructs, and halos represent SEM (**G**). Finally, the scatter plot represents the correlation of orientation between cells and fibres in aligned constructs (r=0.9793, p>0.0001) (**H**). Blue dots on scatter plots indicate strong correlation (r>0.5) and yellow dots indicate weak correlation (r<0.5) (n=3, two-tailed Spearman correlation test with a 95% confidence interval). The cells were oriented towards the same angle as the aligned constructs.*

As suggested by Tuj-1 staining (**Figure 5.6 A**), approximately 20% of cells in all conditions differentiated into neurons (**Figure 5.6 B**). Neurons on random fibres seemed to be randomly distributed, as suggested by a weak correlation between cell and fibre orientation (r=0.439, p<0.0001) (**Figure 5.6 C-E**), while a cell directionality peak

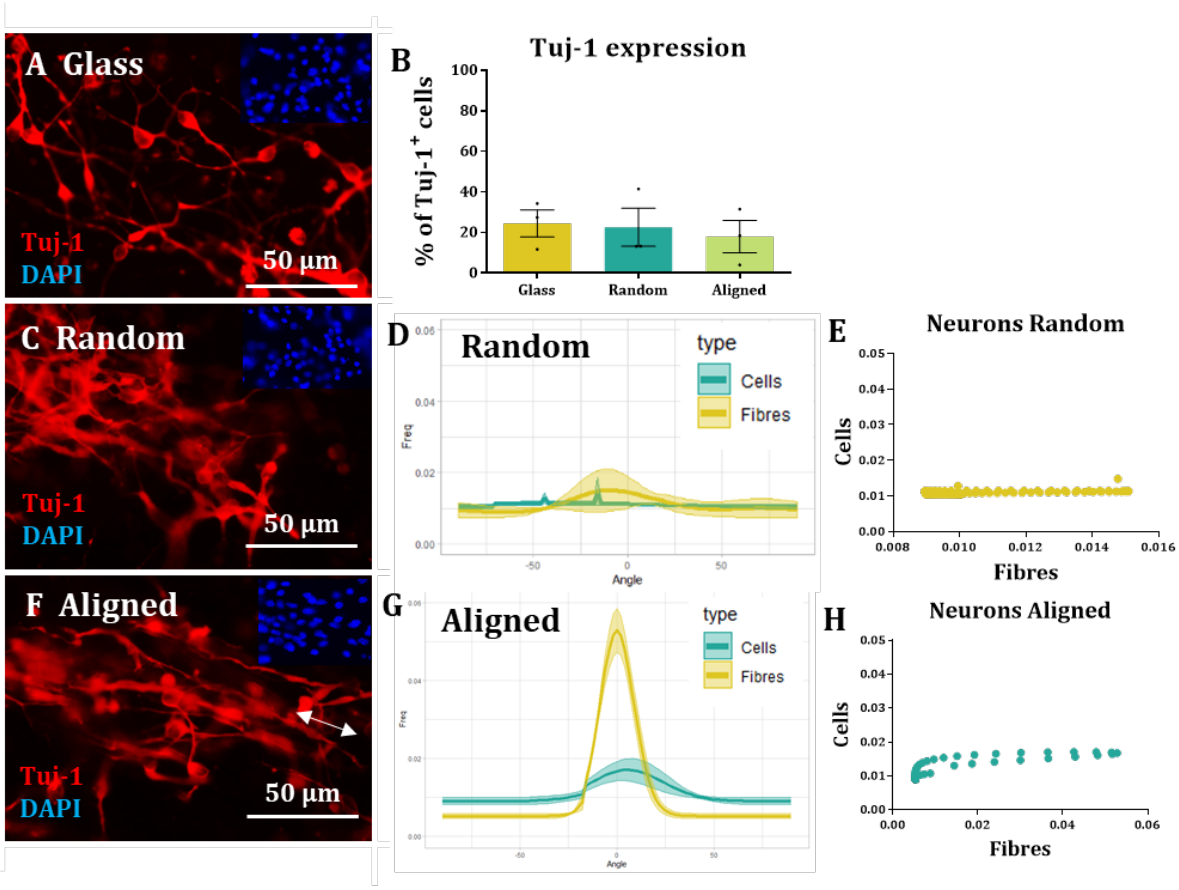

Figure 5.6 Phenotype and orientation of neurons on electrospun fibres*. Representative image of neurons on glass stained with neuronal cytoskeleton marker Tuj-1 (red) with insets showing nuclear marker DAPI (blue) (**A**). Bar graph represents the percentages of Tuj-1 positive cells on glass, random and aligned substrates (Kurskal-Wallis test, n=4, p≥0.005) (**B**) Error bars indicate SEM and scatter dots indicate the mean values of each biological repeat. (**C**) is a representative image of Tuj-1 positive cells on random substrates, with inset representing DAPI stained counterpart. XY graph indicates the frequency at which cells and random fibres are oriented at each angle, with halo representing the SEM (**D**). Scatter plot representing the correlation of directionality between cells and fibres on random substrates (r=0.4390, p=>0.0001) (**E**). Image (**F**) is representative of Tuj-1 positive cells on aligned fibres, with blue inset representing the DAPI stained counterpart and the white arrow indicating the direction of the fibres. XY graph represents the frequency at which cells and fibres are oriented at each angle on aligned constructs, and halos represent SEM (**G**). Finally, the scatter plot represents the correlation of orientation between cells and fibres in aligned constructs (r=0.9109, p>0.0001) (**H**). Blue dots on scatter plots indicate strong correlation (r>0.5) and yellow dots indicate weak correlation (r<0.5) (n=3, two-tailed Spearman correlation test with a 95% confidence interval). The cells were oriented towards the same angle as the aligned constructs.*

corresponded to a fibre directionality peak on aligned constructs with a positive correlation (r=0.911; p<0.0001) (**Figure 5.6 F-H**).

MBP staining (a marker for oligodendrocytes) (**Figure 5.7 A, B**) revealed that approximately 5% of NSCs had differentiated into oligodendrocytes. In this case, both

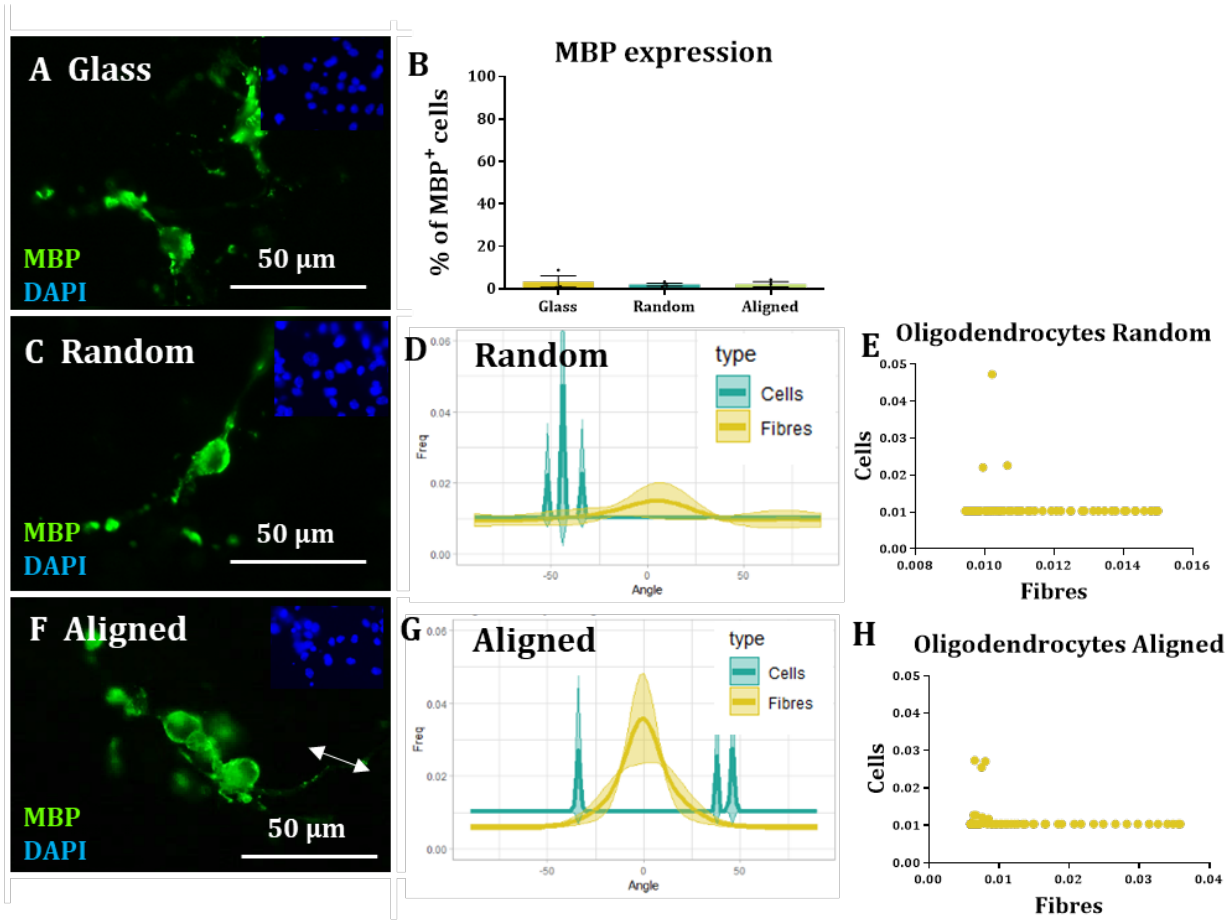

Figure 5.7 Phenotype and orientation of oligodendrocytes on electrospun fibres. *Representative image of oligodendrocytes on glass stained with oligodendrocyte cytoskeleton marker MBP (green) with insets showing nuclear marker DAPI (blue) (**A**). Bar graph represents the percentages of MBP positive cells on glass, random and aligned substrates (Kurskal-Wallis test, n=4, p≥0.005) (**B**) Error bars indicate SEM and scatter dots indicate the mean values of each biological repeat. (**C**) is a representative image of MBP positive cells on random substrates, with inset representing DAPI stained counterpart. XY graph indicates the frequency at which cells and random fibres are oriented at each angle, with halo representing the SEM (**D**). Scatter plot representing the correlation of directionality between cells and fibres on random substrates (r=0.0354, p=0.7387) (**E**). Image (**F**) is representative of MBP positive cells on aligned fibres, with blue inset representing the DAPI stained counterpart and the white arrow indicating the direction of the fibres. XY graph represents the frequency at which cells and fibres are oriented at each angle on aligned constructs, and halos represent SEM (**G**). Finally, the scatter plot represents the correlation of orientation between cells and fibres in aligned constructs (r=0.0887, p>0.4029) (**H**). Yellow dots indicate weak correlation (r<0.5) (n=3, two-tailed Spearman correlation test with a 95% confidence interval). The cells were not oriented towards the same angle as the aligned constructs.*

cells on random fibres (**Figure 5.7 C-E**) and aligned fibres (**Figure 5.7 F-H**) did not show directionality peaks, and cell *vs.* fibre correlation was negative in both cases (oligodendrocytes vs. random fibres (r=0.0354, p=0.7387) and oligodendrocytes vs. aligned fibres (r=0.0887, p>0.4029).

SEM images (**Figure 5.8**) allowed for a more detailed visualisation of the cells on the fibres. The random distribution of NSCs on glass coverslips and random fibres is evident, while the cells seemed to present a more elongated bipolar morphology that orientated towards the same angle as the aligned fibres. Similarly, cells that we putatively identified as astrocytes appeared to have a flattened appearance on glass coverslips and random fibres, covering the bottom of the surface, they seem to present more elongated processes that also follow the direction of fibres on the aligned constructs. Cell with the morphological appearance of neurons and oligodendrocytes were largely found lying on top of astrocytes in all experimental conditions. The processes of those neurons that were in direct contact with the fibres seemed to follow them in isotropic fashion in the case of

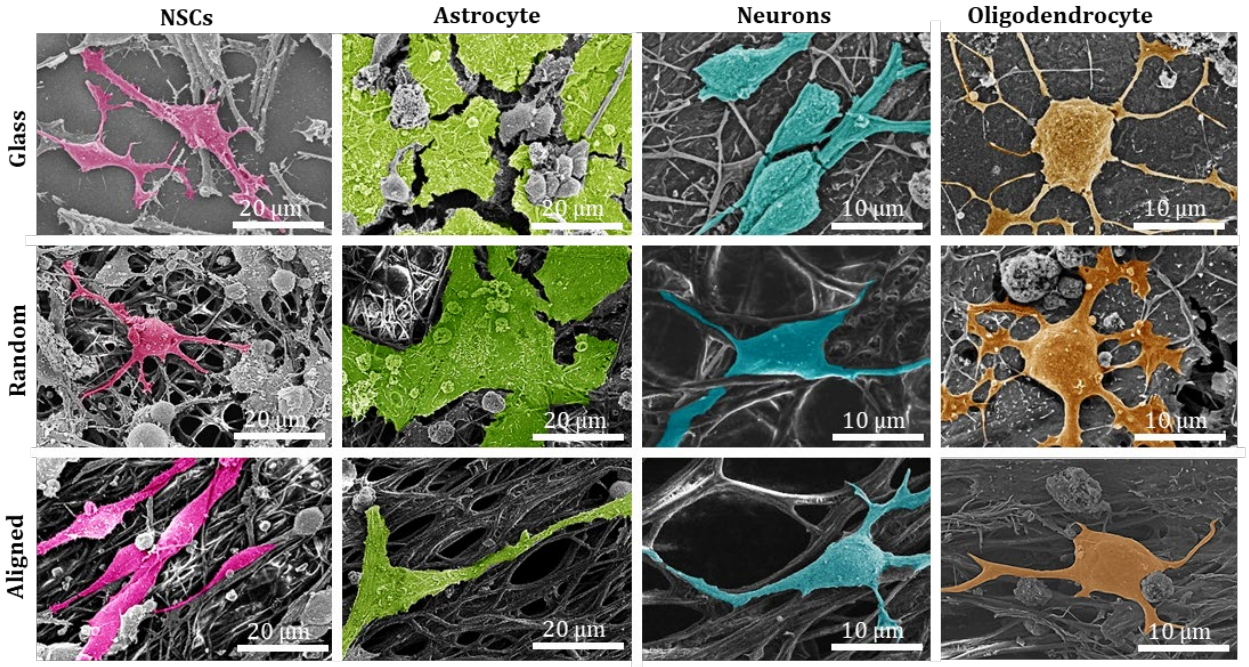

Figure 5.8 OTOTO prepared samples for SEM*. Representative SEM images of NSCs, astrocytes, neurons and oligodendrocytes on glass coverslips, random fibres and aligned fibres. Putative cell types highlighted in colour. SEM images allowed for the direct visualisation of cell-biomaterial interaction and cell morphology.*

random constructs and anisotropic on aligned fibres. Due to the low percentage of oligodendrocytes on the cultures, their visualisation in contact with the fibres was scarce and could only be seen on top of astrocytes.

5.3 DISCUSSION

5.3.1 Summary of aims and results

Here we show that alignment of cells can be reproducibly and quantitatively analysed through the use of a directionality plug in combined with data rotation and a correlation test. Moreover, the alignment of NSCs and their progeny on aligned and random electrospun fibres was robustly analysed, resulting in alignment of NSCs, neurons and astrocytes, but not oligodendrocytes and also showing high survival and standard proliferative capacity of the cultured cells, highlighting the safety and feasibility of culturing NSCs on electrospun fibres. Therefore, we describe a methodology for analysing cellular alignment and we demonstrate alignment of neurons and astrocytes on electrospun fibres, key tools when aiming to promote directed axonal growth for spinal cord repair. These outcomes will be discussed in the following sections.

5.3.2 Establishment of a methodology to quantitatively and reproducibly analyse cell alignment to nanofibres

Multiple studies report cellular alignment on aligned nanofibres. However, alignment analysis is represented either as a qualitative comparison (L. He et al., 2010; F. Yang et al., 2005) or as the quantitative analysis of only one data set without comparison between biological repeats (Silantyeva et al., 2018), making data interpretation not reproducible. Alternatively, other studies have quantified the cell's angle deviation from the fibre they are sitting on (Sharifi et al., 2016; Soliman et al., 2018), resulting in repetitive and time consuming work, which can lead to error and biased results.. Moreover, most studies focus on NSC and neuronal alignment, overlooking glial cell alignment despite their importance in axonal guidance (Alexander et al., 2006; East et al., 2010; Katiyar et al., 2018).

This study reports the establishment of a methodology to reproducibly quantify and statistically analyse cell alignment. The two main impediments when aiming to analyse

cell alignment are the lack of an automated software to analyse orientation of single structures within images and the lack of a normalisation method to compare each image. In order to address the first one, we used the Directionality plug-in in ImageJ, which analyses the angle distribution of structures (Silantyeva et al., 2018). Once these have been quantified, they need to be compared to other biological repeats. In order to do that, a standardisation process was needed, which we achieved by data rotation. Finally, in order to statistically analyse any possible differences in directionality between fibres and cells we did a correlation analysis to quantify whether the cells were following the same direction as the fibres. As shown here, we were able to use this methodology on a primary culture of NSCs and on a culture of differentiated NSCs: astrocytes, neurons and oligodendrocytes.

Therefore, we offer a high-throughput analytical method, which allows for an unbiased, reliable analysis of cell alignment of multiple cells at the same time and for comparison between biological repeats. With the ongoing advances in the field of aligned biomaterial implantation, this methodology can act as a platform for alignment assessment with various cell types, with translational potential when aiming to guide regenerating axons in SCI therapies.

5.3.3 Cellular alignment on aligned electrospun nanofibre constructs

The electrospun 3D-NanoMatrix™ fibres used in this study were kindly donated by Cellevate™. The highly porous, 3D nanofibre networks partially mimic the topographical features of the ECM. In addition, their patented manufacturing process provides well-to-well and batch-to-batch consistency, and therefore, reduces experimental variation. These fibres are made of synthetic, biocompatible and biodegradable (approx. >24 months, but degradation time can be decreased through combination with DL-lactide (Middleton & Tipton, 2000)) poly-u03b5-caprolactone (PCL). This material has been widely used to manufacture electrospun fibres for neural-derived cell culture (Xiaoran Li

et al., 2016; Sharifi et al., 2016; Silantyeva et al., 2018; Soliman et al., 2018). Besides, the constructs are mounted on 3mm high crown inserts, which hold the edges of the fibres and keep them suspended to avoid contact with the bottom of the well.

NSC and neuronal alignment have been repeatedly reported when seeded on aligned fibres (Hurtado et al., 2011; Jakobsson et al., 2017; Sharifi et al., 2016; Silantyeva et al., 2018; Soliman et al., 2018; Sperling et al., 2017; F. Yang et al., 2005). We also report NSC and neuronal alignment on aligned fibres but not on random fibres or glass controls. Neurons were always observed in highly populated groups, rendering it impossible to analyse the impact of the fibres on individual axonal length. It might be desirable to culture a pure neuronal population at a lower density to systematically research the impact of these fibres on axonal length.

Astrocyte alignment has been shown to induce higher neurite outgrowth and neuronal guidance when compared to ... (East et al., 2010). Alignment of glial cells in electrospun fibres has been previously demonstrated (A. Weightman et al., 2014). However, this alignment had not been robustly demonstrated through an established statistical analysis until now. In this report, we show that astrocytes align parallel to the fibres, similarly to neurons and NSCs, and that this alignment is maintained through biological repeats.

While SEM images allowed for the observation that most NSCs, neurons and astrocytes were in direct contact with the fibres, all observed oligodendrocytes were found sitting on top of astrocytes. Therefore, we were not able to see NSC-derived oligodendrocytes aligned on the fibres. This could be due to the low numbers of these cells present in our cultures or due to the tendency to finding these cells sitting on top of astrocytes and not in contact with the fibres. It should also be noted that we identified cells within SEM images using their morphology, which can be subjective. Perhaps, it would be advantageous to use immunogold staining to see a specific cell types under SEM, which

would also facilitate the cell identification. In previous studies, OPC alignment with electrospun fibres was seen with the presence of astrocytes in the culture, but the alignment was lost when OPCs differentiated into mature oligodendrocytes (A. Weightman et al., 2014). In order to address these issues, it would be interesting to culture an enriched population of OPCs on aligned and random fibres in order to establish whether a denser OPC population would result in higher OPC alignment. In fact, these experiments have already been undertaken in our laboratory, using the methodology described here for data analysis, and resulting in OPC alignment on aligned electrospun fibres (data not published yet).

5.3.4 Feasibility of culturing NSCs and daughter cells on electrospun fibre constructs

Here we show that NSCs and their progeny can be successfully cultured in commercially available electrospun fibres. This can increase the reproducibility of this study and allows for highly consistent biological repeats.

Our findings indicate that NSCs can be cultured on electrospun fibres, the topography of which does not alter survival, proliferation or differentiation rates regardless of whether the fibres are aligned or random. Moreover, the survival and proliferation of astrocytes, neurons and oligodendrocytes does not seem to be affected by the fibres either, indicating the safety of the procedure. The utilisation of a random fibre control and a flat surface glass control allowed us to discern whether any significant differences were due to the physical cues provided by the fibre topography or by the chemical properties of the fibre material.

We decided to further functionalise the constructs with laminin to improve cell attachment and migration. It has been reported that the presence of laminin, a molecule present in the ECM, facilitates NSC migration instead of promoting neurosphere

formation (Flanagan *et al.*, 2006; Mogas Barcons *et al*., 2021), rendering the cell-construct complex with more *in vivo*-like properties. Moreover, previous studies have been successful in functionalizing Cellevate™ fibres with poly-L-lysine (PLL) in culture with human neural progenitor cells on random fibres (Jakobsson et al., 2017) and with laminin in culture with retinal cells (Castro et al., 2016). The functionalisation of other PCL aligned fibres with laminin resulted in higher viability rates of neurons and astrocytes than in non-coated fibres (Hyysalo et al., 2017). Therefore, there is substantial evidence to suggest that laminin coating can be routinely used to promote cell adhesion to the fibres, similarly to its standard use in control glass coverslips and to avoid methodological differences between fibres and controls. In our laminin coated materials, we found an even pattern of cell distribution, present as single cells in all experimental groups and similar viability rates when compared to glass controls.

NSC differentiation varies across reports. In past studies, the functionalization of PCL aligned fibres with a peptide sequence found in laminin resulted in the expression of neuronal markers at earlier time points on fibres than on laminin coated coverslips. In this study, the expression of Sox-1, a marker for neural commitment, was upregulated in cells on functionalized fibres but not on coverslips at day 1 of culture. It was also reported that the upregulation of TUBB3 and Gap43 (neuronal markers) was higher on fibres than on coverslips at day 3. However, at day 14 of culture, neuronal numbers were similar in both fibres and coverslips (Silantyeva et al., 2018). Here, we report that the differentiation of NSCs towards a neural phenotype is not altered by the presence or arrangement of the PCL fibres after 7 days of culture. These results are not in contradiction with those reported by Silantyeva et al. since they reported no significant differences in phenotype at day 7 of culture or after.

On the other hand, changes in differentiation rates have been reported in other studies. For example, 10 days after mESC were seeded on aligned and random fibres and a gelatine

control, a co-culture of NSCs, astrocytes, neurons and oligodendrocytes were seen in immunocytochemistry analysis. However, flow cytometry revealed higher upregulation of nestin (an NSC marker) and Tuj-1 (a neuronal marker) on aligned fibres but not on random fibres or gelatine controls (Sperling et al., 2017). Sharifi *et al*. (2016), also reported high numbers of nestin-positive and Tuj-1-positive cells compared to glial markers (*e.g*.: GFAP and RIP) after 7 days. In future studies, it might be interesting to study the differentiation profile of cells with molecular tests, such as Western blot, as well as immunostaining in order to study the timepoints of differentiation with more accuracy.

Fibre diameter has been seen to impact the differentiation rate and phenotype of NSCs. For example, NSCs growing on fibres of 300nm in diameter were seen to differentiate earlier than when grown on 1.5µm fibres regardless of alignment (F. Yang et al., 2005). Adult hippocampal NSCs, in the presence of retinoic acid, differentiated towards neurons in 794nm fibres at a higher rate than in 283nm fibres. The latter were seen to differentiate more towards an oligodendrocytic phenotype after 5 days of culture (Christopherson et al., 2009). Therefore, it seems that an increase in fibre diameter correlates with a decrease in differentiation time and an increase of differentiation towards a neuronal phenotype. The fibres used in this study have an average diameter of 700nm (personal communication, Cellevate™) and the fibres of the Silantyeva et al. (2018) study are also in the nanometer scale. Both Sperling et al. and Sharifi et al. reported their fibres to be in the micrometer scale. This increase in fibre diameter, together with the use of different cell types, could be a potential explanation as to why NSC differentiation varies across reports.

In conclusion, biofunctionalisation with ECM molecules, selection of fibre diameter and fibre orientation could help researchers finely tune a material towards a pro-regenerative final product. Our results suggest that primary culture NSCs, a clinically relevant cell

population, and derived neurons and astrocytes can follow the direction of aligned electrospun fibres.

5.3.5 Future directions

Further work would aim to test the biomaterial for its capacity to guide host cells upon implantation after SCI. This could be done in the organotypic model established in **Chapter 3**. However, the construct would have to be initially modified for implantation. This could be potentially achieved through two different methods: formation of a rolled tube of aligned fibres or embedding of the construct within a hydrogel.

The formation of conduits of aligned electrospun fibres has been previously reported in a study in which collagen fibres were electrospun on aluminium foil and, while the fibres were wet, they were rolled to form a 4–5-layer conduit. Then, the conduits were critical point dried and the aluminium was removed (Liu et al., 2012). Since the fibres used in this study are also electrospun it seems feasible to use a similar protocol. However, the fibres might need to be modified to be stiffer to hold the shape without the ring around them and all the changes would have to be done by the manufacturer.

The other option would be to embed the fibres within a collagen hydrogel. A collagen gel could be allowed to set around the fibres prior to detaching the construct from the ring. This would potentially maintain the structure of the fibres while facilitating implantation.

6 CHICK EMBRYO ORGANOTYPIC SLICES FOR TESTING BIOMATERIAL IMPLANTATION IN SPINAL CORD INJURY SITES

6.1 BACKGROUND

6.1.1 Biomaterial implantation after spinal cord injury *in vivo*

As discussed in **Chapter 1**, the spinal cord does not have the intrinsic capacity for regeneration after injury. In this regard, the implantation of a 3D matrix in the SCI cavity could provide a non-toxic environment for the host tissue cells to regenerate compared to the toxic and reactive environment of the untreated lesion. In fact, biomaterial implantation has been attempted in a clinical trial with two acute SCI patients, one thoracic and one cervical, indicating the promise of the approach. In this trial, a bovine collagen biomaterial laden with umbilical cord MSCs was implanted 24h-8 days after injury. Sensory recovery was observed 2 months post-surgery and bowel and bladder sensation were regained after 9 months. Movement, which was completely lost after injury, started to recover 3 months after surgery and one of the patients was able to walk with the help of braces 12 months after surgery (Xiao et al., 2018).

Biomaterial implantation correlates with better motor recovery and axonal infiltration, highlighting the therapeutic potential of this procedure (**Chapter 1**). However, the complexity of the *in vivo* models hinders the capacity to reliably and reproducibly analyse histological changes in the tissue, such as the formation of a glial scar, microglial infiltration or demyelination, which, in combination with increasing possible permutations of biomaterial testing, highlight the importance of a simpler model in which to carry out these tests.

6.1.2 Biomaterial implantation in organotypic tissue slices

As discussed in **Chapter 3**, organotypic culture slices offer a simpler, more manipulable model of SCI, making them a desirable alternative to *in vivo* models, in which to test a

range of therapies before translation to higher complexity platforms. Typically, organotypic slices have been used as a platform to study neural development or underlying physiological systems of the CNS. However, there has been a recent drive to use this type of culture for neural tissue engineering applications, such as for testing implantation of biomaterials or cell transplant populations in injury sites. A list of relevant reports can be found in **Table 6.1**.

***Table 6.1 Summary of published literature in which a biomaterial or a transplant cell population was implanted in a spinal cord injury organotypic model* in vitro**.
This table summarises the methodology of previous research on SCI theraoies.

Slice orientation	Lesion type	Animal model	Biomaterial	Cell type	Duration of treatment	Reference
Transversal	Demyelination	P16 rats	N/A	hMSCs	1-3 weeks	*Cho et al. 2009*
Sagital	Transecting	P0 – P3 rats	Injectable Fmoc-based	N/A	7 days	*Guijarro-Bermar et al. 2019*
Transveral	Transecting	P21-P28 mice	Alginate-collagen microcapsules in Matrigel	NSCs and DPSC	10 days	*Hidalgo San José et al. 2018*
Sagital	Transecting	P0-P5 mice	PLL nanofibres	N/A	6 days	*Weightman et al. 2014*

For example, treatment of transverse spinal cord slices with lysolecthin can induce demyelination of the slice to represent one aspect of the chronic stage of the injury (Cho et al. 2009). Injection of hMSCs alone into the demyelinated spinal cord promoted endogenous cell survival, including injured neurons, oligodendrocytes and OPCs (Cho et al. 2009). Biomaterial implantation has also been tested on organotypic slices. Longitudinal slices with transecting lesions offer an advantageous platform for biomaterial testing due to the marked lesion edges and retention of ascending and descending tracts, offering an *in vivo*-like structure. In addition, they offer a unique constitution to study axonal growth. In the first described method for safe biomaterial incorporation, a mesh of aligned PLL nanofibres was implanted in the injury gap, inducing enhanced axonal outgrowth aligned with coated nanofibers compared to controls.

Moreover, the reactive astrocytes that were seen in a scar-like formation on untreated slices, showed extensive alignment and extension of processes across the lesion site after implantation of coated PLL nanofibers, inducing a reorganisation of the tissue that would potentially disrupt the glial scar (A. P. Weightman et al., 2014). In another study, an injectable biomaterial functionalised with an Epac2 agonist was implanted within the injury gap of rat spinal cord organotypic slices resulting in reversed inhibition of CSPGs and increased neuronal growth when compared to untreated controls or hydrogel-only treated groups (Guijarro-Belmar et al., 2019). Finally, the feasibility of biomaterial-encapsulated NSC delivery within the lesion gap was tested in a recent study. NSCs encapsulated within alginate-collagen microcapsules were implanted in a mouse spinal cord organotypic slice after a transecting lesion. The cell-laden microcapsules were retained at the lesion site with Matrigel, with high viability rates and retention of differentiation capacities (Hidalgo San Jose et al., 2018).

These studies highlight the possibility of using spinal cord organotypic slices as a neural tissue engineering platform. Taken together, these results suggest that it is possible to implant cells and biomaterials on these slices, and that the complexity of these can be increased by functionalising the biomaterials or by encapsulating cells within them before implantation. Moreover, the accessibility of the model allows for simple analysis of

Table 6.4 Summary of results from published data aiming to improve regeneration after spinal cord injury through biomaterial implantation in organotypic spinal cord injury models. *This table summarises the results of previous research on SCI therapies.*

Reference	Increased axonal infiltration	Reduced glial scarring	Reduced microglial infiltration	Reduced demyelination	Viability of implanted cells	Functional reconnection
Cho et al. 2009	✓	N/A	N/A	✗	✓	N/A
Guijarro-Bermar et al. 2019	✓	✓	✓	N/A	N/A	N/A
Hidalgo San José et al. 2018	N/A	N/A	N/A	N/A	✓	N/A
Weightman et al. 2014	✓	✓	✗	N/A	N/A	N/A

important regenerative responses to biomaterial implantation such as axonal infiltration, glial scar formation, immune response, demyelination and viability of implanted cells (**Table 6.2**).

6.1.3 Knowledge gaps and aims

Despite the simplicity offered by organotypic slices, these mostly rely on rodents for tissue acquisition, increasing the cost of experimentation and being associated with high ethical implications (**Chapter 1**). As discussed in **Chapter 3**, the chick embryo offers a relevant alternative to rodents for establishing spinal cord organotypic slices as a model of spinal cord injury. However, this model has never been tested for biomaterial implantation to date. In addition, in **Chapter 4**, the compatibility of Hemopatch™ to safely encapsulate a relevant transplant cell population was assessed but the biomaterial has never been studied in interaction with injured spinal cord tissue.

Therefore, the aims of this chapter are to:

1. Study the feasibility of interfacing lesioned chick embryo organotypic slices with Hemopatch™ implantation.
2. Study the tissue responses to biomaterial implantation.

6.2 RESULTS

6.2.1 The slices were highly viable regardless of experimental condition

Before the start of the full experiment, the procedure was trialled in order to assess the feasibility of implanting a piece of Hemopatch™ in the injury site. The possibility of staining and visualising cells while maintaining the biomaterial in place was also tested. As seen in **Figure 6.1**, we were able to stain for different cellular markers, in this case lectin and GFAP while maintaining the implant in the lesion gap as well as visualising cellular infiltration in the biomaterial. In addition, the phase image shows the Hemopatch™ piece implanted within the two sides of the lesioned spinal cord.

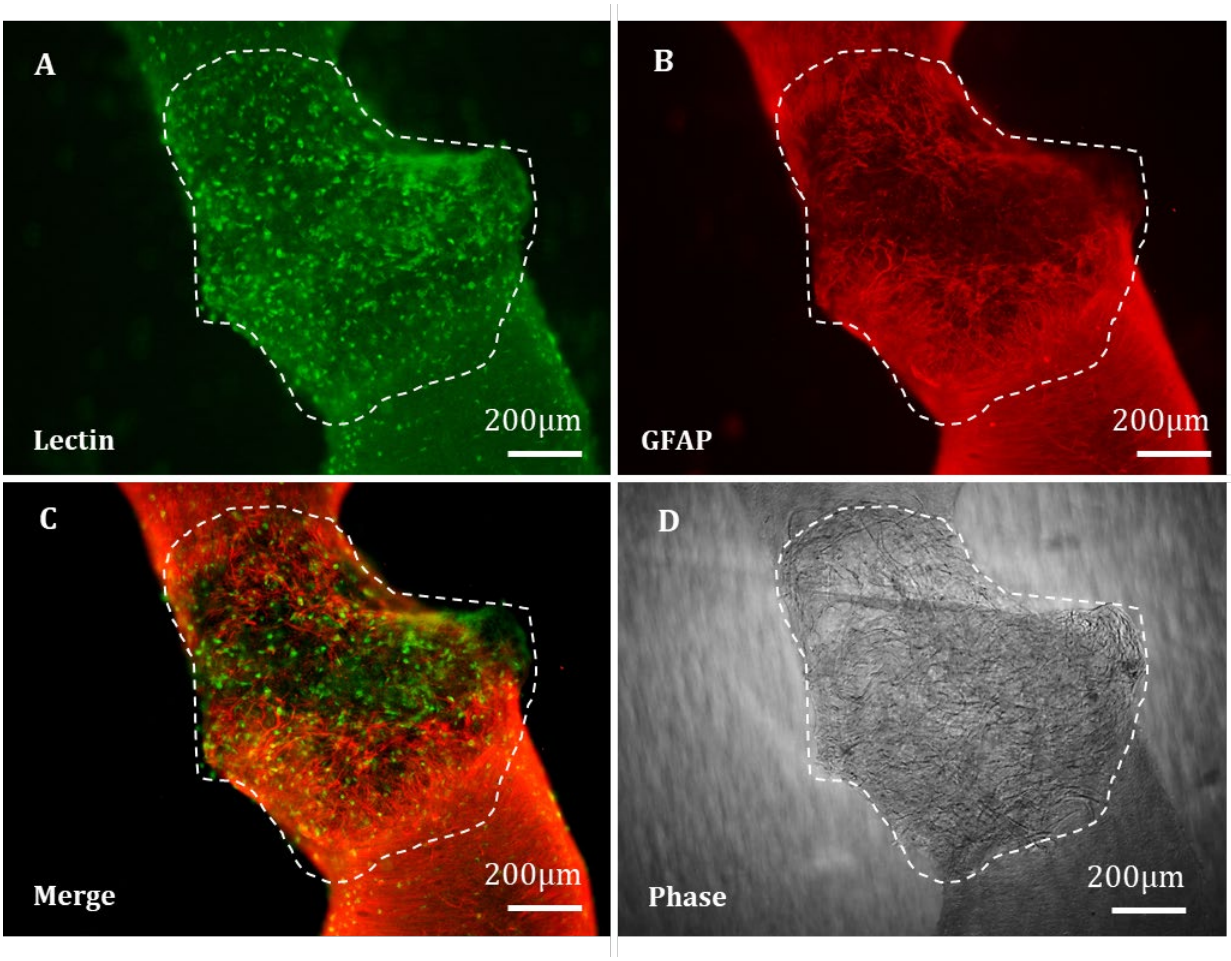

Figure 6.1 Implantation of Hemopatch™ within the lesion gap of organotypic slices. *Images of first Hemopatch™ implantation in a lesioned spinal cord trial showing staining with lectin (**A**), GFAP (**B**), both markers merged (**C**) and a phase image (**D**). White dotted lines indicating the perimeter of the implant. The biomaterial was successfully implanted and it allowed for cell visualisation after immunocytochemistry.*

In the main experiment, all spinal cords were kept in culture for 24 days. Staining revealed highly viable spinal cord slices in all experimental groups as seen by extensive Calcein AM staining throughout the slices compared to the small numbers of red cells corresponding to ethidium homodimer staining (**Figure 6.2 A-C**). The viability index (a measure of comparison between intensity of live versus dead staining) was approximately 60% for all experimental groups without statistically significant differences (**Figure 6.2 D**). We also calculated the viability of host cells infiltrating Hemopatch™, which was also approximately 60%, so similar to slice tissue viability.

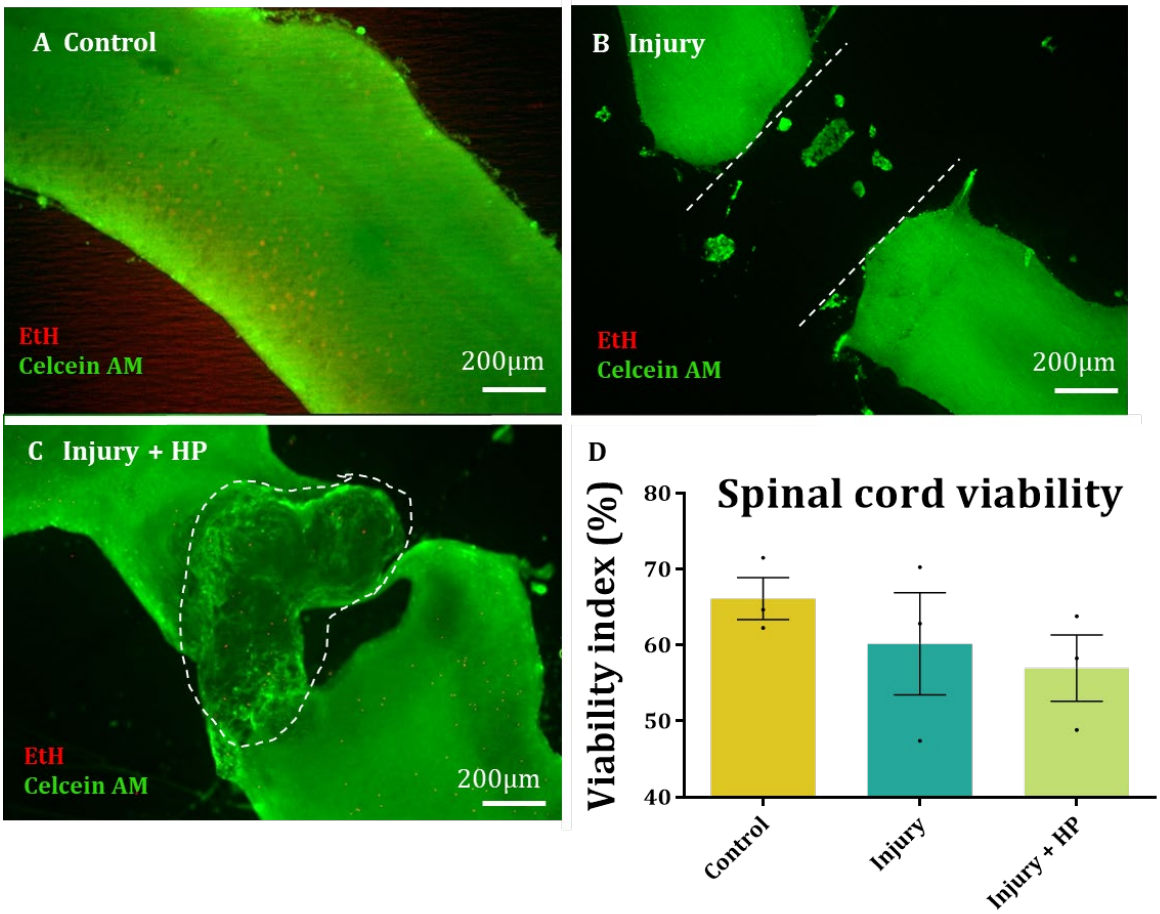

Figure 6.2 Survival of slices after biomaterial implantation*. Representative images of the survival assay on spinal cords showing live Calcein-AM stained tissue (green) and dead Ethidium homodimer (EtH) stained tissue (red) on uninjured control slices (**A**), untreated injured slices (**B**) and treated injured slices (**C**).White lines represent the edges of the lesion on B and the edges of the implanted biomaterial on C. **D** is the graphical representation of the viability index analysis, showing % of Calcein AM OD relative to total OD (Kruskal-Wallis test, n=3, p=0.439). There were no differences between groups.*

6.2.2 The lesion gap was wider after implantation compared to controls

The lesion edges in the control group were easily distinguishable, while the edges after implantation were more difficult to discern due to high host cell infiltration into the biomaterial. However, in all cases a line at which DAPI intensity dropped was visible, which we established to be the lesion edge. As seen in **Figure 6.3**, the OD value for DAPI in the control injury group rapidly decreases to a constant near-zero value, corresponding to the lesion gap, until it rapidly increases again. In contrast, after implantation a peak in DAPI OD can be observed followed by a gradual and small decrease in OD. We interpreted this to correspond to infiltrating host cells, the OD of which start increasing again nearer the opposite end of the lesion.

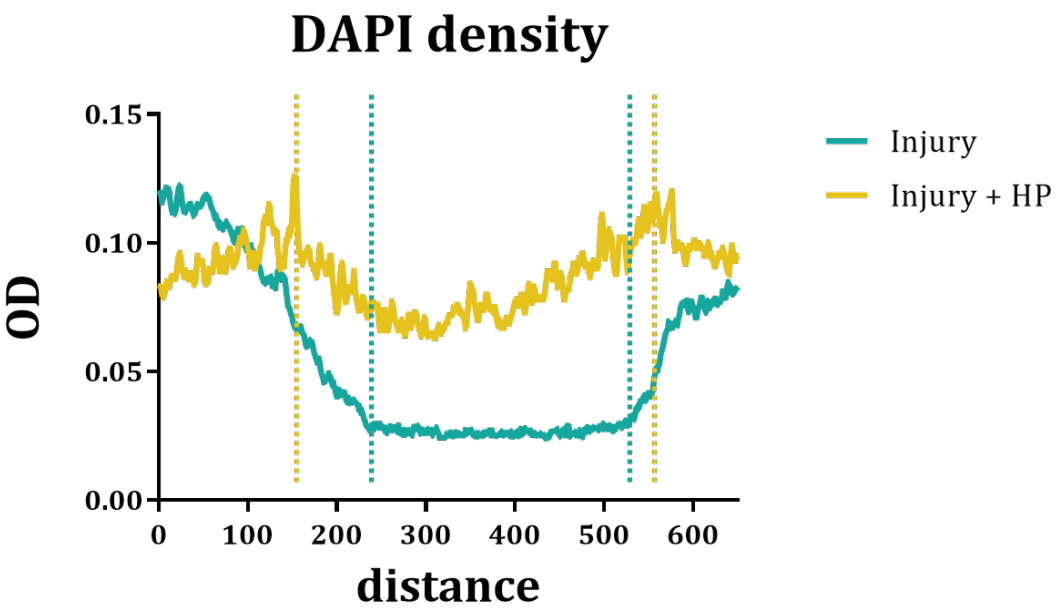

***Figure 6.3 Pattern of DAPI OD in the lesion**. Graphical representation of DAPI optical density profile across the injury on untreated slices (blue) and after biomaterial implantation (orange). The OD is represented in the Y axis and the X axis represents the distance in µm across the spinal cord. Dotted lines representing the putative lesion edge. This study indicates that the DAPI OD decreases at the injury gap.*

In this context, the mean lesion width of untreated slices was 367.6 ± 45.6µm. This was statistically different from 427.3 ± 86.2µm, when Hemopatch™ was implanted immediately after lesioning (Injury + HP) (**Figure 6.4**).

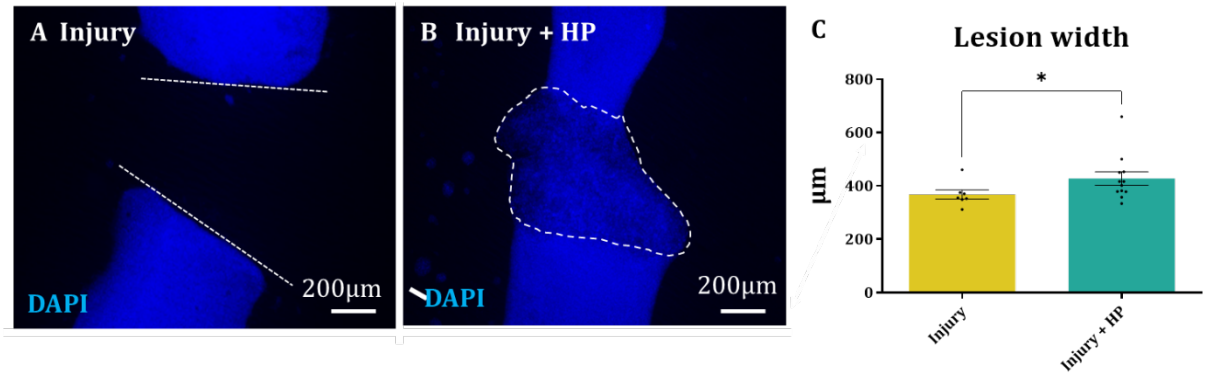

Figure 6.4 Lesion width after biomaterial implantation*. DAPI stained spinal cord slices to represent the lesion width on untreated spinal cords (**A**) and after biomaterial implantation (**B**). White lines represent the edges of the lesion. The bar graph (**C**) is the representation of the lesion width (in µm) analysis comparing injured and treated slices (Mann-Whitney test, n=7 (Injury) and n=12 (Injury + HP), p=0.034). The lesion width was bigger after biomaterial implantation than in untreaded slices.*

6.2.3 GFAP expression was higher at the edge of the lesion only in non-treated slices

Similarly to the previous experiments, the spinal cords in the control group (Injury) seemed to present a higher expression of GFAP at the edge of the lesion, with the cells apparently aligned at 90° to the lesion. This is in stark contrast to the random processes of astrocytes observed in the centre of the slice (**Figure 6.5 A, B**). However, when Hemopatch™ was implanted, GFAP expression did not seem higher at the lesion edge than at the centre of the spinal cord and the orientation of GFAP positive cells seemed random at all distances from the lesion (**Figure 6.5 C, D**). A visual assessment of the treated spinal cord slices seems to indicate that infiltrating GFAP-positive cells expressed more GFAP than those within the tissue (**Figure 6.5 D**). However, their morphology and cytoarchitecture differ from untreated slices (**Figure 6.5 B**) as seen by the loss of polarity

towards the lesion and the lack of a clear band of orientated astrocytes, expressing high levels of GFAP.

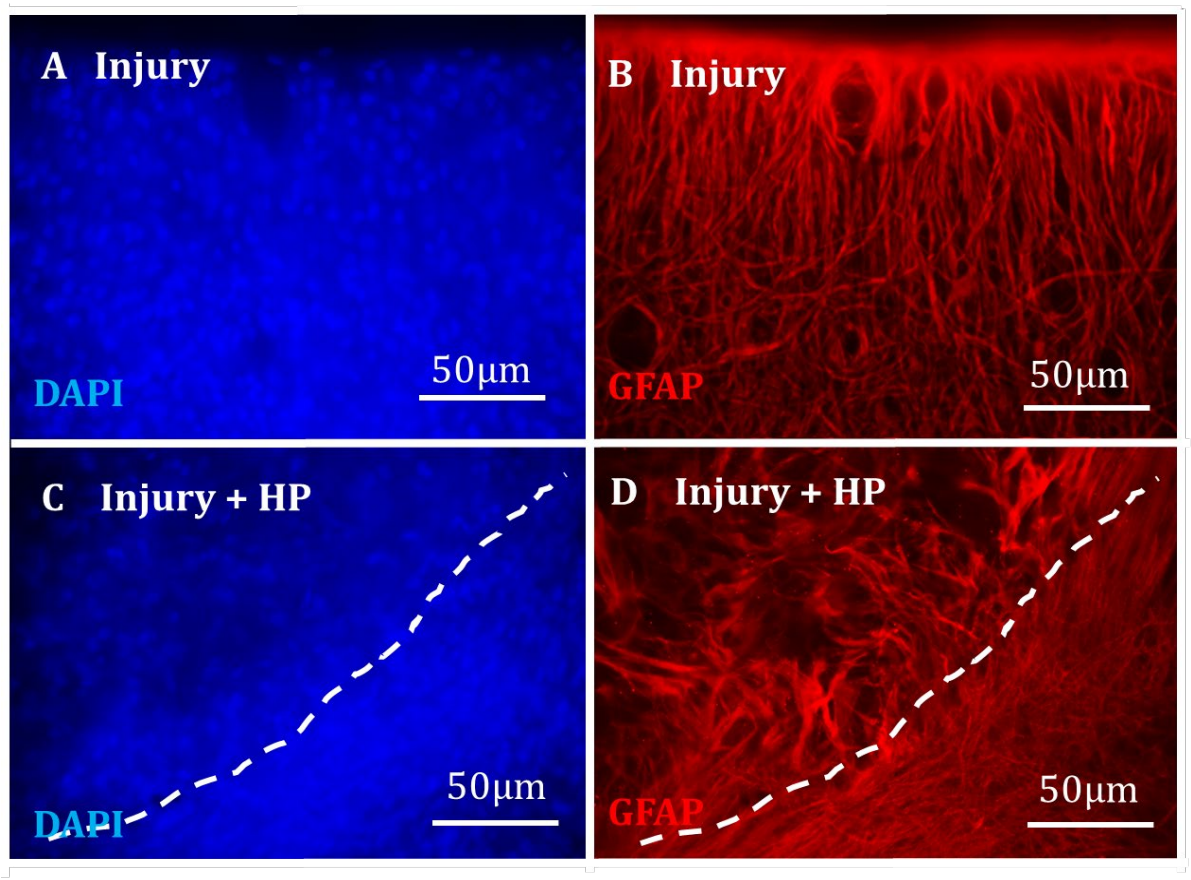

Figure 6.5 Astrocyte morphology at lesion edges*. Representative images of the edge of the lesion showing the presence of nuclei (DAPI) (**A**) and astrocytes (GFAP) (**B**) on untreated slices and nuclei (**C**) and astrocytes (**D**) after implantation. White lines representing the edge of the lesion after implantation. Astrocyte morphology and GFAP OD appeared different in treated and untreated slices.*

Low magnification images revealed an increased GFAP expression at the lesion edge of the injured controls as well as all the borders of the "Injury + HP" group excluding those in contact with Hemopatch™ (**Figure 6.6 A, B**). OD analysis showed a significant increase in GFAP expression at the first 10µm after the lesion compared to 50-60µm and 100-110µm only on the control group (Injury). This increase in GFAP OD was also significantly higher than the lesion edges in the other group (Injury + HP). There were no significant differences within the same spinal cord of GFAP OD at any distance from the lesion when Hemopatch™ was implanted (**Figure 6.6 C**).

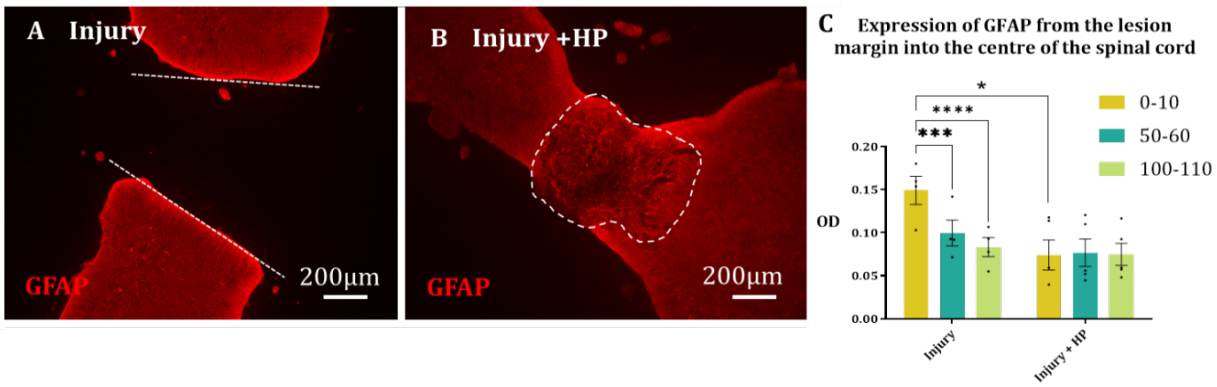

Figure 6.6 Astrocyte OD pattern*. Representative low magnification images showing GFAP (red) activation on untreated slices (**A**) and on Hemopatch™ treated slices (**B**). White lines representing the edges of the lesion. **C** is the graphical representation of the GFAP OD analysis, representing the absolute OD values at the edge of the lesion (0-10µm) and at 50-60µm and 100-110µm from the lesion towards the centre of the spinal cord (Two-way ANOVA, n=4 (Injury) and n=5 (Injury + HP), p<0.05). GFAP OD at the edge of the lesion was higher than at the centre of the spinal cord only in untreated slices.*

6.2.4 Biomaterial implantation increased axonal infiltration through the lesion site

As already seen in **Chapter 3**, untreated lesioned slices displayed weak spontaneous axonal growth in the lesion site, never reconnecting both sides of the lesion (**Figure 6.7 A**). Implantation of Hemopatch™ to the lesion area resulted in robust axonal infiltration within the material and the apparent formation of complex neuronal circuitry (**Figure 6.7 B**). Due to the high numbers of infiltrating axons it was impossible to trace single cells

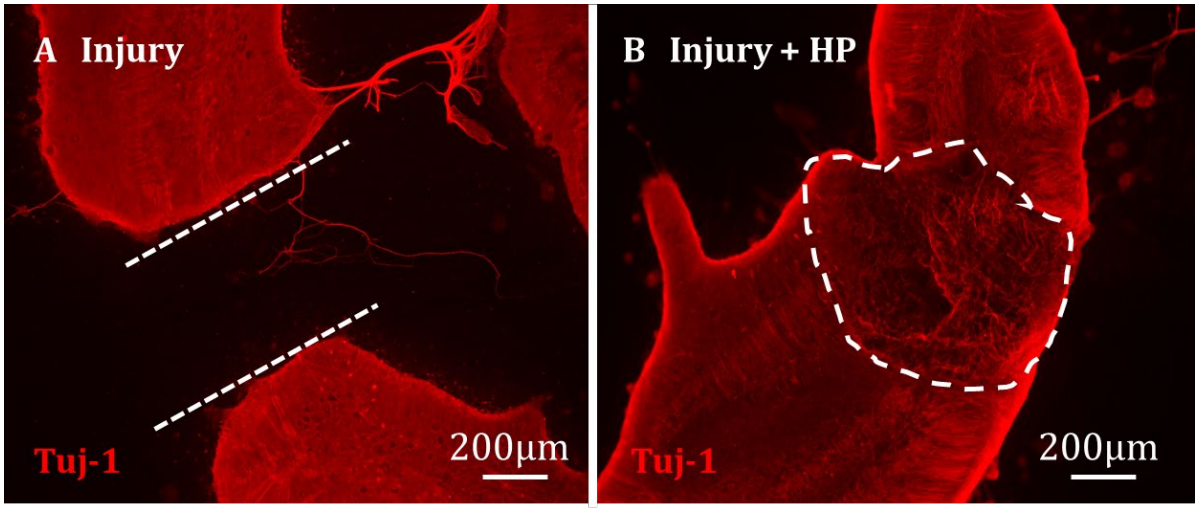

Figure 6.7 Neuronal tract infiltration after biomaterial implantation*. Fluorescence images representing Tuj-1 (red) infiltration into the lesion area in untreated slices (**A**) and biomaterial treated slices (**B**). White lines representing the lesion edges. More axonal infiltration was apparent in treated slices after injury.*

and, therefore, we were unable to analyse the length of each individual axon or determine if axons projecting from one side of the lesion had traversed the entire lesion width.

The total axonal length in each field of high magnification images (**Figure 6.8 A, B**) was analysed and averaged, showing a 1x10^4-fold higher total length of infiltrated neurites in "injury + HP" than in "injury" alone (**Figure 6.8 C**).

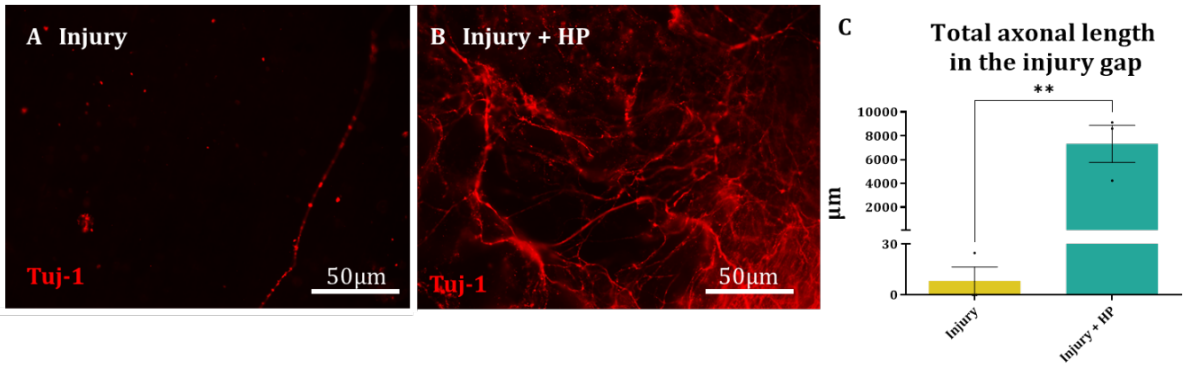

Figure 6.8 Formation of neuronal network after biomaterial implantation. *Fluorescence high magnification images of Tuj-1 fibres infiltrating the lesion site in an untreated injury (**A**) and within implanted Hemopatch™ (**B**). The bar graph (**C**) represents the total length of fibres present in each field (in µm) in untreated slices compared to treated slices (Unpaired t-test, n=3, p=0.009). More axonal infiltration was quantified in treated slices than in untreated slices.*

6.2.5 Biomaterial implantation induced higher microglial infiltration into the lesion area

Biomaterial implantation induced high microglial infiltration into the implanted biomaterial compared to infiltration within the lesioned area alone (**Figure 6.9 A, B**). Visual analysis of the lectin-positive cells morphology suggested most of the infiltrated cells to present an amoeboid or reactive phenotype (**Figure 6.9 C**). The statistical analysis revealed a significant increase in the number of lectin-positive cells in the lesion area after implantation than on untreated slices (**Figure 6.9 D**).

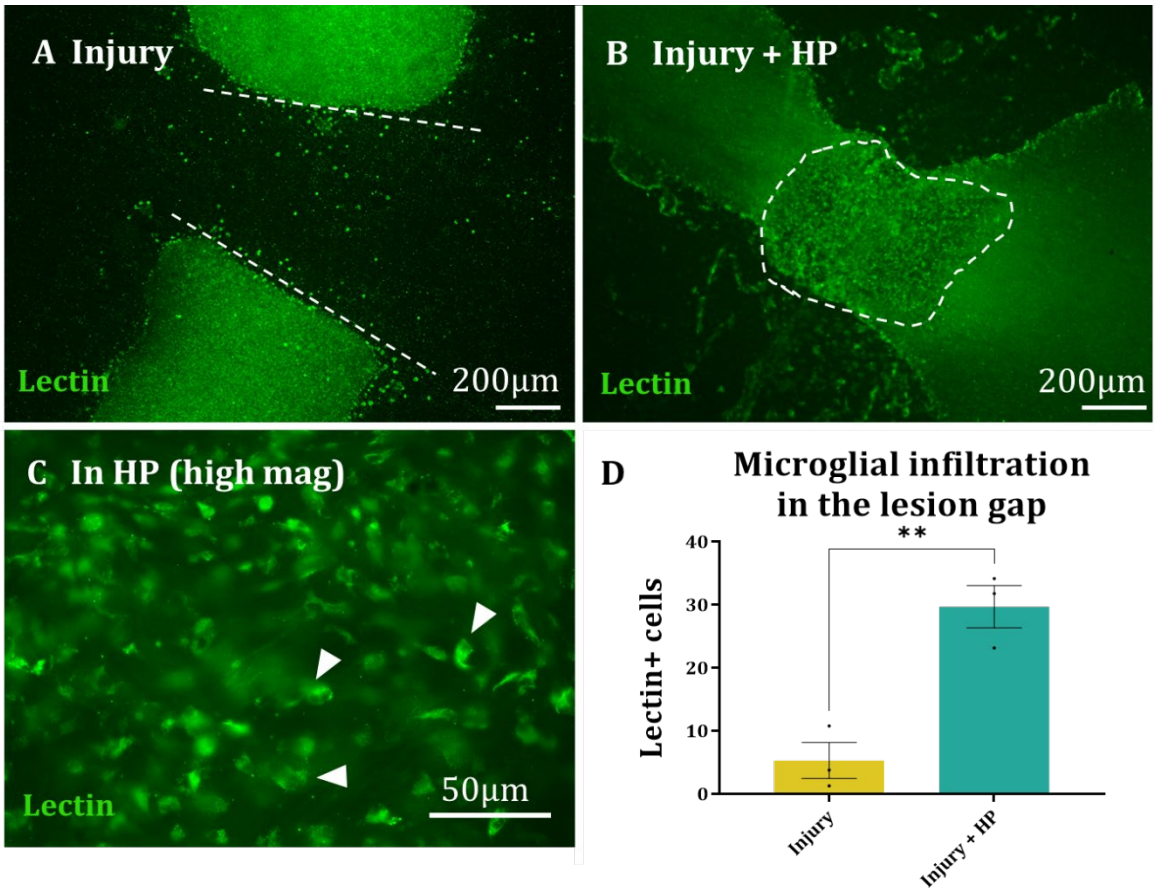

Figure 6.9 Microglial infiltration after biomaterial implantation*. Representative fluorescence images of lectin positive cells (green) on untreated slices (**A**) and after biomaterial implantation (**B**) at low magnification. White lines representing the edges of the lesion. **C** is a representative high magnification image of lectin-positive cells within the implanted biomaterial. White arrow indicating amoeboid cells. The bar graph (**D**) represents the absolute number of lectin-positive cells per unit area within the lesion area on untreated slices compared to treated slices (Unparied t-test, n=3, p=0.005). More microglial infiltration was seen in treated slices than in untreated.*

6.2.6 Analysis of MBP-positive fibre distribution was unreliable due to lack of fibres on control spinal cords

The spinal cord slices were stained and analysed following the protocols established in **Chapter 3**. Despite the successful analysis in **Chapter 3** and in those spinal cords treated with Hemopatch™, these results could not be reliably compared to controls due to the low presence of MBP fibres on the control slices. Although MBP staining was successful, the lack of MBP positive fibres within the control spinal cords (**Figure 6.10 A-C**) make the analysis unreliable in this case. However, a representative number of MBP-positive fibres were observed after implantation (**Figure 6.10 D-F**) and, therefore, the images and quantification are added in this section for representation of putative future results that might originate after further repetition of experiments.

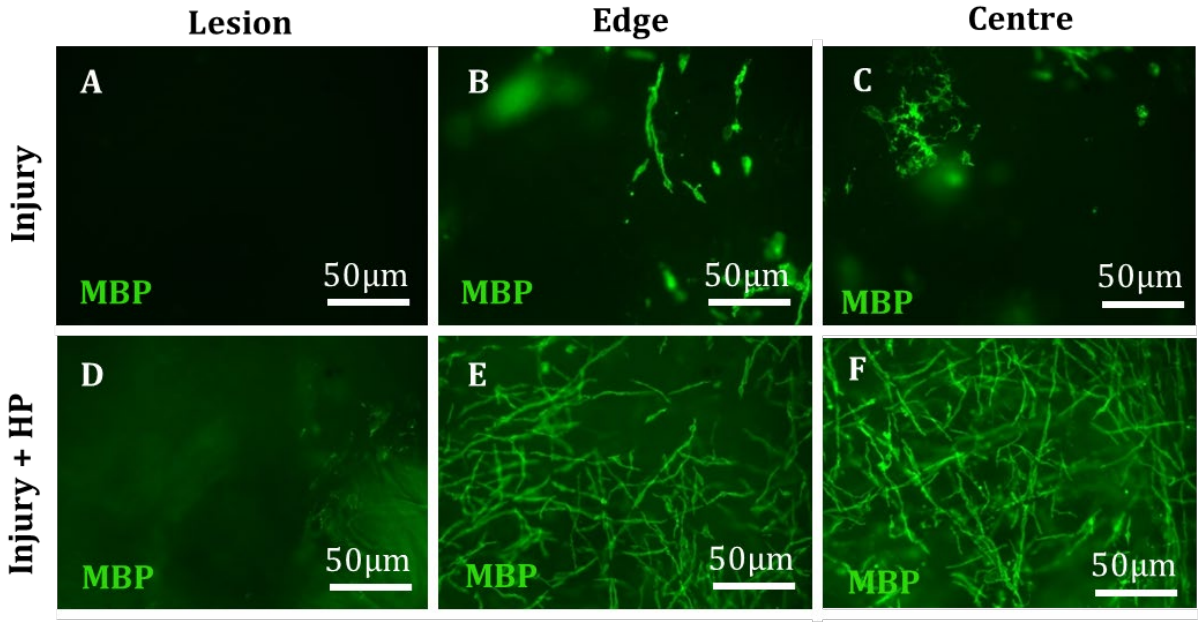

Figure 6.10 Presence of myelin tracts after biomaterial implantation. *Fluorescence images representing MBP-positive fibres (green) on untreated slices in the lesion area (**A**), edge of the lesion (**B**) and centre of the spinal cord (**C**) as well as representative images of spinal cord slices after biomaterial implantation within the implanted biomaterial (**D**), edge of the lesion (**E**) and centre of the spinal cord (**F**). No MBP positive tracts were found in untreated slices.*

The analysis suggested that, after Hemopatch™ implantation there were no differences in the density of MBP tracts between the centre of the spinal cord and the edge of the lesion (**Figure 6.11**). However, there was a significant difference between the centre of the spinal cord and the density inside the implanted scaffold, which was approximately 0%.

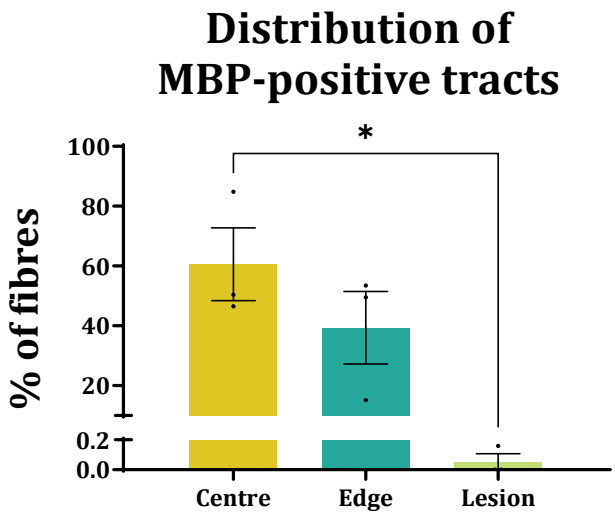

***Figure 6.11 Distribution of MBP-positive tracts**. Graphical representation of the percentage of MBP-positive fibres present in the centre and edge of the spinal cord and within the lesion area in slices after biomaterial implantation (One-way ANOVA, n=3, p<0.05). Less MBP-positive fibres were found in the implanted biomaterial than at the centre of the spinal cord.*

6.3 DISCUSSION

6.3.1 Summary of aims and results

Here we show for the first time that bioscaffolds, in this case a clinically available biomaterial, can be implanted within the transecting injury of a chick embryo spinal cord organotypic slice injury model. Our results suggest that slice viability is retained after implantation and that it is possible to manipulate the samples for immunostaining and imaging. In addition, we show that the slices respond to biomaterial implantation through increased axonal and microglial infiltration and reduced glial scarring. This is the first report of the implantation of clinical a grade material in a SCI model. These results could have a potential impact in increasing the research output on the study of SCI therapies which, in turn, would lead to a faster translation of functional therapies to higher complexity models and, finally, to the clinic. These findings will be discussed in the following sections.

6.3.2 Feasibility of biomaterial implantation in lesioned chick embryo spinal cord organotypic slices

Biomaterial implantation in rodent spinal cord organotypic slices has been tested within the frame of transecting injuries (Guijarro-Belmar et al., 2019; Hidalgo San Jose et al., 2018; A. P. Weightman et al., 2014) due to the gap created between both ends of the lesion in comparison to a demyelinating or compression injury. Moreover, transecting lesions are also used in most *in vivo* studies of biomaterial implantation in SCI (Galli et al., 2018; Wu et al., 2018). In addition, in comparison to transversal slices, longitudinal spinal cord slices maintain the ascending/descending polarity of axons (Guijarro-Belmar et al., 2019; A. P. Weightman et al., 2014), crucial to mimic *in vivo* responses when analysing axonal regeneration. Therefore, transecting lesions on longitudinal slices were used in this study.

The lesioning time point (4 days after dissection) was chosen in accordance with the results in **Chapter 3**, as it was the earliest lesioning time point at which typical responses

to lesioning were observed in the tissue slices. According to the results in **Chapter 3**, astrocytic gliosis in response to injury was only observed 12 days after lesioning, but not 4. In addition, the longest time period the slices were maintained in culture was 24 days. In order to allow enough time for the host tissue to respond to biomaterial implantation, but also to ensure survival, we decided to keep the slices in culture for 24 days (20 days after injury and/or biomaterial implantation).

At the end of the incubation period, the untreated slices (injured and sham) showed high viability rates, similarly to the results obtained in **Chapter 3**. Moreover, implantation of a biomaterial within the injury gap did not have an effect on slice survival, suggesting that Hemopatch™ did not have a toxic effect on the tissue and highlighting the potential of the material for safe implantation.

If cell infiltration was not considered, it was noticed that apparent lesion width was slightly wider after implantation than in untreated controls. A bigger lesion gap after implantation is also reported in *in vivo* studies (Galli et al., 2018), although implantation was also correlated with higher axonal infiltration and motor recovery. This could be due to a further lesion infliction during biomaterial implantation (Yoshii et al., 2004). The use of injectable hydrogels could help overcome this problem. These *in situ*-forming scaffolds can be injected into the patient and gel once they are at the injury site, providing a gentler implantation procedure (Morteza Bahram, 2012). However, upon image examination, it was clear that cellular infiltration covered the width of the lesion gap, closing the distance between both ends of the spinal cord.

In conclusion, we show that Hemopatch™ implantation into the SCI model established in **Chapter 3** can be achieved with similar previously published results using rodent models.

6.3.3 Cellular responses to Hemopatch™ implantation

The second aim of this chapter was to examine the cellular responses to Hemopatch™ implantation. Hemopatch™ was chosen for implantation due to its capacity for NSC encapsulation and potential for clinical translation (**Chapter 4**). Although we reported Cellevate™ to also allow the culture of healthy NSC populations as well as cellular alignment with fibres (**Chapter 5**), this material needs further modifications prior to implantation, for example, formation of conduits instead of coverslip-shaped constructs. Consequently, Hemopatch™ provided a more straightforward path to implantation and was therefore chosen for these experiments. Hemopatch™ was implanted acellularly, to study its regeneration permissiveness as a biomaterial (as well as the possibility of interfacing it with the organotypic slice model) instead of its capacity to deliver transplant cell populations.

Here, we report that GFAP OD at the edge of the lesion was lower after biomaterial implantation than in untreated slices. Moreover, astrocytes, which were polarised in a 90° angle in respect to the untreated lesion, appeared more disperse and less elongated on the treated slices, suggesting a possible inhibition of glial scar formation. These results are in contradiction with some *in vivo* studies, which reported no difference in glial scar formation after biomaterial implantation (Domínguez-Bajo et al., 2020; Galli et al., 2018). In contrast, other studies do report a disruption of the glial scar either through an architectural change *in vivo* (Hurtado et al., 2011) or a decrease in GFAP expression *in vitro* (Guijarro-Belmar et al., 2019; A. P. Weightman et al., 2014). This contradiction within existing literature, all reporting transecting lesions, could be due to the use of different types of biomaterials (*i.e.*: aligned fibres, injectable hydrogels, implantable gels), stressing the importance of biomaterial screening tests before committing to high complexity models. In this case, the data suggests that Hemopatch™ implantation does not result in astrocyte reactivity, emphasizing the potential of the biomaterial as a treatment for SCI.

We also report high axonal infiltration within the implanted biomaterial compared to the untreated lesion, similarly to previously published research *in vivo* (Galli et al., 2018; Wu et al., 2018; Z. Yang et al., 2015) and *in vitro* (Guijarro-Belmar et al., 2019; A. P. Weightman et al., 2014). Due to the high axonal infiltration we were unable to distinguish single axons. This hampered the analysis of single axonal length and we were forced to analyse total axonal length in the field as an indicative of regenerative behaviour. We were also unable to distinguish any possible physical reconnection between axons from each end of the lesion. Nevertheless, due to the high density of axons present within the material, there is a possibility of such synaptic connections existing between the separated tissue. Moreover, the high number of infiltrating axons are regarded as an indicative of the potential pro-regenerative role for axonal growth (or regeneration permissive role) of Hemopatch™ implantation. In fact, experimental grade collagen scaffolds, have previously been shown to promote neuron growth (Kourgiantaki et al., 2020).

In **Chapter 3**, the presence of MBP-positive tracts was reported to be lower at the edge of the lesion than at the centre, suggesting possible demyelination of fibres. Here, we report that MBP-positive fibres are equally present at the edge of the lesion and at the centre of the spinal cord after implantation. This data seems to implicate that biomaterial implantation could have an effect on protecting these tracts. However, it does not seem to allow oligodendrocyte infiltration into the lesion gap, as seen by the low numbers of MBP-positive cells within the biomaterial. This could be due to the inherent low ability of this cell type for migration. The response of oligodendrocytes to the untreated lesion in this chapter, however, could not be analysed due to the low numbers of MBP-positive tracts found in the control slices. We initially hypothesised this was due to the advanced age of the slices. However, upon comparison of slices of the same age from **Chapter 3** (I12F12) to younger slices (I4F4, I4F12), it was concluded that all displayed similar numbers of MBP-positive tracts regardless of age. We, therefore, concluded that perhaps the control

slices that were chosen for experimentation were obtained from a spinal cord slice that had not developed mature oligodendrocytes at the time of dissection and, due to the lack of external physiological input, these did not differentiate in culture either. Therefore, the lack of MBP-positive tracts in control slices forced us to deem the results obtained on treated slices inconclusive.

Finally, the immune response to biomaterial implantation was investigated. Our data indicate that microglial infiltration in the lesion area is higher upon implantation. Moreover, morphological examination seemed to indicate that microglia displayed a reactive phenotype within the biomaterial. Our results are in consonance with previously published research with mouse organotypic models of transecting SCI (Weightman et al., 2014) and *in vivo* models of transecting SCI in rats and mice respectively (Domínguez-Bajo et al., 2020; Kourgiantaki et al., 2020). A reduction in microglial infiltration has only been reported in one study (Guijarro-Belmar et al., 2019), due to the functionalisation of the implanted biomaterial with an Epac2 agonist. Our results constitute the first report of immune cell infiltration in an implant in the chick, providing the model with a multidimensional platform in which to research tissue engineering techniques for regenerative medicine.

In conclusion, here we show that Hemopatch™ implantation elicits cellular responses that could lead to functional regeneration, such as reduced glial scarring and high axonal infiltration compared to controls. These findings, together with the data from **Chapter 4**, highlight the potential of Hemopatch™ as a possible biomaterial for implantation in SCI. Moreover, these results suggest that the chick embryo SCI model described here responds to lesion and biomaterial implantation in a similar fashion to models established using rodents. This has important implications when aiming to test a range of biomaterials for the first time as treatment for SCI, as this model offers a cheaper and easily accessible

platform and allows the scientific community to conduct relevant research while reducing animal suffering.

6.3.4 Future directions

The model described here offers a platform in which to test biomaterial implantation as it mimics *in vivo* responses to injury and implantation. In this case, the material was implanted immediately after lesioning and, therefore, not allowing enough time for scar formation and consecutive disruption. Instead, priority was given to rapid implantation to allow for an extended time period to observe responses to the treatment as shown in previous studies (Guijarro-Belmar et al., 2019; A. P. Weightman et al., 2014). In future studies, it might be desirable to implant the biomaterial 12 days after lesioning to allow formation of the glial scar (**Chapter 3**) and study whether biomaterial implantation results in disruption of an existing glial scar.

As mentioned previously, some slices lacked MBP-positive tracts, which hampered analysis. Although it has been described that oligodendrocytes appear at E5 in the chick embryo (Ono et al., 1995), it might be useful to study the segments of the spinal cord that contain mature oligodendrocytes at E15. A possible short research project could involve the dissection and cryosection of different sections of the spinal cord and consecutive immunostaining with an MBP marker. This may facilitate targeted dissection of those slices which will contain tracts and can therefore be used to study potential de- and remyelination events.

In regard to neuronal reconnection, failure to study functional synaptic reconnection after SCI *in vitro* is a recurrent limitation in the literature. Since most *in vitro* SCI models focus on cytological responses to insult, synaptic functionality is often left to be tested *in vivo* with behavioural tests. The generalist nature of such tests, however, does not account for the study of targeted and efficient synapsis, leading to partial recovery of motor and

sensory function after all experiments to date. We propose that, in order to achieve testing of functional synapsis within the organotypic tissue SCI models, these could be interfaced with electrophysiology equipment, such as multi electrode arrays (MEAs) (Duan et al., 2016) or stained with a calcium dye (O'Donovan et al., 2005) and imaged live.

7 CONCLUSIONS

7.1 SUMMARY AND SCIENTIFIC IMPACT OF RESULTS

The aim of this thesis was to develop a SCI model using chick embryo organotypic slices in order to provide a platform in which to test biomaterial implantation within the framework of the 3Rs principle. Here we demonstrate the establishment of a chick embryo spinal cord organotypic slice model for SCI, which responded to the lesion with typical cellular responses: glial scarring, low axonal regeneration, loss of MBP-positive tracts and microglial infiltration. Next, we tested two biomaterials (Hemopatch™ and Cellevate™) for their capacity to incorporate a clinically relevant cell transplant population. Both biomaterials allowed for safe cell culture. In addition, we were able to improve distribution of cells within Hemopatch™ through laminin engineering and to successfully analyse cell alignment in Cellevate™. Out of the two, Hemopatch™ offered a more straightforward path for implantation and, therefore, it was chosen to be tested in the SCI model established previously. Hemopatch™ implantation in the organotypic SCI model resulted in cellular responses comparable to those obtained *in vivo* and in other murine organotypic models: reduced glial scarring, increased axonal infiltration, microglial response and possible retention of oligodendrocytes. The research conducted for this thesis resulted in relevant outcomes for the study of SCI therapies. These outcomes could be classified into two categories: SCI therapies and SCI models.

In regard to the first category, this constitutes the second ever study involving the culture of a relevant cell transplant population within a clinical grade biomaterial. Moreover, this is the first report of the implantation of clinical a grade material in a SCI model, resulting in increased axonal regeneration. Our results corroborate the fact that such materials have translational potential for implantation in SCI with potential implications in reducing the time it takes for such therapies to reach the clinic. Additionally, we were able

to modify the scaffold through laminin engineering, opening the possibilities of finely tuning the characteristics of these surgical biomaterials in order to optimise them for cell encapsulation. In addition, we describe a methodology for analysing cellular alignment and we demonstrate alignment of neurons and astrocytes on electrospun fibres, key tools when aiming to promote directed axonal growth for spinal cord repair.

In regard to the second category, we report for the first time the establishment of a SCI model using chick embryo organotypic slices. The model, which presents comparable responses to those based on murine models, represents a simpler alternative to previously established models. Here, we offer a cheaper alternative, which is easier to manipulate and linked to fewer ethical implications in the UK. Purchasing fertilised eggs is cheaper and easier than purchasing mice for experimentation. Additionally, the techniques described here do not require licence for animal manipulation in the UK and the maintenance of the eggs does not require specialised facilities or personnel. For these reasons, the model described here offers a system which could be adopted by most biological labs. The adoption of this model could lead to impactful research while maintaining a cost-effective and technically simple methodology. This could have translational potential for other research areas, such as the study of degenerative diseases, and potentially increase the research output on the study of SCI therapies which, in turn, would lead to a faster translation of functional therapies to higher complexity models and, finally, to the clinic.

7.2 FUTURE DIRECTIONS

7.2.1 Implantation of encapsulated neural stem cells within the established model

The next logical step would be to put in practice the model established here by testing a combinatorial therapy of Hemopatch™-encapsulated NSCs implanted within the chick embryo organotypic SCI model. This would allow for a more complete characterisation of Hemopatch™ as a method of delivering NSCs for SCI therapy. A population of mouse-

derived NSCs have been tested in this thesis for encapsulation in the biomaterial. Therefore, it would be logical to test the same cell population for implantation. Previous research has shown that it is feasible to deliver human-derived (Sigurjonsson et al., 2005) and mouse-derived (Clarke et al., 2000) stem cells to the chick embryo, resulting in integration of these cells with the host. This would have the added advantage of being able to detect the species-specific transplant cells to assess important regenerative properties such as survival, integration and differentiation post-transplantation. Alternatively, in order to avoid rejection of the implanted cells, it might be desirable to implant chick-derived NSCs. We have attempted derivation of NSCs from E14 chick embryos in a preliminary study (**Figure 7.1**).

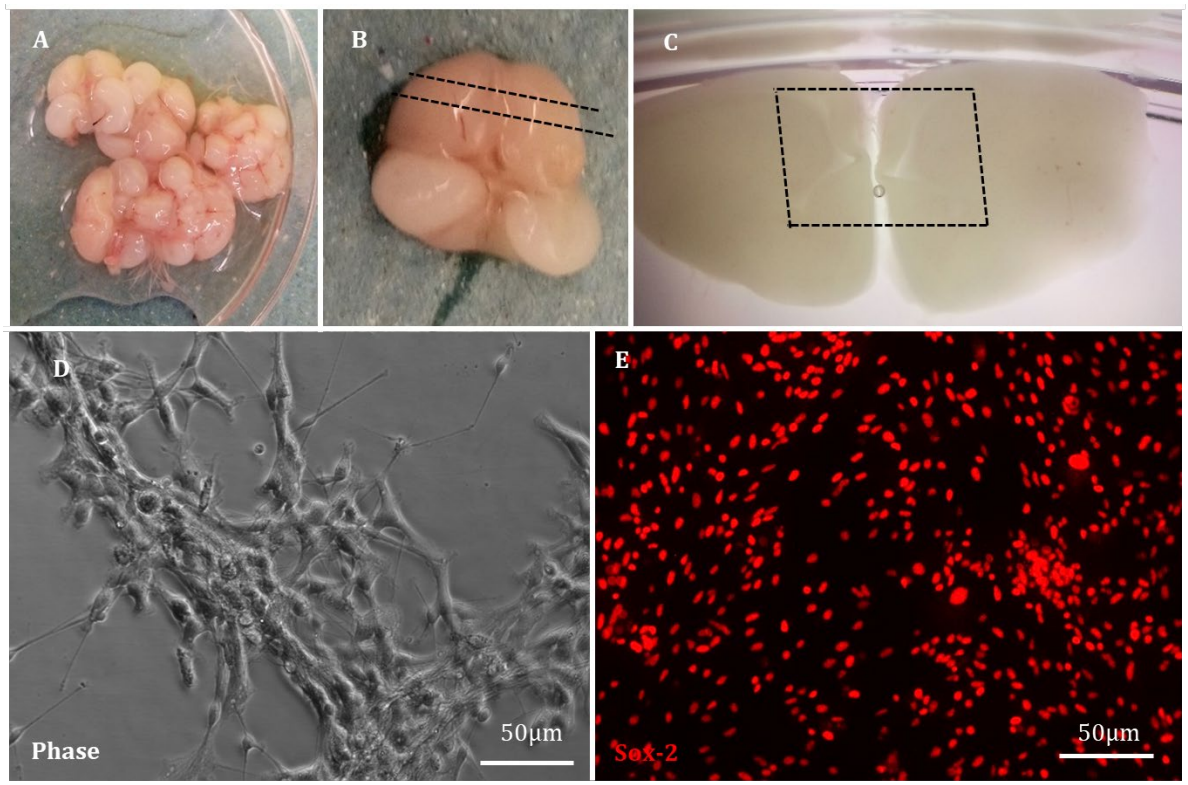

Figure 7.1 *Establishment of an NSC culture from chick embryo brains. Preliminary results showing the process of obtaining chick embryo-derived NSCs showing dissected brains (**A**), detail of one brain with dotted lines marking slicing areas (**B**), sliced brain with dotted line marking the surroundings of the SVZ (**C**), live cells two days after culture on glass coverslips (**D**), and Sox-2 stained NSCs 5 days after culture. (**E**). These images suggest the possibility of establishing the chick embryo NSC* in vitro *culture.*

The results obtained suggested that it would be possible to derive NSCs from chick embryo brains following the same protocols used for mouse-derived NSCs. In addition, it seems feasible to immunostain the cultured cells with Sox-2, an NSC marker. Next steps would involve the study of the proliferative and differentiation capacity of these cells in glass coverslips and within Hemopatch™. Such experiments would further the 3Rs impact of the technique, having all the cells and tissue derived from non-protected species.

Upon implantation in the organotypic model similar landmarks of regeneration as in **Chapter 6** would have to be studied (*i.e.:* glial scarring, axonal infiltration, microglial activation and MBP tract loss) in addition to survival, phenotypical fate and possible migration and integration with the host tissue of the exogenous cells. These landmarks would have to be compared to appropriate controls (i.e.: sham, untreated lesion, lesion treated with acellular Hemopatch™).

Importantly, if derived from chick, the implanted cells would have to be tracked and distinguished from host cells. This could be achieved through genetic engineering for green fluorescent protein (GFP) incorporation. This strategy has been previously achieved successfully in our laboratory using minicircle DNA vectors incorporating GFP and using safe magnetofection technology as a transfection approach (Finch et al., 2020).

7.2.2 Study of molecular responses to lesion and biomaterial implantation

Molecular level responses to SCI (*i.e.:* release of oxygen reactive species, inflammatory cytokines and CSPGs) are a crucial factor to consider when studying regenerative therapies. However, this thesis focuses primarily on cellular responses. Therefore, with the aim of making the characterisation of lesioning and implantation more complete, it might be desirable to study these molecular responses. On the one hand it might be interesting to study landmark molecular responses to injury alone *vs.* implantation (such as the ones described in the previous paragraph) in order to compare their levels and

correlate the results to the cellular responses. On the other hand, it might be interesting to study the molecular effects of NSC implantation such as the release of neurotrophic factors (*i.e.:* BDNF, NT-3) or the molecular profile of NSC differentiation upon implantation. This could be achieved through the study of gene expression, for example using qPCR, or protein expression, for example using mass spectrometry or western blot.

7.2.3 Evaluation of synaptic restoration after spinal cord injury

Despite the promising results in current SCI therapy research, full restoration has not been achieved yet. This could be due to the formation of non-functional synapses. For this reason, it is becoming increasingly evident that targeted axonal regeneration is crucial in order to achieve full restoration of motor and sensory function. Current *in vitro* and *ex vivo* models focus on regenerative evaluation mostly through histological tests but lack techniques for evaluation of functional restoration. *In vivo* models offer the possibility to study functional outcomes through motor and sensory tests. However, these generalist approaches lack the capacity to evaluate synapsis formation and functionality in detail. Therefore, we propose the incorporation of methods for evaluation of electrical neuronal activity with the organotypic model described here.

The entry of extracellular calcium within the neuronal cytoplasm is one hallmark of neuronal excitation, which leads to membrane depolarisation and action potential. Calcium dyes permit the visualisation of calcium transients in cultured cells *in situ*, and have been repeatedly used to research synchronised neuronal firing (O'Donovan et al., 2005). In addition, calcium imaging has already been successfully attempted in hippocampal organotypic slices (Sasaki et al., 2014), leading to hypothesise that the technique could also be successful in spinal cord organotypic slices. This technique could allow for the study of synchronised neuronal activity before and after injury and before and after treatment which, together with histological analysis, would provide the model

with a multidimensional understanding of the regenerative and functional properties of the therapy.

Alternatively, MEAs are culture wells consisting of an array of electrodes capable of recording extracellular changes in ionic levels, which are correlated with neuronal electrical activity. Due to their small size and distribution in the well, MEAs are capable of detecting action potentials at high resolution and have also been used to study neuronal firing synchronicity (Chiappalone et al., 2007). Additionally, these have also been used in combination with brain organotypic cultures (Plenz et al., 2011).

An advantage of MEAs over calcium dyes is the possibility of electrical stimulation of samples. Electrical stimulation of neurons has been correlated with increased axonal length (Bertucci et al., 2019). In fact, electrical stimulation through the implantation of an electrode array after SCI resulted in increased motor improvement in a clinical trial (Wagner et al., 2018). Consequently, incorporating the use of MEAs on the SCI model described here would add a new level of analysis, which could result in a three-dimensional research model including histological, molecular and electrical assays. Moreover, it could lead to the study of a three-way combinatorial approach featuring cell therapy, biomaterial implantation and electrical stimulation.

8 REFERENCES

Aarabi, B., Sansur, C. A., Ibrahimi, D. M., Simard, J. M., Hersh, D. S., Le, E., Diaz, C., Massetti, J., & Akhtar-Danesh, N. (2017). Intramedullary lesion length on postoperative magnetic resonance imaging is a strong predictor of ASIA impairment scale grade conversion following decompressive surgery in cervical spinal cord injury. *Clinical Neurosurgery*, *80*(4), 610–620. https://doi.org/10.1093/neuros/nyw053

Abu-Rub, M., McMahon, S., Zeugolis, D. I., Windebank, A., & Pandit, A. (2010). Spinal cord injury in vitro: Modelling axon growth inhibition. *Drug Discovery Today*, *15*(11–12), 436–443. https://doi.org/10.1016/j.drudis.2010.03.008

Ahuja, C. S., Mothe, A., Khazaei, M., Badhiwala, J. H., Gilbert, E. A., van der Kooy, D., Morshead, C. M., Tator, C., & Fehlings, M. G. (2020). The leading edge: Emerging neuroprotective and neuroregenerative cell-based therapies for spinal cord injury. *Stem Cells Translational Medicine*, *9*(12), 1509–1530. https://doi.org/10.1002/sctm.19-0135

Ahuja, C. S., Nori, S., Tetreault, L., Wilson, J., Kwon, B., Harrop, J., Choi, D., & Fehlings, M. G. (2017a). Traumatic Spinal Cord Injury-Repair and Regeneration. *Neurosurgery*, *80*(3), S9–S22. https://doi.org/10.1093/neuros/nyw080

Ahuja, C. S., Nori, S., Tetreault, L., Wilson, J., Kwon, B., Harrop, J., Choi, D., & Fehlings, M. G. (2017b). Traumatic spinal cord injury - Repair and regeneration. *Clinical Neurosurgery*, *80*(3), S22–S90. https://doi.org/10.1093/neuros/nyw080

Akhtar, A. Z., Pippin, J. J., & Sandusky, C. B. (2009). Animal studies in spinal cord injury: a systematic review of methylprednisolone. *Alternatives to Laboratory Animals : ATLA*, *37*(1), 43–62.

Alaynick, W. A., Jessell, T. M., & Pfaff, S. L. (2011). SnapShot: Spinal cord development. *Cell*,

146(1), 178.e1. https://doi.org/10.1016/j.cell.2011.06.038

Alexander, J. K., Fuss, B., & Colello, R. J. (2006). Electric field-induced astrocyte alignment directs neurite outgrowth. *Neuron Glia Biology*, *2*(2), 93–103. https://doi.org/10.1017/S1740925X0600010X

Amer, M. H., White, L. J., & Shakesheff, K. M. (2015). The effect of injection using narrow-bore needles on mammalian cells: Administration and formulation considerations for cell therapies. *Journal of Pharmacy and Pharmacology*, *67*(5), 640–650. https://doi.org/10.1111/jphp.12362

Anderson, K. D., Martinez-barrizonte, J., Sunn, G. H., Gant, K. L., & Levi, A. D. (2017). Human Neural Stem Cell Transplantation in Chronic Cervical Spinal Cord Injury : Functional Outcomes at 12 Months in a Phase II Clinical Trial. *CLINICAL NEUROSURGERY*, *64*(1), 87–91. https://doi.org/10.1093/neuros/nyx242

Anderson, M. A., Burda, J. E., Ren, Y., Ao, Y., O'Shea, T. M., Kawaguchi, R., Coppola, G., Khakh, B. S., Deming, T. J., & Sofroniew, M. V. (2016). Astrocyte scar formation aids central nervous system axon regeneration. *Nature*, *532*(7598), 195–200. https://doi.org/10.1038/nature17623

Ankeny, D. P., McTigue, D. M., & Jakeman, L. B. (2004). Bone marrow transplants provide tissue protection and directional guidance for axons after contusive spinal cord injury in rats. *Experimental Neurology*, *190*(1), 17–31. https://doi.org/10.1016/j.expneurol.2004.05.045

Assinck, P., Duncan, G. J., Hilton, B. J., Plemel, J. R., & Tetzlaff, W. (2017). Cell transplantation therapy for spinal cord injury. *Nature Neuroscience*, *20*(5), 637–647. https://doi.org/10.1038/nn.4541

Ayuso-Sacido, A., Moliterno, J. A., Kratovac, S., Kapoor, G. S., O'Rourke, D. M., Holland, E. C.,

Garci'a-Verdugo, J. M., Roy, N. S., & Boockvar, J. A. (2010). Activated EGFR signaling increases proliferation, survival,and migration and blocks neuronal differentiation in post-natal neural stem cells. *Journal of Neuro-Oncology*, *97*(3), 323–337. https://doi.org/10.1007/s11060-009-0035-x

Azbill, R. D., Mu, X., & Springer, J. E. (2000). Riluzole increases high-affinity glutamate uptake in rat spinal cord synaptosomes. *Brain Research*, *871*(2), 175–180. https://doi.org/10.1016/S0006-8993(00)02430-6

Ballios, B. G., Cooke, M. J., Donaldson, L., Coles, B. L. K., Morshead, C. M., Kooy, D. Van Der, & Shoichet, M. S. (2015). A Hyaluronan-Based Injectable Hydrogel Improves the Survival and Integration of Stem Cell Progeny following Transplantation. *Stem Cell Reports*, *4*(6), 1031–1045. https://doi.org/10.1016/j.stemcr.2015.04.008

Bardehle, S., Krüger, M., Buggenthin, F., Schwausch, J., Ninkovic, J., Clevers, H., Snippert, H. J., Theis, F. J., Meyer-Luehmann, M., Bechmann, I., Dimou, L., & Götz, M. (2013). Live imaging of astrocyte responses to acute injury reveals selective juxtavascular proliferation. *Nature Neuroscience*, *16*(5), 580–586. https://doi.org/10.1038/nn.3371

Barros, D., Amaral, I. F., & Pêgo, A. P. (2019). Laminin-Inspired Cell-Instructive Microenvironments for Neural Stem Cells. *Biomacromolecules*, *21*(2), 276–293. https://doi.org/10.1021/acs.biomac.9b01319

Baxter Healthcare Corporation. (2019). *Hemopatch Sealing Hemostat*. http://www.hemopatch.com/int/index.html

Bertucci, C., Koppes, R., Dumont, C., & Koppes, A. (2019). Neural responses to electrical stimulation in 2D and 3D in vitro environments. *Brain Research Bulletin*, *152*(February), 265–284. https://doi.org/10.1016/j.brainresbull.2019.07.016

Biernaskie, J., Sparling, J. S., Liu, J., Shannon, C. P., Plemel, J. R., Xie, Y., Miller, F. D., & Tetzlaff, W. (2007). Skin-derived precursors generate myelinating Schwann cells that promote remyelination and functional recovery after contusion spinal cord injury. *Journal of Neuroscience*, *27*(36), 9545–9559. https://doi.org/10.1523/JNEUROSCI.1930-07.2007

BJ Cummings, N Uchida, et al. (2005). Human neural stem cells differentiate and promote locomotor recovery in spinal cord-injured mice. *Proceedings of the National Academy of Sciences of the United States of America*, *102*(39), 14069–14074.

Bjornstad, S., Austdal, L. P. E., Roald, B., Glover, J. C., & Paulsen, R. E. (2015). Cracking the Egg: Potential of the Developing Chicken as a Model System for Nonclinical Safety Studies of Pharmaceuticals. *Journal of Pharmacology and Experimental Therapeutics*, *355*(3), 386–396. https://doi.org/10.1124/jpet.115.227025

Bonner, J. F., Connors, T. M., Silverman, W. F., Kowalski, D. P., & Lemay, M. A. (2011). Grafted Neural Progenitors Integrate and Restore Synaptic Connectivity across the Injured Spinal Cord. *The Journal of Neuroscience*, *31*(12), 4675–4686. https://doi.org/10.1523/JNEUROSCI.4130-10.2011

Bonnici, B., & Kapfhammer, J. P. (2008). Spontaneous regeneration of intrinsic spinal cord axons in a novel spinal cord slice culture model. *European Journal of Neuroscience*, *27*(10), 2483–2492. https://doi.org/10.1111/j.1460-9568.2008.06227.x

Boyd, J. G., & Gordon, T. (2003). Neurotrophic Factors and Their Receptors in Axonal Regeneration and Functional Recovery after Peripheral Nerve Injury. *Molecular Neurobiology*, *27*(3), 277–323. https://doi.org/10.1385/MN:27:3:277

Bradbury, E. J., Moon, L. D. F., Popat, R. J., King, V. R., Bennett, G. S., Patel, P. N., Fawcett, J. W., & McMahon, S. B. (2002). Chondroitinase ABC promotes functional recovery after

spinal cord injury. *Nature*, *416*(6881), 636–640. https://doi.org/10.1038/416636a

Briscoe, J., Pierani, A., Jessell, T. M., & Ericson, J. (2000). A homeodomain protein code specifies progenitor cell identity and neuronal fate in the ventral neural tube. *Cell*, *101*(4), 435–445. https://doi.org/10.1016/S0092-8674(00)80853-3

Brunet, Núria, Tarabal, O., Esquerda, J. E., & Calderó, J. (2009). Excitotoxic motoneuron degeneration induced by glutamate receptor agonists and mitochondrial toxins in organotypic cultures of chick embryo spinal cord. *Journal of Comparative Neurology*, *516*(4), 277–290. https://doi.org/10.1002/cne.22118

Brunet, Nuria, Tarabal, O., Portero-Otin, M., Oppenheim, Ronald, W., Esquerda, J. E., & Caldero, J. (2007). Survival and Death of Mature Avian Motoneurons in Organotypic Slice Culture: Trophic Requirements for Survival and Different Types of Degeneration. *Journal of Comparative Neurology*, *501*(October 2007), 669–690. https://doi.org/10.1002/cne

Bunge, M. B. (2016). Efficacy of Schwann cell transplantation for spinal cord repair is improved with combinatorial strategies. *Journal of Physiology*, *594*(13), 3533–3538. https://doi.org/10.1113/JP271531

Calderó, J., Brunet, N., Tarabal, O., Piedrafita, L., Hereu, M., Ayala, V., & Esquerda, J. E. (2010). Lithium prevents excitotoxic cell death of motoneurons in organotypic slice cultures of spinal cord. *Neuroscience*, *165*(4), 1353–1369. https://doi.org/10.1016/j.neuroscience.2009.11.034

Calderó, Jordi, Brunet, N., Ciutat, D., Hereu, M., & Esquerda, J. E. (2009). Development of microglia in the chick embryo spinal cord: Implications in the regulation of motoneuronal survival and death. *Journal of Neuroscience Research*, *87*(11), 2447–2466. https://doi.org/10.1002/jnr.22084

Carmignac, V., & Durbeej, M. (2012). Cell-matrix interactions in muscle disease. *Journal of Pathology*, *226*(2), 200–218. https://doi.org/10.1002/path.3020

Casha, S., Zygun, D., McGowan, M. D., Bains, I., Yong, V. W., & John Hurlbert, R. (2012). Results of a phase II placebo-controlled randomized trial of minocycline in acute spinal cord injury. *Brain*, *135*(4), 1224–1236. https://doi.org/10.1093/brain/aws072

Castro, M., Johansson, S., Johansson, F., & Englund, U. (2016). Molecular and Cellular Neuroscience Exploration of physical and chemical cues on retinal cell fate. *Molecular and Cellular Neuroscience*, *75*, 122–132. https://doi.org/10.1016/j.mcn.2016.07.006

CE-Marking. (2020). *CE Marking Association*. https://www.cemarkingassociation.co.uk/

Celox-Medical. (2020). *Celox Medical*. celoxmedical.com

Charles W., George P., G. K. (2009). *The Spinal Cord*. Christopher and Dana Reeve Foundation.

Chiappalone, M., Vato, A., Berdondini, L., Koudelka-Hep, M., & Martinoia, S. (2007). Network dynamics and synchronous activity in cultured cortical neurons. *International Journal of Neural Systems*, *17*(2), 87–103. https://doi.org/10.1142/S0129065707000968

Cho, J. S., Park, H. W., Park, S. K., Roh, S., Kang, S. K., Paik, K. S., & Chang, M. S. (2009). Transplantation of mesenchymal stem cells enhances axonal outgrowth and cell survival in an organotypic spinal cord slice culture. *Neuroscience Letters*, *454*(1), 43–48. https://doi.org/10.1016/j.neulet.2009.02.024

Christopherson, G. T., Song, H., & Mao, H. Q. (2009). The influence of fiber diameter of electrospun substrates on neural stem cell differentiation and proliferation. *Biomaterials*, *30*(4), 556–564. https://doi.org/10.1016/j.biomaterials.2008.10.004

Clarke, D. L., Johansson, C. B., Wilbertz, J., Veress, B., Nilsson, E., Karlström, H., Lendahl, U., & Frisén, J. (2000). Generalized potential of adult neural stem cells. *Science*, *288*(5471), 1660–1663. https://doi.org/10.1126/science.288.5471.1660

Coumans, J. V., Lin, T. T. S., Hai Ning Dai, MacArthur, L., McAtee, M., Nash, C., & Bregman, B. S. (2001). Axonal regeneration and functional recovery after complete spinal cord transection in rats by delayed treatment with transplants and neurotrophins. *Journal of Neuroscience*, *21*(23), 9334–9344. https://doi.org/10.1523/jneurosci.21-23-09334.2001

Cullen, D. K., Stabenfeldt, S. E., Simon, C. M., Tate, C. C., & LaPlaca, M. C. (2007). In Vitro Neural Injury Model for Optimization of Tissue-Engineered Constructs. *Journal of Neuroscience Research*, *85*, 3642–3651800. https://doi.org/10.1002/jnr

David, S., & Aguayo, A. J. (1981). Axonal elongation into peripheral nervous system "bridges" after central nervous system injury in adult rats. *Science*, *214*(4523), 931–933. https://doi.org/10.1126/science.6171034

Davies, S. J. A., Fitch, M. T., Memberg, S. P., Hall, A. K., Raisman, G., & Silver, J. (1997). Regeneration of adult axons in white matter tracts of the central nervous system. *Nature*, *390*(6661), 680–683. https://doi.org/10.1038/37776

de la Torre, J. C. (1982). Catecholamine fiber regeneration across a collagen bioimplant after spinal cord transection. *Brain Research Bulletin*, *9*(1–6), 545–552. https://doi.org/10.1016/0361-9230(82)90162-9

Dhillon, S., De Boer, M. T., Papacharalabous, E. N., & Schwartz, M. (2011). Fibrin sealant (Evicel® [quixil®/crosseal™]): A review of its use as supportive treatment for haemostasis in surgery. *Drugs*, *71*(14), 1893–1915. https://doi.org/10.2165/11207700-000000000-00000

Dobbing, J., Morgan, R. S., Reid, R. T. W., & Wright, G. P. (1957). *Neuroglial Development and Myelination in the Spinal Cord of the Chick Embryo*. *5*(December), 428–437.

Domínguez-Bajo, A., González-Mayorga, A., López-Dolado, E., Munuera, C., García-Hernández, M., & Serrano, M. C. (2020). Graphene Oxide Microfibers Promote Regenerative Responses after Chronic Implantation in the Cervical Injured Spinal Cord. *ACS Biomaterials Science and Engineering*, *6*(4), 2401–2414. https://doi.org/10.1021/acsbiomaterials.0c00345

Drury, J. L., & Mooney, D. J. (2003). Hydrogels for tissue engineering: Scaffold design variables and applications. *Biomaterials*, *24*(24), 4337–4351. https://doi.org/10.1016/S0142-9612(03)00340-5

Duan, H., Li, X., Wang, C., Hao, P., Song, W., Li, M., Zhao, W., Gao, Y., & Yang, Z. (2016). Functional hyaluronate collagen scaffolds induce NSCs differentiation into functional neurons in repairing the traumatic brain injury. *Acta Biomaterialia*, *45*, 182–195. https://doi.org/10.1016/j.actbio.2016.08.043

Duarte, A. P., Coelho, J. F., Bordado, J. C., Cidade, M. T., & Gil, M. H. (2012). Surgical adhesives: Systematic review of the main types and development forecast. *Progress in Polymer Science*, *37*(8), 1031–1050. https://doi.org/10.1016/j.progpolymsci.2011.12.003

Duncan, G. J., Manesh, S. B., Hilton, B. J., Assinck, P., Plemel, J. R., & Tetzlaff, W. (2019). The fate and function of oligodendrocyte progenitor cells after traumatic spinal cord injury. *Glia*, *68*(2), 227–245. https://doi.org/10.1002/glia.23706

Dunn, R., Lyman, M. D., Edelman, P. G., & Campbell, P. K. (2001). Evaluation of the SprayGel™ adhesion barrier in the rat cecum abrasion and rabbit uterine horn adhesion models. *Fertility and Sterility*, *75*(2), 411–416.

https://doi.org/10.1016/S0015-0282(00)01677-0

Dwivedi, R., Kumar, S., Pandey, R., Mahajan, A., Nandana, D., Katti, D. S., & Mehrotra, D. (2020). Polycaprolactone as biomaterial for bone scaffolds: Review of literature. *Journal of Oral Biology and Craniofacial Research*, *10*(1), 381–388. https://doi.org/10.1016/j.jobcr.2019.10.003

East, E., De Oliveira, D. B., Golding, J. P., & Phillips, J. B. (2010). Alignment of astrocytes increases neuronal growth in three-dimensional collagen gels and is maintained following plastic compression to form a spinal cord repair conduit. *Tissue Engineering - Part A*, *16*(10), 3173–3184. https://doi.org/10.1089/ten.tea.2010.0017

Eck, J. C., Nachtigall, D., Humphreys, S. C., & Hodges, S. D. (2006). Questionnaire survey of spine surgeons on the use of methylprednisolone for acute spinal cord injury. *Spine*, *31*(9), 250–253. https://doi.org/10.1097/01.brs.0000214886.21265.8c

Ellis, E. F., Mckinney, J. S., Willoughby, K. A., Liang, S., & Povlishock, J. T. (1995). A New Model for Rapid Stretch-Induced Injury of Cells in Culture: Characterization of the Model Using Astrocytes. *Journal of Neurotrauma*, *12*(3), 325–339. https://doi.org/10.1089/neu.1995.12.325

Ericson, J., Rashbass, P., Schedl, A., Brenner-Morton, S., Kawakami, A., Van Heyningen, V., Jessell, T. M., & Briscoe, J. (1997). Pax6 controls progenitor cell identity and neuronal fate in response to graded Shh signaling. *Cell*, *90*(1), 169–180. https://doi.org/10.1016/S0092-8674(00)80323-2

Ericson, Johan, Thor, S., Edlund, T., Jessell, T. M., & Yamada, T. (1992). Early Stages of Motor Neuron Differentiation Revealed by Expression of Homeobox Gene. *Science*, *256*(5063), 1555–1560.

F. Bear, Mark; W. Connors, Barry; A. Paradiso, M. (2007). *Neuroscience: Exploring the brain* (3rd editio). Lippincott Williams & Wilkins.

Fan, B., Wei, Z., Yao, X., Shi, G., Cheng, X., Zhou, X., Zhou, H., Ning, G., Kong, X., & Feng, S. (2018). Microenvironment Imbalance of Spinal Cord Injury. *Cell Transplantation*, *27*(6), 853–866. https://doi.org/10.1177/0963689718755778

Faulkner, J. R., Herrmann, J. E., Woo, M. J., Tansey, K. E., Doan, N. B., & Sofroniew, M. V. (2004). Reactive Astrocytes Protect Tissue and Preserve Function after Spinal Cord Injury. *Journal of Neuroscience*, *24*(9), 2143–2155. https://doi.org/10.1523/JNEUROSCI.3547-03.2004

Fawcett, J. W., & Asher, R. A. (1999). The glial scar and central nervous system repair. *Brain Research Bulletin*, *49*(6), 377–391. https://doi.org/10.1016/S0361-9230(99)00072-6

FDA. (2020). *Food and Drug Administration*. https://www.fda.gov/

Fehlings, M. G., Tetreault, L. A., Wilson, J. R., Kwon, B. K., Burns, A. S., Martin, A. R., Hawryluk, G., & Harrop, J. S. (2017). A Clinical Practice Guideline for the Management of Acute Spinal Cord Injury: Introduction, Rationale, and Scope. *Global Spine Journal*, *7*(3_supplement), 84S-94S. https://doi.org/10.1177/2192568217703387

Fernandes, A. R., Adams, C. F., Furness, D. N., & Chari, D. M. (2015). Early Membrane Responses to Magnetic Particles are Predictors of Particle Uptake in Neural Stem Cells. *Particle and Particle Systems Characterization*, *32*(6), 661–667. https://doi.org/10.1002/ppsc.201400231

Féron, F., Perry, C., Cochrane, J., Licina, P., Nowitzke, A., Urquhart, S., Geraghty, T., & Mackay-Sim, A. (2005). Autologous olfactory ensheathing cell transplantation in human spinal cord injury. *Brain*, *128*(12), 2951–2960.

https://doi.org/10.1093/brain/awh657

Ferretti, P., & Whalley, K. (2008). Molecular and cellular basis of regeneration and tissue repair: Successful neural regeneration in amniotes: The developing chick spinal cord. *Cellular and Molecular Life Sciences*, *65*(1), 45–53. https://doi.org/10.1007/s00018-007-7430-2

Finch, L., Harris, S., Solomou, G., Sen, J., Tzerakis, N., Emes, R. D., Lane, C. S., Hart, S. R., Adams, C. F., & Chari, D. M. (2020). Safe nanoengineering and incorporation of transplant populations in a neurosurgical grade biomaterial, DuraGen PlusTM, for protected cell therapy applications. *Journal of Controlled Release*, *321*, 553–563. https://doi.org/10.1016/j.jconrel.2020.02.028

Flanagan, L. A., Rebaza, L. M., Derzic, S., Schwartz, P. H., & Monuki, E. S. (2006). Regulation of human neural precursor cells by laminin and integrins. *Journal of Neuroscience Research*, *83*(5), 845–856. https://doi.org/10.1002/jnr.20778

Forgione, N., Chamankhah, M., & Fehlings, M. G. (2017). A Mouse Model of Bilateral Cervical Contusion-Compression Spinal Cord Injury. *Journal of Neurotrauma*, *34*(6), 1227–1239. https://doi.org/10.1089/neu.2016.4708

Frisén, J., Johansson, C. B., Török, C., Risling, M., & Lendahl, U. (1995). Rapid, widespread, and longlasting induction of nestin contributes to the generation of glial scar tissue after CNS injury. *Journal of Cell Biology*, *131*(2), 453–464. https://doi.org/10.1083/jcb.131.2.453

Führmann, T., Obermeyer, J., Tator, C. H., & Shoichet, M. S. (2015). Click-crosslinked injectable hyaluronic acid hydrogel is safe and biocompatible in the intrathecal space for ultimate use in regenerative strategies of the injured spinal cord. *Methods*, *84*, 60–69. https://doi.org/10.1016/j.ymeth.2015.03.023

Galli, R., Sitoci-Ficici, K. H., Uckermann, O., Later, R., Marečková, M., Koch, M., Leipnitz, E., Schackert, G., Koch, E., Gelinsky, M., Steiner, G., & Kirsch, M. (2018). Label-free multiphoton microscopy reveals relevant tissue changes induced by alginate hydrogel implantation in rat spinal cord injury. *Scientific Reports*, *8*(1), 1–13. https://doi.org/10.1038/s41598-018-29140-z

Geisler, F. H., Dorsey, F. C., & Coleman, W. P. (1991). Recovery of motor functrion after spinal cord injury - a randomized, placebo-controlled trial with GM-1 ganglioside. *The New England Journal of Medicine*, *325*(26), 1829–1838. https://doi.org/10.1056/NEJM199112053252301

George, E. B., Glass, J. D., & Griffin, J. W. (1995). Axotomy-induced axonal degeneration is mediated by calcium influx through ion-specific channels. *The Journal of Neuroscience : The Official Journal of the Society for Neuroscience*, *15*(October), 6445–6452. https://doi.org/10.1523/JNEUROSCI.5397-08.2009

Gray, M., Palispis, W., Popovich, P., Van Rooijen, N., & Gupta, R. (2007). Macrophage depletion alters the blood nerve barrier without affectin schwann cell function after neural injury. *Journal of Neuroscience Research*, *85*(11), 766–777. https://doi.org/10.1002/jnr

Grégoire, C. A., Goldenstein, B. L., Floriddia, E. M., Barnabé-Heider, F., & Fernandes, K. J. L. (2015). Endogenous neural stem cell responses to stroke and spinal cord injury. *Glia*, *63*(8), 1469–1482. https://doi.org/10.1002/glia.22851

Gregorio, I., Braghetta, P., Bonaldo, P., & Cescon, M. (2018). Collagen VI in healthy and diseased nervous system. *DMM Disease Models and Mechanisms*, *11*(6). https://doi.org/10.1242/dmm.032946

Guijarro-Belmar, A., Viskontas, M., Wei, Y., Bo, X., Shewan, D., & Huang, W. (2019). Epac2

Elevation Reverses Inhibition by Chondroitin Sulfate Proteoglycans In Vitro and Transforms Postlesion Inhibitory Environment to Promote Axonal Outgrowth in an Ex Vivo Model of Spinal Cord Injury. *The Journal of Neuroscience : The Official Journal of the Society for Neuroscience*, *39*(42), 8330–8346. https://doi.org/10.1523/JNEUROSCI.0374-19.2019

Hamburger, V., & Hamilton, H. (1951). A series of normal stages in the development of the chick embryo. *Journal of Morphology*, *88*(1), 49–92. https://doi.org/10.1002/aja.1001950404

Hara, M., Kobayakawa, K., Ohkawa, Y., Kumamaru, H., Yokota, K., Saito, T., Kijima, K., Yoshizaki, S., Harimaya, K., Nakashima, Y., & Okada, S. (2017). Interaction of reactive astrocytes with type i collagen induces astrocytic scar formation through the integrin-N-cadherin pathway after spinal cord injury. *Nature Medicine*, *23*(7), 818–828. https://doi.org/10.1038/nm.4354

Hasan, S. J., Keirstead, H. S., Muir, G. D., & Steeves, J. D. (1993). Axonal regeneration contributes to repair of injured brainstem-spinal neurons in embryonic chick. *The Journal of Neuroscience : The Official Journal of the Society for Neuroscience*, *13*(2), 492–507. http://www.ncbi.nlm.nih.gov/pubmed/8426225

Hawryluk, G. W. J., Mothe, A., Wang, J., Wang, S., Tator, C., & Fehlings, M. G. (2012). An in vivo characterization of trophic factor production following neural precursor cell or bone marrow stromal cell transplantation for spinal cord injury. *Stem Cells and Development*, *21*(12), 2222–2238. https://doi.org/10.1089/scd.2011.0596

He, J., Zhang, N., Zhu, Y., Jin, R., & Wu, F. (2021). MSC spheroids-loaded collagen hydrogels simultaneously promote neuronal differentiation and suppress inflammatory reaction through PI3K-Akt signaling pathway. *Biomaterials*, *265*(August 2020), 120448. https://doi.org/10.1016/j.biomaterials.2020.120448

He, L., Liao, S., Quan, D., Ma, K., Chan, C., Ramakrishna, S., & Lu, J. (2010). Synergistic effects of electrospun PLLA fiber dimension and pattern on neonatal mouse cerebellum C17.2 stem cells. *Acta Biomaterialia*, *6*(8), 2960–2969. https://doi.org/10.1016/j.actbio.2010.02.039

Hemmati-Brivanlou, A., & Melton, D. A. (1994). Inhibition of activin receptor signaling promotes neuralization in Xenopus. *Cell*, *77*(2), 273–281. https://doi.org/10.1016/0092-8674(94)90319-0

Hidalgo San Jose, L., Stephens, P., Song, B., & Barrow, D. (2018). Microfluidic Encapsulation Supports Stem Cell Viability, Proliferation, and Neuronal Differentiation. *Tissue Engineering - Part C: Methods*, *24*(3), 158–170. https://doi.org/10.1089/ten.tec.2017.0368

Himes, B. T., Neuhuber, B., Coleman, C., Kushner, R., Swanger, S. A., Kopen, G. C., Wagner, J., Shumsky, J. S., & Fischer, I. (2006). Recovery of function following grafting of human bone marrow-derived stromal cells into the injured spinal cord. *Neurorehabilitation and Neural Repair*, *20*(2), 278–296. https://doi.org/10.1177/1545968306286976

Hofstetter, C. P., Schwarz, E. J., Hess, D., Widenfalk, J., El Manira, A., Prockop, D. J., & Olson, L. (2002). Marrow stromal cells form guiding strands in the injured spinal cord and promote recovery. *Proceedings of the National Academy of Sciences of the United States of America*, *99*(4), 2199–2204. https://doi.org/10.1073/pnas.042678299

Honmou, O., Felts, P. A., Waxman, S. G., & Kocsis, J. D. (1996). Restoration of normal conduction properties in demyelinated spinal cord axons in the adult rat by transplantation of exogenous Schwann cells. *Journal of Neuroscience*, *16*(10), 3199–3208. https://doi.org/10.1523/jneurosci.16-10-03199.1996

Humpel, C. (2015). Neuroscience forefront review organotypic brain slice cultures: A review. *Neuroscience*, *305*, 86–98. https://doi.org/10.1016/j.neuroscience.2015.07.086

Hung, J., & Colicos, M. A. (2008). Astrocytic Ca2+ waves guide CNS growth cones to remote regions of neuronal activity. *PLoS ONE*, *3*(11). https://doi.org/10.1371/journal.pone.0003692

Hurtado, A., Cregg, J. M., Wang, H. B., Wendell, D. F., Oudega, M., Gilbert, R. J., & McDonald, J. W. (2011). Robust CNS regeneration after complete spinal cord transection using aligned poly-l-lactic acid microfibers. *Biomaterials*, *32*(26), 6068–6079. https://doi.org/10.1016/j.biomaterials.2011.05.006

Hyysalo, A., Ristola, M., Joki, T., Honkanen, M., Vippola, M., & Narkilahti, S. (2017). Aligned Poly(ε-caprolactone) Nanofibers Guide the Orientation and Migration of Human Pluripotent Stem Cell-Derived Neurons, Astrocytes, and Oligodendrocyte Precursor Cells In Vitro. *Macromolecular Bioscience*, *17*(7), 1–8. https://doi.org/10.1002/mabi.201600517

Imanaka, T., Hukuda, S., & Maeda, T. (1996). The role of GM1-ganglioside in the injured spinal cord of rats: an immunohistochemical study using GM1-antisera. *J.Neurotrauma*, *13*(0897-7151 SB-M), 163–170.

Integra-Life. (2020). *Integra Life*. integralife.eu

Iwanami, A., Kaneko, S., Nakamura, M., Kanemura, Y., Mori, H., Kobayashi, S., Yamasaki, M., Momoshima, S., Ishii, H., Ando, K., Tanioka, Y., Tamaoki, N., Nomura, T., Toyama, Y., & Okano, H. (2005). Transplantation of human neural stem cells for spinal cord injury in primates. *Journal of Neuroscience Research*, *80*(2), 182–190. https://doi.org/10.1002/jnr.20436

Jakobsson, A., Ottosson, M., Zalis, M. C., Carroll, D. O., Johansson, U. E., & Johansson, F. (2017). Three-dimensional functional human neuronal networks in uncompressed low-density electrospun fiber scaffolds. *Nanomedicine: Nanotechnology, Biology, and Medicine*, *13*(4), 1563–1573. https://doi.org/10.1016/j.nano.2016.12.023

Jeong, D. K., Taghavi, C. E., Song, K. J., Lee, K. B., & Kang, H. W. (2011). Organotypic human spinal cord slice culture as an alternative to direct transplantation of human bone marrow precursor cells for treating spinal cord injury. *World Neurosurgery*, *75*(3–4), 533–539. https://doi.org/10.1016/j.wneu.2010.10.042

Jessell, T. M. (2000). Neuronal specification in the spinal cord: inductive signals and transcriptional codes. *Nature Reviews Genetics*, *1*(1), 20–29. https://doi.org/10.1038/35049541

Johnson, P. J., Tatara, A., Shiu, A., & Sakiyama-elbert, S. E. (2011). *Controlled release of neurotrophin-3 and plateled derived growth factor from fibrin scaffolds containing neural progenitor cells enchances survuval and differentiation into neurons in a subacute model of SCI*. *19*(1), 89–101. https://doi.org/10.3727/096368909X477273.Controlled

Joosten, E. A. J., Veldhuis, W. B., & Hamers, F. P. T. (2004). Collagen containing neonatal astrocytes stimulates regrowth of injured fibers and promotes modest locomotor recovery after spinal cord injury. *Journal of Neuroscience Research*, *77*(1), 127–142. https://doi.org/10.1002/jnr.20088

Kakulas, B. A. (1999). Review Article The applied neuropathology of human spinal cord injury. *Spinal Cord*, *37*, 79–88.

Karimi-Abdolrezaee, S., Eftekharpour, E., Wang, J., Morshead, C. M., & Fehlings, M. G. (2006). Delayed transplantation of adult neural precursor cells promotes

remyelination and functional neurological recovery after spinal cord injury. *Journal of Neuroscience*, *26*(13), 3377–3389. https://doi.org/10.1523/JNEUROSCI.4184-05.2006

Kassam, A., Horowitz, M., Carrau, R., Snyderman, C., Welch, W., Hirsch, B., Chang, Y. F., Bruce, J. N., Rice, D. H., Hodge, C. J., Sekhar, L. N., & Stimac, D. (2003). Use of tisseel fibrin sealant in neurosurgical procedures: Incidence of cerebrospinal fluid leaks and cost-benefit analysis in a retrospective study. *Neurosurgery*, *52*(5), 1102–1105. https://doi.org/10.1227/01.neu.0000057699.37541.76

Kassam, A., Nemoto, E., Balzer, J., Rao, G., Welch, W. C., Kuwabara, H., Boada, F., & Horowitz, M. (2004). Effects of Tisseel fibrin glue on the central nervous system of nonhuman primates. *Ear, Nose and Throat Journal*, *83*(4), 246–256. https://doi.org/10.1177/014556130408300413

Katiyar, K. S., Winter, C. C., Gordián-Vélez, W. J., O'donnell, J. C., Song, Y. J., Hernandez, N. S., Struzyna, L. A., & Cullen, D. K. (2018). Three-dimensional tissue engineered aligned astrocyte networks to recapitulate developmental mechanisms and facilitate nervous system regeneration. *Journal of Visualized Experiments*, *2018*(131), 1–17. https://doi.org/10.3791/55848

Kawasaki, S., Origasa, H., Tetens, V., & Kobayashi, M. (2017). Comparison of TachoSil and TachoComb in patients undergoing liver resection—a randomized, double-blind, non-inferiority trial. *Langenbeck's Archives of Surgery*, *402*(4), 591–598. https://doi.org/10.1007/s00423-017-1571-z

Kigerl, K. A., Gensel, J. C., Ankeny, D. P., Alexander, J. K., Donnelly, D. J., & Popovich, P. G. (2009). Identification of two distinct macrophage subsets with divergent effects causing either neurotoxicity or regeneration in the injured mouse spinal cord. *Journal of Neuroscience*, *29*(43), 13435–13444. https://doi.org/10.1523/JNEUROSCI.3257-

09.2009

Kirshblum, S. C., Waring, W., Biering-Sorensen, F., Burns, S. P., Johansen, M., Schmidt-Read, M., Donovan, W., Graves, D., Jha, A., Jones, L., Mulcahey, M. J., & Krassioukov, A. (2011). International standards for neurological classification of spinal cord injury (Revised 2011). *Journal of Spinal Cord Medicine*, *34*(6), 547–554. https://doi.org/10.1179/107902611X13186000420242

Koh, H. ., Yong, T., Chan, C. K., & Ramakrishna, S. (2008). Enhancement of neurite outgrowth using nano-structured scaffolds coupled with laminin. *Biomaterials*, *29*, 3574–3589. https://doi.org/doi:10.1016/j.biomaterials.2008.05.014

Kourgiantaki, A., Tzeranis, D. S., Karali, K., Georgelou, K., Bampoula, E., Psilodimitrakopoulos, S., Yannas, I. V., Stratakis, E., Sidiropoulou, K., Charalampopoulos, I., & Gravanis, A. (2020). Neural stem cell delivery via porous collagen scaffolds promotes neuronal differentiation and locomotion recovery in spinal cord injury. *Npj Regenerative Medicine*, *5*(1), 1–14. https://doi.org/10.1038/s41536-020-0097-0

Krämer-Albers, E. M., Bretz, N., Tenzer, S., Winterstein, C., Möbius, W., Berger, H., Nave, K. A., Schild, H., & Trotter, J. (2007). Oligodendrocytes secrete exosomes containing major myelin and stress-protective proteins: Trophic support for axons? *Proteomics - Clinical Applications*, *1*(11), 1446–1461. https://doi.org/10.1002/prca.200700522

Krassioukov, A. V., Ackery, A., Schwartz, G., Adamchik, Y., Liu, Y., & Fehlings, M. G. (2002). An in vitro model of neurotrauma in organotypic spinal cord cultures from adult mice. *Brain Research Protocols*, *10*(2), 60–68. https://doi.org/10.1016/S1385-299X(02)00180-0

Le Douarin, N. M. (2004). Neural crest cell plasticity and its limits. *Development*, *131*(19),

4637–4650. https://doi.org/10.1242/dev.01350

Lee, C. H., Singla, A., & Lee, Y. (2001). Biomedical applications of collagen. *International Journal of Pharmaceutics*, *221*, 1–22. https://doi.org/https://doi.org/10.1016/S0378-5173(01)00691-3

Lee, K. J., & Jessell, T. M. (1999). the Specification of Dorsal Cell Fates in the Vertebrate Central Nervous System. *Annual Review of Neuroscience*, *22*(1), 261–294. https://doi.org/10.1146/annurev.neuro.22.1.261

Leonardi, M., Barbara, C., Simonetti, L., Giardino, R., Nicoli Aldini, N., Fini, M., Martini, L., Masetti, L., Joechler, M., & Roncaroli, F. (2002). Glubran 2: A new acrylic glue for neuroradiological endovascular use: Experimental study on animals. *Interventional Neuroradiology*, *8*(3), 245–250. https://doi.org/10.1177/159101990200800304

Levine, J. M. (1994). Increased expression of the NG2 chondroitin-sulfate proteoglycan after brain injury. *The Journal of Neuroscience : The Official Journal of the Society for Neuroscience*, *14*(8), 4716–4730.

Li, Xiang, Peng, Z., Long, L., Tuo, Y., Wang, L., Zhao, X., Le, W., & Wan, Y. (2020). Wnt4-modified NSC transplantation promotes functional recovery after spinal cord injury. *FASEB Journal*, *34*(1), 82–94. https://doi.org/10.1096/fj.201901478RR

Li, Xiaoran, Fan, C., Xiao, Z., Zhao, Y., Zhang, H., Sun, J., Zhuang, Y., Wu, X., Shi, J., Chen, Y., & Dai, J. (2018). A collagen microchannel scaffold carrying paclitaxel-liposomes induces neuronal differentiation of neural stem cells through Wnt/β-catenin signaling for spinal cord injury repair. *Biomaterials*, *183*, 114–127. https://doi.org/10.1016/j.biomaterials.2018.08.037

Li, Xiaoran, Li, M., Sun, J., Zhuang, Y., Shi, J., Guan, D., Chen, Y., & Dai, J. (2016). Radially Aligned Electrospun Fibers with Continuous Gradient of SDF1α for the Guidance of

Neural Stem Cells. *Small*, *12*(36), 5009–5018. https://doi.org/10.1002/smll.201601285

Li, Xiaoran, Xiao, Z., Han, J., Chen, L., Xiao, H., Ma, F., Hou, X., Li, X., Sun, J., Ding, W., Zhao, Y., Chen, B., & Dai, J. (2013). Promotion of neuronal differentiation of neural progenitor cells by using EGFR antibody functionalized collagen scaffolds for spinal cord injury repair. *Biomaterials*, *34*(21), 5107–5116. https://doi.org/10.1016/j.biomaterials.2013.03.062

Li, Y., Field, P. M., & Raisman, G. (1997). Repair of adult rat corticospinal tract by transplants of olfactory ensheathing cells. *Science*, *277*(5334), 2000–2002. https://doi.org/10.1126/science.277.5334.2000

Liu, T., Houle, J. D., Xu, J., Chan, B. P., & Chew, S. Y. (2012). Nanofibrous collagen nerve conduits for spinal cord repair. *Tissue Engineering - Part A*, *18*(9–10), 1057–1066. https://doi.org/10.1089/ten.tea.2011.0430

Lu, D. C., Niu, T., & Alaynick, W. A. (2015). Molecular and cellular development of spinal cord locomotor circuitry. *Frontiers in Molecular Neuroscience*, *8*(June), 1–18. https://doi.org/10.3389/fnmol.2015.00025

Luo, D., Ruan, S., Liu, A., Kong, X., Lee, I. S., & Chen, C. (2018). Laminin functionalized biomimetic apatite to regulate the adhesion and proliferation behaviors of neural stem cells. *International Journal of Nanomedicine*, *13*, 6223–6233. https://doi.org/10.2147/IJN.S176596

Ma, W., Chen, S., Fitzgerald, W., Maric, D., Lin, H. J., O'Shaughnessy, T. J., Kelly, J., Liu, X.-H. H., & Barker, J. L. (2005). Three-dimensional collagen gel networks for neural stem cell-based neural tissue engineering. *Macromolecular Symposia*, *227*(1), 327–333. https://doi.org/DOI 10.1002/masy.200550933

MacArthur Clark, J. (2018). The 3Rs in research: A contemporary approach to replacement, reduction and refinement. *British Journal of Nutrition*, *120*(s1), S1–S7. https://doi.org/10.1017/S0007114517002227

Macaya, D; Spector, M. (2012). Injectable hydrogel materials for spinal cord regeneration : A review. *Biomedical Materials*, *7*(May), 22pp. https://doi.org/10.1088/1748-6041/7/1/012001

Maitz, M. F. (2015). Applications of synthetic polymers in clinical medicine. *Biosurface and Biotribology*, *1*(3), 161–176. https://doi.org/10.1016/j.bsbt.2015.08.002

Masahira, N., Takebayashi, H., Ono, K., Watanabe, K., Ding, L., Furusho, M., Ogawa, Y., Nabeshima, Y. ichi, Alvarez-Buylla, A., Shimizu, K., & Ikenaka, K. (2006). Olig2-positive progenitors in the embryonic spinal cord give rise not only to motoneurons and oligodendrocytes, but also to a subset of astrocytes and ependymal cells. *Developmental Biology*, *293*(2), 358–369. https://doi.org/10.1016/j.ydbio.2006.02.029

Mcdaid, D., & Park, A. (2019). Understanding and modelling the economic impact of spinal cord injuries in the United Kingdom. *Spinal Cord*. https://doi.org/10.1038/s41393-019-0285-1

McKeon, R. J., Jurynec, M. J., & Buck, C. R. (1999). The Chondroitin Sulfate Proteoglycans Neurocan and Phosphacan Are Expressed by Reactive Astrocytes in the Chronic CNS Glial Scar. *Journal of Neuroscience* , *19*(24), 10778–10788.

Middleton, J. C., & Tipton, A. J. (2000). Synthetic biodegradable polymers as orthopedic devices. *Biomaterials*, *21*(23), 2335–2346. https://doi.org/10.1016/S0142-9612(00)00101-0

Miner, J. H., & Yurchenco, P. D. (2004). Laminin functions in tissue morphogenesis. *Annual*

Review of Cell and Developmental Biology, *20*(M), 255–284. https://doi.org/10.1146/annurev.cellbio.20.010403.094555

Mishra, S. (2017). FDA, CE mark or something else?—Thinking fast and slow. *Indian Heart Journal*, *69*(1), 1–5. https://doi.org/10.1016/j.ihj.2016.11.327

Mitrousis, N., Fokina, A., & Shoichet, M. S. (2018). Biomaterials for cell transplantation. *Nature Reviews Materials*, *3*(11), 441–456. https://doi.org/10.1038/s41578-018-0057-0

Mogas Barcons, A., Chari, D. M., & Adams, C. (2021). Enhancing the regenerative potential of stem cell-laden, clinical-grade implants through laminin engineering. *Materials Science and Engineering: C*, *123*(February), 111931. https://doi.org/10.1016/j.msec.2021.111931

Morteza Bahram, N. M. and M. M. (2012). An introduction to hydrogels and some recent applications. *Intech*, *6*, 111–133. https://doi.org/10.5772/711

Mothe, A. J., Kulbatski, I., Parr, A., Mohareb, M., & Tator, C. H. (2008). Adult spinal cord stem/progenitor cells transplanted as neurospheres preferentially differentiate into oligodendrocytes in the adult rat spinal cord. *Cell Transplantation*, *17*(7), 735–751. https://doi.org/10.3727/096368908786516756

Mothe, A. J., & Tator, C. H. (2012). Advances in stem cell therapy for spinal cord injury. *Thew Journal of Clinical Investigation*, *122*(11), 3824–3834. https://doi.org/10.1172/JCI64124.3824

Muhr, J., Graziano, E., Wilson, S., Jessell, T. M., & Edlund, T. (1999). Convergent inductive signals specify midbrain, hindbrain, and spinal cord identity in Gastrula stage chick embryos. *Neuron*, *23*(4), 689–702. https://doi.org/10.1016/S0896-6273(01)80028-3

Nakajima, H., Uchida, K., Guerrero, A. R., Watanabe, S., Sugita, D., Takeura, N., Yoshida, A., Long, G., Wright, K. T., Johnson, W. E. B., & Baba, H. (2012). Transplantation of mesenchymal stem cells promotes an alternative pathway of macrophage activation and functional recovery after spinal cord injury. *Journal of Neurotrauma*, *29*(8), 1614–1625. https://doi.org/10.1089/neu.2011.2109

Nakhjavan-Shahraki, B., Yousefifard, M., Rahimi-Movaghar, V., Baikpour, M., Nasirinezhad, F., Safari, S., Yaseri, M., Moghadas Jafari, A., Ghelichkhani, P., Tafakhori, A., & Hosseini, M. (2018). Transplantation of olfactory ensheathing cells on functional recovery and neuropathic pain after spinal cord injury; Systematic review and meta-analysis. *Scientific Reports*, *8*(1), 1–12. https://doi.org/10.1038/s41598-017-18754-4

National Spinal Cord Injury Statistical Center. (2019). Spinal Cord Injury Facts and Figures at a Glance. *The Journal of Spinal Cord Medicine*. www.msktc.org/sci/model-system-centers.

NC3Rs. (2021). *National Centre for the Replacement, Reduction and Refinement of Animals in Research*. https://nc3rs.org.uk/

Nemati, S., Jabbari, R., Hajinasrollah, M., Zare Mehrjerdi, N., Azizi, H., Hemmesi, K., Azhdari, Z., Talebi, A., Mohitmafi, S., Vosough Dizaj, A., Sharifi, G., Baharvand, H., Kiani, S., & Rezaee, O. (2013). Transplantation of Adult Monkey Neural Stem Cells into A Contusion Spinal Cord Injury Model in Rhesus Macaque Monkeys. *Cell Journal*, *16*(2), 117–130. http://www.ncbi.nlm.nih.gov/pubmed/24567941

Nguyen, L. H., Gao, M., Lin, J., Wu, W., Wang, J., & Chew, S. Y. (2017). Three-dimensional aligned nanofibers-hydrogel scaffold for controlled non-viral drug/gene delivery to direct axon regeneration in spinal cord injury treatment. *Scientific Reports*, *7*(October 2016), 1–12. https://doi.org/10.1038/srep42212

Nirwane, A., & Yao, Y. (2019). Laminins and their receptors in the CNS. *Biological Reviews*, *94*(1), 283–306. https://doi.org/10.1111/brv.12454

Nissen, L., Hunter, J., Schrøder, H., Rütz, K., & Bollen, P. (2017). Adhesions, infl ammatory response and foreign body giant cells infi ltration of the topical hemostats TachoSil®, Hemopatch™ and Veriset™ – An Animal Study. *Journal of Surgery and Surgical Research*, *3*(2), 038–041. https://doi.org/10.17352/2455-2968.000043

Nori, S., Okada, Y., Yasuda, A., Tsuji, O., Takahashi, Y., Kobayashi, Y., Fujiyoshi, K., Koike, M., Uchiyama, Y., Ikeda, E., Toyama, Y., Yamanaka, S., Nakamura, M., & Okano, H. (2011). Grafted human-induced pluripotent stem-cell-derived neurospheres promote motor functional recovery after spinal cord injury in mice. *Proceedings of the National Academy of Sciences of the United States of America*, *108*(40), 16825–16830. https://doi.org/10.1073/pnas.1108077108

Nowak, S., Schroeder, H. W. S., & Fleck, S. (2019). Hemopatch® as a new dural sealant: A clinical observation. *Clinical Neurology and Neurosurgery*, *176*(November 2018), 133–137. https://doi.org/10.1016/j.clineuro.2018.12.009

O'Donovan, M. J., Bonnot, A., Wenner, P., & Mentis, G. Z. (2005). Calcium imaging of network function in the developing spinal cord. *Cell Calcium*, *37*(5 SPEC. ISS.), 443–450. https://doi.org/10.1016/j.ceca.2005.01.012

Ogawa, Y., Sawamoto, K., Miyata, T., Miyao, S., Watanabe, M., Nakamura, M., Bregman, B. S., Koike, M., Uchiyama, Y., Toyama, Y., & Okano, H. (2002). Transplantation of in vitro-expanded fetal neural progenitor cells results in neurogenesis and functional recovery after spinal cord contusion injury in adult rats. *Journal of Neuroscience Research*, *69*(6), 925–933. https://doi.org/10.1002/jnr.10341

Okado, N., & Oppenheim, R. W. (1985). The onset and development of descending

pathways to the spinal cord in the chick embryo. *Journal of Comparative Neurology*, *232*(2), 143–161. https://doi.org/10.1002/cne.902320202

Ono, K., Bansal, R., Payne, J., Rutishauser, U., & Miller, R. H. (1995). Early development and dispersal of oligodendrocyte precursors in the embryonic chick spinal cord. *Development (Cambridge, England)*, *121*(6), 1743–1754.

Pakulska, M. M., Ballios, B. G., & Shoichet, M. S. (2012). Injectable hydrogels for central nervous system therapy. *Biomedical Materials*, *7*(2), 024101. https://doi.org/10.1088/1748-6041/7/2/024101

Pandamooz, S., Salehi, M. S., Zibaii, M. I., Ahmadiani, A., Nabiuni, M., & Dargahi, L. (2018). Epidermal neural crest stem cell-derived glia enhance neurotrophic elements in an ex vivo model of spinal cord injury. *Journal of Cellular Biochemistry*, *119*(4), 3486–3496. https://doi.org/10.1002/jcb.26520

Parr, A. M., Kulbatski, I., & Tator, C. H. (2007). Transplantation of adult rat spinal cord stem/progenitor cells for spinal cord injury. *Journal of Neurotrauma*, *24*(5), 835–845. https://doi.org/10.1089/neu.2006.3771

Patar, A., Dockery, P., Howard, L., & McMahon, S. (2019a). Analysis of reactive astrocytes and NG2 proteoglycan in ex vivo rat models of spinal cord injury. *Journal of Neuroscience Methods*, *311*, 418–425. https://doi.org/10.1016/j.jneumeth.2018.09.027

Patar, A., Dockery, P., Howard, L., & McMahon, S. S. (2019b). Cell viability in three ex vivo rat models of spinal cord injury. *Journal of Anatomy*, *234*(2), 244–251. https://doi.org/10.1111/joa.12909

Patel, V., Joseph, G., Patel, A., Patel, S., Bustin, D., Mawson, D., Tuesta, L. M., Puentes, R., Ghosh, M., & Pearse, D. D. (2010). Suspension matrices for improved Schwann-cell

survival after implantation into the injured rat spinal cord. *Journal of Neurotrauma*, *27*(5), 789–801. https://doi.org/10.1089/neu.2008.0809

Patten, I., & Placzek, M. (2000). The role of Sonic hedgehog in neural tube patterning. *Cellular and Molecular Life Sciences : CMLS*, *57*, 1695–1708. https://doi.org/10.1007/PL00000652

Plenz, D., Stewart, C. V., Shew, W., Yang, H., Klaus, A., & Bellay, T. (2011). Multi-electrode array recordings of neuronal avalanches in organotypic cultures. *Journal of Visualized Experiments*, *54*, 1–7. https://doi.org/10.3791/2949

Pringle, N. P. (2003). Fgfr3 expression by astrocytes and their precursors: evidence that astrocytes and oligodendrocytes originate in distinct neuroepithelial domains. *Development*, *130*(1), 93–102. https://doi.org/10.1242/dev.00184

Pringle, Nigel P., Yu, W. P., Guthrie, S., Roelink, H., Lumsden, A., Peterson, A. C., & Richardson, W. D. (1996). Determination of neuroepithelial cell fate: Induction of the oligodendrocyte lineage by ventral midline cells and Sonic hedgehog. *Developmental Biology*, *177*(1), 30–42. https://doi.org/10.1006/dbio.1996.0142

Prior, J. J., Wallace, D. G., Harner, A., Prior, D. J. J., Wallace, D. G., & Noe, M. (1999). A sprayable hemostat containing fibrillar collagen, bovine thrombin and aoutologous plasma. *The Society of Thoracic Surgeons*, *4975*(99).

Quertainmont, R., Cantinieaux, D., Botman, O., Sid, S., Schoenen, J., & Franzen, R. (2012). Mesenchymal stem cell graft improves recovery after spinal cord injury in adult rats through neurotrophic and pro-angiogenic actions. *PLoS ONE*, *7*(6). https://doi.org/10.1371/journal.pone.0039500

Ramón-Cueto, A., Cordero, M. I., Santos-Benito, F. F., & Avila, J. (2000). Functional recovery of paraplegic rats and motor axon regeneration in their spinal cords by olfactory

ensheathing glia. *Neuron*, *25*(2), 425–435. https://doi.org/10.1016/S0896-6273(00)80905-8

Rashidi, H., & Sottile, V. (2009). The chick embryo: Hatching a model for contemporary biomedical research. *BioEssays*, *31*(4), 459–465. https://doi.org/10.1002/bies.200800168

Roberts, T. T., Leonard, G. R., & Cepela, D. J. (2017). Classifications In Brief: American Spinal Injury Association (ASIA) Impairment Scale. *Clinical Orthopaedics and Related Research*, *475*(5), 1499–1504. https://doi.org/10.1007/s11999-016-5133-4

Robins, S. L., & Fehlings, M. G. (2008). Models of experimental spinal cord injury: Translational relevance and impact. *Drug Discovery Today: Disease Models*, *5*(1), 5–11. https://doi.org/10.1016/j.ddmod.2008.07.001

Robinson, S., Tani, M., Strieter, R. M., Ransohoff, R. M., & Miller, R. H. (1998). The chemokine growth-regulated oncogene-alpha promotes spinal cord oligodendrocyte precursor proliferation. *The Journal of Neuroscience*, *18*(24), 10457–10463. http://www.ncbi.nlm.nih.gov/pubmed/9852583

Rösner, H., & Vacun, G. (1997). Organotypic spinal cord culture in serum-free fibrin gel: A new approach to study three-dimensional neurite outgrowth and of neurotoxicity testing: Effects of modulating the actin and tubulin dynamics and protein kinase activities. *Journal of Neuroscience Methods*, *78*(1–2), 93–103. https://doi.org/10.1016/S0165-0270(97)00132-5

Ruzicka, J., Romanyuk, N., Jirakova, K., Hejcl, A., Janouskova, O., Machova, L. U., Bochin, M., Pradny, M., Vargova, L., & Jendelova, P. (2019). The Effect of iPS-Derived Neural Progenitors Seeded on Laminin-Coated pHEMA-MOETACl Hydrogel with Dual Porosity in a Rat Model of Chronic Spinal Cord Injury. *Cell Transplantation*, *28*(4),

400–412. https://doi.org/10.1177/0963689718823705

Sadler, T. W. (2005). Embryology of neural tube development. *American Journal of Medical Genetics - Seminars in Medical Genetics*, *135 C*(1), 2–8. https://doi.org/10.1002/ajmg.c.30049

Sanz-Herrera, J. A., & Reina-Romo, E. (2011). Cell-biomaterial mechanical interaction in the framework of tissue engineering: Insights, computational modeling and perspectives. *International Journal of Molecular Sciences*, *12*(11), 8217–8244. https://doi.org/10.3390/ijms12118217

Sasaki, T., Ishikawa, T., Abe, R., Nakayama, R., Asada, A., Matsuki, N., & Ikegaya, Y. (2014). Astrocyte calcium signalling orchestrates neuronal synchronization in organotypic hippocampal slices. *Journal of Physiology*, *592*(13), 2771–2783. https://doi.org/10.1113/jphysiol.2014.272864

Schoenwolf, G. C., & Smith, J. L. (1990). Mechanisms of neurulation: traditional viewpoint and recent advances. *Development (Cambridge, England)*, *109*(2), 243–270. http://www.ncbi.nlm.nih.gov/pubmed/2205465

Seabrook, T. J., Jiang, L., Maier, M., & Lemere, C. A. (2006). Minocycline affects microglia actibation, A beta deposition, and behaviour in APP-tg mice. *Glia*, *53*, 776–782. https://doi.org/10.1002/glia

Selden, N. R., Al-Uzri, A., Huhn, S. L., Koch, T. K., Sikora, D. M., Nguyen-Driver, M. D., Guillaume, D. J., Koh, J. L., Gultekin, S. H., Anderson, J. C., Vogel, H., Sutcliffe, T. L., Jacobs, Y., & Steiner, R. D. (2013). Central nervous system stem cell transplantation for children with neuronal ceroid lipofuscinosis. *Journal of Neurosurgery: Pediatrics*, *11*(6), 643–652. https://doi.org/10.3171/2013.3.PEDS12397

Shamir, E. R., & Ewald, A. J. (2014). Three-dimensional organotypic culture: Experimental

models of mammalian biology and disease. *Nature Reviews Molecular Cell Biology*, *15*(10), 647–664. https://doi.org/10.1038/nrm3873

Sharif-Alhoseini, M., Khormali, M., Rezaei, M., Safdarian, M., Hajighadery, A., Khalatbari, M. M., Safdarian, M., Meknatkhah, S., Rezvan, M., Chalangari, M., Derakhshan, P., & Rahimi-Movaghar, V. (2017). Animal models of spinal cord injury : a systematic review. *Nature Publishing Group*, *55*(8), 714–721. https://doi.org/10.1038/sc.2016.187

Sharifi, F., Patel, B. B., Dzuilko, A. K., Montazami, R., Sakaguchi, D. S., & Hashemi, N. (2016). Polycaprolactone Microfibrous Scaffolds to Navigate Neural Stem Cells. *Biomacromolecules*, *17*(10), 3287–3297. https://doi.org/10.1021/acs.biomac.6b01028

Sharma, K., Korade, Z., & Frank, E. (1994). Development of specific muscle and cutaneous sensory projections in cultured segments of spinal cord. *Development*, *120*(5), 1315–1323.

Sharma, Kamal, & Frank, E. (1998). Sensory axons are guided by local cues in the developing dorsal spinal cord. *Development*, *125*(4), 635–643.

Shimizu, I., Oppenheim, R. W., O'Brien, M., & Shneiderman, a. (1990). Anatomical and functional recovery following spinal cord transection in the chick embryo. *J Neurobiol*, *21*(6), 918–937. https://doi.org/10.1002/neu.480210609

Shinozaki, Y., Shibata, K., Yoshida, K., Shigetomi, E., Gachet, C., Ikenaka, K., Tanaka, K. F., & Koizumi, S. (2017). Transformation of Astrocytes to a Neuroprotective Phenotype by Microglia via P2Y1 Receptor Downregulation. *Cell Reports*, *19*(6), 1151–1164. https://doi.org/10.1016/j.celrep.2017.04.047

Shoulders, M. D., & Raines, R. T. (2009). Collagen structure and stability. *Annual Review of*

Biochemistry, *78*, 929–958. https://doi.org/10.1146/annurev.biochem.77.032207.120833

Shuliang Chen, Peter Novick, and S. F.-N. (2017). Elastic sealants for surgical applications Nasim. *Physiology & Behavior*, *176*(3), 139–148. https://doi.org/10.1016/j.physbeh.2017.03.040

Siddiqui, N., Asawa, S., Birru, B., Baadhe, R., & Rao, S. (2018). PCL-Based Composite Scaffold Matrices for Tissue Engineering Applications. *Molecular Biotechnology*, *60*(7), 506–532. https://doi.org/10.1007/s12033-018-0084-5

Sigurjonsson, O. E., Perreault, M.-C., Egeland, T., & Glover, J. C. (2005). Adult human hematopoietic stem cells produce neurons efficiently in the regenerating chicken embryo spinal cord. *Proceedings of the National Academy of Sciences of the United States of America*, *102*(14), 5227–5232. https://doi.org/10.1073/pnas.0501029102

Silantyeva, E. A., Nasir, W., Carpenter, J., Manahan, O., Becker, M. L., & Willits, R. K. (2018). Accelerated neural differentiation of mouse embryonic stem cells on aligned GYIGSR-functionalized nanofibers. *Acta Biomaterialia*, *75*, 129–139. https://doi.org/10.1016/j.actbio.2018.05.052

Sofroniew, M. V., Pearson, R. C. A., Cuello, A. C., Tagari, P. C., & Stephens, P. H. (1986). Parenterally administered GM1ganglioside prevents retrograde degeneration of cholinergic cells of the rat basal forebrain. *Brain Research*, *398*(2), 393–396. https://doi.org/10.1016/0006-8993(86)91503-9

Soliman, E., Bianchi, F., Sleigh, J. N., George, J. H., Cader, M. Z., Cui, Z., & Ye, H. (2018). Aligned electrospun fibers for neural patterning. *Biotechnology Letters*, *40*(3), 601–607. https://doi.org/10.1007/s10529-017-2494-z

Sperling, L. E., Reis, K. P., Pozzobon, L. G., Girardi, C. S., & Pranke, P. (2017). Influence of

random and oriented electrospun fibrous poly(lactic-co-glycolic acid) scaffolds on neural differentiation of mouse embryonic stem cells. *Journal of Biomedical Materials Research - Part A*, *105*(5), 1333–1345. https://doi.org/10.1002/jbm.a.36012

Stern, C. D. (2005). The chick: A great model system becomes even greater. *Developmental Cell*, *8*(1), 9–17. https://doi.org/10.1016/j.devcel.2004.11.018

Steyn, J. S., & Andras, P. (2017). Analysis of the dynamics of temporal relationships of neural activities using optical imaging data. *Journal of Computational Neuroscience*, *42*(2), 107–121. https://doi.org/10.1007/s10827-016-0630-8

Stoeckli, E. T. (2018). Understanding axon guidance: Are we nearly there yet? *Development (Cambridge)*, *145*(10). https://doi.org/10.1242/dev.151415

Tahara, Y., & Obara, K. (2014). A novel shell-less culture system for chick embryos using a plastic film as culture vessels. *Egyptian Journal of Neurology, Psychiatry and Neurosurgery*, *51*(3), 307–312. https://doi.org/10.2141/jpsa.0130043

Takada, Y., Ye, X., & Simon, S. (2007). The integrins. *Genome Biology*, *8*(5). https://doi.org/10.1186/gb-2007-8-5-215

Takahashi, Y., Tsuji, O., Kumagai, G., Hara, C. M., Okano, H. J., Miyawaki, A., Toyama, Y., Okano, H., & Nakamura, M. (2011). Comparative study of methods for administering neural stem/progenitor cells to treat spinal cord injury in mice. *Cell Transplantation*, *20*(5), 727–739. https://doi.org/10.3727/096368910X536554

Tang-schomer, M. D. (2018). 3D axon growth by exogenous electrical stimulus and soluble factors. *Brain Research*, *1678*, 288–296. https://doi.org/10.1016/j.brainres.2017.10.032

Tapia, N., & Scholer, H. R. (2016). Molecular Obstacles to Clinical Translation of iPSCs. *Cell Stem Cell*, 1–12. https://doi.org/10.1016/j.stem.2016.06.017

Tate, C. C., Shear, D. A., Tate, M. C., Archer, D. R., Stein, D. G., & La Placa, M. C. (2009). Laminin and fibronectin scaffolds enhance neural stem cell transplantation into the injured brain. *J Tissue Eng Regen Med*, *3*(August), 208–217. https://doi.org/10.1002/term

Tricol-Biomedical. (2020). *Tricol Biomedical*. https://www.tricolbiomedical.com/

Tunnicliff, G., Cho, Y. D., Blackwell, N., Martin, R. O., & Wood, J. D. (1973). The uptake of γ aminobutyrate by organotypic cultures of chick spinal cord. *Biochemical Journal*, *134*, 27–32. https://doi.org/10.1042/bj1340027

Van Norman, G. A. (2016). Drugs, Devices, and the FDA: Part 2: An Overview of Approval Processes: FDA Approval of Medical Devices. *JACC: Basic to Translational Science*, *1*(4), 277–287. https://doi.org/10.1016/j.jacbts.2016.03.009

Van Straaten, H. W., Janssen, H. C., Peeters, M. C., Copp, A. J., & Hekking, J. W. (1996). Neural tube closure in the chick embryo is multiphasic. *Dev Dyn*, *207*(3), 309–318. http://www.ncbi.nlm.nih.gov/entrez/query.fcgi?cmd=Retrieve&db=PubMed&dopt=Citation&list_uids=8922530

Van Straaten, H. W. M., Peeters, M. C. E., Szpak, K. F. W., & Hekking, J. W. M. (1997). Initial closure of the mesencephalic neural groove in the chick embryo involves a releasing zipping-up mechanism. *Developmental Dynamics*, *209*(4), 333–341. https://doi.org/10.1002/(SICI)1097-0177(199708)209:4<333::AID-AJA1>3.0.CO;2-J

Wagner, F. B., Mignardot, J. B., Le Goff-Mignardot, C. G., Demesmaeker, R., Komi, S., Capogrosso, M., Rowald, A., Seáñez, I., Caban, M., Pirondini, E., Vat, M., McCracken, L. A., Heimgartner, R., Fodor, I., Watrin, A., Seguin, P., Paoles, E., Van Den Keybus, K., Eberle, G., … Courtine, G. (2018). Targeted neurotechnology restores walking in

humans with spinal cord injury. *Nature*, *563*(7729), 65–93. https://doi.org/10.1038/s41586-018-0649-2

Waller, A. (1850). Experiments on the Section of the Glossopharyngeal and Hypoglossal Nerves of the Frog, and Observations of the Alterations Produced Thereby in the Structure of Their Primitive Fibres. *Philosophical Transactions of the Royal Society of London*, *140*(0), 423–429. https://doi.org/10.1098/rstl.1850.0021

Wang, B., Xiao, Z., Chen, B., Han, J., Gao, Y., Zhang, J., Zhao, W., Wang, X., & Dai, J. (2008). Nogo-66 promotes the differentiation of neural progenitors into astroglial lineage cells through mTOR-STAT3 pathway. *PLoS ONE*, *3*(3). https://doi.org/10.1371/journal.pone.0001856

Weightman, A., Jenkins, S., Pickard, M., Chari, D., & Yang, Y. (2014). Alignment of multiple glial cell populations in 3D nanofiber scaffolds: Toward the development of multicellular implantable scaffolds for repair of neural injury. *Nanomedicine: Nanotechnology, Biology, and Medicine*, *10*(2), 291–295. https://doi.org/10.1016/j.nano.2013.09.001

Weightman, A. P., Pickard, M. R., Yang, Y., & Chari, D. M. (2014). An in vitro spinal cord injury model to screen neuroregenerative materials. *Biomaterials*, *35*(12), 3756–3765. https://doi.org/10.1016/j.biomaterials.2014.01.022

Wells, J. E. A., Hurlbert, J., Fehlings, M. G., & Yong, V. W. (2003). Neuroprotection by minocycline facilitates significant recovery from spinal cord injury in mice. *Brain*, *126*(7), 1628–1637. https://doi.org/10.1093/brain/awg178

Whalley, K., O'Neill, P., & Ferretti, P. (2006). Changes in response to spinal cord injury with development: Vascularization, hemorrhage and apoptosis. *Neuroscience*, *137*(3), 821–832. https://doi.org/10.1016/j.neuroscience.2005.07.064

Whalley, Katherine, Gögel, S., Lange, S., & Ferretti, P. (2009). Changes in progenitor populations and ongoing neurogenesis in the regenerating chick spinal cord. *Developmental Biology*, *332*(2), 234–245. https://doi.org/10.1016/j.ydbio.2009.05.569

WHO. (2018). *World Health Organisation*. http://www.who.int/mediacentre/factsheets/fs384/en/

Wiliams, R. R., & Bunge, M. B. (2012). Schwann cell transplantation: A repair strategy for spinal cord injury? In *Progress in Brain Research* (1st ed., Vol. 201). Elsevier B.V. https://doi.org/10.1016/B978-0-444-59544-7.00014-7

Wong, I., Liao, H., Bai, X., Zaknic, A., Zhong, J., Guan, Y., Li, H. Y., Wang, Y. J., & Zhou, X. F. (2010). ProBDNF inhibits infiltration of ED1+ macrophages after spinal cord injury. *Brain, Behavior, and Immunity*, *24*(4), 585–597. https://doi.org/10.1016/j.bbi.2010.01.001

Wu, G. H., Shi, H. J., Che, M. T., Huang, M. Y., Wei, Q. S., Feng, B., Ma, Y. H., Wang, L. J., Jiang, B., Wang, Y. Q., Han, I., Ling, E. A., Zeng, X., & Zeng, Y. S. (2018). Recovery of paralyzed limb motor function in canine with complete spinal cord injury following implantation of MSC-derived neural network tissue. *Biomaterials*, *181*, 15–34. https://doi.org/10.1016/j.biomaterials.2018.07.010

Xiao, Z., Tang, F., Zhao, Y., Han, G., Yin, N., Li, X., Chen, B., Han, S., Jiang, X., Yun, C., Zhao, C., Cheng, S., Zhang, S., & Dai, J. (2018). Significant Improvement of Acute Complete Spinal Cord Injury Patients Diagnosed by a Combined Criteria Implanted with NeuroRegen Scaffolds and Mesenchymal Stem Cells. *Cell Transplantation*, *27*(6), 907–915. https://doi.org/10.1177/0963689718766279

Xie, J., MacEwan, M. R., Schwartz, A. G., & Xia, Y. (2010). Electrospun nanofibers for neural

tissue engineering. *Nanoscale*, *2*(1), 35–44. https://doi.org/10.1039/b9nr00243j

Yaginuma, H., Shiga, T., Homma, S., Ishihara, R., & Oppenheim, R. W. (1990). Identification of early developing axon projections from spinal interneurons in the chick embryo with a neuron specific beta-tubulin antibody: evidence for a new "pioneer" pathway in the spinal cord. *Development (Cambridge, England)*, *108*(4), 705–716. http://www.ncbi.nlm.nih.gov/pubmed/2387240

Yamamoto, Y., & Henderson, C. E. (1999). Patterns of programmed cell death in populations of developing spinal motoneurons in chicken, mouse, and rat. *Developmental Biology*, *214*(1), 60–71. https://doi.org/10.1006/dbio.1999.9413

Yang, F., Murugan, R., Wang, S., & Ramakrishna, S. (2005). Electrospinning of nano/micro scale poly(l-lactic acid) aligned fibers and their potential in neural tissue engineering. *Biomaterials*, *26*(15), 2603–2610. https://doi.org/10.1016/j.biomaterials.2004.06.051

Yang, Z., Zhang, A., Duan, H., Zhang, S., Hao, P., Ye, K., Sun, Y. E., & Li, X. (2015). NT3-chitosan elicits robust endogenous neurogenesis to enable functional recovery after spinal cord injury. *Proceedings of the National Academy of Sciences of the United States of America*, *112*(43), 13354–13359. https://doi.org/10.1073/pnas.1510194112

Yoshii, S., Oka, M., Shima, M., Taniguchi, A., Taki, Y., & Akagi, M. (2004). Restoration of function after spinal cord transection using a collagen bridge. *Journal of Biomedical Materials Research. Part A*, *70*(4), 569–575. https://doi.org/10.1002/jbm.a.30120

Zawadzka, M., Rivers, L. E., Fancy, S. P. J., Zhao, C., Tripathi, R., Jamen, F., Young, K., Goncharevich, A., Pohl, H., Rizzi, M., Rowitch, D. H., Kessaris, N., Suter, U., Richardson, W. D., & Franklin, R. J. M. (2010). CNS-Resident Glial Progenitor/Stem Cells Produce Schwann Cells as well as Oligodendrocytes during Repair of CNS Demyelination. *Cell*

Stem Cell, *6*(6), 578–590. https://doi.org/10.1016/j.stem.2010.04.002

Zhang, H. T., Gao, Z. Y., Chen, Y. Z., & Wang, T. H. (2008). Temporal changes in the level of neurotrophins in the spinal cord and associated precentral gyrus following spinal hemisection in adult Rhesus monkeys. *Journal of Chemical Neuroanatomy*, *36*(3–4), 138–143. https://doi.org/10.1016/j.jchemneu.2008.07.004

Zhang, N., Yan, H., & Wen, X. (2005). Tissue-engineering approaches for axonal guidance. *Brain Research Reviews*, *49*(1), 48–64. https://doi.org/10.1016/j.brainresrev.2004.11.002

Zhang, Y., Li, L., Mu, J., Chen, J., Feng, S., & Gao, J. (2020). Implantation of a functional TEMPO-hydrogel induces recovery from rat spinal cord transection through promoting nerve regeneration and protecting bladder tissue. *Biomaterials Science*. https://doi.org/10.1039/c9bm01530b

Zukor, K., Kent, D., & Odelberg, S. (2011). Relationships in Intact and Regenerating Adult Newt Spinal Cords. *Developmental Dynamics*, *239*(11), 3048–3057. https://doi.org/10.1002/dvdy.22441.Fluorescent